Strategies to Hunt for New Physics with Strange Beauty Mesons

Robert Jan Knegjens

Cover: designed by the author, using an image generated by the Paperscape project on which the author worked together with Damien George (`http://paperscape.org`). Prepared for print by Emile Holmewood. It shows a map of scientific papers drawn as circles, which have been been arranged according to how they cite each other. A paper's size is determined by its number of citations and its colour by its scientific category. The map is zoomed in on the *flavour physics peninsula*, and the author's papers have been highlighted by white halos.

ISBN: 978-90-8891-815-5
Printed by: Proefschriftmaken.nl || Uitgeverij BOXPress
Published by: Uitgeverij BOXPress, 's-Hertogenbosch

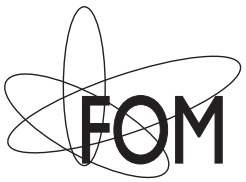

This work is part of the research program of the Foundation for Fundamental Research on Matter (FOM), which is part of The Netherlands Organisation for Scientific Research (NWO).

VRIJE UNIVERSITEIT

Strategies to Hunt for New Physics with Strange Beauty Mesons

ACADEMISCH PROEFSCHRIFT

ter verkrijging van de graad Doctor aan
de Vrije Universiteit Amsterdam,
op gezag van de rector magnificus
prof.dr. F.A. van der Duyn Schouten,
in het openbaar te verdedigen
ten overstaan van de promotiecommissie
van de Faculteit der Exacte Wetenschappen
op dinsdag 11 maart 2014 om 11.45 uur
in het aula van de universiteit,
De Boelelaan 1105

door

Robert Jan Knegjens

geboren te Soest

promotor: prof.dr. R. Fleischer

Contents

Publications

The main chapters of this thesis are based on the following publications:
Chapter 3:

- R. Fleischer and R. Knegjens, *Effective Lifetimes of B_s Decays and their Constraints on the B_s^0-$\bar{B}_s^0$ Mixing Parameters*, **Eur. Phys. J. C 71**, 1789 (2011)
- K. De Bruyn, R. Fleischer, R. Knegjens, P. Koppenburg, M. Merk and N. Tuning, *Branching Ratio Measurements of B_s Decays*, **Phys. Rev. D 86**, 014027 (2012)

Chapter 4:

- R. Fleischer and R. Knegjens, *In Pursuit of New Physics with $B_s^0 \to K^+K^-$*, **Eur. Phys. J. C 71**, 1532 (2010)
- K. De Bruyn, R. Fleischer, R. Knegjens, M. Merk, M. Schiller and N. Tuning, *Exploring $B_s \to D_s^{(*)\pm}K^{\mp}$ Decays in the Presence of a Sizable Width Difference $\Delta\Gamma_s$*, **Nucl. Phys. B 868**, 351-367 (2012)

Chapter 5:

- R. Fleischer, R. Knegjens and G. Ricciardi, *Anatomy of $B_{s,d}^0 \to J/\psi f_0(980)$*, **Eur. Phys. J. C 71**, 1832 (2011)
- R. Fleischer, R. Knegjens and G. Ricciardi, *Exploring CP Violation and η-η' Mixing with the $B_{s,d}^0 \to J/\psi\eta^{(\prime)}$ Systems*, **Eur. Phys. J. C 71**, 1798 (2011)

Chapter 6:

- K. De Bruyn, R. Fleischer, R. Knegjens, P. Koppenburg, M. Merk, A. Pellegrino and N. Tuning, *Probing New Physics via the $B_s^0 \to \mu^+\mu^-$ Effective Lifetime*, **Phys. Rev. Lett. 109**, 041801 (2012)
- A. Buras, R. Fleischer, J. Girrbach, R. Knegjens, *Probing New Physics with the $B_s \to \mu^+\mu^-$ Time-dependent Rate*, **JHEP 1307 77** (2013)
- A. Buras, F. De Fazio, J. Girrbach, R. Knegjens, M. Nagai, *The Anatomy of Neutral Scalars with FCNCs in the Flavour Precision Era*, **JHEP 1306 111** (2013)

Other publications and proceedings contributions:

- M. Herquet, R. Knegjens and E. Laenen, *Single top production in a non-minimal supersymmetric model*, **Phys. Lett. B 693**, 591 (2010)
- R. Knegjens, *An exploration of* $B_s \to J/\psi s\bar{s}$, **Nucl. Phys. Proc. Suppl. 241-242**, 164-169 (2012)
- R. Knegjens, *Phenomenology with a non-zero* B_s *Decay Width Difference*, **PoS Beauty2013 053**, (2013)

Chapter 1

Introduction

The starting date of this thesis research closely coincided with the first proton-proton collisions at the Large Hadron Collider (LHC) at CERN[1]. At that time there was not yet any evidence for the Higgs boson, and there was a strong hope that the LHC's record centre of mass energy of 7 TeV would reveal clear signals of so-called *New Physics*. New Physics essentially refers to any phenomena that cannot be described by the so far very successful Standard Model of particle physics, which is by now almost 40 years old. It may be searched for by conjecturing specific new models, known as the *top down* approach, or by studying deviations from the Standard Model in generic observables, which is called the *bottom up* approach. An example of the top down approach is the class of models based on weak scale supersymmetry, which can address a range of Standard Model shortcomings, including the origin of dark matter [1], the naturalness of the Higgs boson mass and the unification of forces [2, 3].

Several years on from the startup of the LHC, in July 2012 to be precise, the ATLAS and CMS detectors at the LHC proudly reported the discovery of a Higgs-like particle with a mass of 126 GeV [4, 5]. On the other hand, all direct searches for New Physics to date have returned results compatible with the Standard Model. As a result, models of New Physics, such as supersymmetry, now have a significantly constrained parameter space and strict lower bounds for the masses of possible new particles [6, 7, 8]. This is the status quo of what may be called the *high energy frontier*.

Equally important is the *precision frontier*, where New Physics is looked for indirectly by precisely measuring the decays of well-understood particles to well-understood final states. Particularly interesting are decays of meson particles, as these often involve processes in which quarks change flavour via the weak force. In the Standard Model such processes can violate Charge-Parity (CP) symmetry. The violation of this symmetry is interesting in its own right, as well as a necessary condition to explain the matter–antimatter asymmetry of the Universe [9]. In addition, when quarks with the same charge change flavour, they do so via virtual loop interactions in which heavy new

[1]The starting date was on the 1st of February 2010 and the first proton-proton collisions took place on March 30th that same year.

particles can also participate. Thus, by measuring these processes very precisely, we can discern the presence or absence of New Physics particles that are too heavy to have a direct impact on the high energy frontier.

The violation of CP symmetry was first discovered by the observation of long-lived neutral kaons decaying to two pions [10]. Besides from being an unexpected result, it was, in hindsight, also a somewhat unlikely process to discover CP violation with, given that the observed asymmetry is of the order 10^{-3}. Much bigger effects, as it turns out, occur in decays involving B mesons. To study the CP violation present in these decays, the so-called B-factories BaBar, at SLAC, and Belle, at KEKB, were commissioned in 1999. These e^+e^- colliders operated primarily at the $\Upsilon(4S)$ resonance, allowing them to produce over a billion pairs of B_d^0–$\overline{B}_d^0$ and B_u^+–B_u^- mesons. A key highlight of the B-factory era was the measurement of a sizable CP-violating B_d^0–$\overline{B}_d^0$ mixing phase with a time-dependent analysis of the decay mode $B_d \to J/\psi K_S$ [11, 12]. On the whole, after ten years of operation, the B-factories helped to establish a very consistent picture of CP violation in the Standard Model. However, some corners of quark flavour mixing were left unconstrained, in particular quark transitions to which the neutral B_s meson system is sensitive.

Around the time the LHC started up, the properties of the neutral B_s meson system were still largely undetermined, while existing determinations of its CP violating mixing phase were causing excitement. Specifically, measurements of this phase by the Tevatron detectors DØ and CDF were showing deviations from the Standard Model prediction by two standard deviations [13]. Since then the LHC's LHCb detector has considerably sharpened this picture. As we will present in Chapter 3, the B_s mixing phase has now been more accurately measured, and it appears to reside close to the Standard Model prediction, already ruling out a smoking gun signal of New Physics. The same holds true for other B_s observables that could have revealed a large New Physics signal, such as the rare decay $B_s \to \mu^+\mu^-$ that we will discuss in more detail below. The LHCb experiment has recently reported small hints of New Physics in the B_d meson system, although these are far from conclusive. Namely, in the angular distribution of the $B_d \to K^*\mu^+\mu^-$ decay [14, 15] and in an isospin relation involving the $B_d \to K\mu^+\mu^-$ decay [16].

With the status quo of the precision frontier delivering no clear cut signals of New Physics either, we must await further precision from the LHC experiments. However, as theorists, we should not wait by idly. If there are small signals of New Physics hidden in future precision measurements, precise Standard Model predictions are required in order to identify them. The most challenging aspect of improving these predictions is due to the difficult hadronic nature of meson decays, which involve long-distance strong interactions. To this end, we can make use of a well developed theoretical framework, known as the Operator Product Expansion (OPE), which allows us to split short from long distance contributions. In some cases the long distance contributions can be further simplified with an approximation known as factorization. We will introduce both of these theoretical tools in Chapter 2. Unfortunately, these tools alone are often not sufficient to

factor out the presence of hadronic physics. Methods to directly compute the hadronic amplitudes exist, such as lattice QCD or QCD sum rules, but the associated theoretical uncertainties are still sizable. In this thesis we will chiefly attempt to deal with hadronic physics by making use of the approximate flavour symmetries of QCD, as we will also introduce in Chapter 2.

Our goal in this thesis is to develop and improve strategies for searching for New Physics in the form of new sources of CP violation and modified flavour changing quark couplings using the B_s meson system. We will mainly follow the bottom up approach, which means that we apply a general, model-independent, parameterization to observable processes that can be compared with Standard Model predictions. In essence this involves puzzling together various related meson decay modes and their observables in order to extract parameters, such as CP violating phases, while minimizing the theoretical uncertainty. Several of the strategies that we discuss complement more conventional determinations of the same parameters. Overconstraining these parameters in this way is crucial. Firstly, it combines analyses with different experimental systematics and different theoretical uncertainties, thereby increasing our overall confidence in the final result. And secondly, comparing the same result from two vastly different analyses may reveal something unexpected. For example, if a parameter determined from processes with only tree topologies differs from that extracted from a processes dominated by loop topologies this could be an indication of heavy new particles contributing to the latter.

A particularly useful feature of the B_s meson system, in contrast to the B_d meson system, is that its mass-eigenstates have a sizable lifetime difference, as we will explain in Chapter 3. This makes it possible, from a time-dependent analysis, to distinguish the relative decay rates of the two mass eigenstates to a specific final state i.e. to measure a *mass-eigenstate rate asymmetry*. Such an analysis does not require so-called flavour tagging, where an attempt is made to identify which flavour state the B_s meson is in before it decays, and is thereby experimentally more efficient and available sooner. The observable sensitive to this asymmetry that is typically quoted by experiments is the *effective lifetime*, which we will also introduce in Chapter 3. Throughout this thesis effective lifetimes will play a prominent role in our hunt for New Physics.

Another consequence of the sizable decay width difference of the two B_s mass-eigenstates is that the definition of their branching ratio becomes ambiguous. This is not surprising, because in general there is no obvious way to define a single branching ratio for two different physical states. In the neutral kaon system, for example, the total decay widths of the mass-eigenstates $K_{\rm S}$ and $K_{\rm L}$ are very different, so it is not intuitively clear what a single branching ratio would mean in this case. However, in the neutral B_d and B_s systems, where the total widths are similar (almost exactly so in the B_d case), it is tempting to have such a definition. In Chapter 3 we will discuss two definitions currently in use, with one corresponding to how a B_s branching ratio is experimentally measured and the other how it is theoretically calculated. In particular, we will present the dictionary necessary to convert between them. To avoid making theoretical assumptions in such a conversion, it is possible to use information from the

effective lifetime measurement of the decay channel in question.

The CP violation present in the Standard Model can be described by a triangle constructed in the complex plane, describing the unitarity of the quark mixing matrix, which we will elaborate on in Chapter 2. The apex of this triangle has already been constrained using many different analyses (for a review see, for example, Ref. [17]), which so far gives a consistent picture. However, one angle of this triangle, referred to as γ, has yet to be accurately determined directly. In Chapter 4 we will discuss strategies for determining this angle using two different B_s meson decays: $B_s \to K^+K^-$ and $B_s \to D_s^{(*)}K$. These two decays complement each other in an interesting way. Specifically, the first decay is driven by virtual loop processes and is thereby also sensitive to New Physics effects. The second decay, on the other hand, receives no contributions from such loop diagrams. Furthermore, a time-dependent analysis of the second decay is theoretically clean. It will therefore be interesting to eventually compare the results of the strategies of these two decays, as this may indicate the presence of New Physics.

A possible hiding place for new sources of CP violation is in the mixing of the B_s meson system, a phenomenon we will introduce in detail in Chapter 3. The CP violation that enters this mixing is parameterised by a phase ϕ_s. The flagship experimental analysis for probing this phase is a time-dependent angular analysis of the decay mode $B_s \to J/\psi\phi$, which includes flavour tagging. In Chapter 5 we will, as we discussed and motivated above, present alternative strategies and decay modes for extracting this phase. In particular, we will consider the decay modes $B_s \to J/\psi f_0(980)$ and $B_s \to J/\psi\eta^{(\prime)}$. The advantage of these modes is that their determination depends on different experimental techniques, such as requiring no angular analysis. The disadvantage, as we will discuss, is the uncertain composition of the $f_0(980)$ and $\eta^{(\prime)}$ isospin singlet states. In this chapter we will also present a strategy for extracting the phase ϕ_s and the B_s decay width difference using only a pair of effective lifetimes, which involves no flavour tagging, and compare the result with the flagship analysis.

A good place to look for New Physics is within decays that are very suppressed in the Standard Model. A prime example of such a rare decay is $B_s \to \mu^+\mu^-$, which in the Standard Model is expected to occur only once for every 300 million B_s mesons. It was long hoped that the branching ratio measurement of this decay would be orders of magnitude larger than expected and thereby reveal a clear signal of New Physics. Alas, recent measurements of this branching ratio, as we will present in Chapter 6, turn out to be in the ballpark of the Standard Model. This makes the issue of how a branching ratio is defined, as we discussed above, very relevant for this decay mode, and we will present the necessary correction in Chapter 6. We will also discuss how an effective lifetime measurement for this decay complements the branching ratio. Essentially the effective lifetime is sensitive to features of New Physics models that the branching ratio is not. Furthermore, we will discuss how the combination of the branching ratio with the time-dependent $B_s \to \mu^+\mu^-$ observables can discriminate between different classes of New Physics models.

Brief outline of this thesis

The outline of this thesis is as follows. In Chapter 2 we introduce some of the existing theoretical tools and frameworks common to our analysis strategies. In Chapter 3 we present the B_s meson system, and focus in particular on the observables and subtle effects that originate from the sizable decay width difference of the mass-eigenstates of this system. In Chapter 4 various strategies for extracting the angle γ of the unitarity triangle using the decay modes $B_s \to K^+K^-$ and $B_s \to D_s^{(*)}K$ are discussed. The former decay mode is dominated by QCD penguin topologies whereas the latter is governed purely by tree topologies and is theoretically clean. In Chapter 5 we turn our attention to determining the B_s mixing parameters, particularly the mixing phase ϕ_s. To this end we analyse decay modes of the form $B_s \to J/\psi s\bar{s}$, with the $s\bar{s}$ state taken to be the $f_0(980)$ or the $\eta^{(\prime)}$ mesons. We also present an analysis strategy for pinpointing the mixing parameters based only on a pair of effective lifetime measurements. In Chapter 6 we discuss how an untagged time-dependent analysis of the rare decay $B_s \to \mu^+\mu^-$ offers complementary information to the branching ratio, which can help to discriminate between various models of New Physics. In addition we point out how this branching ratio must be corrected due to the B_s decay width difference. In Chapter 7 we summarise the findings of this thesis and provide an outlook.

Chapter 2

Technology

2.1 Quark flavour mixing and CP violation

The cornerstone of our modern understanding of particle physics is *gauge theory*. Gauge theory in this context is an extension of quantum field theory, which describes particles by fields. In a gauge theory such fields are required to be invariant under a particular continuous symmetry at every point in space. In order to enforce this *local symmetry*, additional fields known as gauge bosons must be introduced to communicate changes in the *gauge* degrees of freedom protected by the symmetry. A consequence of this communication mechanism is that otherwise freely moving particles begin to interact, attracting or repelling each other. Thereby gauge bosons mediate forces. Or, to put it differently, each of the known forces, bar perhaps gravity, can be associated with a specific continuous local symmetry.

The Standard Model of particle physics is a gauge theory that has the continuous gauge-symmetry

$$SU(3)_C \times SU(2)_L \times U(1)_Y. \tag{2.1}$$

The symmetry $SU(3)_C$, describing a conserved colour charge, represents the strong force with gauge bosons called gluons. The fermion fields of the Standard Model that carry a non-trivial colour charge are classified as *quarks* and the rest as *leptons*. The unique feature of the strong force, to which it owes its name, is that it forces quarks together into strongly bound states known as hadrons. A combination of three quarks is called a baryon, and a quark together with an antiquark a meson. The Standard Model has a total of six *flavours* of quarks and antiquarks, which, in order of increasing mass, are labeled u, d, s, c, b and t. In this thesis our focus will be on the decays of the mesons B_s^0 and $\overline{B}_s^0$, which have the flavour content $\bar{b}s$ and $b\bar{s}$, respectively. To this end we will first explain the mechanisms responsible for such decays, and for this we need to discuss the other two Standard Model forces.

Quarks and leptons are described in the Standard Model by Dirac fermions[1]. A Dirac

[1]Neutrinos may yet prove to be Majorana fermions instead

fermion ψ can be decomposed into left and right handed *chiral* components, $\psi_{L,R}$, using the projection matrices $P_{\binom{L}{R}} \equiv (1 \mp \gamma_5)/2$. The Standard Model symmetry $SU(2)_L$, which represents the weak force, only acts on left-handed fermions. Specifically, the left-handed quark doublets

$$\begin{pmatrix} u_L \\ d_L \end{pmatrix}_1, \quad \begin{pmatrix} c_L \\ s_L \end{pmatrix}_2, \quad \begin{pmatrix} t_L \\ b_L \end{pmatrix}_3, \tag{2.2}$$

transform under the fundamental representation of $SU(2)_L$. We will collectively refer to these doublets as $Q_{L,i}$, and use $i \in \{1, 2, 3\}$ as a general label for the three fermion *generations* e.g. $u_{L,i} = \{u_L, c_L, t_L\}$. The three generations of left-handed lepton doublets,

$$\begin{pmatrix} \nu_{eL} \\ e_L \end{pmatrix}_1, \quad \begin{pmatrix} \nu_{\mu L} \\ \mu_L \end{pmatrix}_2, \quad \begin{pmatrix} \nu_{\tau L} \\ b_L \end{pmatrix}_3, \tag{2.3}$$

transform in the same way, and will be referred to by $L_{L,i}$. Finally each Standard Model fermion also carries a non-trivial hypercharge associated to the symmetry $U(1)_Y$. We may thus conclude that left-handed quarks are the most sociable species of elementary particles that we know about, as only they are charged under each symmetry of the Standard Model gauge group.

The fact that the left-handed quarks and leptons participate in the $SU(2)_L$ chiral symmetry, requires the Standard Model to have a special mechanism for generating their masses. This is because ordinarily fermion mass terms mix chirality and therefore break this symmetry. An elegant solution, proposed by Brout, Englert and Higgs [18, 19], is to introduce additional fields that dynamically break the electroweak symmetry, and in turn generate all the masses of the theory. To this end a combination of scalar fields are introduced that are charged under $SU(2)_L \times U(1)_Y$, and that have a carefully chosen scalar potential so that one of the real scalar fields takes a non-zero vacuum expectation value v at its minimum. To be precise, a doublet of complex scalars is introduced

$$H = \begin{pmatrix} H^+ \\ H^0 \end{pmatrix}, \tag{2.4}$$

transforming under the fundamental representation of $SU(2)_L$ and with a hypercharge of 1. The desired minimum then occurs at the vacuum expectation value

$$\langle H \rangle = \begin{pmatrix} 0 \\ \frac{1}{\sqrt{2}} v \end{pmatrix}, \tag{2.5}$$

as the generators of $SU(2)_L \times U(1)_Y$ acting on this minima do not leave it invariant, bar one exception: the combination $I_3 + Y/2 \equiv Q$, where I_3 is the diagonal generator of $SU(2)_L$ and Y the generator of hypercharge. Thus the continuous local symmetry $SU(2)_L \times U(1)_Y$ is spontaneously broken at this minimum, leaving only the subgroup $U(1)_Q$ intact, the gauge symmetry of electromagnetism. In place of the three broken symmetries we recover three Goldstone bosons, whose degrees of freedom are captured by

the corresponding gauge bosons, $W^{\pm}$ and Z^0, to become their longitudinal components. Via this so-called Brout–Englert–Higgs mechanism, these gauge bosons also pick up a mass proportional to the Higgs vacuum expectation value. The remaining massless gauge boson, corresponding to the gauge symmetry $U(1)_Q$ that is preserved at the minimum of the scalar potential, is the photon γ familiar from electromagnetism.

In order to also give a mass to quarks and leptons, they too must be coupled to the Higgs doublet field. The electroweak gauge invariant way to do this is via so-called Yukawa terms, which in general are given for quarks by

$$\mathcal{L}_{\text{Yukawa}} = \sum_{i,j} y_u^{ij} \left(\overline{Q_{L,i}} \cdot i\sigma_2 H^*\right) u_{R,j} + \sum_{i,j} y_d^{ij} \left(\overline{Q_{L,i}} \cdot H\right) d_{R,j} + \text{h.c.}, \tag{2.6}$$

where the latin indices sum over quark flavour (as mentioned earlier), and the dot product refers to an inner product of $SU(2)_L$ doublets. The matrices $\mathbf{y}_u$ and $\mathbf{y}_d$ are generalized Yukawa terms in flavour space, and not necessarily diagonal. After electroweak symmetry breaking this produces the mass terms

$$\mathcal{L}_{\text{mass}} = \sum_{i,j} m_u^{ij} \overline{u_{L,i}}\, u_{R,j} + \sum_{i,j} m_d^{ij} \overline{d_{L,i}}\, d_{R,j} + \text{h.c.}, \tag{2.7}$$

where $\mathbf{m}_{u,d} \equiv v\,\mathbf{y}_{u,d}/\sqrt{2}$. Because the mass matrices are in general also not diagonal, we recover the quark mass-eigenstates with the unitary transformations[2]

$$\begin{aligned} u'_{L,i} &= \sum_j U^u_{L,ij}\, u_{L,j}, \quad u'_{R,i} = \sum_j U^u_{R,ij}\, u_{R,j}, \quad \text{diag}(m_{u'}, m_{c'}, m_{t'}) = \mathbf{U}_L^{u\dagger}\, \mathbf{m}_u\, \mathbf{U}_R^u, \\ d'_{L,i} &= \sum_j U^d_{L,ij}\, d_{L,j}, \quad d'_{R,i} = \sum_j U^d_{R,ij}\, d_{R,j}, \quad \text{diag}(m_{d'}, m_{s'}, m_{b'}) = \mathbf{U}_L^{d\dagger} \mathbf{m}_d\, \mathbf{U}_R^d. \end{aligned} \tag{2.8}$$

where, for temporary clarity, we denote the mass-eigenstates with a prime.

The unitarity of the transformation matrices $\mathbf{U}^{u,d}_{L,R}$ ensures that the neutral vector currents of the Standard Model are unaffected by the change of basis, for example:

$$\bar{\boldsymbol{u}}_{\boldsymbol{L}} \gamma^\mu \boldsymbol{u}_{\boldsymbol{L}} \to \bar{\boldsymbol{u}}'_{\boldsymbol{L}} \gamma^\mu \boldsymbol{u}'_{\boldsymbol{L}}. \tag{2.9}$$

This is not true for the charged weak force current which becomes

$$\frac{i\,g_2}{\sqrt{2}} W^+_\mu \bar{\boldsymbol{u}}_{\boldsymbol{L}} \gamma^\mu \boldsymbol{d}_{\boldsymbol{L}} + \text{h.c} \to \frac{i\,g_2}{\sqrt{2}} W^+_\mu \bar{\boldsymbol{u}}'_{\boldsymbol{L}} \left(\mathbf{U}_L^u \mathbf{U}_L^{d\dagger}\right) \gamma^\mu \boldsymbol{d}'_{\boldsymbol{L}} + \text{h.c.} \tag{2.10}$$

The matrix $\mathbf{V} \equiv \mathbf{U}_L^u \mathbf{U}_L^{d\dagger}$, if not purely diagonal, therefore enables flavour changing charged currents between different generations of left-handed quarks, and is named after its developers Cabibbo, Kobayashi and Maskawa (CKM) [20, 21]. Being a product of two unitary matrices, it is itself also unitary (at least in the Standard Model). Our focus

[2]It is assumed that $\mathbf{m}_{u,d}$ can be transformed into a real diagonalized form.

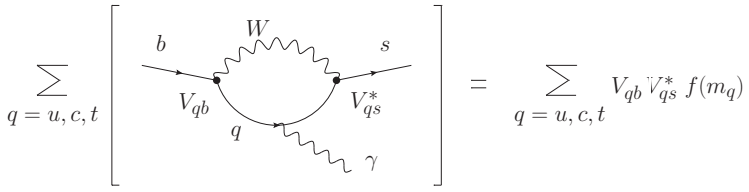

Figure 2.1: The *flavour changing neutral current* (FCNC) decay $b \to s\gamma$, where the function $f(m_q)$ describes the general dynamics of the loop process. In the limit $m_u = m_c = m_t$ the amplitude would vanish due to the unitarity of the CKM matrix.

has been on the left-handed quarks, but we should note that the same arguments hold for left-handed leptons. In the lepton case the mixing matrix is named after Pontecorvo, Maki, Nakagawa and Sakata [22, 23, 24] (PMNS). Over the past decade neutrino flavour mixing has been observed, dispelling the long held idea that neutrinos are massless [25]. It is still an open question, however, whether neutrinos are Dirac or Majorana fermions.

We already noted that the unitarity of the transformations to the mass-eigenstate basis prevent flavour changing neutral currents (FCNCs) at tree level in the Standard Model. This feature is known as the GIM-mechanism, which is named after Glashow, Iliopoulos and Maiani who proposed the existence of the charm quark to explain the absence of $s \leftrightarrow d$ transitions at tree-level [26]. At loop level, however, such a neutral current is achievable by combining two flavour changing charged currents. For example, a b quark can decay to an s quark and a photon via a loop process involving a W boson and up-type quarks as shown in Figure 2.1. Such a process is then proportional to

$$M(b \to s\,\gamma) \propto \sum_i V_{i2}^* V_{i3}\, f_i, \tag{2.11}$$

where f_i specifies the loop dynamics associated to the up-type quark $u_i = \{u, c, t\}$ (from here on we will always refer to quark mass-eigenstates, and stop denoting them with a prime). In the Standard Model the dynamics differ only with respect to the quark masses, so that $f_i = f(m_{q_i})$. Thus, if the mediating quarks (in the example up-type) are degenerate in mass, the unitarity of the CKM matrix would ensure a perfect cancellation for such a transition. An approximate cancellation due to nearly degenerate quark masses is often referred to as a GIM-suppression. The quark masses (determined in the $\overline{\text{MS}}$-scheme) are given as follows [27, 28, 17]:

$$\begin{aligned} m_u(2\,\text{GeV}) &= (2.1 \pm 0.1)\,\text{MeV}, & m_d(2\,\text{GeV}) &= (4.73 \pm 0.12)\,\text{MeV}, \\ m_s(2\,\text{GeV}) &= (93.4 \pm 1.1)\,\text{MeV}, & m_c(m_c) &= (1.279 \pm 0.013)\,\text{GeV}, \\ m_b(m_b) &= (4.18 \pm 0.05)\,\text{GeV}, & m_t(m_t) &= (163 \pm 1)\,\text{GeV}. \end{aligned} \tag{2.12}$$

We see that up-type FCNCs, dependent on down-type quark mass differences, are more strongly GIM-suppressed.

Let us now consider the CKM matrix in more detail. Being unitary, the CKM matrix

can be parameterized in terms of three Euler angles and one CP-violating phase [17]:

$$V = \begin{pmatrix} 1 & 0 & 0 \\ 0 & c_{23} & s_{23} \\ 0 & -s_{23} & c_{23} \end{pmatrix} \begin{pmatrix} c_{13} & 0 & s_{13}\, e^{-i\delta_{13}} \\ 0 & 1 & 0 \\ -s_{13}\, e^{i\delta_{13}} & 0 & c_{13} \end{pmatrix} \begin{pmatrix} c_{12} & s_{12} & 0 \\ -s_{12} & c_{12} & 0 \\ 0 & 0 & 1 \end{pmatrix}, \tag{2.13}$$

where $s_{ij} = \sin\theta_{ij}$ and $c_{ij} = \cos\theta_{ij}$. Experimentally it has been established that $s_{13} \ll s_{23} \ll s_{12} \ll 1$, which has prompted the use of the more convenient Wolfenstein parameterization [29]:

$$s_{12} = \lambda, \qquad s_{23} = A\lambda^2, \qquad s_{13}\, e^{-i\delta_{13}} = A\lambda^3(\rho - i\eta). \tag{2.14}$$

As $\lambda \ll 1$ we may use it as an expansion parameter, resulting in a clearer depiction of the relative coupling strengths of the flavour changing weak processes:

$$V = \begin{pmatrix} 1 - \frac{1}{2}\lambda^2 & \lambda & A\lambda^3(\rho - i\eta) \\ -\lambda & 1 - \frac{1}{2}\lambda^2 & A\lambda^2 \\ A\lambda^3(1 - \rho - i\eta) & -A\lambda^2 & 1 \end{pmatrix} + \mathcal{O}(\lambda^4). \tag{2.15}$$

The unitarity of the CKM matrix gives six orthogonality conditions that can be depicted as triangles in the complex plane in the presence of a non-trivial CP-violating phase. The angles and lengths of these triangles can often be probed directly by experiments, and it is therefore useful to reparameterize the CKM matrix in terms of them. Of particular interest is the normalized unitarity condition

$$1 + \frac{V_{ud}V_{ub}^*}{V_{cd}V_{cb}^*} + \frac{V_{td}V_{tb}^*}{V_{cd}V_{cb}^*} = 0 \tag{2.16}$$

as it gives one of two triangles in the complex plane with sides in equal proportion to order λ. This triangle is shown in the left panel of Figure 2.2, and is often referred to as *the* unitarity triangle. Expanding to sixth order in λ, this triangle's vertex is given by [30]

$$\bar{\rho} = \rho(1 - \frac{1}{2}\lambda^2), \qquad \bar{\eta} = \eta(1 - \frac{1}{2}\lambda^2), \tag{2.17}$$

its sides by

$$R_b \equiv \left|\frac{V_{ud}V_{ub}^*}{V_{cd}V_{cb}^*}\right| = \sqrt{\bar{\rho}^2 + \bar{\eta}^2}, \qquad R_t \equiv \left|\frac{V_{td}V_{tb}^*}{V_{cd}V_{cb}^*}\right| = \sqrt{(1-\bar{\rho})^2 + \bar{\eta}^2}, \tag{2.18}$$

and its angles by

$$\begin{aligned} \alpha &\equiv \arg\left(-\frac{V_{td}V_{tb}^*}{V_{ud}V_{ub}^*}\right) = \frac{1}{2}\sin^{-1}\left[\frac{2\bar{\eta}(\bar{\eta}^2 + \bar{\rho}^2 - \bar{\rho})}{(\bar{\rho}^2 + \bar{\eta}^2)((1-\bar{\rho})^2 + \bar{\eta}^2)}\right], \\ \beta &\equiv \arg\left(-\frac{V_{cd}V_{cb}^*}{V_{td}V_{tb}^*}\right) = \frac{1}{2}\sin^{-1}\left[\frac{2\bar{\eta}(1-\bar{\rho})}{(1-\bar{\rho})^2 + \bar{\eta}^2}\right], \\ \gamma &\equiv \arg\left(-\frac{V_{ud}V_{ub}^*}{V_{cd}V_{cb}^*}\right) = \frac{1}{2}\sin^{-1}\left[\frac{2\bar{\rho}\,\bar{\eta}}{\bar{\rho}^2 + \bar{\eta}^2}\right], \end{aligned} \tag{2.19}$$

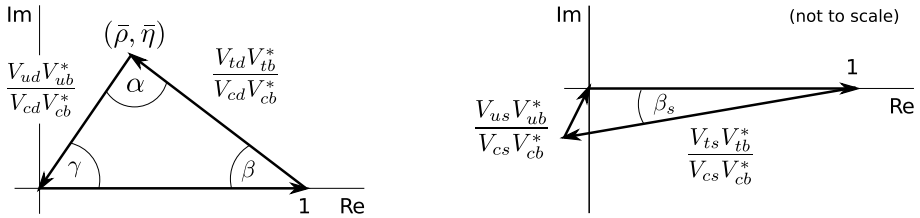

Figure 2.2: Two normalized unitarity conditions of the CKM matrix as triangles in the complex plane. The left triangle is the famous unitarity triangle with sides of equal proportion. The right triangle shows the small angle β_s.

with $\alpha + \beta + \gamma = \pi$.

At higher orders in λ we also find another, very squashed, unitarity triangle due to the phase of V_{ts} in the Wolfenstein parameterization. This triangle is shown (not to scale) in the right panel of Figure 2.2. The definition of this small angle is given by

$$\beta_s \equiv \arg\left(-\frac{V_{ts}V_{tb}^*}{V_{cs}V_{cb}^*}\right) = \lambda^2\eta. \tag{2.20}$$

As will be discussed in Section 3.1, this phase can be probed by B_s^0–$\overline{B}_s^0$ mixing. If we expand the Wolfenstein parameterization of the CKM matrix to $\mathcal{O}(\lambda^5)$, its components can be written in terms of the angle β, γ and β_s in the following way:

$$V = \begin{pmatrix} 1-\frac{1}{2}\lambda^2-\frac{1}{8}\lambda^4 & \lambda & \left[A\lambda^3\, R_b/(1-\frac{1}{2}\lambda^2)\right]\, \boldsymbol{e^{-i\gamma}} \\ -\lambda & 1-\frac{1}{2}\lambda^2-\frac{1}{8}\lambda^4(1-4A^2) & A\lambda^2 \\ A\lambda^3\, R_t\, \boldsymbol{e^{-i\beta}} & -A\lambda^2\, \boldsymbol{e^{i\beta_s}} & 1-\frac{1}{2}A^2\lambda^4 \end{pmatrix} + \mathcal{O}(\lambda^5). \tag{2.21}$$

All of the triangles corresponding to the six unitarity conditions have the same area, which is given by half the Jarlskog parameter [31]

$$\begin{aligned} J_{\rm CP} &\equiv \mathrm{Im}(V_{ik}V_{jl}V_{il}^*V_{jk}^*), \quad (i \neq j, k \neq l) \\ &= A^2\lambda^6\eta \sim 10^{-5}. \end{aligned} \tag{2.22}$$

The Jarslkog parameter is a measure of the amount of CP violation present in the mixing matrix, and vanishes in the absence of a CP-violating phase. It so happens that the observed CP violation in the Standard Model CKM matrix is a thousand times less than the maximum that is possible in a unitary 3×3 matrix.

Part of the goal of this thesis is to probe the consistency of the CKM matrix. Essentially, we seek to establish if the Standard Model CKM matrix gives the complete picture of CP violation, or if there are other sources of CP violation. Simultaneously, we also seek to answer whether there are new mechanisms or particles responsible for enhanced (or suppressed) flavour changing currents among quarks.

2.2 Operator product expansion for weak decays

We would like to study quark flavour changing processes and CP violation using B_s meson decays. As discussed in Section 2.1, these two phenomena occur in the Standard Model via the weak interaction. This confronts us with a large discrepancy in scales. Namely, hadrons decay with energies of the order of their mass, $E \sim m_b \approx 4\,\text{GeV}$ in the case of B_s mesons, whereas the weak decay is mediated by W bosons with a mass of $M_W \approx 80\,\text{GeV}$. Clearly $E \ll M_W$, so any W boson produced will be highly virtual. In other words, to a decaying meson an intermediate W boson is not resolvable and the associated weak transition will effectively appear as a four-fermion point interaction. If we let $k \sim E$ be the momentum transfer of a W boson, then its momentum-space propagator expanded in powers of k^2/M_W^2 becomes

$$\Delta^{\mu\nu}(k) = \frac{-1}{k^2 - M_W^2}\left(g^{\mu\nu} - \frac{k^\mu k^\nu}{M_W^2}\right) \to \frac{g^{\mu\nu}}{M_W^2} + \mathcal{O}\left(\frac{k^2}{M_W^4}\right), \tag{2.23}$$

i.e. at leading order it represents a purely local interaction. Often in this limit the W boson is said to be *integrated out*, which refers to the formal procedure of removing it from the generating functional by integrating over its fields in the absence of any source terms.

By integrating out the heavy W boson we can construct a low-energy effective field theory. At tree level the corresponding effective interaction Hamiltonian for quarks and leptons is given by

$$\mathcal{H}_{\text{eff}}^{\text{tree}} = \frac{G_F}{\sqrt{2}}\mathcal{J}_\mu \mathcal{J}^{\mu\dagger} \tag{2.24}$$

where

$$\mathcal{J}_\mu = \sum_{ij} V_{ij}^{\text{CKM}} \bar{u}_i \gamma_\mu (1-\gamma_5) d_j + \sum_{ij} V_{ij}^{\text{PMNS}} \bar{\nu}_i \gamma_\mu (1-\gamma_5) l_j. \tag{2.25}$$

The Fermi constant,

$$G_F \equiv \frac{\sqrt{2}\, g_2^2}{8\, M_W^2}, \tag{2.26}$$

was introduced in the original Fermi theory [32] that described weak decays in terms of four-fermion interactions before the discovery of the mediating W boson. In Figure 2.3 we illustrate how the W boson propagator is replaced by a local four point interaction.

As the weak decays we will be interested in involve hadrons, QCD effects will play an important role. In particular, as hadrons are strongly bound states, we will have to contend with QCD in its non-perturbative low-energy regime. To this end we introduce the Operator Product Expansion (OPE) for weak decays [33, 34, 35],

$$\mathcal{H}_{\text{eff}} = \frac{G_F}{\sqrt{2}} \sum_i C_i \mathcal{O}_i, \tag{2.27}$$

which generalizes the tree-level effective theory above. The $\mathcal{O}_i$ represent a basis of operators, typically of mass dimension six, relevant for the process under consideration.

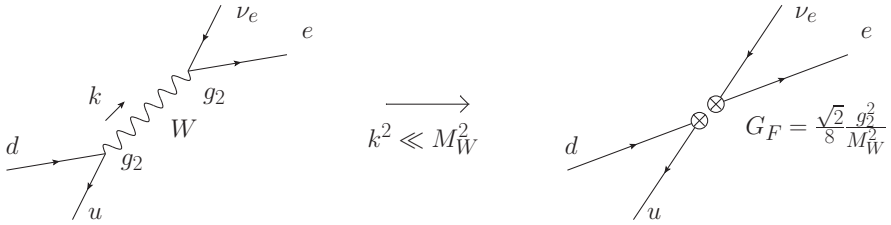

Figure 2.3: Illustration of how the W propagator is replaced by a local four point interaction in the low energy effective theory.

As before, higher dimensional operators that are suppressed by additional powers of the heavy scale, $1/M_W$, are neglected. The C_i are *Wilson coefficients*, essentially the coupling constants of this new operator basis. The basic idea is that the high energy dynamics of the theory are contained in these Wilson coefficients. This includes both the heavy fields above the typical interaction that have been integrated out, such as the W and Z bosons and the top quark, and QCD effects above this energy scale.

The utility of the OPE can be better understood in the context of an amplitude computation. Consider for example the transition of some initial hadronic state i to some final state f. Using the effective Hamiltonian in (2.27) the amplitude becomes

$$\langle f|H_{\text{eff}}|i\rangle = \frac{G_F}{\sqrt{2}} \sum_j C_j(\mu)\langle \mathcal{O}_j(\mu)\rangle, \tag{2.28}$$

where we have made explicit the renormalization scale μ. In a dimensional regularization scheme (such as $\overline{\text{MS}}$) this is the scale introduced in order to keep the strong coupling constant dimensionless in $d \neq 4$ dimensions. The effect of using the OPE is that the amplitude is factorised into two parts describing two different energy regimes. The Wilson coefficients describe the short-distance physics with energies above the scale μ, whereas the operator matrix elements $\langle \mathcal{O}_j(\mu)\rangle$ describe long-distance physics with energies below this scale. In this sense the scale μ doubles as a factorisation scale. The physical amplitude in (2.28) cannot depend on the scale μ. Therefore the μ dependence of the Wilson coefficients and the operator matrix elements must cancel each other. In practice the dependence on μ is expressed in terms of a truncated series in $\alpha_s(\mu)$ and the cancellation is effective up to this order in the series.

Due to the asymptotic freedom of QCD, the Wilson coefficients can be computed straightforwardly using perturbation theory. The matrix elements, however, describe an energy regime where the strong coupling constant can no longer be treated perturbatively. Their determination in principle requires more involved theoretical calculations with larger theoretical uncertainties. We will return to their evaluation in Section 2.3.

The Wilson coefficients are determined by *matching* amplitude calculations using the effective theory with calculations using the full theory at a given order in the strong coupling constant α_s. However, beyond zeroth order in QCD the amplitudes in both theories must first be renormalized. As only the short-distance physics is meant to

be encapsulated into the Wilson coefficients, infrared or collinear divergences are of no concern provided they are regulated consistently in both calculations[3]. Specifically, they are simply absorbed into the operator matrix elements, which anyway represent the long-distance non-perturbative physics.

For the effective field theory it is conventional to renormalize the operators rather than the couplings (Wilson coefficients). Consider for example a single generic operator

$$\mathcal{O}_2 = (\bar{q}_{1\alpha}\Gamma_1\, b_\alpha)(\bar{q}_{2\beta}\Gamma_2\, q_{3\beta}), \tag{2.29}$$

where $\{\Gamma_1, \Gamma_2\}$ represents some Dirac matrix structure and the Greek indices denote the colour flow of the quarks (with Einstein summation implied). Once QCD corrections are included there will be gluon exchanges between the quark legs that will not only introduce ultraviolet (UV) divergences but also change the colour flow of this effective operator. Therefore in order to successfully subtract the divergences a second operator with the following colour structure is required:

$$\mathcal{O}_1 = (\bar{q}_{1\alpha}\Gamma_1\, b_\beta)(\bar{q}_{2\beta}\Gamma_2\, q_{3\alpha}). \tag{2.30}$$

And, likewise, the renormalization of this operator requires the presence of the original one, so that this pair of operators is said to *mix* under renormalization. In general, a set of bare operators $\mathcal{O}_i^{(0)}$ is renormalized by

$$\mathcal{O}_i^{(0)} = Z_{ij}\mathcal{O}_j, \tag{2.31}$$

and mixes as a result. The associated anomalous dimension matrix is given by

$$\hat{\boldsymbol{\gamma}} \equiv \boldsymbol{Z}^{-1}\frac{d}{d\ln\mu}\boldsymbol{Z}. \tag{2.32}$$

The mixed operators can for convenience be transformed back into an unmixed diagonal basis. Either way, after renormalization the Wilson coefficients in the desired basis are extracted by equating the renormalized amplitudes of the effective and full theory calculations.

We are not quite done, however. After renormalizing the QCD corrections we find logarithm terms of the form $\ln M_W^2/\mu^2$ in the Wilson coefficients. For a factorisation scale μ set to a typical meson decay energy of $\mathcal{O}(1\,\mathrm{GeV})$, these logarithms are large and, because they accompany the strong coupling constant $\alpha_s(\mu)$, can ruin the perturbative expansion. The solution is to use the Renormalization Group Equations (RGE) for the Wilson coefficients

$$\frac{d}{d\ln\mu}\boldsymbol{C}(\mu) = \hat{\boldsymbol{\gamma}}^T\boldsymbol{C}(\mu), \tag{2.33}$$

where $\hat{\boldsymbol{\gamma}}$ was given in (2.32) and $\boldsymbol{C}(\mu)$ is a column vector of the Wilson coefficients introduced in (2.28). With this equation in hand we can first evaluate the Wilson

[3]Amplitude calculations can in fact often be simplified by picking an unphysical setup, such as setting all external momenta equal, at the cost of introducing infrared divergences.

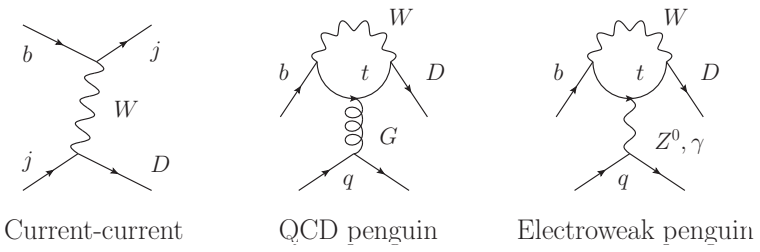

Figure 2.4: Diagrams in the full theory of the Standard Model that result in the equivalently labeled operators in the $\Delta B = 1$ effective Hamiltonian presented in the text. Here $D \in \{d, s\}$ corresponds to $\Delta S = 0$ or $\Delta S = 1$ Hamiltonian, respectively, $j \in \{u, c\}$ and $q \in \{u, d, s, c, b\}$.

coefficients at a high energy scale $\mu = M_W$, at which the troublesome logarithms become small or vanish, and then evolve them down to the lower factorisation scale μ. For example, suppose in renormalizing the effective theory we had kept terms up to order $\alpha_s(\mu) \ln M_W^2/\mu^2$, the so-called *leading log approximation* [35]. Then, at leading order in the anomalous dimension the solution to (2.33) is given by

$$\begin{aligned} \boldsymbol{C}(\mu) &= \left[\frac{\alpha_s(M_W)}{\alpha_s(\mu)}\right]^{\hat{\boldsymbol{\gamma}}^{T(0)}/2\beta_0} \boldsymbol{C}(M_W) \\ &= \left[\frac{1}{1 + \frac{\beta_0}{4\pi}\alpha_s(\mu)\ln(M_W^2/\mu^2)}\right]^{\hat{\boldsymbol{\gamma}}^{T(0)}/2\beta_0} \boldsymbol{C}(M_W). \end{aligned} \tag{2.34}$$

We thus see that solving the RGEs has the effect of resumming terms of the form $(\alpha_s(\mu)\, \ln M_W^2/\mu^2)^n$ to all orders of n. This is called the *renormalization group improved* perturbation theory. Had we kept terms to the next-to-leading-log order, $\alpha_s^2 \ln M_W^2/\mu^2$, then the RGEs would let us resum the terms $\alpha_s(\alpha_s\, \ln M_W^2/\mu^2)^n$ to all order in n, and so on.

We will now give the $\Delta B = 1$ effective Hamiltonian relevant for the Standard Model. We introduce the quark label $D \in \{d, s\}$ to describe both $\Delta S = 0$ and $\Delta S = 1$ transitions, respectively. Along with the W and Z bosons we also integrate out the top quark, which results in penguin operators originating from top quark loops shown in Figure 2.4. The unitarity of the CKM matrix further allows us to express

$$V_{tD}^* V_{tb} = -V_{uD}^* V_{ub} - V_{cD}^* V_{cb}. \tag{2.35}$$

The effective Hamiltonian is then given by

$$\begin{aligned} \mathcal{H}_{\text{eff}} = \frac{G_F}{\sqrt{2}} \sum_{j=u,c} V_{jD}^* V_{jb} \Big[&\sum_{k=1}^{2} C_k(\mu)\mathcal{O}_k^j + \sum_{k=3}^{10} C_k(\mu)\mathcal{O}_k \\ &+ C_{7\gamma}(\mu)\mathcal{O}_{7\gamma} + C_{8g}(\mu)\mathcal{O}_{8g} \Big] + \text{h.c.} \end{aligned} \tag{2.36}$$

We will make use of the notation $(\bar{q}q')_{\mathrm{V}\pm\mathrm{A}} = \bar{q}\gamma_\mu(1\pm\gamma_5)q'$, Greek indices denote colour flow (with summation implied) and $q \in \{u, d, s, c, b\}$. The effective operators $\mathcal{O}$ are then given by [35]:

Current–current

$$\mathcal{O}_1^j = (\overline{D}_\alpha j_\beta)_{\mathrm{V-A}}(\bar{j}_\beta b_\alpha)_{\mathrm{V-A}} \qquad \mathcal{O}_2^j = (\overline{D}_\alpha j_\alpha)_{\mathrm{V-A}}(\bar{j}_\beta b_\beta)_{\mathrm{V-A}}; \tag{2.37}$$

QCD penguin

$$\begin{aligned} \mathcal{O}_3 &= (\overline{D}_\alpha b_\alpha)_{\mathrm{V-A}}\sum_q(\bar{q}_\beta q_\beta)_{\mathrm{V-A}} \qquad \mathcal{O}_4 = (\overline{D}_\alpha b_\beta)_{\mathrm{V-A}}\sum_q(\bar{q}_\beta q_\alpha)_{\mathrm{V-A}} \\ \mathcal{O}_5 &= (\overline{D}_\alpha b_\alpha)_{\mathrm{V-A}}\sum_q(\bar{q}_\beta q_\beta)_{\mathrm{V+A}} \qquad \mathcal{O}_6 = (\overline{D}_\alpha b_\beta)_{\mathrm{V-A}}\sum_q(\bar{q}_\beta q_\alpha)_{\mathrm{V+A}}; \end{aligned} \tag{2.38}$$

Electroweak penguin (e_q is the quark electric charge)

$$\begin{aligned} \mathcal{O}_7 &= \frac{3}{2}(\overline{D}_\alpha b_\alpha)_{\mathrm{V-A}}\sum_q e_q\,(\bar{q}_\beta q_\beta)_{\mathrm{V+A}} \qquad \mathcal{O}_8 = \frac{3}{2}(\overline{D}_\alpha b_\beta)_{\mathrm{V-A}}\sum_q e_q\,(\bar{q}_\beta q_\alpha)_{\mathrm{V+A}} \\ \mathcal{O}_9 &= \frac{3}{2}(\overline{D}_\alpha b_\alpha)_{\mathrm{V-A}}\sum_q e_q\,(\bar{q}_\beta q_\beta)_{\mathrm{V-A}} \qquad \mathcal{O}_{10} = \frac{3}{2}(\overline{D}_\alpha b_\beta)_{\mathrm{V-A}}\sum_q e_q\,(\bar{q}_\beta q_\alpha)_{\mathrm{V-A}}; \end{aligned} \tag{2.39}$$

Magnetic penguin

$$\mathcal{O}_{7\gamma} = \frac{e}{8\pi^2}m_b\overline{D}_\alpha\sigma^{\mu\nu}(1+\gamma_5)b_\alpha F_{\mu\nu} \qquad \mathcal{O}_{8g} = \frac{g_s}{8\pi^2}m_b\overline{D}_\alpha\sigma^{\mu\nu}(1+\gamma_5)t^a_{\alpha\beta}b_\beta G^a_{\mu\nu}. \tag{2.40}$$

At a renormalization scale of $\mu \sim m_b$ the current–current Wilson coefficients are of the order $C_2(m_b) \sim 1$ and $C_1(m_b) \sim 10^{-1}$ when QCD corrections are included. This is as expected, because the operator $\mathcal{O}_1$ requires gluon exchanges to alter the colour flow. The QCD penguin coefficients are suppressed by an additional factor $\alpha_s(m_b)/4\pi$ and therefore take values of the order $C_{3-6} \sim 10^{-2}$. Likewise electroweak penguins are suppressed by a factor $\alpha_{\mathrm{QED}}/4\pi$, and are in general an order of magnitude smaller still. The magnetic penguins contribute in the Standard Model with $C_{7\gamma,8g} \sim 10^{-1}$. We have not included the Standard Model semi-leptonic $\Delta B = 1$ operators above. These will be presented in the context of the decay $B_s \to \mu^+\mu^-$ in Chapter 6.

As a model–independent description of low energy hadronic physics, the OPE lends itself well to studies of New Physics. In this case additional effective operators may need to be introduced that are not present or negligibly small in the Standard Model. A model describing new scalar particles that interact in a flavour changing way with quarks, for example, may require additional $\Delta B = 1$ operators of the form:

$$\mathcal{O}_{\mathrm{SLL}} = (\overline{D}P_L j)(\bar{j}P_L b), \quad \mathcal{O}_{\mathrm{LR}} = (\overline{D}P_L j)(\bar{j}P_R b), \quad \text{etc.} \tag{2.41}$$

In Chapter 6 we will consider such New Physics scalar operators in the context of $\Delta B = 1$ semi-leptonic transitions and $\overline{B}^0_s$–B^0_s mixing.

2.3 Factorising hadronic matrix elements

In the previous section we presented a low energy effective theory as a means to factorise amplitudes involving hadrons into two parts. One part, the Wilson coefficients, describe the short-distance physics above the factorisation scale. And the other part, the hadronic matrix elements, describe the long-distance physics below this scale. At short distances, or equivalently high energies, the strong coupling constant is small and therefore the Wilson coefficients can be determined perturbatively. However, at long distances, or low energies, the strong coupling constant is no longer small, and we can not use perturbation theory in the standard way to compute the hadronic matrix elements. To simplify this problem somewhat we attempt to *factorise* hadronic matrix elements into simpler matrix elements, namely decay constants and form factors [36, 37]. The latter still represent hadronic physics, but are in general universal for the transitions they represent. It is therefore possible to use their experimental determination in one process to make a prediction about another. Alternatively, decay constants and form factors can also be calculated theoretically using tools such as lattice QCD and QCD sum rules. These calculations typically suffer from large theoretical uncertainties, but are steadily improving with time.

The simplest example of factorising a hadronic matrix element into simpler hadronic components is given by purely leptonic meson decays. Because there are no hadrons in the final state and the leptons carry no colour charge, the quark currents in the effective operator can be evaluated between the decaying meson and the vacuum. This defines the meson *decay constants*. For example, the decay constant f_P for a pseudoscalar meson P with momentum p is defined in general with respect to its axial-vector quark current as

$$\langle 0|\bar{q}\gamma_\mu\gamma_5 q'|P(p)\rangle \equiv i f_P\, p_\mu. \tag{2.42}$$

Because the strong force conserves the parity symmetry the vector current vanishes. Contracting the above expression with p and applying the Dirac equation gives

$$\langle 0|\bar{q}\gamma_5 q'|P(p)\rangle = -i\frac{M_P^2}{m_q + m_{q'}} f_P \tag{2.43}$$

for the pseudoscalar current. For scalar mesons parity conservation implies that its decay constant f_S is defined analogously to the pseudoscalar meson but with respect to a vector current, which we will discuss further in Chapter 5. In Chapter 6 we will discuss the purely leptonic decay $B_s \to \mu^+\mu^-$.

Another simple but illustrative example of factorisation is for semi-leptonic meson decays, which lets us introduce the general formalism of *form factors*. Consider, for example, the decay $P \to P'\bar{l}l'$ for two pseudoscalars P and P' with momenta p and p', respectively. The lepton current can be separated from the hadronic transition $P \to P'$, and the hadronic matrix element can be conveniently described in terms of the following

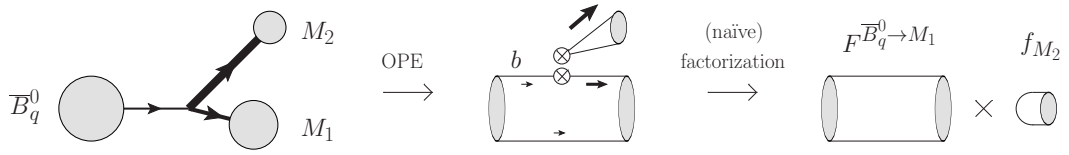

Figure 2.5: Schematic illustration of (naïve) factorization applied to a $\overline{B}_q^0 \to M_1\, M_2$ decay. The arrows show the relative momentum flow, with their size indicating the magnitude.

form factors:

$$\begin{aligned}\langle P'(p')|\bar{q}\gamma_\mu q'|P(p)\rangle = &\left[(p+p')_\mu - \frac{M_P^2 - M_{P'}^2}{k^2}k_\mu\right] F_1^{P\to P'}(k^2) \\ &+ \left[\frac{M_P^2 - M_{P'}^2}{k^2}k_\mu\right] F_0^{P\to P'}(k^2),\end{aligned} \tag{2.44}$$

where $k = p - p'$ is the momentum transfered to the leptons. Analogous expressions holds for a $P \to S$ or $S \to P$ transition mediated by an axial-vector quark current (so that parity is conserved by strong interactions). The expressions for the non-vanishing scalar and pseudoscalar currents $\bar{q}q'$ and $\bar{q}\gamma_5 q'$ can be derived by contracting with q^μ and applying the Dirac equation. A leptonic current of the form $\bar{l}\gamma_\mu(1-\gamma_5)l'$ contracted with the transfered momentum k^μ gives terms proportional to the lepton masses due to the Dirac equation. Therefore, for semi-leptonic decays of the form given in (2.44), the form factor $F_0^{P\to P'}$ will be suppressed relative to $F_1^{P\to P'}$ for small lepton masses, and the latter can then be probed experimentally directly from the decay rate.

Having defined mesonic form factors and decay constants, we can now more precisely present the idea behind factorisation for non-leptonic decays. For concreteness we will consider the pseudoscalar decay $\overline{B}_q^0 \to M_1\, M_2$, where M_1 and M_2 are generic mesons and $q \in \{d, s\}$. Essentially we wish to express the hadronic matrix element for a given operator $\mathcal{O}_i$ as

$$\langle M_1 M_2|\mathcal{O}_i|\overline{B}_q^0\rangle \sim F^{\overline{B}_q^0\to M_1}\, f_{M_2}, \tag{2.45}$$

where $F^{\overline{B}_q^0\to M_1}$ is a form factor for the $\overline{B}_q^0 \to M_1$ transition and f_{M_2} the decay constant of the M_2 meson. The dynamic assumptions leading to factorisation are sketched in Figure 2.5 and can be understood intuitively as follows: the heavy b quark in the $\overline{B}_q^0$ meson decays via a flavour changing process to three lighter quarks, as described by the relevant operator in the effective theory. Two of these quarks, having first arranged themselves in a colour-singlet configuration, move away quickly due to the kinetic energy released from the heavier b quark, and form the meson M_2. The third quark meets up with the spectator quark q of the $\overline{B}_q^0$ meson to form the meson M_1. Because the quarks that form the M_2 meson have managed to spatially separate themselves before the hadronization takes place, soft, long-distance, interactions between the two hadronization processes are assumed to be negligible. This leads to so-called *naïve factorisation*, which assumes

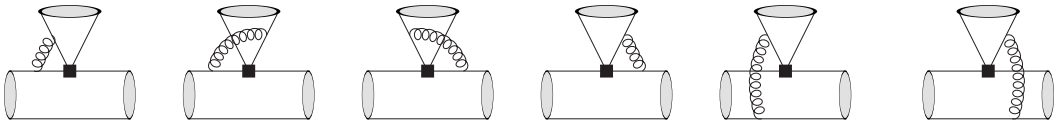

Figure 2.6: Diagrams that are considered *non-factorisable* in *naïve factorisation*. In the *QCD factorisation* formalism hard gluon corrections of this type can be calculated and soft gluon exchanges are shown to be suppressed by a power of $\Lambda_{\rm QCD}/m_b$.

that both soft and hard gluon exchanges between the quarks that form M_2 and the quarks of the $\overline{B}{}^0_q \to M_1$ system may be ignored [36, 37]. In Figure 2.6 we show such gluon exchange processes, which represent *non-factorisable* corrections to naïve factorisation. Later in this section we will present a formalism that extends and strengthens this assumption.

There are of course some caveats to this intuitive picture (for a detailed discussion see Ref. [38] and references therein). Firstly, let us note that the b quark is considered to be a *heavy* quark, and combined with a light quark q the $\overline{B}{}^0_q$ is labeled a *heavy meson*. The charm quark is also relatively heavy, and thus combinations of charm quarks with light quarks (D mesons) are labeled heavy mesons too. Somewhat surprisingly, as we will come back to later, is that $\bar{c}c$ bound states (charmonium mesons) are not considered to be heavy mesons in this context.

With the above definitions in place we can consider what happens if M_1 or M_2 is a heavy meson. The case of M_1 being heavy and M_2 light, most closely fits the intuitive picture sketched above. In this case the third quark from the b quark decay will not carry too much kinetic energy and can easily meet up with the slow spectator quark in order to hadronize. If, however, M_1 is also light, then the third quark will be travelling much faster than the spectator quark. In this case a hard gluon interaction with another quark in the game is needed to allow them to meet up, which suppresses the likelihood of this process. Finally, if the M_2 meson is heavy the idea of factorisation is no longer valid. This is because we can no longer assume that the two quarks that will hadronize to give M_2 have first travelled sufficiently far away for soft interactions with the $\overline{B}{}^0_q \to M_1$ hadronic transition to be negligible.

In Section 2.2 we saw how the renormalization of QCD corrections to the effective operators led them to mix. An operator that has the wrong colour flow to contribute to a decay process can exchange a hard gluon (i.e. with a transition energy greater than the factorisation scale μ) to remedy this. Therefore effective operators with a specific Dirac matrix structure, $\{\Gamma_1, \Gamma_2\}$ typically contribute to an amplitude in pairs. Let us

consider a generic pair of operators[4]

$$\begin{aligned}\mathcal{O}_1 &= (\bar{q}_{1\alpha}\Gamma_1\, b_\beta)(\bar{q}_{2\beta}\Gamma_2\, q_{3\alpha}),\\ \mathcal{O}_2 &= (\bar{q}_{1\alpha}\Gamma_1\, b_\alpha)(\bar{q}_{2\beta}\Gamma_2\, q_{3\beta}),\end{aligned} \tag{2.46}$$

where Greek indices denote colour. Because mesons are colour-singlet states, it is necessary for the quark currents involved in the separate hadronizations to be in colour-singlet states in order for factorisation to make sense. Therefore for some processes we need to Fierz rearrange the above operators to get

$$\begin{aligned}\tilde{\mathcal{O}}_1 &= (\bar{q}_{2\alpha}\tilde{\Gamma}_1\, b_\alpha)(\bar{q}_{1\beta}\tilde{\Gamma}_2\, q_{3\beta}),\\ \tilde{\mathcal{O}}_2 &= (\bar{q}_{2\beta}\tilde{\Gamma}_1\, b_\alpha)(\bar{q}_{1\alpha}\tilde{\Gamma}_2\, q_{3\beta}),\end{aligned} \tag{2.47}$$

where the Dirac matrix structure $\{\tilde{\Gamma}_1, \tilde{\Gamma}_2\}$ is in principle different. Factorisation for the colour-singlet combinations can now be defined as

$$\langle M_1 M_2|\tilde{\mathcal{O}}_1|\overline{B}_q^0\rangle_F \equiv \langle M_1|(\bar{q}_2\tilde{\Gamma}_1\, b)|\overline{B}_q^0\rangle\langle M_2|(\bar{q}_1\tilde{\Gamma}_2\, q_3)|0\rangle, \tag{2.48}$$

$$\langle M_1 M_2|\mathcal{O}_2|\overline{B}_q^0\rangle_F \equiv \langle M_1|(\bar{q}_1\Gamma_1\, b)|\overline{B}_q^0\rangle\langle M_2|(\bar{q}_2\Gamma_2\, q_3)|0\rangle, \tag{2.49}$$

either of which may vanish depending on the process in question.

For definiteness let us consider the effective operators in (2.46) with $\Gamma_1 = \gamma_\mu(1-\gamma_5)$ and $\Gamma_2 = \gamma^\mu(1-\gamma_5)$, which is commonly denoted as $(\bar{q}_1\, b)_{V-A}(\bar{q}_2\, q_3)_{V-A}$. Furthermore, let us assume that a matching of the above operators to the full theory at tree-level results in the Wilson coefficients $C_2 = 1$ and $C_1 = 0$, as is the case in the Standard Model. In other words, the operator $\mathcal{O}_1$ describes QCD corrections to $\mathcal{O}_2$. We will now give the different possible factorised amplitudes based on the classification introduced in Ref. [39].

A so-called Class I decay is an initial–final state configuration for which only

$$\langle M_1 M_2|\mathcal{O}_2|\overline{B}_q^0\rangle_F$$

is non-vanishing in the absence of QCD corrections. An example of such a process is given in the top row of Figure 2.7. In order to express the amplitude purely in terms of $\mathcal{O}_2$ we can make use of the $SU(3)$ relation

$$\delta_{\alpha\delta}\delta_{\beta\gamma} = \frac{1}{N}\delta_{\alpha\beta}\delta_{\gamma\delta} + 2\, t^a_{\alpha\beta}t^a_{\gamma\delta}, \tag{2.50}$$

for the colour indices to write

$$C_1\mathcal{O}_1 + C_2\mathcal{O}_2 = \left(C_2 + \frac{1}{N}C_1\right)\mathcal{O}_2 + 2\, C_1\mathcal{O}^8, \tag{2.51}$$

[4]We choose the labels "1" and "2" so that we can later relate them to the current-current operators defined in (2.36).

where N is the number of colours and

$$\mathcal{O}^8 \equiv (\bar{q}_1 t^a \Gamma_1 \, b)(\bar{q}_2 t^a \Gamma_2 \, q_3). \tag{2.52}$$

In factorisation the two separate currents give colour-singlets. If there is no gluon exchange to alter the existing colour structure, the key assumption of naïve factorisation, then the resulting trace over the colour generators will cause the matrix element of this octet operator to vanish. In naïve factorisation we are then left with the Class I amplitude

$$\langle M_1 M_2 | H_{\text{eff}} | \overline{B}^0_q \rangle_I = \frac{G_f}{\sqrt{2}} K_{\text{CKM}} a_1(\mu) \langle M_1 M_2 | \mathcal{O}_2 | \overline{B}^0_q \rangle_F \tag{2.53}$$

where K_{CKM} represents the relevant CKM matrix terms and

$$a_1(\mu) \equiv C_2(\mu) + \frac{1}{N} C_1(\mu). \tag{2.54}$$

A Class II decay is defined as the contrary situation where only $\langle M_1 M_2 | \tilde{\mathcal{O}}_1 | \overline{B}^0_q \rangle_F$ is non-vanishing when QCD correctons are absent. See the bottom row of Figure 2.7 for an example of such a process. Following similar steps as before we find

$$\langle M_1 M_2 | H_{\text{eff}} | \overline{B}^0_q \rangle_{II} = \frac{G_f}{\sqrt{2}} K_{\text{CKM}} a_2(\mu) \langle M_1 M_2 | \tilde{\mathcal{O}}_1 | \overline{B}^0_q \rangle_F \tag{2.55}$$

with

$$a_2(\mu) \equiv C_1(\mu) + \frac{1}{N} C_2(\mu). \tag{2.56}$$

Finally, we have a Class III decay when both matrix elements are non-vanishing and $a_1(\mu)$ and $a_2(\mu)$ interfere.

At a scale μ where the QCD corrections are small it follows that $a_1(\mu) \sim 1$ and $a_2(\mu) \sim 1/N$ i.e. Class II decay amplitudes are suppressed by the number of colours $N = 3$. Therefore Class I decays are said to be *colour-allowed* and Class II decays *colour-suppressed*. This can be intuitively seen in Figure 2.7, where we show the tree level Feynman diagrams corresponding to colour-allowed and colour-suppressed amplitudes in the full and effective theories. In colour-allowed amplitudes colour can be summed over individually for the two final state mesons, whereas in the colour-suppressed decay there is only one colour sum. In the Standard Model an example of a Class I (colour-allowed) decay is $\overline{B}^0_d \to D^+ \pi^-$, a Class II (colour-suppressed) decay is $\overline{B}^0_d \to \bar{K}^0 J/\psi$, and of a Class III decay is $B^- \to D^0 K^-$ [40].

The last step in naïve factorisation is to substitute the form factors and decay constants into the factorised matrix elements $\langle \mathcal{O}_2 \rangle_F$ or $\langle \tilde{\mathcal{O}}_1 \rangle_F$. For example, consider a decay to two pseudoscalars, $\overline{B}^0_q \to P_1 P_2$, that proceeds via a tree-level colour-allowed amplitude (top diagrams in Figure 2.7). Plugging the form factor and decay constant definitions of (2.44) and (2.42), respectively, into the factorised matrix element expression given in (2.49), the amplitude of this decay is given by

$$\langle P_1 P_2 | H_{\text{eff}} | \overline{B}^0_q \rangle = i \frac{G_F}{\sqrt{2}} K_{\text{CKM}} a_1(\mu) \, f_{P_2} \, F_0^{\overline{B}^0_q \to P_1}(M^2_{P_2}) \left(M^2_{B_q} - M^2_{P_1} \right). \tag{2.57}$$

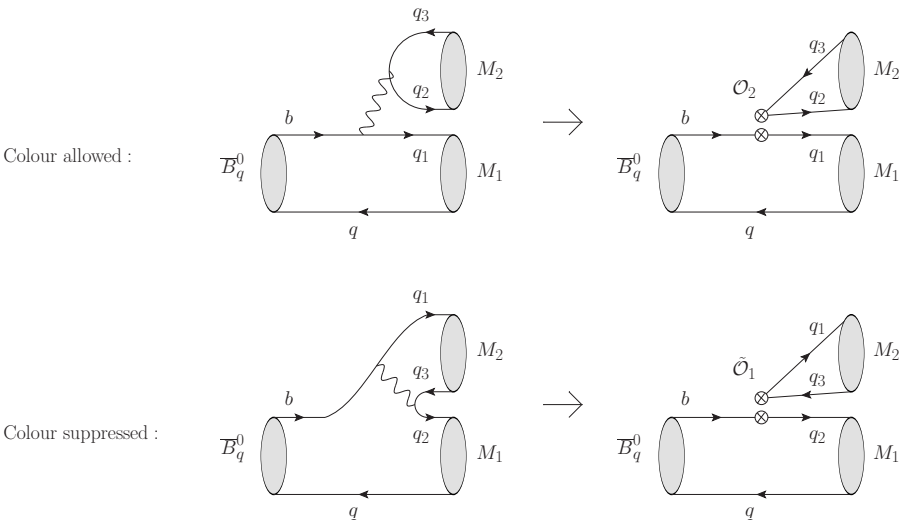

Figure 2.7: Colour allowed (Class I) and colour suppressed (Class II) non-leptonic meson decays in the full theory of the Standard Model (left) and in terms of the effective theory's OPE at zeroth order in QCD (right). For the latter decay the effective operators $\mathcal{O}_i$ have been Fierz rearranged into $\tilde{\mathcal{O}}_i$ in preparation for *factorisation* as discussed in the text.

We have thus succeeded to factorise the amplitude into a theoretically computable term $a_1(\mu)$ describing the short distance behaviour, and the form factors and decay constants describing the long distance behaviour. These form factors and decay constants are universal in the sense that they also enter semi-leptonic and fully leptonic decays as discussed earlier. Therefore, besides from being theoretically computable, they can in principle also be determined experimentally from such processes.

Closer inspection of (2.57), however, reveals a problem with the factorisation approach we have taken so far. Namely, the dependence of the hadronic matrix element on the renormalization scale μ has disappeared. Consequently, the dependence of the Wilson coefficients on μ, described by $a_1(\mu)$, no longer cancels and the amplitude becomes dependent on this unphysical scale. Nonetheless, for any given process there may be a particular factorisation scale at which naïve factorisation works well. Attempts to properly determine this scale are known as *generalized factorisation* [41, 42]. They involve introducing additional parameters, representing non-factorisable corrections, that exactly cancel the μ dependence in $a_{1,2}(\mu)$, leaving μ-independent coefficients $a_{1,2}^{\text{eff}}$. The idea is that these parameters can be determined by experiment at some scale μ, and then evolved to their vanishing point using the renormalization group equations. The scale at which they vanish is then the optimal factorisation scale for the process under consideration. The problem with this approach, however, is that it cannot account for the renormalization scheme used to compute the Wilson coefficients [43]. Thus the factorisation scale deduced is scheme dependent and thereby still unphysical.

There have been several attempts to go beyond generalized factorisation. A notable

example is *perturbative QCD* (PQCD) [44, 45, 46], which, contrary to the factorisation picture defined above, separates the hard and soft components of a non-leptonic decay by absorbing the latter into hadronic wave functions to be determined experimentally. Most interesting for the present discussion, however, is *QCD factorisation* (QCDF) [38, 47, 48], which gives a formal description of the intuitive heavy b quark picture we sketched earlier and reduces to naïve factorisation at leading order. Note that the terms "pertubative QCD" and "QCD factorization" have broader or different meanings in QCD outside the current context of hadronic matrix elements for beauty mesons.

QCD factorisation is formulated in the *heavy quark limit* i.e. it assumes $m_b \gg \Lambda_{\rm QCD}$ and treats $\Lambda_{\rm QCD}/m_b$ as an expansion parameter. At leading order in the $\Lambda_{\rm QCD}/m_b$ expansion the hadronic matrix element for a given operator $\mathcal{O}_i$ is given by

$$\begin{aligned}\langle M_1 M_2|\mathcal{O}_i(\mu)|\overline{B}_q^0\rangle = &\sum_j F_j^{\overline{B}_q^0\to M_1}(M_{M_2}^2)\, T_{ij}^I(\mu) * f_{M_2}\Phi_{M_2}(\mu) + \ (M_1 \leftrightarrow M_2) \\ &+ \ T_i^{II}(\mu) * f_{B_q}\Phi_{B_q}(\mu) * f_{M_1}\Phi_{M_1}(\mu) * f_{M_2}\Phi_{M_2}(\mu). \end{aligned} \tag{2.58}$$

For heavy-light final states, as opposed to light-light final states, the last term on the right receives a relative $\Lambda_{\rm QCD}/m_b$ power suppression and can be ignored (and also the second interchanged term is irrelevant). Here the Φ_M are light-cone distribution amplitudes, which parameterise the probability of a meson to hadronize for a given momentum fraction of the constituent quarks. The $T^{I,II}$ are hard-scattering functions, which also depend on the aforementioned momentum fractions, and parameterise the hard gluon exchanges between the interacting quarks. A star is used to denote an integration over the relevant momentum fractions. The dependence of Φ_M and $T^{I,II}$ on the renormalization scale μ and renormalization scheme is precisely canceled by that of the Wilson coefficients. QCDF therefore accomplishes the goal of generalized factorisation by allowing us to replace $a_i(\mu) \to a_i^{\rm eff}$ as in (2.53) or (2.55), and subsequently compute these coefficients systematically beyond leading order in α_s.

The most powerful result of QCDF is that the soft non-factorisable corrections from Figure 2.6 only contribute at the next power in the $\Lambda_{\rm QCD}/m_b$ expansion. In addition, the hard non-factorisable corrections are described by the hard-scattering functions and can be computed perturbatively in this framework, appearing from $\mathcal{O}(\alpha_s)$ onwards. This also means non-factorisable effective operator configurations that create a quark pair in a non-colour-singlet configuration are consistently included in QCDF at NLO. An important consequence of QCDF is that at leading order in $\Lambda_{\rm QCD}/m_b \sim 5\%$ and α_s it gives naïve factorisation:

$$\langle M_1 M_2|\mathcal{O}_i|\overline{B}_q^0\rangle = \langle M_1 M_2|\mathcal{O}_i|\overline{B}_q^0\rangle\Big|_{\text{naive fact.}} \times \left[1 + \mathcal{O}(\alpha_s) + \mathcal{O}\left(\frac{\Lambda_{\rm QCD}}{m_b}\right)\right]. \tag{2.59}$$

QCDF makes our earlier statement regarding light-heavy final states, where the meson M_2 that flies off is heavy, more precise. Specifically, it follows from QCDF that soft non-factorisable corrections in this case are not power suppressed in $\Lambda_{\rm QCD}/m_b$ i.e.

they enter at $\mathcal{O}(1)$. If, instead, the M_2 meson is a $c\bar{c}$ charmonium state and c is treated as a heavy quark, $m_c \sim m_b$, the soft corrections are power-suppressed, though only by a factor $\Lambda_{\rm QCD}/(m_b\alpha_s)$. In practice the charm quark, being both almost heavy and almost light, requires special care in QCDF.

In QCDF the imaginary part of an amplitude is also suppressed either by $\mathcal{O}(\alpha_s)$ in the hard-scattering case or $\Lambda_{\rm QCD}/m_b$ for soft corrections. It therefore follows that in general CP-conserving strong phases are small. Exceptions to this rules occur when also the real part is suppressed by some other mechanism. For example, in the Class II decays introduced earlier the leading-order diagrams are colour suppressed, which can lead to sizable strong phases for such decays. Also CKM suppression or small Wilson coefficients can enhance strong phases, though this is seldom the case in B_q decays.

2.4 Flavour symmetries

In the previous section we discussed how the amplitudes of B_q meson decays can be factorized into two parts: one describing the short-distance physics and the other the long-distance hadronic physics. In particular the latter part can be notoriously difficult to compute theoretically, and current attempts to do so with lattice QCD or QCD sum rules still come with sizable theoretical errors. In this section we will discuss an alternative approach to deal with the hadronic nature of this physics that takes advantage of the approximate symmetries between quarks of different flavours in QCD. These will allow us to relate together hadronic matrix elements from different decay processes. In some cases this lets us factor them out of the relevant observables completely, and in others we may constrain them using experimentally available data.

Let us consider the QCD Lagrangian with N flavours of massless quarks

$$\mathcal{L} = i\sum_j^N \overline{q_{L,j}} \not{D}\, q_{L,j} + i\sum_i^N \overline{q_{R,j}} \not{D}\, q_{R,j} - \frac{1}{4} G^{a\,\mu\nu} G^a_{\mu\nu} \tag{2.60}$$

where D_μ is the standard covariant derivative of $SU(3)_C$ and $G^a_{\mu\nu}$ the gluon field strength tensor. This Lagrangian has a global $U(N)_L \times U(N)_R$ chiral symmetry transforming as

$$q_{L,i} \to (U_L)_{ij}\; q_{L,j} = \exp\left(-i\theta^a_L t^a_{ij} - i\theta_L \delta_{ij}\right) q_{L,j} \tag{2.61}$$

$$q_{R,i} \to (U_R)_{ij}\; q_{R,j} = \exp\left(-i\theta^a_R t^a_{ij} - i\theta_R \delta_{ij}\right) q_{R,j} \tag{2.62}$$

with $\boldsymbol{t}^a$ the N^2-1 generators of $SU(N)$. For clarity we will use latin indices or a bold font to denote the flavour vector space. The $2N^2$ conserved currents associated with this symmetry can be expressed as [49]

$$V^{\mu,a} = \bar{\boldsymbol{q}}_{\boldsymbol{L}}\gamma^\mu \boldsymbol{t}^a \boldsymbol{q}_{\boldsymbol{L}} + \bar{\boldsymbol{q}}_{\boldsymbol{R}}\gamma^\mu \boldsymbol{t}^a \boldsymbol{q}_{\boldsymbol{R}} = \bar{\boldsymbol{q}}\gamma^\mu \boldsymbol{t}^a \boldsymbol{q}, \tag{2.63}$$

$$A^{\mu,a} = \bar{\boldsymbol{q}}_{\boldsymbol{L}}\gamma^\mu \boldsymbol{t}^a \boldsymbol{q}_{\boldsymbol{L}} - \bar{\boldsymbol{q}}_{\boldsymbol{R}}\gamma^\mu \boldsymbol{t}^a \boldsymbol{q}_{\boldsymbol{R}} = \bar{\boldsymbol{q}}\gamma^\mu\gamma_5 \boldsymbol{t}^a \boldsymbol{q}, \tag{2.64}$$

$$V^{\mu} = \bar{\boldsymbol{q}}_{\boldsymbol{L}}\gamma^\mu \boldsymbol{q}_{\boldsymbol{L}} + \bar{\boldsymbol{q}}_{\boldsymbol{R}}\gamma^\mu \boldsymbol{q}_{\boldsymbol{R}} = \bar{\boldsymbol{q}}\gamma^\mu \boldsymbol{q}, \tag{2.65}$$

$$A^{\mu} = \bar{\boldsymbol{q}}_{\boldsymbol{L}}\gamma^\mu \boldsymbol{q}_{\boldsymbol{L}} - \bar{\boldsymbol{q}}_{\boldsymbol{R}}\gamma^\mu \boldsymbol{q}_{\boldsymbol{R}} = \bar{\boldsymbol{q}}\gamma^\mu\gamma_5 \boldsymbol{q}, \tag{2.66}$$

where V and A denote vector and axial-vector currents respectively. We note, however, that the singlet axial vector current $U(1)_A$ is only conserved classically. After quantization it picks up an anomaly [50]:

$$\partial_\mu A^\mu = \frac{N\, g_s^2}{3\pi}\epsilon_{\mu\nu\rho\sigma}G_a^{\mu\nu}G_a^{\rho\sigma}. \tag{2.67}$$

Of course, as presented in (2.12), quarks are not massless. However, if we add a diagonal mass term to the QCD Lagrangian of the form

$$\mathcal{L}_M = -\bar{\boldsymbol{q}}\,\boldsymbol{M}\,\boldsymbol{q} = -\bar{\boldsymbol{q}}_{\boldsymbol{R}}\,\boldsymbol{M}\,\boldsymbol{q}_{\boldsymbol{L}} - \bar{\boldsymbol{q}}_{\boldsymbol{L}}\,\boldsymbol{M}\,\boldsymbol{q}_{\boldsymbol{R}}, \tag{2.68}$$

then we find that it mixes the left and right handed fields, and thereby explicitly breaks the chiral symmetry. Specifically, the currents listed in (2.66) then have the following divergences [49]:

$$\partial_\mu V^{\mu,a} = i\bar{\boldsymbol{q}}[\boldsymbol{M},\boldsymbol{t}^a]\boldsymbol{q}, \tag{2.69}$$
$$\partial_\mu A^{\mu,a} = i\bar{\boldsymbol{q}}\{\boldsymbol{M},\boldsymbol{t}^a\}\boldsymbol{q}, \tag{2.70}$$
$$\partial_\mu V^{\mu} = 0, \tag{2.71}$$
$$\partial_\mu A^{\mu} = 2\,i\bar{\boldsymbol{q}}\boldsymbol{M}\gamma_5\boldsymbol{q} + \frac{N\, g_s^2}{3\pi}\epsilon_{\mu\nu\rho\sigma}G_a^{\mu\nu}G_a^{\rho\sigma}. \tag{2.72}$$

We see that the mass term breaks the axial vector currents. The vector currents $V^{\mu,a}$ on the other hand can remain conserved if the masses of the quarks are degenerate i.e. if $\boldsymbol{M} \propto \boldsymbol{1}$ so that $[\boldsymbol{M},\boldsymbol{t}^a] = 0$. Only the singlet vector current remains conserved regardless of the quark masses introduced.

Assuming that the three lightest quarks are degenerate in mass gives the $SU(3)_{\mathrm{F}} \equiv SU(3)_V$ flavour symmetry of Gell-Mann and Ne'eman [51, 52]. At an energy scale of 1 GeV, which is much larger than the three light quark masses, the $SU(3)$ axial vector current could be expected to be approximately conserved. However, if it were, we would expect to see *parity doubling*. Namely, if both Q_V^a and Q_A^a commute with the QCD Hamiltonian, then the fact that Q_A^a has negative parity means we would expect a negative parity state for every positive parity one. But we do not observe a negative parity baryon octet for example. The absence of approximately conserved $A^{\mu,a}$ axial vector currents can be explained by the spontaneous breaking of $SU(3)_L \times SU(3)_R \to SU(3)_V$. The presence of a scalar quark condensate is sufficient for this symmetry breaking to take place [49]. The pseudo-Goldstone bosons that result from the eight broken axial vector generators give the eight pseudoscalar mesons $\pi^\pm, \pi^0, K^\pm, K^0, \bar{K}^0, \eta$.

We may also assume $m_u = m_d$, $m_d = m_s$ and $m_u = m_s$ on an individual basis, which give the $SU(2)$ flavour symmetries known as *isospin*, *U-spin* and *V-spin*, respectively. These three symmetries are subgroups of $SU(3)_{\mathrm{F}}$. To see this explicitly, consider $\boldsymbol{q} \equiv (u\ d\ s)^T$ transforming under the fundamental representation of $SU(3)_{\mathrm{F}}$. In this representation the $SU(3)$ generators can be described in terms of the Gell-Mann matrices

$\boldsymbol{t}^a = \boldsymbol{\lambda}_a/2$, where

$$\boldsymbol{\lambda}_1 = \begin{pmatrix} 0 & 1 & 0 \\ 1 & 0 & 0 \\ 0 & 0 & 0 \end{pmatrix} \qquad \boldsymbol{\lambda}_2 = \begin{pmatrix} 0 & -i & 0 \\ i & 0 & 0 \\ 0 & 0 & 0 \end{pmatrix} \qquad \boldsymbol{\lambda}_3 = \begin{pmatrix} 1 & 0 & 0 \\ 0 & -1 & 0 \\ 0 & 0 & 0 \end{pmatrix}$$
$$\boldsymbol{\lambda}_4 = \begin{pmatrix} 0 & 0 & 1 \\ 0 & 0 & 0 \\ 1 & 0 & 0 \end{pmatrix} \qquad \boldsymbol{\lambda}_5 = \begin{pmatrix} 0 & 0 & -i \\ 0 & 0 & 0 \\ i & 0 & 0 \end{pmatrix} \qquad \boldsymbol{\lambda}_6 = \begin{pmatrix} 0 & 0 & 0 \\ 0 & 0 & 1 \\ 0 & 1 & 0 \end{pmatrix}$$
$$\boldsymbol{\lambda}_7 = \begin{pmatrix} 0 & 0 & 0 \\ 0 & 0 & -i \\ 0 & i & 0 \end{pmatrix} \qquad \boldsymbol{\lambda}_8 = \frac{1}{\sqrt{3}} \begin{pmatrix} 1 & 0 & 0 \\ 0 & 1 & 0 \\ 0 & 0 & -2 \end{pmatrix}. \tag{2.73}$$

By defining

$$\begin{aligned} \boldsymbol{I}_1 &\equiv \boldsymbol{t}^1, & \boldsymbol{I}_2 &\equiv \boldsymbol{t}^2, & \boldsymbol{I}_3 &\equiv \boldsymbol{t}^3, \\ \boldsymbol{V}_1 &\equiv \boldsymbol{t}^4, & \boldsymbol{V}_2 &\equiv \boldsymbol{t}^5, & \boldsymbol{V}_3 &\equiv \frac{1}{2}\left(\sqrt{3}\,\boldsymbol{t}^8 + \boldsymbol{t}^3\right), \\ \boldsymbol{U}_1 &\equiv \boldsymbol{t}^6, & \boldsymbol{U}_2 &\equiv \boldsymbol{t}^7, & \boldsymbol{U}_3 &\equiv \frac{1}{2}\left(\sqrt{3}\,\boldsymbol{t}^8 - \boldsymbol{t}^3\right), \end{aligned} \tag{2.74}$$

we see that

$$[\boldsymbol{I}_i, \boldsymbol{I}_j] = i\,\varepsilon_{ijk}\boldsymbol{I}_k, \qquad [\boldsymbol{U}_i, \boldsymbol{U}_j] = i\,\varepsilon_{ijk}\boldsymbol{U}_k, \qquad [\boldsymbol{V}_i, \boldsymbol{V}_j] = i\,\varepsilon_{ijk}\boldsymbol{V}_k, \tag{2.75}$$

and thus recover the isospin, U-spin and V-spin $SU(2)$ subgroups, which rotate the pairs of quarks (u, d), (d, s) and (u, s), respectively.

To illustrate how flavour symmetries can be a useful tool for analysing meson decays, let us consider an example involving isospin symmetry. Specifically, we can use isospin symmetry to derive a relation between the transition amplitudes of the decays $B_d^0 \to \pi^+\pi^-$, $B_u^+ \to \pi^+\pi^0$ and $B_d^0 \to \pi^0\pi^0$. Such a relation is used for example in the Gronau–London method [53] to control penguin contributions to the decay $B_d \to \pi^+\pi^-$, and thereby extract the CP angle α from its time-dependent analysis, but we will not discuss this further. In Chapter 4 we will present an alternative strategy for extracting the CP violating angle γ from this decay mode using its U-spin symmetry relation to $B_s \to K^+K^-$.

Under the $SU(2)$ isospin symmetry the mesons $B_d^0 \equiv \bar{b}d$ and $B_u^+ \equiv \bar{b}u$ transform as an isodoublet $(B_u^+ \; B_d^0)^T$, and the pions $\pi^+ \equiv u\bar{d}$, $\pi^0 \equiv \frac{1}{\sqrt{2}}(d\bar{d} - u\bar{u})$ and $\pi^- \equiv -d\bar{u}$ as an isotriplet $(\pi^+ \; \pi^0 \; \pi^-)^T$. The two pion final states of the decays in question are therefore described by the isospin tensor product $1 \otimes 1$, and decompose to

$$\begin{aligned} \langle\pi^+\pi^-| &= \sqrt{\frac{1}{3}}\langle 2,0| + \sqrt{\frac{2}{3}}\langle 0,0|, \\ \langle\pi^0\pi^0| &= \sqrt{\frac{2}{3}}\langle 2,0| - \sqrt{\frac{1}{3}}\langle 0,0|, \\ \langle\pi^+\pi^-| &= \langle 2,1|. \end{aligned} \tag{2.76}$$

Given the initial isospin states $|B_d^0\rangle = |\frac{1}{2}, -\frac{1}{2}\rangle$ and $|B_u^+\rangle = |\frac{1}{2}, \frac{1}{2}\rangle$, the contributing transition matrix elements must involve a change of isospin of either $\Delta I = \frac{1}{2}$, $\Delta I = \frac{3}{2}$ or $\Delta I = \frac{5}{2}$. We may thus express the effective Hamiltonian in terms of the following components:

$$\mathcal{H}_{\text{eff}} = \mathcal{H}_{\text{eff}}^{\frac{1}{2}} \oplus \mathcal{H}_{\text{eff}}^{\frac{3}{2}} \oplus \mathcal{H}_{\text{eff}}^{\frac{5}{2}}, \tag{2.77}$$

where the superscript denotes the change in isospin.

To limit the number of distinct amplitudes we end up with, we can use the Wigner-Eckart theorem to express the amplitudes in terms of *reduced matrix elements*, which have no orientation in isospin space. Specifically, the Wigner-Eckart theorem states that

$$\langle J, M|\mathcal{H}_{\text{eff}}^{j_2,m_2}|j_1, m_1\rangle = C_{j_1\, j_2}(J\, M; m_1\, m_2)\langle J||\mathcal{H}_{\text{eff}}^{j_2}||j_1\rangle, \tag{2.78}$$

where $C_{j_1\, j_2}(J\, M; m_1\, m_2)$ is a Clebsch–Gordon coefficient and $\langle J||\mathcal{H}^{(j_2)}||j_1\rangle$ a reduced matrix element. As a result, we can express the three decay amplitudes in terms of three distinct reduced matrix elements:

$$\begin{aligned}
\langle\pi^+\pi^-|\mathcal{H}_{\text{eff}}|B_d^0\rangle &= -\sqrt{\frac{1}{3}}\Big\langle 0\Big|\Big|\mathcal{H}_{\text{eff}}^{\frac{1}{2}}\Big|\Big|\frac{1}{2}\Big\rangle + \sqrt{\frac{1}{6}}\Big\langle 2\Big|\Big|\mathcal{H}_{\text{eff}}^{\frac{3}{2}}\Big|\Big|\frac{1}{2}\Big\rangle - \sqrt{\frac{1}{6}}\Big\langle 2\Big|\Big|\mathcal{H}_{\text{eff}}^{\frac{5}{2}}\Big|\Big|\frac{1}{2}\Big\rangle,\\
\langle\pi^0\pi^0|\mathcal{H}_{\text{eff}}|B_d^0\rangle &= \sqrt{\frac{1}{6}}\Big\langle 0\Big|\Big|\mathcal{H}_{\text{eff}}^{\frac{1}{2}}\Big|\Big|\frac{1}{2}\Big\rangle + \sqrt{\frac{1}{3}}\Big\langle 2\Big|\Big|\mathcal{H}_{\text{eff}}^{\frac{3}{2}}\Big|\Big|\frac{1}{2}\Big\rangle - \sqrt{\frac{1}{3}}\Big\langle 2\Big|\Big|\mathcal{H}_{\text{eff}}^{\frac{5}{2}}\Big|\Big|\frac{1}{2}\Big\rangle,\\
\langle\pi^+\pi^0|\mathcal{H}_{\text{eff}}|B_u^+\rangle &= \sqrt{\frac{3}{4}}\Big\langle 2\Big|\Big|\mathcal{H}_{\text{eff}}^{\frac{3}{2}}\Big|\Big|\frac{1}{2}\Big\rangle + \sqrt{\frac{1}{3}}\Big\langle 2\Big|\Big|\mathcal{H}_{\text{eff}}^{\frac{5}{2}}\Big|\Big|\frac{1}{2}\Big\rangle.
\end{aligned} \tag{2.79}$$

Of the reduced matrix elements, the $\Delta I = \frac{1}{2}$ and $\Delta I = \frac{3}{2}$ transitions receive contributions from short-distance physics [54]. Namely, the current–current and electroweak penguin operators of the low-energy effective theory (see Section 2.2) contribute to both, whereas QCD penguins contribute only to $\Delta I = \frac{1}{2}$ transitions. The $\Delta I = \frac{5}{2}$ transitions on the other hand are only generated in the Standard Model by long-distance electromagnetic rescattering effects [55]. They are hereby effectively suppressed by a factor α_{QED} with respect to the $\Delta I = \frac{1}{2}$ transition and can be neglected to this order. The remaining two reduced matrix elements in (2.79) then allow us to write the following amplitude relation in the limit of isospin symmetry:

$$\langle\pi^+\pi^-|\mathcal{H}_{\text{eff}}|B_d^0\rangle + \sqrt{2}\,\langle\pi^0\pi^0|\mathcal{H}_{\text{eff}}|B_d^0\rangle - \sqrt{2}\,\langle\pi^+\pi^0|\mathcal{H}_{\text{eff}}|B_u^+\rangle = 0. \tag{2.80}$$

It is similarly possible to derive amplitude relations assuming an exact $SU(3)_{\text{F}}$ flavour symmetry e.g. for the triplet $(B_u^+\ B_d^0\ B_s^0)^T$ transforming under the fundamental representation [56, 57]. However, an $SU(3)_F$ decomposition of a decay amplitude typically involves many more reduced matrix elements, which complicates the construction and usefulness of the resulting amplitude relations. Because the reduced matrix elements can receive contributions from various decay topologies, it is in general difficult to neglect specific ones on dynamical grounds in order to simplify the amplitude relations. Therefore a better basis is offered by the decay topologies themselves, which can be straightforwardly mapped to the reduced matrix elements [56, 58, 59].

For the $\Delta S = 0$ $B \to \pi\pi$ transitions considered above, a simplified topology basis is given by: T (colour-allowed tree), C (colour-suppressed tree), P (penguin), E (exchange) and PA (penguin annihilation). Using this basis we find that [58]

$$\langle \pi^+\pi^-|\mathcal{H}_{\text{eff}}|B_d^0\rangle = -(T + P + E + PA), \tag{2.81}$$

$$\langle \pi^0\pi^0|\mathcal{H}_{\text{eff}}|B_d^0\rangle = \frac{1}{\sqrt{2}}\left(-C + P + E + PA\right), \tag{2.82}$$

$$\langle \pi^+\pi^0|\mathcal{H}_{\text{eff}}|B_u^+\rangle = -\frac{1}{\sqrt{2}}(C + T), \tag{2.83}$$

which indeed also satisfies the amplitude relation given in (2.80):

$$-(T + P + E + PA) + (-C + P + E + PA) + (C + T) = 0. \tag{2.84}$$

Note that the amplitudes written in this way include CKM factors.

The topology basis for $\Delta S = 1$ transition can be defined analagously to the $\Delta S = 0$ basis above, and distinguished with a prime. For example, by making the $SU(3)_{\text{F}}$ decomposition [58]

$$\langle \pi^-K^+|\mathcal{H}_{\text{eff}}|B_d^0\rangle = -(T' + P'), \tag{2.85}$$

$$\langle K^+K^-|\mathcal{H}_{\text{eff}}|B_s^0\rangle = -(T' + P' + E' + PA'), \tag{2.86}$$

$$\langle \pi^+\pi^-|\mathcal{H}_{\text{eff}}|B_s^0\rangle = -(E' + PA'), \tag{2.87}$$

we find the amplitude relation

$$\langle \pi^-K^+|\mathcal{H}_{\text{eff}}|B_d^0\rangle - \langle K^+K^-|\mathcal{H}_{\text{eff}}|B_s^0\rangle + \langle \pi^+\pi^-|\mathcal{H}_{\text{eff}}|B_s^0\rangle = 0, \tag{2.88}$$

or, equivalently,

$$-(T' + P') + (T' + P' + E' + PA') - (E' + PA') = 0. \tag{2.89}$$

Let us now make a dynamical assumption regarding the topology amplitudes. Namely, assuming that the spectator quark is unlikely to interact with the b quark, the so-called *spectator approximation*, we can neglect the exchange (E') and penguin annihilation (PA') topologies. In this case the decay amplitude for $B_s \to \pi^+\pi^-$ vanishes, and we find the squared amplitude relation

$$\langle \pi^-K^+|\mathcal{H}_{\text{eff}}|B_d^0\rangle = \langle K^+K^-|\mathcal{H}_{\text{eff}}|B_s^0\rangle, \tag{2.90}$$

which we will return to in Chapter 4. This illustrates the usefulness of the topology basis over the reduced matrix element basis, and of flavour symmetries in general.

We observe from (2.81) and (2.86) that the decay amplitudes of $B_d \to \pi^+\pi^-$ and $B_s \to K^+K^-$ have the same classes of topology amplitudes contributing. As we will discuss in Chapter 4, after factoring out CKM couplings, it turns out that U-spin symmetry implies a 1–1 mapping between the hadronic matrix elements of these two decays.

In Chapter 5 we will use U-spin in a similar way to find control channels for decays of the form $B_s \to J/\psi s\bar{s}$. Here, however, it will be necessary to make dynamical assumptions about the relative contributions of some decay topologies. Of course, U-spin is not an exact symmetry, and when we use it we must also take U-spin breaking corrections into account. Such corrections depend on the dynamics of the processes in question and are therefore difficult to estimate a priori. The quantities $f_K/f_\pi - 1$ or $(m_s - m_d)/\Lambda_{\rm QCD}$ give a ballpark estimate of 20%.

Chapter 3

Observables of the B_S meson system

3.1 The B_s meson system

Flavour, CP and mass basis states

In Chapter 2 we briefly introduced the B_s flavour states B_s^0 and $\overline{B}_s^0$ as the strongly bound states of the quark–antiquark combinations $\bar{b}s$ and $b\bar{s}$, respectively. These flavour states are related to each other by the CP transformations

$$\mathcal{CP}|B_s^0\rangle = e^{i\xi_{B_s}}|\overline{B}_s^0\rangle, \qquad \mathcal{CP}|\overline{B}_s^0\rangle = e^{-i\xi_{B_s}}|B_s^0\rangle, \tag{3.1}$$

where ξ_{B_s} is an arbitrary, convention-dependent, phase. As a consequence of this relation, they can be expressed in a basis of CP–eigenstates

$$|B_{s,\pm}\rangle \equiv \frac{1}{\sqrt{2}}\left(|B_s^0\rangle \pm e^{i\xi_{B_s}}|\overline{B}_s^0\rangle\right), \tag{3.2}$$

with eigenvalues of ± 1, corresponding to *CP-even* and *CP-odd* states, respectively.

As discussed in the introduction, the B_s meson system's flavour states B_s^0 and $\overline{B}_s^0$ can oscillate before decaying. This oscillation can be described in terms of a time-dependent quantum mechanical state [54]

$$|B_s(t)\rangle = a(t)|B_s^0\rangle + b(t)|\overline{B}_s^0\rangle, \tag{3.3}$$

where t is the time in the B_s^0–$\overline{B}_s^0$ rest frame. This is called the Wigner-Weisskopf approximation, as we have ignored other possible intermediate states. This is valid if we start with only these flavour states and consider times much larger than the interaction scale. If at time $t = 0$ a given state has $b(0) = 0$ or $a(0) = 0$, then we will simply label it as $|B_s^0(t)\rangle$ or $|\overline{B}_s^0(t)\rangle$, respectively.

The Schrödinger equation that describes the mixing and decay of this state is

$$i\frac{d}{dt}\boldsymbol{\psi}(t) = \left(\mathbf{M} - \frac{i}{2}\mathbf{\Gamma}\right)\boldsymbol{\psi}(t), \qquad \boldsymbol{\psi}(t) \equiv \begin{pmatrix} a(t) \\ b(t) \end{pmatrix}, \tag{3.4}$$

where $\mathbf{M}$ and $\mathbf{\Gamma}$ are the mass and decay matrices respectively. For the B_s meson system to decay with time we require that

$$\begin{aligned}\frac{d}{dt}\left(\boldsymbol{\psi}^\dagger(t)\boldsymbol{\psi}(t)\right) &= -i\boldsymbol{\psi}^\dagger(t)\left(-\boldsymbol{M}^\dagger - \frac{i}{2}\mathbf{\Gamma}^\dagger + \boldsymbol{M} - \frac{i}{2}\mathbf{\Gamma}\right)\boldsymbol{\psi}(t) \\ &= -\boldsymbol{\psi}^\dagger(t)\,\mathbf{\Gamma}\,\boldsymbol{\psi}(t). \end{aligned} \tag{3.5}$$

Thus the matrix $\mathbf{M} - \frac{i}{2}\mathbf{\Gamma}$ cannot be Hermitian, but instead $\mathbf{M}$ and $\mathbf{\Gamma}$ must be separately Hermitian. For the number of B_s mesons to decrease with time, $\mathbf{\Gamma}$ should also be positive definite. The matrices $\mathbf{M}$ and $\mathbf{\Gamma}$ obey two additional constraints if we make the experimentally supported assumption that the combination of discrete symmetries CPT is respected by Nature. To derive these we consider the matrices in second-order perturbation theory as a sum over intermediate states n [54]. Under a CPT transformation the flavour states transform as

$$\mathcal{CPT}|B_s^0\rangle = e^{i\nu_{B_s}}|\overline{B}_s^0\rangle, \qquad \mathcal{CPT}|\overline{B}_s^0\rangle = e^{i\nu_{B_s}}|B_s^0\rangle, \tag{3.6}$$

where ν_{B_s} is a convention-dependent phase. Then, given that $[\mathcal{H}, \mathcal{CPT}] = 0$, we find

$$\begin{aligned} M_{11} &= m_0 + \langle B_s^0|\mathcal{H}|B_s^0\rangle + \sum_n P\frac{\langle B_s^0|\mathcal{H}|n\rangle\langle n|\mathcal{H}|B_s^0\rangle}{m_0 - E_n} \\ &= m_0 + \langle \overline{B}_s^0|\mathcal{H}|\overline{B}_s^0\rangle + \sum_n P\frac{\langle \overline{B}_s^0|\mathcal{H}|n\rangle\langle n|\mathcal{H}|\overline{B}_s^0\rangle}{m_0 - E_n} = M_{22}, \end{aligned} \tag{3.7}$$

$$\begin{aligned} \Gamma_{11} &= 2\pi\sum_n \delta(m_0 - E_n)\langle B_s^0|\mathcal{H}|n\rangle\langle n|\mathcal{H}|B_s^0\rangle \\ &= 2\pi\sum_n \delta(m_0 - E_n)\langle \overline{B}_s^0|\mathcal{H}|n\rangle\langle n|\mathcal{H}|\overline{B}_s^0\rangle = \Gamma_{22}, \end{aligned} \tag{3.8}$$

where P denotes the principal part. Thus, including the constraints $M_0 \equiv M_{11} = M_{22}$ and $\Gamma_0 \equiv \Gamma_{11} = \Gamma_{22}$, there are a total of six mixing degrees of freedom remaining in $\mathbf{M} - \frac{i}{2}\mathbf{\Gamma}$, which we will now discuss and present in terms of convenient parameters.

The oscillating system of flavour states can be diagonalized to give mass-eigenstates, the normal modes of this coupled system. These physical states evolve in time independently of each other

$$|B_{\rm H}(t)\rangle = e^{-i\lambda_{\rm H}t}|B_{\rm H}\rangle, \qquad |B_{\rm L}(t)\rangle = e^{-i\lambda_{\rm L}t}|B_{\rm L}\rangle, \tag{3.9}$$

with eigenvalues

$$\lambda_{\left(\begin{smallmatrix}\rm H\\ \rm L\end{smallmatrix}\right)} = M_{\left(\begin{smallmatrix}\rm H\\ \rm L\end{smallmatrix}\right)} - \frac{i}{2}\Gamma_{\left(\begin{smallmatrix}\rm H\\ \rm L\end{smallmatrix}\right)}, \tag{3.10}$$

where $M_{\left(\begin{smallmatrix}\rm H\\ \rm L\end{smallmatrix}\right)}$ and $\Gamma_{\left(\begin{smallmatrix}\rm H\\ \rm L\end{smallmatrix}\right)}$ are the mass and decay width of these physical particles, respectively. It is conventional, as we have done, to label these mass-eigenstates by their

relative mass, heavy (H) and light (L). They are related to the matrix elements in the flavour basis by [60]

$$M_{\binom{\mathrm{H}}{\mathrm{L}}} \equiv M_0 \pm \mathrm{Re}\left[\left(M_{12} - \frac{i}{2}\Gamma_{12}\right)\alpha\right], \tag{3.11}$$

$$\Gamma_{\binom{\mathrm{H}}{\mathrm{L}}} \equiv \Gamma_0 \mp 2\mathrm{Im}\left[\left(M_{12} - \frac{i}{2}\Gamma_{12}\right)\alpha\right], \tag{3.12}$$

with

$$\alpha \equiv \sqrt{\frac{M_{12}^* - \frac{i}{2}\Gamma_{12}^*}{M_{12} - \frac{i}{2}\Gamma_{12}}}. \tag{3.13}$$

Similarly the mass-eigenstates are expressed in terms of the flavour states by[1]

$$\left|B_{s,\binom{\mathrm{H}}{\mathrm{L}}}\right\rangle = \frac{1}{\sqrt{1+|\alpha|^2}}\left(|B_s^0\rangle \pm \alpha|\overline{B_s^0}\rangle\right). \tag{3.14}$$

Having already labeled the eigenstates by their relative mass, the B_s mass difference places the following condition on the matrix elements:

$$\Delta M_s \equiv M_\mathrm{H} - M_\mathrm{L} = 2\mathrm{Re}\left[\left(M_{12} - \frac{i}{2}\Gamma_{12}\right)\alpha\right] > 0. \tag{3.15}$$

We also define the B_s mass, decay width difference and mean decay width as[2]

$$M_{B_s} \equiv \frac{M_\mathrm{H} + M_\mathrm{L}}{2} = M_0 \tag{3.16}$$

$$\Delta\Gamma_s \equiv \Gamma_\mathrm{L} - \Gamma_\mathrm{H} = 4\mathrm{Im}\left[\left(M_{12} - \frac{i}{2}\Gamma_{12}\right)\alpha\right], \tag{3.17}$$

$$\Gamma_s \equiv \frac{\Gamma_\mathrm{L} + \Gamma_\mathrm{L}}{2} = \Gamma_0, \tag{3.18}$$

respectively. Throughout this thesis we will often find it convenient to replace the latter two parameters with the following ones:

$$y_s \equiv \frac{\Gamma_\mathrm{L} - \Gamma_\mathrm{H}}{\Gamma_\mathrm{L} + \Gamma_\mathrm{H}} = \frac{\Delta\Gamma_s}{2\,\Gamma_s}, \qquad \tau_{B_s} \equiv \frac{1}{\Gamma_s}. \tag{3.19}$$

The latter parameter is referred to as the B_s *mean lifetime*. We will find that the parameters in (3.13), (3.15) and (3.17) simplify if we take into consideration the relative magnitude of M_{12} to Γ_{12}. To that end we proceed to consider these matrix elements separately.

[1] In the literature the notation $\alpha = q/p$ is also commonly used.

[2] Our use of natural units ($\hbar = c = 1$) allows us to relate mass and frequencies in this way. Taking these constants as non-trivial gives $M_{B_s} = (\hbar/c^2)M_0$.

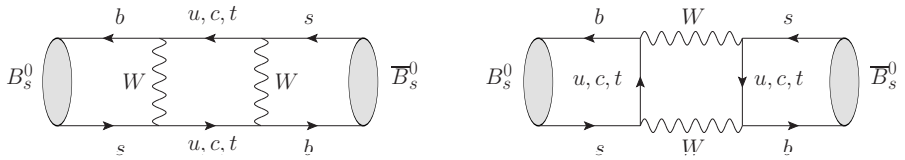

Figure 3.1: Diagrams in the Standard Model that contribute to M_{12} and Γ_{12}. The former receives contributions from virtual intermediate quarks, especially a virtual top, and the latter when the intermediate quarks are on-shell, especially the charm.

B_s^0–$\overline{B}_s^0$ mixing in the Standard Model

The matrix element $M_{21} = M_{12}^*$ is responsible for the virtual, dispersive, transition of a B_s^0 to a $\overline{B}_s^0$ meson. In the Standard Model it is driven by box diagrams involving virtual W bosons and top quarks as shown in Figure 3.1. The corresponding four-quark operator in the low energy effective theory is

$$\mathcal{O}_1^{\mathrm{VLL}} = (\bar{b}_\alpha \gamma_\mu P_L s_\alpha)\,(\bar{b}_\beta \gamma^\mu P_L s_\beta), \tag{3.20}$$

where the label VLL refers to the presence of two left-handed vector currents. It is part of a general model-independent operator basis for $|\Delta B| = 2$ transitions to be presented in Section 6.4.1. The OPE gives [35]

$$M_{12}^*|_{\mathrm{SM}} = \frac{G_{\mathrm{F}}^2\, M_{\mathrm{W}}^2}{4\pi^2}\,(V_{ts}V_{tb}^*)^2\, C_1^{\mathrm{VLL}}(\mu_b)\langle \overline{B}_s^0|\mathcal{O}_1^{\mathrm{VLL}}(\mu_b)|B_s^0\rangle, \tag{3.21}$$

where $\mu_b = \mathcal{O}(m_b)$ is the appropriate factorization scale.

The long-distance physics is contained in the hadronic matrix element and is parameterized by

$$\langle \overline{B}_s^0|\mathcal{O}_1^{\mathrm{VLL}}(\mu_b)|B_s^0\rangle \equiv \frac{1}{3} M_{B_s} f_{B_s}^2 B_1^{\mathrm{VLL}}(\mu_b)\, e^{i(\xi_{B_s}+\xi_s-\xi_b-\pi)}, \tag{3.22}$$

where f_{B_s} is the B_s decay constant and the ξs are CP transformation phases. The parameter $B_1^{\mathrm{VLL}}(\mu_b)$ is historically referred to as a bag parameter, with a deviation from unity indicating a departure from the vacuum insertion approximation [61]. In lattice calculations of the hadronic matrix element it is typically the combination $f_{B_s}^2 B_1^{\mathrm{VLL}}(\mu_b)$ that is measured. The bag parameter in the context of the Standard Model is often denoted as $B_{B_s}(\mu_b) \equiv B_1^{\mathrm{VLL}}(\mu_b)$, which we will use now to simplify comparisons with the literature.

The short-distance physics is contained in the Wilson coefficient

$$C_1^{\mathrm{VLL}}(\mu_b) = \hat{\eta}_B(\mu_b) S_0(x_t). \tag{3.23}$$

In this expression

$$S_0(x_t) = \frac{4x_t - 11x_t^2 + x_t^3}{4(1-x_t)^2} - \frac{3x_t^3 \ln x_t}{2(1-x_t)^3} \tag{3.24}$$

is the Inami-Lim function with $x_t = m_t^2/M_{\rm W}^2$ [62]. It describes the dynamics of the box diagrams with the W boson and top quark integrated out. The factor $\hat{\eta}_B(\mu_b)$ describes the short-distance perturbative QCD corrections.

In the above formulation the quantities $\hat{\eta}_B(\mu_b)$ and $B_{B_s}(\mu_b)$ share a renormalization scale and scheme dependence. It is possible to transfer this scale and scheme dependence to the bag parameter, which results in the combination of independent parameters $\eta_B \hat{B}_{B_s} = \hat{\eta}_B(\mu_b) B_{B_s}(\mu_b)$ with $\eta_B = 0.55$ [63]. Combining the above ingredients then finally gives

$$M_{12}^*|_{\rm SM} = \frac{G_{\rm F}^2 M_{\rm W}^2}{12\pi^2} M_{B_s} f_{B_s}^2 \eta_B \hat{B}_{B_s} \left(V_{ts} V_{tb}^*\right)^2 S_0(x_t)\, e^{i(\xi_{B_s} + \xi_s - \xi_b - \pi)}. \tag{3.25}$$

We will generalise the $|\Delta B| = 2$ OPE to include additional operators when we discuss models of New Physics in Section 6.4.1.

The matrix element $\Gamma_{21} = \Gamma_{12}^*$ is responsible for on-shell, absorptive, B_s^0 to $\overline{B}_s^0$ transitions. This means that all B_s final states carrying no net strangeness contribute to it. In the Standard Model the leading contributions are given by the box diagrams shown in Figure 3.1 for on-shell intermediate quarks. Thus the intermediate top quarks can be neglected as they are far too heavy. Furthermore, an intermediate up quark is Cabibbo suppressed relative to a charm quark. Therefore the dominant contributions come from $b \to c\bar{c}s$ transitions. In order to theoretically estimate Γ_{12}^* one can take an exclusive or inclusive approach. In the exclusive approach an attempt is made to sum over all exclusive B_s hadronic final states, of which the modes $B_s^0 \to D_s^{(*)} \overline{D}_s^{(*)} \to \overline{B}_s^0$ dominate [64, 65]. In the inclusive approach it assumed that the sum over exclusive decays is equal to the sum over all intermediate quark states, which is known as *quark-hadron duality*.

Following the inclusive approach, we can express the $b \to c\bar{c}s$ transitions in terms of the $|\Delta B| = 1$ effective theory given in Section 2.2, of which $\mathcal{O}_1^c$ and $\mathcal{O}_2^c$ are the dominant operators. Because the heavy b quark results in an interaction distance $1/m_b$ much smaller than the hadronic distance scale, the combination of the two $|\Delta B| = 1$ local operators is effectively also a local operator. This second effective theory is derived by expanding in powers of the heavy b quark mass m_b, known as the *heavy quark expansion* (HQE), which is schematically given by [66]

$$\mathrm{Im}\, i \int d^4x T \left(\mathcal{O}^{\Delta B=1}(x)\, \mathcal{O}^{\Delta B=1}(0)\right) = \sum_n \frac{C_n}{m_b^n} \mathcal{O}_n^{\Delta B=2}(0), \tag{3.26}$$

where C_n are the corresponding Wilson Coefficients of this theory. The resulting $|\Delta B| = 2$ operators at leading order in the mass expansion are $\mathcal{O}_1^{\rm VLL}$, as given in (3.20), and the operator

$$\mathcal{O}_1^{\rm SLL} = (\bar{b}_\alpha P_L s_\alpha)\, (\bar{b}_\beta P_L s_\beta), \tag{3.27}$$

where the label SLL similarly refers to the presence of two scalar left handed currents. Its hadronic matrix element is defined as

$$\langle \overline{B}_s^0 | \mathcal{O}_1^{\rm SLL}(\mu_b) | B_s^0 \rangle \equiv -\frac{5}{24} M_{B_s} \frac{M_{B_s}^2}{(m_b + m_s)^2} f_{B_s}^2 B_1^{\rm SLL}(\mu_b)\, e^{i(\xi_{B_s} + \xi_s - \xi_b - \pi)}. \tag{3.28}$$

At leading order in $1/m_b$ and CKM factors, the absorptive transition is thus given by [67]

$$\begin{aligned}\Gamma_{12}^* = & -\frac{G_F^2\, m_b^2 M_{B_s} f_{B_s}^2}{12\pi}\,(V_{cs}V_{cb}^*)^2\; e^{i(\xi_{B_s}+\xi_s-\xi_b-\pi)} \\ & \times\left[\frac{1}{3}G^{cc}\,B_1^{\rm VLL}(\mu_b)+\frac{5}{24}G_S^{cc}\frac{M_{B_s}^2}{(m_b+m_s)^2}B_1^{\rm SLL}(\mu_b)\right]+\mathcal{O}\left(\frac{1}{m_b},\lambda_{\rm CKM}\right), \qquad (3.29)\end{aligned}$$

where the coefficients $G_{(S)}^{cc}$ are defined in terms of the Wilson coefficients of the $|\Delta B|=1$ effective theory. Note that this expression does not represent the state of the art, and in the given basis of operators the $1/m_b$ corrections can be as large as 40% [67]. A modern calculation of Γ_{12}^*, including next-to-leading order corrections in $1/m_b$ and α_s in an optimized operator basis, is given in Ref. [68].

We are now in a position to qualitatively consider the relative magnitudes of M_{12}^* and Γ_{12}^*. Assuming $G_{(S)}^{cc}=\mathcal{O}(1)$, $B_1^{\rm VLL}\approx B_1^{\rm SLL}$ and using the approximation $S_0(x_t)\sim x_t=m_t^2/M_W^2$ we find

$$\left.\frac{\Gamma_{12}^*}{M_{12}^*}\right|_{\rm SM}\sim-\frac{\pi}{\hat\eta_B\,S_0(x_t)}\left(\frac{m_b^2}{M_{\rm W}^2}\right)=\mathcal{O}\left(\frac{m_b^2}{m_t^2}\right)=\mathcal{O}(10^{-4}). \qquad (3.30)$$

Thus in the Standard Model we can safely conclude that $|\Gamma_{12}/M_{12}|$ is a valid expansion parameter. Also beyond the Standard Model this is a safe assumption, as the dramatic New Physics necessary to increase this quantity several orders of magnitude has not been seen experimentally. Specifically, Γ_{12} is driven by $b\to c\bar cs$ transitions and no anomalously large branching ratios are observed for exclusive decays in which this quark level transition is also dominant.

Before expanding in powers of $|\Gamma_{12}/M_{12}|$ it will be convenient to define the following convention independent phases

$$\phi_s\equiv\arg(M_{12})-\pi+\xi_{B_s}+\xi_s-\xi_b, \qquad (3.31)$$

$$\tilde\phi_s\equiv\arg(-M_{12}/\Gamma_{12}), \qquad (3.32)$$

where the convention dependent ξ phases exactly cancel those in (3.25). The expansion then gives

$$\alpha=-e^{-i\phi_s}\,e^{i(\xi_{B_s}+\xi_s-\xi_b)}\left[1-\frac{1}{2}\left|\frac{\Gamma_{12}}{M_{12}}\right|\sin\tilde\phi_s+\mathcal{O}\left(\left|\frac{\Gamma_{12}}{M_{12}}\right|^2\right)\right], \qquad (3.33)$$

$$\Delta M_s=2\,|M_{12}|\left[1+\mathcal{O}\left(\left|\frac{\Gamma_{12}}{M_{12}}\right|^2\right)\right], \qquad (3.34)$$

$$\Delta\Gamma_s=2\,|\Gamma_{12}|\cos\tilde\phi_s\left[1+\mathcal{O}\left(\left|\frac{\Gamma_{12}}{M_{12}}\right|^2\right)\right]. \qquad (3.35)$$

At leading order we see that the B_s mass difference depends only on M_{12}, the decay width difference only on Γ_{12} and its phase relative to M_{12} and the mixing parameter α only on the phase of M_{12}.

A closer look at the mixing parameters

A deviation of $|\alpha|$ from one would imply the presence of CP violation in B_s^0–$\overline{B}_s^0$ mixing. Experimentally this can be probed using *flavour specific* decays, which are decays for which the channels $B_s^0 \to f$ and $\overline{B}_s^0 \to \bar{f}$ are allowed but $\overline{B}_s^0 \to f$ and $B_s^0 \to \bar{f}$ are forbidden. A typical example are semi-leptonic decays of the form $B_s \to X\ell\bar{\nu}$. Consequently, the so-called *semi-leptonic asymmetry* is defined as

$$\begin{aligned} a_{\rm SL}^s &\equiv \frac{\Gamma(\overline{B}_s^0(t) \to X\ell\bar{\nu}) - \Gamma(B_s^0(t) \to \overline{X}\bar{\ell}\nu)}{\Gamma(\overline{B}_s^0(t) \to X\ell\bar{\nu}) + \Gamma(B_s^0(t) \to \overline{X}\bar{\ell}\nu)} = \frac{1-|\alpha|^4}{1-|\alpha|^4} \\ &= \left|\frac{\Gamma_{12}}{M_{12}}\right| \sin\tilde{\phi}_s + \mathcal{O}\left[(|\alpha|-1)^2\right], \end{aligned} \tag{3.36}$$

where we have made the safe assumption that semi-leptonic decays have no direct CP violation. One avenue to measure this asymmetry is to search for final states containing two leptons with the same charge, as this implies that for an initial pair of B_s^0–$\overline{B}_s^0$ mesons one necessarily mixed into the other. The theoretical prediction for this asymmetry is tiny [68]:

$$a_{\rm SL}^s\big|_{\rm SM} = (1.9 \pm 0.3) \times 10^{-5}. \tag{3.37}$$

The latest experimental results give

$$a_{\rm SL}^s = \begin{cases} (-1.81 \pm 1.06)\% & : \text{ di-muon, DØ [69]} \\ (-1.12 \pm 0.74 \pm 0.17)\% & : B_s \to D_s\,\mu\nu X, \text{ DØ [70]} \\ (-0.06 \pm 0.50 \pm 0.36)\% & : B_s \to D_s\,\mu\nu, \text{ LHCb [71]} \end{cases}, \tag{3.38}$$

which are largely consistent with the Standard Model. Throughout this thesis we will assume for simplicity that $a_{\rm SL}^s = 0$ and thus that $|\alpha| = 1$.

Having established that $\Delta M_s = 2|M_{12}|$ to an excellent accuracy, we can use (3.25) to give a theoretical estimate. The main source of uncertainty are the long-distance hadronic parameters $f_{B_s}^2 B_{B_s}$. The current lattice QCD world average[3] is [27]

$$f_{B_s}\sqrt{B_{B_s}} = (226 \pm 12) \ \text{MeV}, \tag{3.39}$$

at the scale $\mu_b = m_b$. Using this value together with standard inputs from Ref. [17] gives the Standard Model prediction

$$\Delta M_s\big|_{\rm SM} = (19.0 \pm 2.1) \ \text{ps}^{-1}. \tag{3.40}$$

This can be compared to the Heavy Flavour Averaging Group (HFAG) experimental average [73]

$$\Delta M_s = (17.73 \pm 0.05) \ \text{ps}^{-1}. \tag{3.41}$$

[3]The recent lattice calculation of Ref. [72] is not included in this average. We will discuss its inclusion in Section 6.4.1.

We also established to an excellent accuracy that $\Delta\Gamma_s = 2\,|\Gamma_{12}|\cos\tilde{\phi}_s$ and, likewise, $y_s = (|\Gamma_{12}|/\Gamma_s)\cos\tilde{\phi}_s$. It is therefore possible to theoretically estimate them using the HQE expansion discussed above. The authors of Ref. [68] find

$$\Delta\Gamma_s^{\mathrm{Th}} \equiv 2\,|\Gamma_{12}| = (0.087 \pm 0.021)\ \mathrm{ps}^{-1}, \tag{3.42}$$

$$y_s^{\mathrm{Th}} \equiv \frac{|\Gamma_{12}|}{\Gamma_s} = 0.067 \pm 0.016, \tag{3.43}$$

$$\tilde{\phi}_s^{\mathrm{SM}} = (0.22 \pm 0.06)^\circ. \tag{3.44}$$

As mentioned earlier, New Physics contributions to Γ_{12} are expected to be small because the $b \to c\bar{c}s$ transitions, which give the dominant contribution, are strongly constrained by experiment. Because in the Standard Model $\tilde{\phi}_s^{\mathrm{SM}} \approx 0$, if we assume Γ_{12} is unaffected by New Physics, it follows from

$$y_s = y_s^{\mathrm{Th}}\cos\tilde{\phi}_s \tag{3.45}$$

that New Physics can only decrease the B_s decay width difference [74]. Furthermore, under this assumption New Physics contributions to ϕ_s and $\tilde{\phi}_s$ will come only from M_{12} and will be the same. If we let the parameter ϕ_s^{NP} represent New Physics contribution to M_{12}, we may express the phases defined in (3.31) and (3.32) by

$$\phi_s = \phi_s^{\mathrm{SM}} + \phi_s^{\mathrm{NP}}, \qquad \tilde{\phi} = \tilde{\phi}_s^{\mathrm{SM}} + \phi_s^{\mathrm{NP}}, \tag{3.46}$$

with [75]

$$\phi_s^{\mathrm{SM}} \equiv 2\arg\left(V_{ts}^* V_{tb}\right) = -2\,\beta_s = -(2.11 \pm 0.08)^\circ. \tag{3.47}$$

The experimental determination of the mixing parameters y_s and ϕ_s is one of the focus points of this thesis. Therefore for now it will suffice to point out that the most accurate determination of y_s and ϕ_s comes from the LHCb experiment's analysis of the $B_s \to J/\psi\phi$ decay [76], which gives

$$\phi_s = (4.0 \pm 5.2)^\circ\,, \tag{3.48}$$

$$y_s = 0.075 \pm 0.012. \tag{3.49}$$

In addition, the S-wave modes of the decay $B_s \to J/\psi K^+K^-$ have been used to rule out the discrete ambiguity $\phi_s \to \phi_s + \pi$ and $y_s \to -y_s$ [77].

Thus a positive non-zero B_s decay width difference has been experimentally established. This means that the lighter mass eigenstate, $B_{s,\mathrm{L}}$, will on average decay faster than the heavier one, $B_{s,\mathrm{H}}$. Why this is the case can be understood in analogy to the kaon system, where the mass and CP eigenstates are almost aligned. In this case one mass-eigenstate is much shorter lived because it has exclusive access to the kinematically favoured two pion CP-even decay modes. In the B_s system the situation is similar because the majority of the CKM-favoured modes $B_s \to D_s^{(*)}\overline{D}_s^{(*)}$ are CP even. Therefore

a non-zero width difference also suggests an alignment between mass and CP eigenstates in the B_s system. Combining the expressions for the B_s CP and mass eigenstates in (3.2) and (3.14) together with α as defined in (3.33) gives

$$\begin{pmatrix} |B_{s,\mathrm{L}}\rangle \\ |B_{s,\mathrm{H}}\rangle \end{pmatrix} = e^{-i\bar{\phi}_s/2} \begin{pmatrix} \cos(\bar{\phi}_s/2) & i\sin(\bar{\phi}_s/2) \\ i\sin(\bar{\phi}_s/2) & \cos(\bar{\phi}_s/2) \end{pmatrix} \begin{pmatrix} |B_{s,+}\rangle \\ |B_{s,-}\rangle \end{pmatrix}, \tag{3.50}$$

where $\bar{\phi}_s \equiv \phi_s - \xi_s + \xi_b$. Thus the phase $\bar{\phi}_s$ determines the alignment of the two bases. Note, however, that the presence of the convention-dependent quark phases $\xi_{b,s}$ means that the CP basis is only physically meaningful when considered in the context of a decay where these phases cancel. The point to be made is that the decay width difference and mixing phase are closely related, as also expressed in (3.45).

In this section we have discussed the six degrees of freedom that are present in the mixing matrix $\mathbf{M} - \frac{i}{2}\mathbf{\Gamma}$ of (3.4) if we allow for CP violation, and expressed them in terms of the six parameters

$$M_{B_s}, \qquad \tau_{B_s}, \qquad \Delta M_s, \qquad y_s, \qquad \phi_s, \qquad \tilde{\phi}_s. \tag{3.51}$$

The current HFAG experimental averages [73] for the B_s mass and mean lifetime are

$$M_{B_s} = (5.3663 \pm 0.0006) \ \text{GeV}, \tag{3.52}$$

$$\tau_{B_s} = (1.516 \pm 0.011) \ \text{ps}, \tag{3.53}$$

For completeness we also briefly discuss B^0_d–$\overline{B}^0_d$ mixing, which can be parameterised in an analogous way. A notable difference in this system is that the decay width difference is expected to be vanishingly small in the Standard Model [68]:

$$y_d^{\mathrm{Th}} = \left(23^{+5}_{-6}\right) \times 10^{-4}. \tag{3.54}$$

As a consequence, much of the phenomenology involving untagged observables that we will discuss in the following sections for the B_s system does not apply for B_d. In the Standard Model the B^0_d–$\overline{B}^0_d$ mixing phase is given by

$$\phi_d^{\mathrm{SM}} \equiv 2 \arg\left(V_{td}^* V_{tb}\right) = 2\beta. \tag{3.55}$$

which is significantly larger than the Standard Model prediction for ϕ_s given in (3.47). This phase is conventionally determined experimentally from an analysis of the decay modes $B_d \to J/\psi K_{\mathrm{S,L}}$. Including corrections from doubly Cabibbo-suppressed penguin topologies, which can be deduced from the flavour symmetry relation of these decays to $B^0_d \to J/\psi\pi^0$, gives the result [78]

$$\phi_d = (42.4^{+3.4}_{-1.7})^\circ. \tag{3.56}$$

The B_d counterpart of (3.32) is theoretically estimated to be $\tilde{\phi}_d^{\mathrm{SM}} = (-4.3 \pm 1.4)^\circ$ [68]. Finally, the current HFAG experimental averages for the remaining three parameters

are [73]

$$\Delta M_d = (0.510 \pm 0.004)\ \text{ps}^{-1}, \tag{3.57}$$
$$M_{B_d} = (5.27958 \pm 0.00017)\ \ \text{GeV}, \tag{3.58}$$
$$\tau_{B_d} = (1.519 \pm 0.007)\ \text{ps}. \tag{3.59}$$

Thus the masses and mean lifetimes are similar, but the B_d meson system is seen to oscillate at a much slower rate than the B_s mesons do.

3.2 Time-dependent observables

For a given decay mode $B_s \to f$ we naturally expect the distribution of observed events to decrease with time. However, because this is a coupled system of oscillating flavour states, we will see that the resulting distribution is not necessarily described by a usual exponential function. Consider a sample $N_{B_s^0}$ of B_s mesons that are all initially in the flavour state B_s^0. Letting t represent their proper time, we define their *time-dependent decay rate* as [79]

$$\Gamma(B_s^0(t) \to f) \equiv \frac{1}{N_{B_s^0}} \frac{dN(B_s^0(t) \to f)}{dt}, \tag{3.60}$$

where $dN(B_s^0(t) \to f)$ represents the number of decays in the time window $[t, t + dt]$. The decay rate defined in this way accounts for the probability that the state may already have decayed at the given time t. The time-dependent decay rate $\Gamma(\overline{B}_s^0(t) \to f)$ is defined in an analogous way.

At $t = 0$ the definition in (3.60) reduces to the usual notion of an *instantaneous decay rate*, which for a $B_s \to f$ transition is given by

$$\Gamma(B_s \to f) \equiv \frac{1}{2\,M_{B_s}} \int d\Phi \left|\langle f|\mathcal{H}|B_s\rangle\right|^2, \tag{3.61}$$

where $d\Phi$ is an integral over the final state's phase space. Here B_s is used to denote a flavour, mass or CP state, and each is assumed to have the same well-defined mass M_{B_s}. As the phase space integral should not depend on the proper time, we may thus express the time-dependent decay rate for any $B_s(t) \to f$ transition as

$$\Gamma(B_s(t) \to f) \equiv \frac{1}{2\,M_{B_s}} \int d\Phi \left|\langle f|\mathcal{H}|B_s(t)\rangle\right|^2. \tag{3.62}$$

We will now evaluate this time-dependent squared matrix element.

The time-dependence of the B_s flavour states can be found by combining equations (3.14) and (3.9), which gives

$$\begin{aligned} |B_s^0(t)\rangle &= g_+(t)|B_s^0\rangle + \alpha g_-(t)|\overline{B}_s^0\rangle, \\ |\overline{B}_s^0(t)\rangle &= \frac{1}{\alpha} g_-(t)|B_s^0\rangle + g_+(t)|\overline{B}_s^0\rangle, \end{aligned} \tag{3.63}$$

where

$$g_{\pm}(t) = \frac{1}{2}\left(e^{-i\lambda_{\rm H} t} \pm e^{-i\lambda_{\rm L} t}\right). \tag{3.64}$$

Let us consider a final state f to which both B_s^0 and $\overline{B}_s^0$ can decay. Then the following convention independent quantity can be defined:

$$\lambda_f \equiv \alpha \, \frac{\langle f|\mathcal{H}|\overline{B}_s^0\rangle}{\langle f|\mathcal{H}|B_s^0\rangle} = -e^{-i\phi_s}\left[1 - \frac{1}{2}a_{\rm SL}\right]\frac{\langle f|\mathcal{H}|\overline{B}_s^0\rangle}{\langle f|\mathcal{H}|B_s^0\rangle}, \tag{3.65}$$

where we will typically assume $a_{\rm SL} = 0$ as discussed earlier. In terms of this parameter the squared amplitudes for the B_s flavour states decaying to the final state f exhibit the time evolution [80]

$$\begin{aligned}
\left|\langle f|\mathcal{H}|B_s^0(t)\rangle\right|^2 = \; & \left|\langle f|\mathcal{H}|B_s^0\rangle\right|^2 \frac{e^{-t/\tau_{B_s}}}{2}\Big\{ \\
& + \left(1 - |\lambda_f|^2\right)\cos(\Delta M_s\, t) + 2{\rm Im}[\lambda_f]\sin(\Delta M_s\, t) \\
& + \left(1 + |\lambda_f|^2\right)\cosh\left(y_s\, t/\tau_{B_s}\right) + 2{\rm Re}[\lambda_f]\sinh\left(y_s\, t/\tau_{B_s}\right)\Big\}, \\
\left|\langle f|\mathcal{H}|\overline{B}_s^0(t)\rangle\right|^2 = \; & |\alpha|^{-2}\left|\langle f|\mathcal{H}|B_s^0\rangle\right|^2 \frac{e^{-t/\tau_{B_s}}}{2}\Big\{ \\
& - \left(1 - |\lambda_f|^2\right)\cos(\Delta M_s\, t) - 2{\rm Im}[\lambda_f]\sin(\Delta M_s\, t) \\
& + \left(1 + |\lambda_f|^2\right)\cosh\left(y_s\, t/\tau_{B_s}\right) + 2{\rm Re}[\lambda_f]\sinh\left(y_s\, t/\tau_{B_s}\right)\Big\},
\end{aligned} \tag{3.66}$$

This is in contrast to the mass-eigenstates, for which the time evolution to this final state follows from (3.9), and is simply given by

$$\begin{aligned}
\left|\langle f|\mathcal{H}|B_{s,{\rm H}}(t)\rangle\right|^2 &= e^{-\Gamma_{\rm H}\, t}\left|\langle f|\mathcal{H}|B_{s,{\rm H}}\rangle\right|^2, \\
\left|\langle f|\mathcal{H}|B_{s,{\rm L}}(t)\rangle\right|^2 &= e^{-\Gamma_{\rm L}\, t}\left|\langle f|\mathcal{H}|B_{s,{\rm L}}\rangle\right|^2.
\end{aligned} \tag{3.67}$$

3.2.1 To tag or not to tag

Being able to experimentally identify, or *tag*, the flavour states B_s^0 and $\overline{B}_s^0$ before they decay is very useful for studying their oscillations. Unfortunately, flavour-tagging generally has a low experimental efficiency, and first requires many events to be recorded for a given $B_s \to f$ transition. Given an equal number of produced B_s^0 and $\overline{B}_s^0$ mesons and no attempt to distinguish between them, the quantity that is experimentally probed is the *untagged decay rate*:

$$\langle\Gamma(B_s(t) \to f)\rangle \equiv \Gamma(B_s^0(t) \to f) + \Gamma(\overline{B}_s^0(t) \to f), \tag{3.68}$$

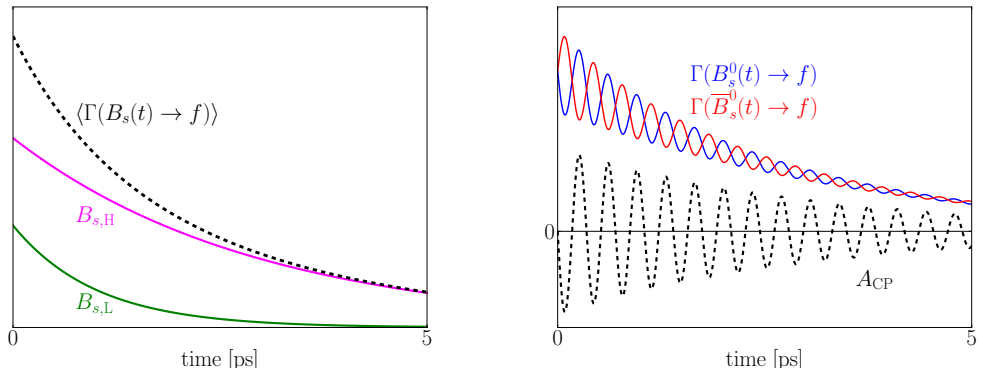

Figure 3.2: *Left panel:* illustration of the untagged decay rate $\langle\Gamma(B_s(t) \to f)\rangle$ as a sum of the mass-eigenstate exponential decay slopes. *Right panel:* illustration mixing-induced CP asymmetry $\mathcal{A}_{\mathrm{CP}}$ from flavour-tagging. Neither plot represents the Standard Model mixing parameters.

presuming both flavour states can decay to the final state f. The untagged decay rate can also be expressed in terms of the mass-eigenstates [79]

$$\begin{aligned}\langle\Gamma(B_s(t) \to f)\rangle &= \Gamma(B_{s,\mathrm{H}} \to f)\, e^{-\Gamma_{\mathrm{H}}\, t} + \Gamma(B_{s,\mathrm{L}} \to f)\, e^{-\Gamma_{\mathrm{L}}\, t} + \mathcal{O}(a_{\mathrm{SL}}) \\ &= [\Gamma(B_{s,\mathrm{H}} \to f) + \Gamma(B_{s,\mathrm{L}} \to f)] \\ &\quad \times\ e^{-t/\tau_{B_s}} \left\{\cosh\left(y_s\, t/\tau_{B_s}\right) + \sinh\left(y_s\, t/\tau_{B_s}\right)\, \mathcal{A}^f_{\Delta\Gamma}\right\} + \mathcal{O}(a_{\mathrm{SL}}), \quad (3.69)\end{aligned}$$

where

$$\mathcal{A}^f_{\Delta\Gamma} \equiv \frac{\Gamma(B_{s,\mathrm{H}} \to f) - \Gamma(B_{s,\mathrm{L}} \to f)}{\Gamma(B_{s,\mathrm{H}} \to f) + \Gamma(B_{s,\mathrm{L}} \to f)}, \quad (3.70)$$

is the *mass-eigenstate rate asymmetry*. Thus if the lifetimes of the two mass eigenstates differ, as we have observed they do, then a time-dependent analysis is sensitive not only to the total summed rate, $\Gamma(B_{s,\mathrm{H}} \to f) + \Gamma(B_{s,\mathrm{L}} \to f)$, but also to the mass-eigenstate rate asymmetry $\mathcal{A}^f_{\Delta\Gamma}$. This is illustrated in the left panel of Figure 3.2, where the untagged decay rate is shown as the sum of two exponential functions with different lifetimes and is thereby itself not an exponential function. The deviation of the untagged rate from a pure exponential is what is experimentally observable. It probes the parameters responsible: y_s and $\mathcal{A}^f_{\Delta\Gamma}$.

The mass eigenstate rate asymmetry $\mathcal{A}^f_{\Delta\Gamma}$ depends on the final state f and, as we will discuss below, is potentially sensitive to New Physics. By substituting (3.66) into (3.68) it follows that in terms of the convention independent parameter λ_f it is given by

$$\mathcal{A}^f_{\Delta\Gamma} = \frac{2\,\mathrm{Re}[\lambda_f]}{1 + |\lambda_f|^2} + \mathcal{O}(a_{\mathrm{SL}}). \quad (3.71)$$

For flavour-specific final states this asymmetry vanishes. In the absence of CP violation it takes a maximal value of ± 1 for CP eigenstate final states as we will discuss in Section 3.2.2.

If the B_s flavour states are distinguished at birth using *flavour-tagging*, then it is possible to construct the CP asymmetry:

$$\begin{aligned} A_{\rm CP} &\equiv \frac{\Gamma(B_s^0(t) \to f) - \Gamma(\overline{B}_s^0(t) \to f)}{\Gamma(B_s^0(t) \to f) + \Gamma(\overline{B}_s^0(t) \to f)} \\ &= \frac{C_f \cos(\Delta M_s\, t) + S_f \sin(\Delta M_s\, t)}{\cosh\left(y_s\, t/\tau_{B_s}\right) + \mathcal{A}^f_{\Delta\Gamma} \sinh\left(y_s\, t/\tau_{B_s}\right)}, \end{aligned} \tag{3.72}$$

where

$$C_f \equiv \frac{1 - |\lambda_f|^2}{1 + |\lambda_f|^2}, \qquad S_f \equiv \frac{2{\rm Im}[\lambda_f]}{1 + |\lambda_f|^2}, \tag{3.73}$$

and $\mathcal{A}^f_{\Delta\Gamma}$ is given in (3.71). From equations (3.71) and (3.73) it follows that the observables must satisfy the constraint[4]

$$|C_f|^2 + |S_f|^2 + |\mathcal{A}^f_{\Delta\Gamma}|^2 = 1. \tag{3.74}$$

In the right panel of Figure 3.2 we illustrate the oscillating time-dependent decay rates for the flavour states and the resulting asymmetry $A_{\rm CP}$. Note that it is not necessary for the final state f to be a CP eigenstate final state. In Section 4.3 we discuss such an example. Next we consider CP eigenstate final states.

3.2.2 CP-eigenstate final states

Let us consider a general final state f which is a CP eigenstate with eigenvalue η_f such that

$$\mathcal{CP}|f\rangle = \eta_f |f\rangle. \tag{3.75}$$

In this case the observable C_f defined in (3.73) is equal to the *direct* CP violation present in the $B_s \to f$ decay mode:

$$C_f = \frac{\Gamma(B_s^0 \to f) - \Gamma(\overline{B}_s^0 \to f)}{\Gamma(B_s^0 \to f) + \Gamma(\overline{B}_s^0 \to f)} \equiv \mathcal{A}^{\rm dir}_{\rm CP}(B_s \to f). \tag{3.76}$$

Given this context, the observable S_f can then be denoted $\mathcal{A}^{\rm mix}_{\rm CP}(B_s \to f)$ to indicate that it probes *mixing-induced* CP violation.

[4]By defining the mass-eigenstate rate asymmetry as in (3.70) this constraint is technically only valid up to $\mathcal{O}(a_{\rm SL})$ corrections.

Finding strategies to determine the B_s mixing phase ϕ_s is a central goal of this thesis. To this end it is convenient to introduce the parameter $\Delta\phi_f$ representing the phase shift to ϕ_s coming from the decay amplitudes. To be precise, we define

$$\Delta\phi_f \equiv \arg\left(\eta_f \frac{\langle f|\mathcal{H}|B_s^0\rangle}{\langle f|\mathcal{H}|\overline{B}_s^0\rangle}\right) - \xi_{B_s} - \xi_s + \xi_b. \tag{3.77}$$

We may then rewrite (3.65) as

$$\lambda_f = -\eta_f \sqrt{\frac{1-C_f}{1+C_f}}\, e^{-i(\phi_s+\Delta\phi_f)}, \tag{3.78}$$

and consequently [81]

$$\mathcal{A}^f_{\Delta\Gamma} = -\eta_f \sqrt{1-C_f}\,\cos(\phi_s+\Delta\phi_f), \tag{3.79}$$

$$\mathcal{S}_f = \eta_f \sqrt{1-C_f}\,\sin(\phi_s+\Delta\phi_f). \tag{3.80}$$

In the Standard Model we can use the unitarity of the CKM matrix to express the amplitude for a $B_s^0 \to f$ decay in terms of two components with different CP violating phases:

$$\langle f|\mathcal{H}|B_s^0\rangle = A_1^f e^{i\delta_1^f} e^{i\varphi_1^f} + A_2^f e^{i\delta_2^f} e^{i\varphi_2^f}. \tag{3.81}$$

Here $A^f_{1,2}$ and $\delta^f_{1,2}$ represent CP conserving strong amplitudes and their accompanying phases, whereas $\varphi^f_{1,2}$ are CP violating weak phases originating from the CKM matrix. We thus have

$$\begin{aligned}\frac{\langle f|\mathcal{H}|\overline{B}_s^0\rangle}{\langle f|\mathcal{H}|B_s^0\rangle} &= \frac{\langle f|\mathcal{CP}^{-1}\,\mathcal{CP}\,\mathcal{H}\,\mathcal{CP}^{-1}\,\mathcal{CP}|\overline{B}_s^0\rangle}{\langle f|\mathcal{H}|B_s^0\rangle} \\ &= \eta_f e^{i(\xi_{B_s}+\xi_s-\xi_b)}\left[\frac{e^{-i\varphi_1^f} + h_f e^{i\delta_f} e^{-i\varphi_2^f}}{e^{i\varphi_1^f} + h_f e^{i\delta_f} e^{i\varphi_2^f}}\right],\end{aligned} \tag{3.82}$$

where

$$h_f e^{i\delta_f} \equiv \frac{A_2^f}{A_1^f} e^{i(\delta_2^f-\delta_1^f)}. \tag{3.83}$$

In this notation the direct CP asymmetry of the $B_s \to f$ decay becomes:

$$C_f = \frac{2\,h_f \sin\delta_f \sin(\varphi_1^f-\varphi_2^f)}{1+2h_f\cos\delta_f\cos(\varphi_1^f-\varphi_2^f)+h_f^2}. \tag{3.84}$$

Thus for a B_s decay mode to exhibit direct CP violation, it must have at least two contributing decay topologies with different strong phases. The phase shift $\Delta\phi_f$ is given

by [81, 82]

$$\sin\Delta\phi_f = \frac{\sin 2\varphi_1^f + 2h_f\cos\delta_f\sin(\varphi_1^f+\varphi_2^f) + h_f^2\sin 2\varphi_2^f}{\sqrt{1-C_f^2}\left(1+2h_f\cos\delta_f\cos(\varphi_1^f-\varphi_2^f)+h_f^2\right)}, \tag{3.85}$$

$$\cos\Delta\phi_f = \frac{\cos 2\varphi_1^f + 2h_f\cos\delta_f\cos(\varphi_1^f+\varphi_2^f) + h_f^2\cos 2\varphi_2^f}{\sqrt{1-C_f^2}\left(1+2h_f\cos\delta_f\cos(\varphi_1^f-\varphi_2^f)+h_f^2\right)}, \tag{3.86}$$

or more compactly as

$$\Delta\phi_f = \tan^{-1}\left[\frac{\sin 2\varphi_1^f + 2h_f\cos\delta_f\sin(\varphi_1^f+\varphi_2^f) + h_f^2\sin 2\varphi_2^f}{\cos 2\varphi_1^f + 2h_f\cos\delta_f\cos(\varphi_1^f+\varphi_2^f) + h_f^2\cos 2\varphi_2^f}\right]. \tag{3.87}$$

The twofold ambiguity for $\Delta\phi_f$ arising from the latter expression can be resolved using sign information from $\sin\Delta\phi_f$ or $\cos\Delta\phi_f$.

3.3 Effective lifetimes

3.3.1 Single exponential fit

An *effective lifetime* for a B_s decay mode is obtained in practice by fitting a single exponential function to its untagged rate. As an untagged rate is in general described by two exponentials, corresponding to two mass-eigenstates with different lifetimes, the single exponential fit is an approximation. Nonetheless, it is possible to derive an analytic expression for this fitted effective lifetime, which we will denote τ_f. To this end we follow the appendix of Ref. [83].

Let the untagged rate be the *true* Probability Distribution Function (PDF), and the single exponent function the *fitted* PDF, such that

$$f_{\text{true}}(t) \equiv \frac{A(t)\,\langle\Gamma(B_s(t)\to f)\rangle}{\int_0^\infty A(t)\,\langle\Gamma(B_s(t)\to f)\rangle\,dt}, \tag{3.88}$$

$$f_{\text{fit}}(t;\tau_f) \equiv \frac{A(t)\,e^{-t/\tau_f}}{\int_0^\infty A(t)\,e^{-t/\tau_f}\,dt}, \tag{3.89}$$

where $A(t)$ is an acceptance efficiency function. The likelihood or χ^2 function for the fit in question is then built using the above PDFs, and maximised or minimised, respectively, in the limit of infinitesimally spaced bins. Specifically, for n events the following functions are minimised:

$$-\log L(\tau_f) = -n\int_0^\infty dt\; f_{\text{true}}(t)\log\left[f_{\text{fit}}(t;\tau_f)\right], \tag{3.90}$$

$$\chi^2(\tau_f) = n\int_0^\infty dt\,\frac{\left[f_{\text{true}}(t)-f_{\text{fit}}(t;\tau_f)\right]^2}{f_{\text{fit}}(t;\tau_f)}, \tag{3.91}$$

for a maximum likelihood and a least squares fit, respectively. In a modified least squares fit, where data is used to estimate the error, the denominator in the χ^2 integrand should be replaced by $f_{\rm true}(t)$. For the maximum likelihood fit, taking the infinitesimal bin limit is equivalent to an unbinned fit.

The effective lifetime τ_f resulting from these fits is then given implicitly by the formula:

$$\frac{\int_0^\infty t\, e^{-t/\tau_f}\, A(t)\, dt}{\int_0^\infty e^{-t/\tau_f}\, A(t)\, dt} = \frac{\int_0^\infty t\, g(t;\tau_f) A(t)\, dt}{\int_0^\infty g(t;\tau_f) A(t)\, dt}, \tag{3.92}$$

where

$$g(t;\tau_f) \equiv \begin{cases} \langle\Gamma(t)\rangle & : \text{ maximum likelihood} \\ \langle\Gamma(t)\rangle^2\, e^{\,t/\tau_f} & : \text{ least squares} \\ \langle\Gamma(t)\rangle^{-1}\, e^{-2\,t/\tau_f} & : \text{ modified least squares.} \end{cases}$$

If the untagged rate is taken to be a single exponential, then all fits agree and give the correct lifetime.

If we assume a trivial acceptance function $A(t) = 1$ then a maximum likelihood fit of the untagged rate returns the conventional definition of the *effective lifetime* [84]:

$$\tau_f = \frac{\int_0^\infty t\, \langle\Gamma(B_s(t) \to f)\rangle\, dt}{\int_0^\infty \langle\Gamma(B_s(t) \to f)\rangle\, dt} = \frac{\Gamma(B_{s,\rm H} \to f)/\Gamma_{\rm H}^2 + \Gamma(B_{s,\rm L} \to f)/\Gamma_{\rm L}^2}{\Gamma(B_{s,\rm H} \to f)/\Gamma_{\rm H} + \Gamma(B_{s,\rm L} \to f)/\Gamma_{\rm L}} \tag{3.93}$$

The final expression was first presented in Ref. [85]. In terms of the mass-eigenstate rate asymmetry this effective lifetime is given, relative to the B_s mean lifetime, by

$$\begin{aligned} \frac{\tau_f}{\tau_{B_s}} &= \frac{1}{1-y_s^2}\left(\frac{1 + 2\mathcal{A}^f_{\Delta\Gamma}\, y_s + y_s^2}{1 + \mathcal{A}^f_{\Delta\Gamma}\, y_s}\right) \\ &= 1 + \mathcal{A}^f_{\Delta\Gamma}\, y_s + \left[2 - (\mathcal{A}^f_{\Delta\Gamma})^2\right] y_s^2 + \mathcal{O}(y_s^3). \end{aligned} \tag{3.94}$$

A measurement of the effective lifetime for a $B_s \to f$ decay thereby effectively probes the combination $\mathcal{A}^f_{\Delta\Gamma}\, y_s$. In Section 3.5 we briefly discuss the consequences of non-trivial acceptance function.

3.3.2 Lifetime contours in the ϕ_s–$\Delta\Gamma_s$ plane

The effective lifetime relates the parameters y_s and $\mathcal{A}^f_{\Delta\Gamma}$. As the latter parameter is potentially sensitive to the B_s mixing phase ϕ_s, an effective lifetime measurement can give a contour in the ϕ_s–$\Delta\Gamma_s$ plane. This section is based on the work presented in Ref. [82]. Let us take a closer look at (3.94), which we can write as the following cubic equation for the real parameter y_s:

$$y_s^3 + a_2 y_s^2 + a_1 y_s + a_0 = 0, \tag{3.95}$$

where

$$a_0 \equiv \frac{\tau_{B_s} - \tau_f}{\tau_f \mathcal{A}^f_{\Delta\Gamma}}, \quad a_1 \equiv \frac{2\,\tau_{B_s} - \tau_f}{\tau_f}, \quad a_2 \equiv \frac{\tau_{B_s} + \tau_f}{\tau_f \mathcal{A}^f_{\Delta\Gamma}}. \tag{3.96}$$

In order to solve this cubic equation, it is useful to rewrite it in the reduced form

$$\left(y_s + \frac{a_2}{3}\right)^3 + P\left(y_s + \frac{a_2}{3}\right) + Q = 0 \tag{3.97}$$

with

$$P \equiv a_1 - \frac{a_2^2}{3}, \quad Q \equiv \frac{2a_2^3}{27} - \frac{a_2 a_1}{3} + a_0. \tag{3.98}$$

Applying Cardano's formula then yields the solutions

$$y_s = -\frac{a_2}{3} + e^{i\omega}\sqrt[3]{R + \sqrt{D}} + e^{-i\omega}\sqrt[3]{R - \sqrt{D}} \tag{3.99}$$

with $\omega \in \{0, 2\pi/3, -2\pi/3\}$, where

$$R \equiv -\frac{Q}{2} = \frac{1}{54}\left(9\,a_1\,a_2 - 27\,a_0 - 2\,a_2^3\right) \tag{3.100}$$

$$D \equiv \left(\frac{P}{3}\right)^3 + \left(\frac{Q}{2}\right)^2 = \frac{1}{108}\left(27\,a_0^2 - 18\,a_0\,a_1\,a_2 + 4\,a_0\,a_2^3 + 4\,a_1^3 - a_1^2 a_2^2\right). \tag{3.101}$$

For $\mathcal{A}^f_{\Delta\Gamma} = 0$, this solution is not valid as (3.94) is then a quadratic equation in y_s. Furthermore, the above expressions may prove cumbersome to use in practice. A convenient approximate solution is obtained by solving the expansion in (3.94) up to quadratic order in y_s:

$$y_s \approx -\frac{1}{2}\left[\frac{\mathcal{A}^f_{\Delta\Gamma}}{2 - (\mathcal{A}^f_{\Delta\Gamma})^2}\right] \pm \frac{1}{2}\sqrt{\left[\frac{\mathcal{A}^f_{\Delta\Gamma}}{2 - (\mathcal{A}^f_{\Delta\Gamma})^2}\right]^2 + \frac{4}{\tau_{B_s}}\left[\frac{\tau_f - \tau_{B_s}}{2 - (\mathcal{A}^f_{\Delta\Gamma})^2}\right]}. \tag{3.102}$$

This quadratic solution agrees very well with the corresponding branches of the exact solution (3.99) in the numerical analyses that we will consider.

For illustration we consider two B_s decays to CP eigenstates, $B_s \to f_+$ and $B_s \to f_-$, with positive and negative CP eigenvalues, respectively. Further, we assume no CP violation in these decay modes, so that

$$h_{f_\pm} = 0, \quad \varphi_1^{f_\pm} = 0 \tag{3.103}$$

for these decays, yielding $C_{f_\pm} = 0$ and $\Delta\phi_{f_\pm} = 0$. In Fig. 3.3, we show the lifetime constraints that are compatible with the theoretical SM calculation of $\Delta\Gamma_s$ given in (3.43). Using the B_s mean lifetime given in (3.53) results in the SM effective lifetimes $\tau_{f_+} = 1.42\,\text{ps}$ and $\tau_{f_-} = 1.62\,\text{ps}$. The difference in behaviour for CP-odd and CP-even

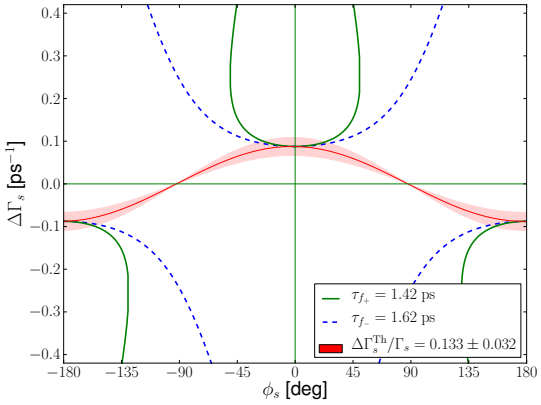

Figure 3.3: Illustration of the lifetimes that are compatible with the SM value of $\Delta\Gamma_s/\Gamma_s$ given in (3.43) for CP-even and CP-odd final states f_+ and f_-, respectively. The decay amplitudes are assumed to have no CP-violating phases. We also show the constraint from the theoretical value of $\Delta\Gamma_s^{\rm Th}/\Gamma_s$ given in (3.43), as discussed in the text.

eigenstates is due to the non-linear dependence on y_s in (3.94). Said differently, if (3.94) is expanded and only terms up to linear order in y_s are kept, the two curves in Fig. 3.3 would overlap. In Fig. 3.3, we have also included the theoretical constraint given in (3.45).

The formalism developed above is also valid for non-CP eigenstates provided the final state is accessible to both B_s^0 and $\bar{B}_s^0$ so that mixing is possible. Examples of such states are $B_s \to D_s K^{(*)}$, which we will study in Chapter 4. For these decays the CP eigenvalue η_f in (3.79) should be replaced by $(-1)^L$, where L denotes the relative orbital angular momentum of the decay products [86].

3.4 Branching ratios

The sizable decay width difference of the B_s meson system has a subtle but important effect on how a B_s branching ratio is defined, which we will address in this section. To this end, we will follow the work presented in Ref. [83].

At hadron colliders a B_s branching ratio to a specific final state f is measured by counting all untagged events over the accessible decay time, and normalizing this count against a known branching ratio measured at a B-factory. It is therefore defined with respect to the untagged time-dependent rate given in (3.69) as [79, 83]

$$\overline{\rm BR}(B_s \to f) \equiv \frac{1}{2}\int_0^\infty \langle \Gamma(B_s(t) \to f)\rangle \, dt = \frac{1}{2}\left[\frac{\Gamma(B_{s,\rm H} \to f)}{\Gamma_{\rm H}} + \frac{\Gamma(B_{s,\rm L} \to f)}{\Gamma_{\rm L}}\right]. \quad (3.104)$$

This definition gives the average branching ratio of the two mass eigenstates.

From a theoretical perspective, squared amplitudes for $B_s \to f$ transitions are customarily computed in the flavour basis rather than the mass eigenstate basis. However, the lifetime of a non-mass eigenstate is not well defined, so instead the mean B_s lifetime τ_{B_s}, defined in (3.19), is substituted. This leads to the following definition for a B_s branching ratio:

$$\begin{aligned}\mathrm{BR}(B_s \to f) \equiv \frac{\tau_{B_s}}{2} \left\langle \Gamma(B_s(t) \to f) \right\rangle\big|_{t=0} &= \frac{1}{2}\left[\frac{\Gamma(B_s^0(t) \to f)\big|_{t=0}}{\frac{1}{2}(\Gamma_\mathrm{H}+\Gamma_\mathrm{L})} + \frac{\Gamma(\overline{B}_s^0(t) \to f)\big|_{t=0}}{\frac{1}{2}(\Gamma_\mathrm{H}+\Gamma_\mathrm{L})}\right] \\ &= \frac{1}{2}\left[\frac{\Gamma(B_{s,\mathrm{H}} \to f)}{\frac{1}{2}(\Gamma_\mathrm{H}+\Gamma_\mathrm{L})} + \frac{\Gamma(B_{s,\mathrm{L}} \to f)}{\frac{1}{2}(\Gamma_\mathrm{H}+\Gamma_\mathrm{L})}\right], \end{aligned} \tag{3.105}$$

where the last equality can be directly compared to (3.104).

We observe that if $\Gamma_\mathrm{H} = \Gamma_\mathrm{L}$ the definitions in (3.104) and (3.105) are equivalent. This is effectively the case for B_d meson system, where $y_d \approx 0$ as given in (3.54). In the B_s meson system, however, it has been experimentally established in (3.49) that y_s is non-zero. Thus in this case it becomes necessary to be able to convert between the theoretical and experimental definitions. The dictionary to convert between these definitions is compactly given by

$$\overline{\mathrm{BR}}(B_s \to f) = \mathrm{BR}(B_s \to f)\left[\frac{1 + y_s\, \mathcal{A}^f_{\Delta\Gamma}}{1 - y_s^2}\right]. \tag{3.106}$$

We see that the required correction depends on the final state specific quantity $\mathcal{A}^f_{\Delta\Gamma}$. This quantity can either be extracted from a time-dependent measurement (such as an effective lifetime as we discuss in the previous section) or computed theoretically. In Figure 3.4 we show the dictionary for various values of $\mathcal{A}^f_{\Delta\Gamma}$.

The effective lifetime can be substituted into the branching ratio dictionary (3.106) to give

$$\mathrm{BR}(B_s \to f) = \overline{\mathrm{BR}}(B_s \to f)\left[2 - (1 - y_s^2)\frac{\tau_f^f}{\tau_{B_s}}\right]. \tag{3.107}$$

In this form the theoretical branching ratio is expressed entirely in terms of measurable quantities.

Another application is given by B_s transitions into two vector mesons, such as $B_s \to J/\psi\phi$, $B_s \to K^{*0}\bar{K}^{*0}$ and $B_s \to D_s^{*+}D_s^{*-}$. Here an angular analysis of the decay products of the vector mesons has to be performed to disentangle the CP-even and CP-odd final states, which affects the branching fraction determination in a subtle way, as recognized in Refs. [87, 88]. Expressing the vector mesons by their linear polarization states, the decay amplitude can be described in a *transversity basis* [89]. This basis, which we label with the index k, consists of longitudinal ($k = 0$) and parallel ($k = \|$) component amplitudes that are CP even, $\eta_k = +1$, and of a perpendicular component ($k = \perp$) that

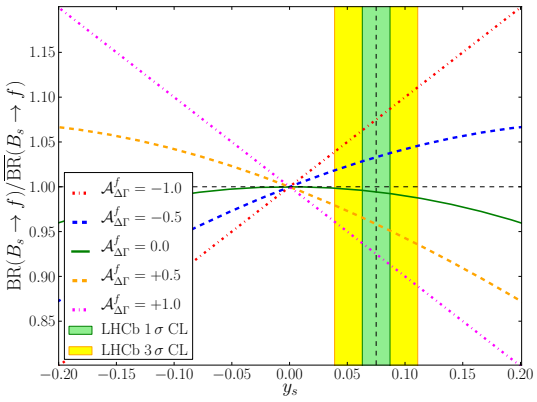

Figure 3.4: Illustration of Eq. (3.106) for various values of $\mathcal{A}^f_{\Delta\Gamma}$. We also show the current LHCb measurement of y_s [76].

is CP odd, $\eta_k = -1$. The generalization of Eq. (3.106) is then given by

$$\mathrm{BR}^{VV} = \left(1 - y_s^2\right) \left[\sum_{k=0,\|,\perp} \frac{\overline{f}_{VV,k}}{1 + y_s \mathcal{A}^{VV,k}_{\Delta\Gamma}}\right] \overline{\mathrm{BR}}^{VV}, \tag{3.108}$$

where $\overline{f}_{VV,k} = \overline{\mathrm{BR}}^{VV,k}/\overline{\mathrm{BR}}^{VV}$ and $\overline{\mathrm{BR}}^{VV} \equiv \sum_k \overline{\mathrm{BR}}^{VV,k}$ so that $\sum_k \overline{f}_{VV,k} = 1$. As discussed in Ref. [82], assuming the SM structure for the decay amplitudes, we can write

$$\mathcal{A}^{VV,k}_{\Delta\Gamma} = -\eta_k \sqrt{1 - C^2_{VV,k}} \cos(\phi_s + \Delta\phi_{VV,k}), \tag{3.109}$$

where $C_{VV,k}$ describes direct CP violation and $\Delta\phi_{VV,k}$ is a non-perturbative hadronic phase shift. In Ref. [87] these expressions are given for the decay $B_s \to K^{*0}\bar{K}^{*0}$ at leading order in y_s, assuming $\phi_s = 0$ and negligible hadronic corrections. The generalization of Eq. (3.107) is given by

$$\mathrm{BR}^{VV} = \overline{\mathrm{BR}}^{VV} \sum_{k=0,\|,\perp} \left[2 - \left(1 - y_s^2\right) \frac{\tau^{VV}_k}{\tau_{B_s}}\right] \overline{f}_{VV,k}, \tag{3.110}$$

and does not require knowledge of the $\mathcal{A}^{VV,k}_{\Delta\Gamma}$ observables.

3.5 Experimental considerations

Additional subtleties arise in the experimental determination of B_s branching ratios and effective lifetimes, in particular at a hadron collider environment where many final-state particles are produced in the fragmentation. It is the purpose of this section to

conceptually sketch some of the experimental issues that arise due to a non-zero B_s decay width difference and the associated mass-eigenstate rate asymmetry $\mathcal{A}^f_{\Delta\Gamma}$. In practice these effects are much more complicated to properly account for.

At hadron collider experiments the separation of B_s signal decays from the background is typically based on the flight distance of the B_s meson or the impact parameter of its decay products, which leads to a decay-time dependent acceptance efficiency. By rejecting short-lived B_s meson candidates, the relative amounts of $B_{s,\mathrm{L}}$ and $B_{s,\mathrm{H}}$ mesons in the remaining data sample change. As a result the branching ratio or effective lifetime determinations are biased.

To illustrate this bias we consider a toy acceptance function, namely the step function

$$A(t) = \theta(t - t_{\min})(1 - \theta(t - t_{\max})), \tag{3.111}$$

with $t_{\min} = 0.5$ ps and $t_{\max} = 15$ ps. In the left panel of Figure 3.5 we show the deviation that results between a maximum likelihood fit of the effective lifetime with this acceptance versus its ideal functional dependence given in (3.93). We observe that the resulting error for this exaggerated acceptance function is only of the order of 0.1%.

A hadron collider environment is too messy to account for all B_s decay events. Therefore an experimental B_s branching ratio is measured relative to another branching ratio, whose value is known from B–factory experiments. Specifically, an experiment measures the ratio

$$\frac{\overline{\mathrm{BR}}(B_s \to f)_{\mathrm{meas}}}{\overline{\mathrm{BR}}(B_{s,d} \to f')_{\mathrm{meas}}} \equiv \frac{\int_0^\infty A(t)\langle\Gamma(B_s(t) \to f)\rangle\, dt}{\int_0^\infty A'(t)\langle\Gamma(B_{s,d}(t) \to f')\rangle\, dt}, \tag{3.112}$$

where $B_{s,d} \to f'$ is a decay with a known branching ratio $\overline{\mathrm{BR}}(B_{s,d} \to f')$, and $A^{(\prime)}(t)$ are the acceptance functions of the decays in question. An extraction of the experimental branching ratio

$$\overline{\mathrm{BR}}(B_s \to f) = \left(\frac{\epsilon^{f'}_{s,d}}{\epsilon^f_s}\right) \frac{\overline{\mathrm{BR}}(B_s \to f)_{\mathrm{meas}}}{\overline{\mathrm{BR}}(B_{s,d} \to f')_{\mathrm{meas}}} \overline{\mathrm{BR}}(B_{s,d} \to f'), \tag{3.113}$$

thus requires an estimate of the efficiency ratio $\epsilon^{f'}_{s,d}/\epsilon^f_s$, where

$$\epsilon^f_{s,d} \equiv \frac{\int_0^\infty A(t)\,\langle\Gamma(B_{s,d}(t) \to f)\rangle\, dt}{\int_0^\infty \langle\Gamma(B_{s,d}(t) \to f)\rangle\, dt}. \tag{3.114}$$

A good choice for the reference decay $\overline{\mathrm{BR}}(B_{s,d} \to f')$ is one with a similar acceptance efficiency to the considered decay. However, ϵ_s retains an a priori unknown dependence on $\mathcal{A}^f_{\Delta\Gamma}$. In the right panel of Figure 3.5 we show for illustration the bias that is introduced if a B_d decay is chosen for the reference decay, assuming the same acceptance function for both decays is given by (3.111) and, for example, a Standard Model estimate of $\mathcal{A}^f_{\Delta\Gamma} = 0$. In this scenario the error can be as large as $\pm 3\%$ if in fact $\mathcal{A}^f_{\Delta\Gamma} = \pm 1$.

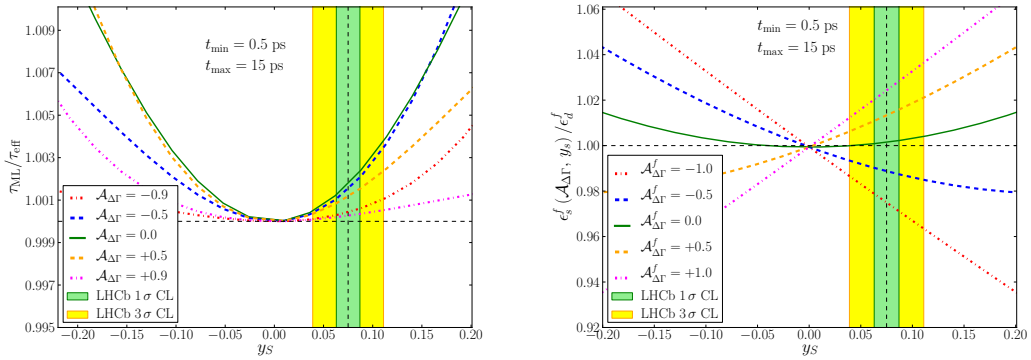

Figure 3.5: The effect of a non-trivial acceptance efficiency on effective lifetime (left panel) and branching ratio (right panel) determinations. See discussion in text.

It is also worth briefly considering the effect of a B_s production asymmetry on both the effective lifetime and branching ratio of $B_s \to f$ decay. This asymmetry is expected to be about 1% at the LHC [90]. Let us define this asymmetry as

$$\mathcal{A}_{\rm prod} = \frac{N_{B_s^0} - N_{\overline{B}_s^0}}{N_{B_s^0} + N_{\overline{B}_s^0}}, \tag{3.115}$$

where $N_{B_s^0}$ and $N_{\overline{B}_s^0}$ are the number of produced B_s^0 and $\overline{B}_s^0$ mesons at a given experiment. It then follows that the time-dependent untagged decay rate defined in (3.68) should be modified to

$$\langle \tilde{\Gamma}(B_s(t) \to f) \rangle \equiv [1 + \mathcal{A}_{\rm prod}]\, \Gamma(B_s^0(t) \to f) + [1 - \mathcal{A}_{\rm prod}]\, \Gamma(\overline{B}_s^0(t) \to f), \tag{3.116}$$

where we denote this modification with tilde. This gives

$$\begin{aligned} \langle \tilde{\Gamma}(B_s(t) \to f) \rangle = {} & [\Gamma(B_{s,\rm H} \to f) + \Gamma(B_{s,\rm L} \to f)] \\ & \times\ e^{-t/\tau_{B_s}} \Big\{ \cosh\left(y_s\, t/\tau_{B_s}\right) + \sinh\left(y_s\, t/\tau_{B_s}\right)\, \mathcal{A}^f_{\Delta\Gamma} \\ & + \left[\cos(\Delta M_s\, t)\, C_f + \sin(\Delta M_s\, t)\, S_f\right] \mathcal{A}_{\rm prod} \Big\} + \mathcal{O}(a_{\rm SL}). \end{aligned} \tag{3.117}$$

The modified branching ratio is given by

$$\begin{aligned} \frac{\overline{\rm BR}(B_s(t) \to f)\big|_{\rm prod}}{\overline{\rm BR}(B_s(t) \to f)} &= 1 + \mathcal{A}_{\rm prod} \left(\frac{1 - y_s^2}{1 + y_s\, \mathcal{A}^f_{\Delta\Gamma}} \right) \left(C_f\, \frac{1}{1 + x_s^2} + S_f\, \frac{x_s}{1 + x_s^2} \right) \\ &= 1 + \mathcal{A}_{\rm prod} (1 + y_s\, \mathcal{A}^f_{\Delta\Gamma} - y_s^2)\, \frac{1}{x_s}\, S_f + \mathcal{O}(x_s^{-2}, y_s^3). \end{aligned} \tag{3.118}$$

where $x_s \equiv \tau_{B_s}\Delta M_s = 26.9 \pm 0.2$ using the inputs from (3.41) and (3.53). Similarly, the measured effective lifetime, assuming a trivial acceptance function, is given by

$$\frac{\tau_f\big|_{\text{prod}}}{\tau_f} = 1 - \mathcal{A}_{\text{prod}}(1 + y_s\,\mathcal{A}^f_{\Delta\Gamma} - y_s^2)\,\frac{1}{x_s}\,S_f + \mathcal{O}(x_s^{-2}, y_s^3). \tag{3.119}$$

The suppression by the factor $1/x_s$ can be intuitively attributed to the very rapid oscillations of the B_s flavour states, which have little influence when integrated over large time-scales. At leading order, a production asymmetry of 1% and a maximal mixing-induced CP violation of $|S_f| = 1$ would result in a deviation of 0.4% for both the branching ratio and the effective lifetime. For a very precise effective lifetime measurement this error may be relevant. However, for the effective lifetime measurements we consider in this thesis, the Standard Model predictions for S_f are close to zero, thereby suppressing the effect even further.

Chapter 4

Extracting CKM angles from penguins or trees

4.1 Introduction

In this chapter we consider various strategies, involving two different B_s decay modes, for determining the angle γ of the unitary triangle (see the left panel of Figure 2.2). Namely, we will consider strategies involving the time-dependent analyses of the decay modes $B_s \to K^+K^-$ and $B_s \to D_s^{(*)}K$ in Sections 4.2 and 4.3, respectively. In the first decay mode QCD penguin topologies play a dominant role, whereas the second mode is governed only by tree topologies. The former mode, in contrast to the latter, is thereby also sensitive to possible New Physics effects that can enter virtually via loops. Furthermore, a time-dependent analysis of the latter mode, as we will discuss, is theoretically clean. It will therefore be interesting to eventually be able to compare both results for γ.

The final state K^+K^- is a CP-eigenstate, which means both the B_s^0 and $\overline{B}_s^0$ mesons can decay to it. The latter also holds for the final states $D_s^{\pm(*)}K^{\mp}$, even though they are not CP-eigenstates. As a result both decay modes are sensitive to B_s^0–$\overline{B}_s^0$ mixing phase ϕ_s as discussed in Section 3.1. In fact, in the $B_s \to D_s^{(*)}K$ case it is the combination $\phi_s + \gamma$ that can be extracted. An optimal determination of γ using either mode will therefore require an accurate measurement of ϕ_s. Considering the recent progress of determining ϕ_s with the decay mode $B_s \to J/\psi\phi$ as given in (3.48), this should be achievable. In Chapter 5 we will also explore the potential of other $B_s \to J/\psi\, s\bar{s}$ modes for measuring the phase ϕ_s.

For both the $B_s \to K^+K^-$ and $B_s \to D_s^{(*)}K$ decay modes we can utilise U-spin symmetry, as introduced in Section 2.4, to relate them to B_d decays whose observables have been measured. The U-spin relation of the $B_s \to K^+K^-$ mode to the $B_s \to \pi^+\pi^-$ mode is in fact crucial for controlling hadronic parameters and extracting γ. The optimal determination, involving the time-dependent CP asymmetries of both modes, requires

knowledge of both mixing phases ϕ_d and ϕ_s, as we already mentioned. However, we will also consider strategies where we employ only the time-integrated branching ratio from the $B_s \to K^+K^-$ mode. As a result we may reverse our method, and use the time-dependent observables of $B_s \to K^+K^-$ to probe the mixing phase ϕ_s. The U-spin relation of the $B_s \to D_s^{\pm(*)}K^{\mp}$ modes to their $B_d \to D^{\pm(*)}\pi^{\mp}$ counterparts can be used to predict the observables of the former in the Standard Model.

In this chapter we will in particular point out the utility of effective lifetimes, as discussed in Section 3.3, for measuring the CKM angles and probing New Physics. The effective lifetime of the $B_s \to K^+K^-$ mode for instance can give a contour in the ϕ_s–$\Delta\Gamma_s$ plane. For the $B_s \to D_s^{(*)}K$ modes the mass-eigenstate rate asymmetries, which are probed by effective lifetimes, can resolve the discrete ambiguities in determining $\phi_s + \gamma$.

4.2 Extracting γ with penguin topologies: $B_s \to K^+K^-$

The topologies of $B_s^0 \to K^+K^-$ are shown in Figure 4.1. This decay mode has the feature that its tree topologies, labeled *current-current* in the figure, are doubly Cabibbo suppressed with respect to the penguin topologies. Therefore the QCD penguins dominate this decay. As already mentioned in the introduction, this decay is related by the U-spin symmetry of strong interactions to the decay $B_d \to \pi^+\pi^-$. A major difference between these two decay modes is that for the latter decay the tree topologies do not receive a relative double Cabibbo suppression.

The novel feature of the U-spin relation under consideration with respect to other $SU(3)_{\rm F}$ flavour symmetry strategies is that there is a complete mapping of topologies i.e. there are no residual topologies present in either decay that must be explained away by invoking dynamical assumptions. Also the electroweak penguins are invariant under U-spin, in contrast to the isospin and V-spin subgroups.

In Ref. [91] a strategy for determining the angle γ was proposed using this U-spin pair of decays. This was developed upon further in Ref. [92] in light of new experimental results, including a discussion of U-spin breaking tests. The work to be presented in this section is based on Ref. [84]. We take an updated look at the extraction of γ given new CP asymmetry measurements for both decay modes, as well as an updated form factor ratio that enters the U-spin analysis.

It is unfortunately still too early to perform the optimal determination of γ presented in Ref. [92]. However, we do perform a first determination using other U-spin related inputs and find a remarkable agreement with complementary methods. The main new feature we present is the utility of a time-dependent untagged $B_s \to K^+K^-$ measurement, specifically in the form of an effective lifetime, to probe New Physics in B_s^0–$\overline{B}_s^0$ mixing. We provide Standard Model predictions for this observable, as well as for the tagged time-dependent CP observables, which turn out to be quite robust with respect to U-spin breaking errors.

The outline of this section is as follows: in Section 4.2.1 we present the relevant

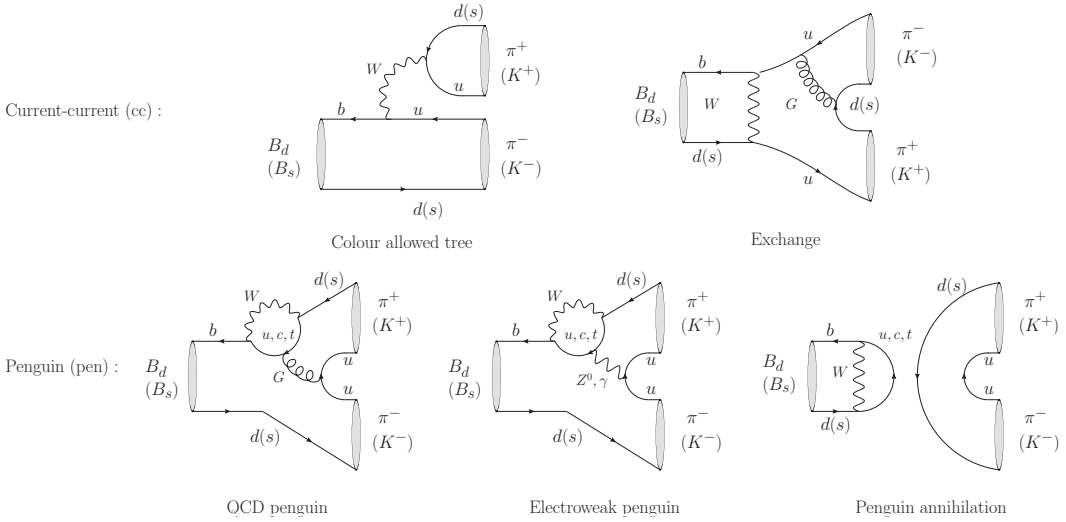

Figure 4.1: Current-current and penguin diagrams contributing to $B_d \to \pi^+\pi^-$ and $B_s \to K^+K^-$ decays.

amplitudes of the decay modes in question and in Section 4.2.2 we discuss the determination of γ arising from the current data. In Section 4.2.3, we calculate the effective lifetime $\tau_{K^+K^-}$ and study its correlation with the CP-violating B_s^0–$\bar{B}_s^0$ mixing phase. A similar analysis is performed for the mixing-induced CP asymmetry of $B_s^0 \to K^+K^-$ in Section 4.2.4. In Section 4.2.5, we discuss and illustrate the optimal determination of γ using the CP asymmetries of $B_s \to K^+K^-$. Finally, we summarize our conclusions in Section 4.4.

4.2.1 Amplitudes

In the Standard Model the $B_s \to K^+K^-$ and $B_d \to \pi^+\pi^-$ decays are governed by the tree and penguin topologies shown in Figure 4.1. We observe that the former is related to the latter by an interchange of s with d quarks. In terms of the strong QCD dynamics contributing to these decay topologies an invariance under such an interchange would imply a U-spin symmetry as defined in Section 2.4. Of course, because the s and d quarks are not degenerate in mass, U-spin symmetry is only an approximate symmetry.

In order to utilise the U-spin symmetry we should first extract the CKM elements entering each topology for both decays, as charged weak interactions badly break this symmetry. To this end we define the CKM parameters

$$\lambda_j^{(q)} \equiv V_{jq}V_{jb}^*, \tag{4.1}$$

for $j \in \{u, c, t\}$ and $q \in \{d, s\}$. We may thus write the general amplitude as

$$A(B_q \to U_q \bar{U}_q) = \lambda_u^{(q)} A_{\rm cc}^{u,(q)} + \sum_j^{\{u,c,t\}} \lambda_j^{(q)} A_{\rm pen}^{j,(q)}, \tag{4.2}$$

where $U_d \equiv \pi^-$ and $U_s \equiv K^-$. The unitarity of the CKM matrix implies

$$\lambda_t^{(q)} = -\lambda_c^{(q)} - \lambda_u^{(q)}, \tag{4.3}$$

and thus

$$A(B_q \to U_q \bar{U}_q) = \left(A_{\rm cc}^{u,(q)} + A_{\rm pen}^{ut,(q)}\right) \lambda_u^{(q)} \left(1 + \frac{\lambda_c^{(q)}}{\lambda_u^{(q)}} \frac{A_{\rm pen}^{ct,(q)}}{A_{\rm cc}^{u,(q)} + A_{\rm pen}^{ut,(q)}}\right), \tag{4.4}$$

where $A_{\rm pen}^{jt,(q)} \equiv A_{\rm pen}^{j,(q)} - A_{\rm pen}^{t,(q)}$ for $j \in \{u, c\}$.

By taking $q = d$ in (4.4) and using the Wolfenstein parameterization (see Section 2.1), we that find the $B_d \to \pi^+\pi^-$ decay amplitude becomes [91]

$$A(B_d \to \pi^+\pi^-) = e^{i\gamma}\, \mathcal{C} \left[1 - d\, e^{i\theta} e^{-i\gamma}\right], \tag{4.5}$$

where

$$\mathcal{C} \equiv A\lambda^3 R_b \left(A_{\rm cc}^{u,d} + A_{\rm pen}^{ut,d}\right), \qquad d\, e^{i\theta} \equiv \frac{1}{R_b} \frac{A_{\rm pen}^{ct,d}}{A_{\rm cc}^{u,d} + A_{\rm pen}^{ut,d}}. \tag{4.6}$$

Similarly, setting $q = s$ in (4.4) gives

$$A(B_s \to K^+K^-) = \sqrt{\epsilon}\; e^{i\gamma} \mathcal{C}' \left[1 + \frac{1}{\epsilon} d' e^{i\theta'} e^{-i\gamma}\right], \tag{4.7}$$

where

$$\mathcal{C}' \equiv A\lambda^3 R_b \left(A_{\rm cc}^{u,s} + A_{\rm pen}^{ut,s}\right), \qquad d' e^{i\theta'} \equiv \frac{1}{R_b} \frac{A_{\rm pen}^{ct,s}}{A_{\rm cc}^{u,s} + A_{\rm pen}^{ut,s}}, \tag{4.8}$$

and

$$\epsilon \equiv \frac{\lambda^2}{1 - \lambda^2}. \tag{4.9}$$

The $\mathcal{C}^{(\prime)}$ and $d^{(\prime)} e^{i\theta^{(\prime)}}$ are CP-conserving hadronic parameters. The former are dominated by the colour-allowed tree contributions and the latter by the ratio of QCD penguins to these tree amplitudes.

An exact U-spin symmetry implies the relations [91]

$$d' = d, \quad \theta' = \theta. \tag{4.10}$$

As was pointed out in Ref. [91], these relations are not affected by factorizable U-spin-breaking corrections, i.e. the relevant form factors and decay constants cancel. An exact U-spin symmetry also implies $|\mathcal{C}'/\mathcal{C}| = 1$. Here, however, the corresponding decay constants and form factors do not cancel, so that we obtain the following result in the factorization approximation (see Section 2.3):

$$\left|\frac{\mathcal{C}'}{\mathcal{C}}\right|_{\text{fact}} = \frac{f_K}{f_\pi}\frac{F_{B_sK}(M_K^2;0^+)}{F_{B_d\pi}(M_\pi^2;0^+)}\left(\frac{M_{B_s}^2 - M_K^2}{M_{B_d}^2 - M_\pi^2}\right). \tag{4.11}$$

The QCD light-cone sum rule calculation of Ref. [93] gives

$$\left|\frac{\mathcal{C}'}{\mathcal{C}}\right|_{\text{fact}}^{\text{QCDSR}} = 1.41^{+0.20}_{-0.11}. \tag{4.12}$$

4.2.2 Early determination of γ

For the extraction of γ, it is useful to introduce the following ratio of theoretical branching ratios:

$$\begin{aligned} K &\equiv \frac{1}{\epsilon}\left|\frac{\mathcal{C}}{\mathcal{C}'}\right|^2\left[\frac{M_{B_s}}{M_{B_d}}\frac{\Phi(M_\pi/M_{B_d}, M_\pi/M_{B_d})}{\Phi(M_K/M_{B_s}, M_K/M_{B_s})}\frac{\tau_{B_d}}{\tau_{B_s}}\right]\left[\frac{\text{BR}(B_s\to K^+K^-)}{\text{BR}(B_d\to\pi^+\pi^-)}\right] \\ &= \frac{1}{\epsilon^2}\left[\frac{\epsilon^2 + 2\epsilon d'\cos\theta'\cos\gamma + d'^2}{1 - 2d\cos\theta\cos\gamma + d^2}\right] \end{aligned} \tag{4.13}$$

where we have used (4.5) and (4.7). Here the phase space of the decay is given in by the function

$$\Phi(x,y) \equiv \sqrt{[1-(x+y)^2]\,[1-(x-y)^2]}. \tag{4.14}$$

The $B_s \to K^+K^-$ theoretical branching ratio can be expressed terms of experimentally measurable quantities using (3.107):

$$\text{BR}(B_s\to K^+K^-) = \overline{\text{BR}}(B_s\to K^+K^-)\left[2 - (1-y_s^2)\frac{\tau_{K^+K^-}}{\tau_{B_s}}\right]. \tag{4.15}$$

The $B_s^0 \to K^+K^-$ decay is now well established and the Heavy Flavour Averaging Group (HFAG) gives the following average for its branching ratio [73]:

$$\overline{\text{BR}}(B_s\to K^+K^-) = (26.4\pm 2.8)\times 10^{-6}, \tag{4.16}$$

The most accurate determination of the effective lifetime is currently given by LHCb [94]

$$\tau_{K^+K^-} = [1.455 \pm 0.046 \pm 0.006]\ \text{ps}. \tag{4.17}$$

Using the HFAG average $\text{BR}(B_d \to \pi^+\pi^-) = (5.15 \pm 0.22)\times 10^{-6}$ and the result of (4.11) we find the numerical value

$$K \overset{\text{exp}}{=} 52.1^{+11}_{-14}. \tag{4.18}$$

The $B_s^0 \to K^+K^-$ and $B_d^0 \to \pi^+\pi^-$ decays are into CP-even eigenstates and thereby give us access to the time-dependent CP asymmetry observables $\mathcal{A}_{\rm CP}^{\rm dir}(B_q \to f)$ and $\mathcal{A}_{\rm CP}^{\rm mix}(B_q \to f)$ (as discussed in Section 3.2.2). For the $B_s^0 \to K^+K^-$ channel the following CP asymetries have been measured for the first time by the LHCb experiment [95]

$$\begin{aligned}\mathcal{A}_{\rm CP}^{\rm dir}(B_s \to K^+K^-) &= 0.14 \pm 0.11 \pm 0.03,\\ \mathcal{A}_{\rm CP}^{\rm mix}(B_s \to K^+K^-) &= -0.30 \pm 0.12 \pm 0.04.\end{aligned} \tag{4.19}$$

Unfortunately these errors are still too large to perform an accurate determination of γ. We will return to this point in Section 4.2.5.

The most accurate measurements of the CP-violating observables of the $B_d^0 \to \pi^+\pi^-$ channel have been performed at the B factories, although LHCb has now also entered the game [96]. By using (4.5), we can derive the expressions

$$\begin{aligned}\mathcal{A}_{\rm CP}^{\rm dir}(B_d \to \pi^+\pi^-) &= -\left[\frac{2\,d\sin\theta\sin\gamma}{1-2\,d\cos\theta\cos\gamma+d^2}\right],\\ \mathcal{A}_{\rm CP}^{\rm mix}(B_d \to \pi^+\pi^-) &= +\left[\frac{\sin(\phi_d+2\gamma)-2\,d\,\cos\theta\,\sin(\phi_d+\gamma)+d^2\sin\phi_d}{1-2\,d\cos\theta\cos\gamma+d^2}\right]\end{aligned} \tag{4.20}$$

where ϕ_d denotes the CP-violating B_d^0–$\bar{B}_d^0$ mixing phase given in (3.56).

The current experimental status of the CP violation in $B_d^0 \to \pi^+\pi^-$ is

$$\mathcal{A}_{\rm CP}^{\rm mix}(B_d \to \pi^+\pi^-) = \left\{\begin{array}{ll}0.68 \pm 0.10 \pm 0.03 & \text{(BaBar [97])}\\ 0.64 \pm 0.08 \pm 0.03 & \text{(Belle [98])}\\ 0.56 \pm 0.17 \pm 0.03 & \text{(LHCb [96])}\end{array}\right. \stackrel{\rm HFAG}{=} 0.65 \pm 0.06, \tag{4.21}$$

$$\mathcal{A}_{\rm CP}^{\rm dir}(B_d \to \pi^+\pi^-) = \left\{\begin{array}{ll}-0.25 \pm 0.08 \pm 0.02 & \text{(BaBar [97])}\\ -0.33 \pm 0.06 \pm 0.03 & \text{(Belle [98])}\\ -0.11 \pm 0.21 \pm 0.03 & \text{(LHCb [96])}\end{array}\right. \stackrel{\rm HFAG}{=} -0.29 \pm 0.05. \tag{4.22}$$

where the final equality for both observables gives the HFAG average [73][1]. We observe that the large discrepancy between the BaBar and Belle results for $\mathcal{A}_{\rm CP}^{\rm dir}(B_d \to \pi^+\pi^-)$, which was discussed in Ref. [84], has been resolved due to the updated Belle value approaching the BaBar one.

A test of the $B_d^0 \to \pi^+\pi^-$ direct CP asymmetry is offered by the relation [99]

$$\mathcal{A}_{\rm CP}^{\rm dir}(B_d \to \pi^+\pi^-) = -\left(\frac{f_\pi}{f_K}\right)^2\left[\frac{\rm BR(B_d \to \pi^\mp K^\pm)}{\rm BR(B_d \to \pi^+\pi^-)}\right]\mathcal{A}_{\rm CP}^{\rm dir}(B_d \to \pi^\mp K^\pm), \tag{4.23}$$

which follows from $SU(3)$ flavour symmetry and a neglect of exchange and penguin annihilation topologies (see Section 2.4). The HFAG average for the direct CP violation in $B_d^0 \to \pi^- K^+$ is $\mathcal{A}_{\rm CP}^{\rm dir}(B_d \to \pi^\mp K^\pm) = 0.082 \pm 0.006$ [73], which results in the estimate $\mathcal{A}_{\rm CP}^{\rm dir}(B_d \to \pi^+\pi^-) = -0.26 \pm 0.03$. This result is seen to be in excellent agreement with

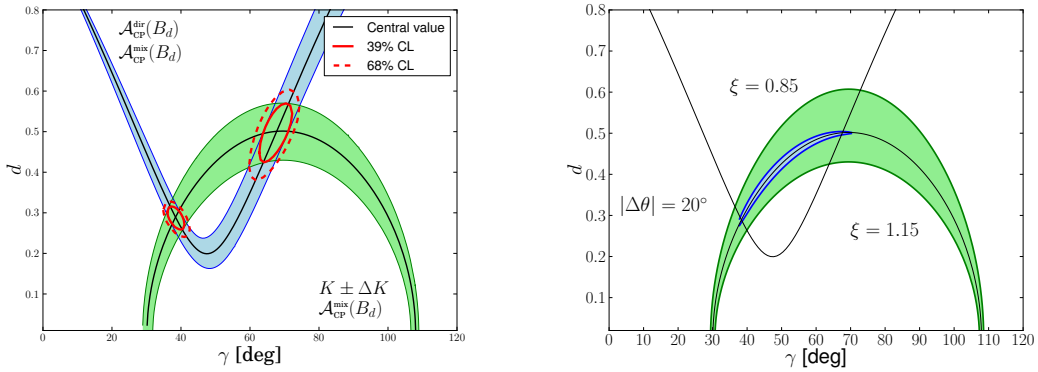

Figure 4.2: The contours in the γ–d plane fixed through the CP-violating $B_d^0 \to \pi^+\pi^-$ observables and K. Left panel: $1\,\sigma$ error bands and the 68% C.L. regions, right panel: illustration of U-spin-breaking effects.

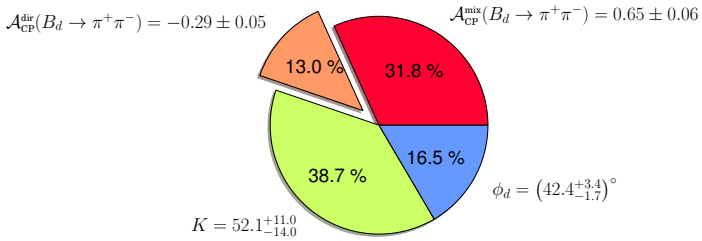

Figure 4.3: The error budget for the extracted value of γ in (4.26) that is associated with the used input data.

the HFAG average in (4.22), which gives confidence in our use of flavour symmetries for these decays.

In order to determine γ, we can convert the direct and mixing-induced CP asymmetry of the $B_d^0 \to \pi^+\pi^-$ channel into a theoretically clean contour in the γ–d plane; the corresponding formulae are given in Ref. [91]. Furthermore, using the U-spin relation (4.10) in (4.13), we can determine a second contour. The intersection of both contours then allows us to determine γ and d, so that we can also extract the strong phase θ. In Figure 4.2, we show the situation arising for the current data. The plot on the left-hand side shows the $1\,\sigma$ error bands and the 39% and 68% confidence regions arising from a χ^2 fit, whereas the plot on the right-hand side illustrates the impact of U-spin-breaking corrections to (4.10), which we have parameterized as

$$\xi \equiv d'/d = 1 \pm 0.15, \tag{4.24}$$

$$\Delta\theta \equiv \theta' - \theta = \pm 20^\circ. \tag{4.25}$$

[1]The updated LHCb results given in Ref. [95] have not yet been included in this HFAG average.

As discussed in Ref. [92], the discrete ambiguities for γ can be resolved using arguments from factorisation, yielding

$$\gamma = (67.7^{+4.5}_{-5.0}|_{\rm input}{}^{+5.0}_{-3.7}|_{\xi}{}^{+0.1}_{-0.2}|_{\Delta\theta})^\circ \tag{4.26}$$

and

$$d = 0.501^{+0.069}_{-0.076}|_{\rm input}{}^{+0.101}_{-0.074}|_{\xi}{}^{+0.002}_{-0.005}|_{\Delta\theta}, \quad \theta = (150.4^{+6.4}_{-8.2}|_{\rm input}{}^{+3.8}_{-3.9}|_{\xi}{}^{+0.1}_{-0.2}|_{\Delta\theta})^\circ, \tag{4.27}$$

where the input errors are the 68% confidence intervals of the χ^2 fit. In Figure 4.3, we show the error budget for γ coming from the individual input quantities. We observe that K and $\mathcal{A}_{\rm CP}^{\rm mix}(B_d \to \pi^+\pi^-)$ have a similar impact on the error, while $\mathcal{A}_{\rm CP}^{\rm dir}(B_d \to \pi^+\pi^-)$ plays a significantly less important role. Also ϕ_d has a small but non-negligible impact on the overall error. Its error, driven mostly by the uncertainty of penguin effects, can be improved in the future using a flavour symmetry strategy involving the decay $B_s^0 \to J/\psi K_{\rm S}$ [100].

The extracted value given in (4.26) is in excellent agreement with the fits of the unitarity triangle:

$$\gamma = \begin{cases} (67.7^{+4.1}_{-4.3})^\circ & \text{(CKMfitter [75])} \\ (69.2 \pm 3.2)^\circ & \text{(UTfit [101]).} \end{cases} \tag{4.28}$$

We may therefore conclude that no large New Physics effects enter the decay amplitudes. In the next section we will therefore assume the Standard Model amplitude expressions given in (4.7) and (4.5) to hold. In Section 4.2.5 we return to the optimal determination of γ using the time-dependent CP asymmetry observables from $B_s \to K^+K^-$.

4.2.3 Mass-eigenstate rate asymmetry

Due to the sizable decay width difference of the B_s meson system discussed in Chapter 3, a time-dependent analysis of the decay $B_s \to K^+K^-$ can probe the mass-eigenstate rate asymmetry $\mathcal{A}_{\Delta\Gamma}(B_s \to K^+K^-)$ as defined in (3.70). We note that this observable is not independent from the other two CP asymmetry observables, $\mathcal{A}_{\rm CP}^{\rm dir}(B_s \to K^+K^-)$ and $\mathcal{A}_{\rm CP}^{\rm mix}(B_s \to K^+K^-)$, due to the relation given in (3.74). It is, however, the only one of the three that can be extracted with an untagged time-dependent decay sample. Using the parametrization in (4.7), we obtain from (3.71) and the associated formalism the expression

$$\mathcal{A}_{\Delta\Gamma}(B_s \to K^+K^-) = -\left[\frac{d'^2\cos\phi_s + 2\epsilon\, d'\cos\theta'\cos(\phi_s+\gamma) + \epsilon^2\cos(\phi_s+2\gamma)}{d'^2 + 2\epsilon\, d'\cos\theta'\cos\gamma + \epsilon^2}\right]. \tag{4.29}$$

We could proceed to use the results given in (4.26) and (4.27) in combination with the U-spin symmetry assumption to give a numerical estimate of $\mathcal{A}_{\Delta\Gamma}(B_s \to K^+K^-)$ for a given value of the B_s^0–$\bar{B}_s^0$ mixing phase ϕ_s. However, in the original analysis of Ref. [84] (on which this section is based), there was a discrepancy present between the BaBar and Belle values of $\mathcal{A}_{\rm CP}^{\rm dir}(B_d \to \pi^+\pi^-)$, as we discussed above. This motivated us

to consider an alternative strategy to estimate the hadronic parameters d' and θ' that does not rely on using this direct CP asymmetry as an input. Although the discrepancy is now resolved, we will nonetheless continue with the alternative strategy because it highlights the consistency of the flavour symmetry picture.

In this alternative strategy, we assume that γ is known, with a value of $\gamma = (68 \pm 7)^\circ$ in agreement with (4.26) and the fits of the UT in (4.28). It is then possible to combine K, as given in (4.13), with the U-spin relation (4.10) and the direct CP asymmetry,

$$\mathcal{A}_{\rm CP}^{\rm dir}(B_s \to K^+K^-) = \frac{2\epsilon d' \sin\theta' \sin\gamma}{d'^2 + 2\epsilon d' \cos\theta' \cos\gamma + \epsilon^2}, \tag{4.30}$$

to determine d' and $\cos\theta'$. Parametrizing the U-spin-breaking effects for $d^{(\prime)}$ through (4.24), the corresponding formulae from which d' and $\cos\theta'$ can be extracted are

$$2d'\cos\theta' = \frac{-d'^2 + \epsilon^2\left[K(1+d'^2\xi^{-2}) - 1\right]}{\epsilon\cos\gamma\,(1+\epsilon\xi^{-1}K)}, \tag{4.31}$$

$$d'^2 = \epsilon^2\left[\frac{b \pm \sqrt{b^2 - ac}}{a}\right], \tag{4.32}$$

with

$$a = \epsilon^2\xi^{-2}\left(1+\epsilon\xi^{-1}\right)^2(\mathcal{A}_{\rm CP}^{\rm dir})^2K^2\cot^2\gamma + \left(1-\epsilon^2\xi^{-2}K\right)^2, \tag{4.33}$$

$$b = -\epsilon\xi^{-1}\left(1+\epsilon\xi^{-1}\right)^2(\mathcal{A}_{\rm CP}^{\rm dir})^2K^2\cot^2\gamma + 2\cos^2\gamma\left(1+\epsilon\xi^{-1}K\right)^2 \tag{4.34}$$

$$+ (K-1)(1-\epsilon^2\xi^{-2}K), \tag{4.35}$$

$$c = \left(1+\epsilon\xi^{-1}\right)^2(\mathcal{A}_{\rm CP}^{\rm dir})^2K^2\cot^2\gamma + (K-1)^2, \tag{4.36}$$

where $\mathcal{A}_{\rm CP}^{\rm dir} \equiv \mathcal{A}_{\rm CP}^{\rm dir}(B_s \to K^+K^-)$. The U-spin-breaking effects of $\theta^{(\prime)}$, as given in (4.25), are difficult to include in the above analytic expressions but are straightforward to calculate numerically.

The CP-violating observables of the $B_s^0 \to K^+K^-$ channel given in (4.19) are not sufficiently accurate for the numerical analysis we have in mind. However, as the $B_d^0 \to \pi^-K^+$ and $B_s^0 \to K^+K^-$ channels differ only in their spectator quarks, we expect

$$\mathcal{A}_{\rm CP}^{\rm dir}(B_s \to K^+K^-) \approx \mathcal{A}_{\rm CP}^{\rm dir}(B_d \to \pi^\mp K^\pm) = 0.082 \pm 0.006. \tag{4.37}$$

In order to take possible corrections into account, we increase the error generously and use

$$\mathcal{A}_{\rm CP}^{\rm dir}(B_s \to K^+K^-) = 0.082 \pm 0.04 \tag{4.38}$$

in the following numerical analysis. This estimate is consistent with the LHCb result given in (4.19).

Given all of these inputs and including the U-spin breaking effects in (4.24) and (4.25), we arrive at the following results for the hadronic parameters:

$$d' = 0.505^{+0.080}_{-0.097}, \quad \cos\theta' = -0.920^{+0.107}_{-0.067}, \tag{4.39}$$

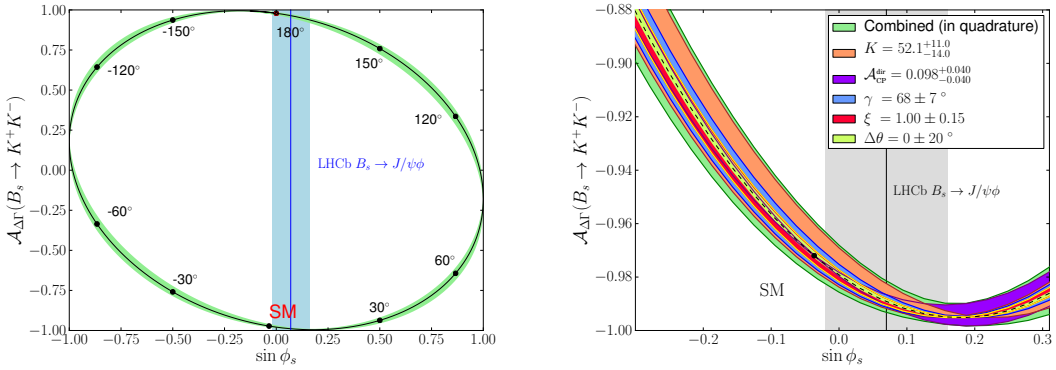

Figure 4.4: Left panel: correlation between $\mathcal{A}_{\Delta\Gamma}(B_s \to K^+K^-)$ and $\sin\phi_s$. Right panel: errors associated with the input observables/parameters, zoomed in on the SM region $\phi_s \in [-17°, 17°]$ and overlayed on top of one another. The legend lists the error contributions from largest to smallest. In both plots we also show for comparison the determination of ϕ_s from the the $B_s \to J/\psi\phi$ analysis as given in (3.48).

where all errors were added in quadrature. A comparison with the results given in (4.27) under the U-spin assumption of (4.10) reveals a very consistent flavour symmetry picture.

Using the SM prediction for the B_s^0–$\bar{B}_s^0$ mixing phase given in (3.47) we find the following prediction for the mass-eigenstate rate asymmetry:

$$\begin{aligned}\mathcal{A}_{\Delta\Gamma}(B_s \to K^+K^-)\Big|_{\rm SM} &= -0.97200^{+0.0119}_{-0.0056}\Big|^{+0.0047}_{K\,-0.0046}\Big|^{+0.00004}_{\gamma\,-0.00002}\Big|^{+0.0022}_{\mathcal{A}_{\rm CP}^{\rm dir}\,-0.0031}\Big|^{+0.0015}_{\xi\,-0.0006}\Big|_{\Delta\theta} \\ &= -0.972^{+0.013}_{-0.008}, \end{aligned} \tag{4.40}$$

where all errors have again been combined in quadrature. Particularly interesting is the small influence of the U-spin breaking errors and direct CP violation, $\mathcal{A}_{\rm CP}^{\rm dir}(B_s \to K^+K^-)$, on the total error. In Figure 4.4 we treat ϕ_s as a free parameter and show the correlation between $\mathcal{A}_{\Delta\Gamma}(B_s \to K^+K^-)$ and $\sin\phi_s$, as well as errors related to the input quantities overlayed on top of one another and centred on the central value. We observe that $\mathcal{A}_{\Delta\Gamma}(B_s \to K^+K^-)$ is very robust with respect to the input errors for the whole range of ϕ_s. However, recent determinations of ϕ_s using the $B_s \to J/\psi\phi$ mode, as given in (3.48), are already quite constraining, which we have indicated with $1\,\sigma$ bands in these plots.

As discussed in Section 3.3, the observable $\mathcal{A}_{\Delta\Gamma}(B_s \to K^+K^-)$ can be experimentally probed by fitting an exponential function to the time-dependent untagged decay rate. The resulting observable is the effective lifetime and is given by

$$\tau_{K^+K^-} = \frac{\tau_{B_s}}{1-y_s^2}\left[\frac{1+2\mathcal{A}_{\Delta\Gamma}(B_s \to K^+K^-)y_s + y_s^2}{1+\mathcal{A}_{\Delta\Gamma}(B_s \to K^+K^-)y_s}\right] \tag{4.41}$$

We can estimate the effective lifetime in the Standard Model by combining (4.40) with the theoretical estimate of y_s given in (3.43). We thus obtain the following SM prediction

of the effective lifetime ratio:

$$\frac{\tau_{K^+K^-}}{\tau_{B_s}}\Big|_{\rm SM} = 0.9398^{+0.0010}_{-0.0006}\Big|_{\mathcal{A}_{\Delta\Gamma}}{}^{+0.0137}_{-0.0132}\Big|_{\Delta\Gamma_s/\Gamma_s} = 0.940^{+0.014}_{-0.013}, \tag{4.42}$$

where the errors have been added in quadrature. Combining this with the measurement of τ_{B_s} given in (3.53) gives a SM prediction for the lifetime of

$$\tau_{K^+K^-}|_{\rm SM} = (1.425 \pm 0.023)\,\text{ps}. \tag{4.43}$$

This prediction is compatible with the LHCb measurement given in (4.17).

It is also possible to use the measured $B_s \to K^+K^-$ effective lifetime from (4.17) together with the measurement of y_s given in (3.49) to give the estimate:

$$\mathcal{A}_{\Delta\Gamma}(B_s \to K^+K^-)\Big|_{\tau_{KK}} = -0.65^{+0.38}_{-0.36}\Big|_{\tau_{KK}}{}^{+0.05}_{-0.08}\Big|_{y_s}{}^{+0.08}_{-0.08}\Big|_{\tau_{B_s}} = -0.65^{+0.39}_{-0.38}. \tag{4.44}$$

Alternatively, in Ref. [96] the $B_s \to K^+K^-$ CP asymmetries are fitted for assuming the relation

$$\mathcal{A}^{\rm dir}_{\rm CP}(B_s \to K^+K^-)^2 + \mathcal{A}^{\rm mix}_{\rm CP}(B_s \to K^+K^-)^2 + \mathcal{A}_{\Delta\Gamma}(B_s \to K^+K^-)^2 = 1. \tag{4.45}$$

Then, using the CP symmetry measurements given in (4.19), we find

$$|\mathcal{A}_{\Delta\Gamma}(B_s \to K^+K^-)|\Big|_{\text{CP meas}} = 0.985^{+0.000}_{-0.021}\Big|_{\mathcal{A}^{\rm dir}_{\rm CP}}{}^{+0.015}_{-0.051}\Big|_{\mathcal{A}^{\rm mix}_{\rm CP}} = 0.985^{+0.015}_{-0.055}. \tag{4.46}$$

It would be interesting to compare the precision found for this observable if the relation in (4.45) is not included in the experimental fit.

Following the general formalism set up in Section 3.2.2 for CP-eigenstate final states, we may express the mass-eigenstate rate asymmetry as

$$\mathcal{A}_{\Delta\Gamma}(B_s \to K^+K^-) = -\sqrt{1 - \mathcal{A}^{\rm dir}_{\rm CP}(B_s \to K^+K^-)}\cos\left(\phi_s + \Delta\phi_{K^+K^-}\right). \tag{4.47}$$

In (3.87) the hadronic phase shift $\Delta\phi_{K^+K^-}$ is expressed in terms of the parameters

$$h_{K^+K^-} = d/\epsilon, \quad \delta_{K^+K^-} = \theta, \quad \phi_1^{K^+K^-} = \gamma, \quad \phi_2^{K^+K^-} = 0. \tag{4.48}$$

and thus, using the numerical analysis of this section, evaluates to

$$\Delta\phi_{K^+K^-} = -\left(10.7^{+2.8}_{-2.1}\right)^\circ, \tag{4.49}$$

Combining this input with (4.38), the remaining degree of freedom in $\mathcal{A}_{\Delta\Gamma}(B_s \to K^+K^-)$ is ϕ_s. Therefore, as outlined in Section 3.3.2, the effective lifetime measurement gives a contour in the ϕ_s–$\Delta\Gamma_s$ plane. In Figure 4.5 we show this contour, along with the corresponding experimental errors of the effective lifetime measurement (left panel) and the effect of the hadronic phase shift (right panel). In Chapter 5 we also add the effective lifetime for a CP-odd final state to this plane.

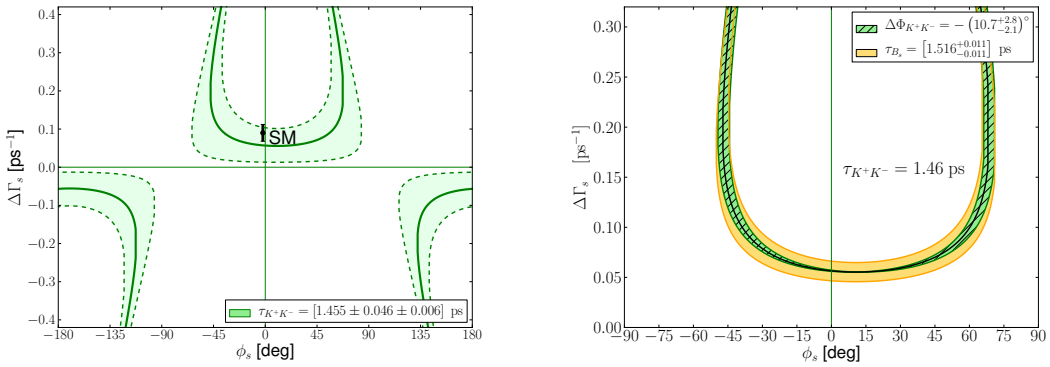

Figure 4.5: Measurement of the $B_s \to K^+K^-$ lifetime projected onto the ϕ_s–$\Delta\Gamma_s$ plane. Error bands correspond to the effective lifetime measurement (left panel) and the hadronic phase shift and mean B_s lifetime (right panel).

4.2.4 Mixing-induced CP violation

The final observable that is offered by the $B_s^0 \to K^+K^-$ channel is its mixing-induced CP asymmetry (see Section 3.2.2). It takes the following form [91]:

$$\mathcal{A}_{\rm CP}^{\rm mix}(B_s \to K^+K^-) = + \left[\frac{d'^2 \sin\phi_s + 2\epsilon d' \cos\theta' \sin(\phi_s+\gamma) + \epsilon^2 \sin(\phi_s+2\gamma)}{d'^2 + 2\epsilon d' \cos\theta' \cos\gamma + \epsilon^2}\right]. \quad (4.50)$$

The structure of this expression is very similar to (4.29), i.e. the strong phase enters only as $\cos\theta'$. Consequently, we can use the formulae given in the previous section to perform an analysis of $\mathcal{A}_{\rm CP}^{\rm mix}(B_s \to K^+K^-)$ that is analogous to that of $\mathcal{A}_{\Delta\Gamma}(B_s \to K^+K^-)$. For the SM we obtain the prediction

$$\begin{aligned}\mathcal{A}_{\rm CP}^{\rm mix}(B_s \to K^+K^-)\Big|_{\rm SM} &= -0.220^{+0.027}_{-0.047}\Big|^{+0.021}_{K\,-0.020}\Big|^{+0.019}_{\gamma\,-0.011}\Big|^{+0.014}_{\mathcal{A}_{\rm CP}^{\rm dir}\,-0.010}\Big|^{+0.003}_{\xi\,-0.006}\Big|_{\Delta\theta} \\ &= -0.220^{+0.042}_{-0.054}, \end{aligned} \quad (4.51)$$

where the errors have been combined in quadrature. This prediction can now be directly compared to (4.19), where it is observed to be compatible. In Figure 4.6, we show the dependence of $\mathcal{A}_{\rm CP}^{\rm mix}(B_s \to K^+K^-)$ on $\sin\phi_s$, with a range of ϕ_s points marked explicitly. The latter quantity is conventionally measured through the CP-violating effects in the $B_s^0 \to J/\psi\phi$ angular distribution, as discussed above. The error bars on the SM point correspond to those given above. This plot illustrates two interesting features:

- $\mathcal{A}_{\rm CP}^{\rm mix}(B_s \to K^+K^-)$ offers a complementary tool to search for footprints of a NP contribution to the phase ϕ_s, and deviates already significantly from the SM value for moderate values of this phase.
- $\mathcal{A}_{\rm CP}^{\rm mix}(B_s \to K^+K^-)$ allows us to resolve the twofold ambiguity for the value of ϕ_s resulting from the analyses of $B_s^0 \to J/\psi\phi$. In particular, we can then distinguish

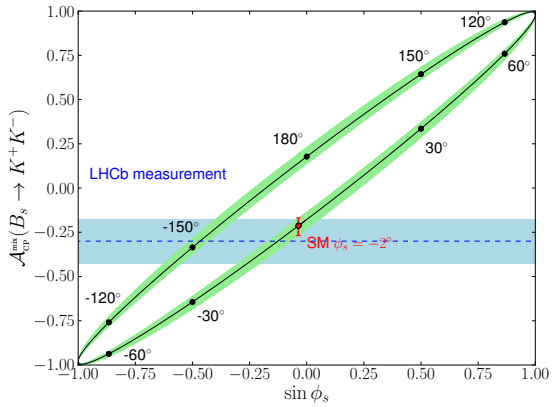

Figure 4.6: The correlation between $\mathcal{A}_{\rm CP}^{\rm mix}(B_s \to K^+K^-)$ and $\sin\phi_s$. The error band takes the uncertainties due to the input parameters and observables into account, as well as possible U-spin-breaking corrections. The numbers label the values of ϕ_s. The blue band gives the LHCb measurement of this quantity as given in (4.19).

between the SM case with $\phi_s \sim 0°$ and a NP scenario with $\phi_s \sim 180°$, both leading to small CP violation in $B_s^0 \to J/\psi\phi$. However, the S-wave modes of the $B_s \to J/\psi K^+K^-$ decay have already been used to resolve this ambiguity [77].

The correlation in Figure 4.6 was first discussed in Ref. [92]. Here we have gone beyond that analysis by making a detailed analysis of the corresponding errors and using γ as an input. As in the previous section, we observe that the calculation is remarkably stable with respect to possible U-spin-breaking corrections and input errors. In Figure 4.7, we show the error budget corresponding to the various input parameters and observables: for the SM case we give both a pie chart of the relative contribution of each error and show the errors overlayed on top of one another and centred on the central value.

4.2.5 Optimal determination of γ

We will now discuss the optimal strategy for determining γ. This will be the major application of the $B_s \to K^+K^-$ decay mode once more precise measurements of its tagged time-dependent CP observables $\mathcal{A}_{\rm CP}^{\rm dir}(B_s \to K^+K^-)$ and $\mathcal{A}_{\rm CP}^{\rm mix}(B_s \to K^+K^-)$ have been made. The idea is that these observables can be converted into a clean contour in the γ–d' plane, in analogy the γ–d contour corresponding to the time-dependent CP observables of $B_d \to \pi^+\pi^-$ shown in Figure 4.2. The single U-spin relation $d = d'$ is then sufficient to determine γ and d from the intersection of the contours. Also θ and θ' can then be determined independently, which will allow us to test the validity of the U-spin symmetry assumption. Furthermore, the quantity K has not yet entered this strategy. It can therefore be used to measure the ratio $|\mathcal{C}'/\mathcal{C}|$, and compare this with the theoretical calculation given in (4.12).

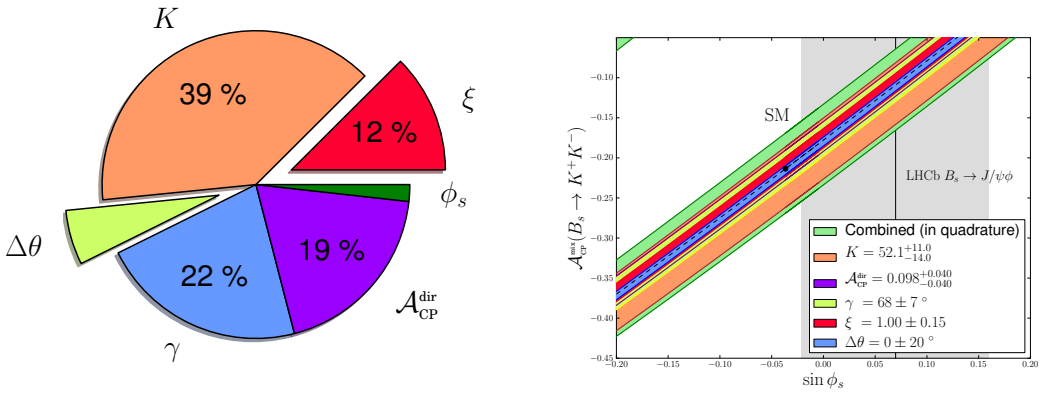

Figure 4.7: The error budget for $\mathcal{A}_{\rm CP}^{\rm mix}(B_s \to K^+K^-)$. Left panel: pie chart of the relative contribution of each input error for the SM case of $\phi_s^{\rm SM}$. Right panel: errors overlayed on top of one another for the correlation in Figure 4.6. The legend lists the error contributions from largest to smallest. We also show for comparison the determination of ϕ_s from the the $B_s \to J/\psi\phi$ analysis as given in (3.48).

In Figure 4.8, we illustrate the corresponding contour in the γ–d' plane To do so, we make use of the γ analysis of Section 4.2.2. Using the values of γ, d and θ in (4.26) and (4.27), and neglecting the corresponding U-spin-breaking errors, we obtain

$$\mathcal{A}_{\rm CP}^{\rm dir}(B_s \to K^+K^-) = 0.094^{+0.044}_{-0.039}, \tag{4.52}$$

$$\mathcal{A}_{\rm CP}^{\rm mix}(B_s \to K^+K^-)|_{\rm SM} = -0.217^{+0.037}_{-0.036}. \tag{4.53}$$

These numbers are fully consistent with (4.38) and (4.51), which rely on different inputs, and thereby further support our numerical analysis. The green band in Figure 4.8, referring to the CP-violating $B_s^0 \to K^+K^-$ observables, corresponds to the central values in (4.52) and (4.53) and their 1σ ranges. The $B_d^0 \to \pi^+\pi^-$ contour is the same as in the left panel of Figure 4.2, and, in order to guide the eye, we have also included the central value of the contour fixed through K and $\mathcal{A}_{\rm CP}^{\rm mix}(B_d \to \pi^+\pi^-)$. It is interesting to observe that the $B_s^0 \to K^+K^-$ and $B_d^0 \to \pi^+\pi^-$ contours are intersecting with a large angle, thereby leading again to a situation that is very robust with respect to possible U-spin-breaking corrections to $d' = d$. In the right panel of Figure 4.8 we show the contour resulting from the measured CP observables of $B_s \to K^+K^-$ given in (4.19). This illustrates our earlier point that for an optimal determination of γ we are eagerly awaiting more precise measurements from LHCb.

4.3 Extracting γ from tree topologies: $B_s \to D_s^{(*)}K$

Two interesting features of $B_s \to D_s^{(*)\pm}K^{\mp}$ decays are that they are governed only by tree diagram topologies and that both flavour states, B_s^0 and $\overline{B}_s^0$, can decay to each of

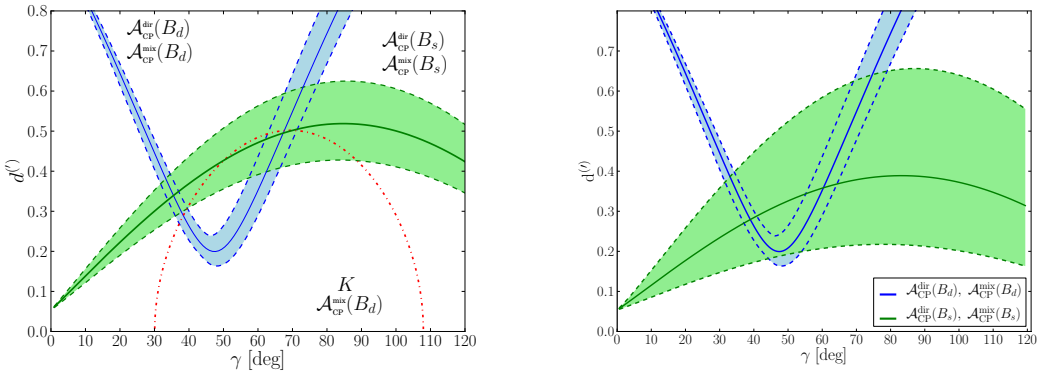

Figure 4.8: Illustration of the optimal determination of γ from the CP-violating observables of the $B_s \to K^+K^-$, $B_d \to \pi^+\pi^-$ system in the SM. *Left panel:* The green contour illustrates the 1σ errors in the CP asymmetries of $B_s \to K^+K^-$ given in (4.52) and (4.53). *Right panel:* the green contour corresponds to the latest LHCb results given in (4.19).

them. The dominant colour-allowed tree diagram topologies of these decays are shown in Figure 4.9. The latter feature leads to interference effects between B_s mixing and the decay. By measuring the time-dependent observables of one of these decay modes and its CP conjugate, for example $B_s \to D_s^+ K^-$ and $B_s \to D_s^- K^+$, a theoretically clean determination of the CP violating phase $\phi_s + \gamma$ is possible [102, 103]. As we discussed in the introduction of this chapter, the phase ϕ_s should be determined quite accurately from separate analyses in advance of the decays discussed here. Thus it should be possible to extract γ from these decay modes. A central question is whether this value will agree with γ determinations from decays with penguin contributions from Section 4.2.

This section is based on the work presented in Ref. [86]. We will assume throughout that the relevant decay amplitudes are described by the Standard Model. Applying the formalism developed in Ref. [103], we shall explore the $B_s \to D_s^{(*)\pm} K^\mp$ channels both in view of recent experimental developments as well as measurements to be performed by the LHCb collaboration in this decade.

Measurements of the $B_s \to D_s^\pm K^\mp$ branching ratios are available from the CDF [104], Belle [105] and LHCb [106] collaborations:

$$\frac{\overline{\rm BR}(B_s \to D_s^\pm K^\mp)}{\overline{\rm BR}(B_s \to D_s^\pm \pi^\mp)} = \begin{cases} 0.097 \pm 0.018\,(\text{stat.}) \pm 0.009\,(\text{syst.}) & [\text{CDF}], \\ 0.065^{+0.035}_{-0.029}\,(\text{stat.}) & [\text{Belle}], \\ 0.0646 \pm 0.0043\,(\text{stat.}) \pm 0.0025\,(\text{syst.}) & [\text{LHCb}]; \end{cases} \tag{4.54}$$

the errors of the Belle result are dominated by the small $B_s \to D_s^\pm K^\mp$ data sample. We will discuss the impact of y_s on this ratio of CP-averaged experimental branching ratios and convert the experimental numbers into constraints on the hadronic parameter characterizing the interference effects discussed above.

The LHCb experiment has also reported a first measurement of the time-dependent

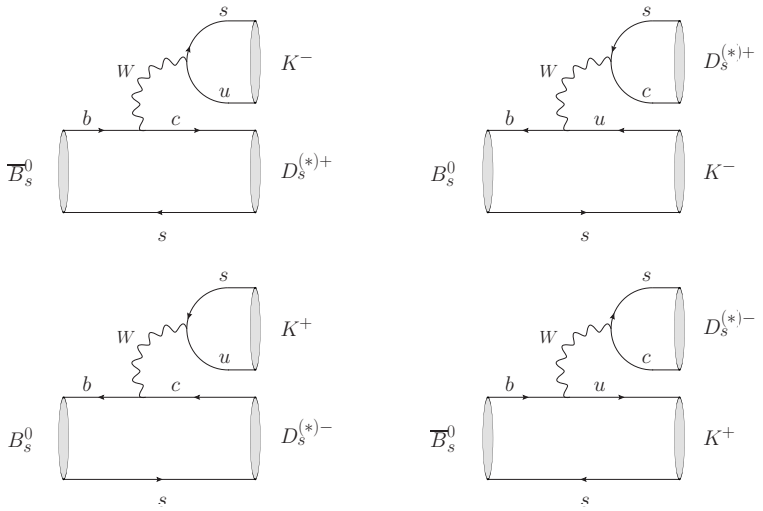

Figure 4.9: The dominant colour-allowed tree topologies contributing to the $B_s^0, \overline{B}_s^0 \to D_s^{(*)+}K^-$ (top row) and $B_s^0, \overline{B}_s^0 \to D_s^{(*)-}K^+$ (bottom row) decay modes.

CP asymmetries for the $B_s \to D_s^{\pm}K^{\mp}$ [107] decays. However, the uncertainties are unfortunately still too large to perform an extraction of $\phi_s + \gamma$, as we will discuss in Section 4.3.4. Instead, following Ref. [103], the observables of the $B_s \to D_s^{(*)\pm}K^{\mp}$ channels can be related to those of the $B_d \to D^{(*)\pm}\pi^{\mp}$ decays through the U-spin symmetry of strong interactions. We shall use B-factory data obtained by the BaBar and Belle collaborations for the latter decays, together with further constraints from $B_d \to D_s^{\pm}\pi^{\mp}$ modes, to make predictions for the $B_s \to D_s^{(*)\pm}K^{\mp}$ observables. These will serve as a guideline for the expected experimental picture. In this analysis, we specifically find that – thanks to the sizable value of y_s – untagged data samples of $B_s \to D_s^{(*)\pm}K^{\mp}$ decays can be efficiently combined with mixing-induced CP asymmetries of tagged analyses to extract $\phi_s + \gamma$ in an unambiguous way.

The outline is as follows: in Section 4.3.1, we discuss untagged measurements of the $B_s \to D_s^{(*)\pm}K^{\mp}$ decays, namely their branching ratios and effective lifetimes. In Section 4.3.2, we apply $SU(3)$ flavour symmetry to extract the hadronic parameters characterizing the $B_s \to D_s^{(*)\pm}K^{\mp}$ decays from the B-factory data for the $B_d \to D^{(*)\pm}\pi^{\mp}$ and $B_d \to D_s^{\pm}\pi^{\mp}$ channels. In Section 4.3.3, we discuss the extraction of $\phi_s + \gamma$ from the tagged and untagged $B_s \to D_s^{(*)\pm}K^{\mp}$ observables, with a special emphasis on resolving the discrete ambiguities. The hadronic parameters obtained in Section 4.3.2 are used in Section 4.3.4 to predict the relevant $B_s \to D_s^{(*)\pm}K^{\mp}$ observables, which then serve as an input for exploring the experimental prospects. We give our conclusions in Section 4.4.

4.3.1 Untagged observables

Following Section 3.2, the time-dependent, untagged $B_s \to D_s^{(*)+} K^-$ decay rates can be written as follows [103]:

$$\begin{aligned}\langle \Gamma(B_s(t) \to D_s^{(*)+} K^-) \rangle &\equiv \Gamma(B_s^0(t) \to D_s^{(*)+} K^-) + \Gamma(\bar{B}_s^0(t) \to D_s^{(*)+} K^-) \\ &= R\, e^{-t/\tau_{B_s}} \left[\cosh\left(y_s \frac{t}{\tau_{B_s}} \right) + \mathcal{A}_{\Delta\Gamma} \sinh\left(y_s \frac{t}{\tau_{B_s}} \right) \right], \end{aligned} \tag{4.55}$$

where

$$R \equiv \langle \Gamma(B_s(t) \to D_s^{(*)+} K^-) \rangle \big|_{t=0} = \langle \Gamma(B_s(t) \to D_s^{(*)-} K^+) \rangle \big|_{t=0}\,. \tag{4.56}$$

The analogous $B_s \to D_s^{(*)-} K^+$ rates can be straightforwardly obtained from (4.55) by replacing $\mathcal{A}_{\Delta\Gamma}$ with $\overline{\mathcal{A}}_{\Delta\Gamma}$. The mass-eigentstate rate asymmetries entering both untagged rate are given by

$$\mathcal{A}_{\Delta\Gamma} = -(-1)^L \frac{2\, x_s}{1 + x_s^2} \cos(\phi_s + \gamma + \delta_s), \quad \overline{\mathcal{A}}_{\Delta\Gamma} = -(-1)^L \frac{2\, x_s}{1 + x_s^2} \cos(\phi_s + \gamma - \delta_s), \tag{4.57}$$

where L denotes the angular momentum of the final state[2]. The hadronic parameter $x_s \propto R_b$ quantifies the strength of the interference effects between the $B_s^0 \to D_s^{(*)+} K^-$ and $\bar{B}_s^0 \to D_s^{(*)+} K^-$ decay processes induced through B_s^0–$\bar{B}_s^0$ mixing, and δ_s is an associated CP-conserving strong phase difference [103].

As discussed in detail in Section 3.4, the branching ratios of B_s decays are determined experimentally as time-integrated untagged rates [79, 83]:

$$\overline{\mathrm{BR}}(B_s \to D_s^{(*)\pm} K^{\mp}) \equiv \frac{1}{2} \int_0^\infty \langle \Gamma(B_s \to D_s^{(*)\pm} K^{\mp}) \rangle \, dt. \tag{4.58}$$

The theoretical branching ratio is given with respect to this measurement by

$$\mathrm{BR}(B_s \to D_s^{(*)+} K^-) = \left[\frac{1 - y_s^2}{1 + \mathcal{A}_{\Delta\Gamma}\, y_s} \right] \overline{\mathrm{BR}}(B_s \to D_s^{(*)+} K^-), \tag{4.59}$$

where an analogous expression involving $\overline{\mathcal{A}}_{\Delta\Gamma}$ holds for the $D_s^{(*)-} K^+$ final states. It is interesting to note that we have

$$\mathrm{BR}(B_s \to D_s^{(*)+} K^-) = \mathrm{BR}(B_s \to D_s^{(*)-} K^+) \tag{4.60}$$

thanks to the expression in (4.56), which implies

$$\frac{\overline{\mathrm{BR}}(B_s \to D_s^{(*)+} K^-)}{\overline{\mathrm{BR}}(B_s \to D_s^{(*)-} K^+)} = \frac{1 + \mathcal{A}_{\Delta\Gamma}\, y_s}{1 + \overline{\mathcal{A}}_{\Delta\Gamma}\, y_s}. \tag{4.61}$$

[2]For simplicity, we did not introduce a label to distinguish between $D_s^+ K^-$ and $D_s^{*+} K^-$.

Consequently, an established difference between the experimental $B_s \to D_s^{(*)-}K^+$ and $B_s \to D_s^{(*)+}K^-$ branching ratios would imply a difference between the $\mathcal{A}_{\Delta\Gamma}$ and $\overline{\mathcal{A}}_{\Delta\Gamma}$ observables (see also Ref. [108]):

$$\frac{\overline{\text{BR}}(B_s \to D_s^{(*)+}K^-) - \overline{\text{BR}}(B_s \to D_s^{(*)-}K^+)}{\overline{\text{BR}}(B_s \to D_s^{(*)+}K^-) + \overline{\text{BR}}(B_s \to D_s^{(*)-}K^+)} = y_s \left[\frac{\mathcal{A}_{\Delta\Gamma} - \overline{\mathcal{A}}_{\Delta\Gamma}}{2 + y_s(\mathcal{A}_{\Delta\Gamma} + \overline{\mathcal{A}}_{\Delta\Gamma})}\right]. \tag{4.62}$$

In order to relate theory to experiment beyond an accuracy of order $y_s \sim 0.1$, we need theoretical input to determine $\mathcal{A}_{\Delta\Gamma}$ and $\overline{\mathcal{A}}_{\Delta\Gamma}$. In Section 4.3.2, we will see that this results in large uncertainties for these observables. However, as discussed in Section 3.4, this input can be avoided with the help of the effective lifetimes, defined as

$$\tau_{\text{eff}} \equiv \frac{\int_0^\infty t\, \langle \Gamma(B_s \to D_s^{(*)+}K^-)\rangle dt}{\int_0^\infty \langle \Gamma(B_s \to D_s^{(*)+}K^-)\rangle dt} = \frac{\tau_{B_s}}{1-y_s^2}\left[\frac{1 + 2\,\mathcal{A}_{\Delta\Gamma}\, y_s + y_s^2}{1 + \mathcal{A}_{\Delta\Gamma}\, y_s}\right], \tag{4.63}$$

with an analogous expression for the lifetimes $\overline{\tau}_{\text{eff}}$ of the CP-conjugate $D_s^{(*)-}K^+$ final states. We then obtain

$$\text{BR}(B_s \to D_s^{(*)+}K^-) = \left[2 - (1-y_s^2)\,\tau_{\text{eff}}\right] \overline{\text{BR}}(B_s \to D_s^{(*)+}K^-), \tag{4.64}$$

and correspondingly for the $D_s^{(*)-}K^+$ final states. These general relations would also hold if the $B_s \to D_s^{(*)\pm}K^\mp$ decay amplitudes were to receive contributions from physics beyond the SM. However, this is not a plausible scenario due to the tree-diagram nature of these decays.

Let us now have a closer look at the ratio (4.54). Since the $B_s^0 \to D_s^-\pi^+$, $\bar{B}_s^0 \to D_s^+\pi^-$ decays are flavour-specific, their $\mathcal{A}_{\Delta\Gamma}$, $\overline{\mathcal{A}}_{\Delta\Gamma}$ observables vanish. The branching ratios entering (4.54) are averages of the experimental branching ratios over the final states:

$$\overline{\text{BR}}(B_s \to D_s^\pm K^\mp) \equiv \frac{1}{2}\left[\overline{\text{BR}}(B_s \to D_s^+K^-) + \overline{\text{BR}}(B_s \to D_s^-K^+)\right], \tag{4.65}$$

with an analogous expression for $\overline{\text{BR}}(B_s \to D_s^\pm\pi^\mp)$. Using (4.56) and its $B_s \to D_s^\pm\pi^\mp$ counterpart yields

$$\frac{\overline{\text{BR}}(B_s \to D_s^{(*)\pm}K^\mp)}{\overline{\text{BR}}(B_s \to D_s^{(*)\pm}\pi^\mp)} = \left[1 + y_s\left(\frac{\mathcal{A}_{\Delta\Gamma} + \overline{\mathcal{A}}_{\Delta\Gamma}}{2}\right)\right]\frac{\text{BR}(B_s \to D_s^{(*)\pm}K^\mp)}{\text{BR}(B_s \to D_s^{(*)\pm}\pi^\mp)}. \tag{4.66}$$

In the language of factorization, as discussed in Section 2.3, the decays $\bar{B}_s^0 \to D_s^{(*)+}K^-$ and $\bar{B}_s^0 \to D_s^{(*)+}\pi^-$ are classed as heavy-light. They are therefore expected to factorise well [37, 36, 109, 110, 111, 38, 112], which is also supported by experimental data [113]. In Figure 4.10, we illustrate the decay topologies characterizing these decays. Using $SU(3)$ flavour symmetry to relate the $\bar{B}_s^0 \to D_s^{(*)+}K^-$ amplitude to that of the $\bar{B}_s^0 \to D_s^{(*)+}\pi^-$ channel (and correspondingly for the CP-conjugate processes), the

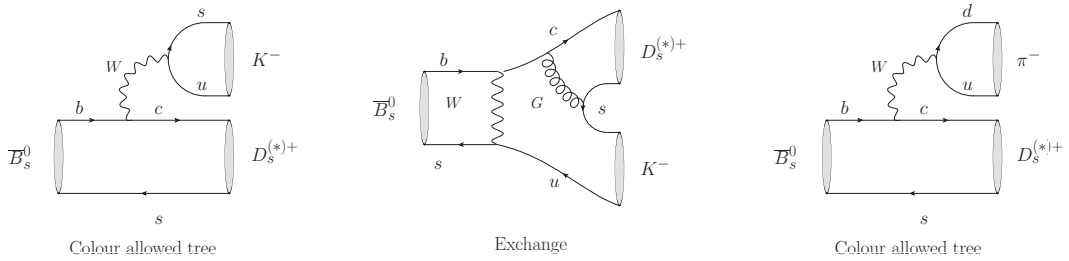

Figure 4.10: The colour-allowed tree and exchange topologies contributing to the $\bar{B}_s^0 \to D_s^{(*)+} K^-$ decay in comparison with the colour-allowed tree topology of the $SU(3)$-related $\bar{B}_s^0 \to D_s^{(*)+} \pi^-$ channel which does not receive exchange contributions because of the flavour content of its final state.

ratio of the theoretical branching ratios in (4.66) allows the extraction of the hadronic parameter x_s [103]:

$$x_s = \sqrt{\left[\frac{\mathcal{C}^{(*)}}{\epsilon}\right]\left[\frac{\mathrm{BR}(B_s \to D_s^{(*)\pm} K^{\mp})}{\mathrm{BR}(B_s \to D_s^{(*)\pm} \pi^{\mp})}\right] - 1}. \tag{4.67}$$

The small CKM parameter ϵ is defined in (4.9), while the $\mathcal{C}^{(*)}$ coefficient can be written in the following form:

$$\mathcal{C}^{(*)} \equiv \frac{\Phi_{D_s^{(*)}\pi}}{\Phi_{D_s^{(*)}K}} \mathcal{N}_F^{(*)} \mathcal{N}_a^{(*)} \mathcal{N}_E^{(*)}, \tag{4.68}$$

where the Φ are phase-space factors defined in (4.14), and

$$\mathcal{N}_F^{(*)} \equiv \left[\frac{f_\pi}{f_K} \frac{F_{B_s \to D_s^{(*)}}(M_\pi^2)}{F_{B_s \to D_s^{(*)}}(M_K^2)}\right]^2 \tag{4.69}$$

describes factorizable $SU(3)$-breaking corrections through the ratios of decay constants $f_K/f_\pi = 1.197 \pm 0.006$ [17] and form factors[3]. On the other hand, the non-factorizable $SU(3)$-breaking corrections affecting the ratio of the colour-allowed tree amplitudes governing the $\bar{B}_s^0 \to D_s^{(*)+} K^-$ and $\bar{B}_s^0 \to D_s^{(*)+} \pi^-$ channels are described by

$$\mathcal{N}_a^{(*)} \equiv \left|\frac{a_1(D_s^{(*)}\pi)}{a_1(D_s^{(*)}K)}\right|^2. \tag{4.70}$$

Finally, $\mathcal{N}_E^{(*)}$ takes into account that the $\bar{B}_s^0 \to D_s^{(*)+} K^-$ decays receive also contributions from exchange topologies, which have no counterparts in the $\bar{B}_s^0 \to D_s^{(*)+} \pi^-$

[3]For the calculation of the form-factor ratio in (4.69) we have assumed that the q^2 dependence is identical to that for $B_d \to D^{(*)-} \ell\nu$ decays [114].

processes, as can be seen in Figure 4.10:

$$\mathcal{N}_E^{(*)} \equiv \left| \frac{T_{D_s^{(*)+}K^-}}{T_{D_s^{(*)+}K^-} + E_{D_s^{(*)+}K^-}} \right|^2 . \tag{4.71}$$

Following the phenomenological analysis of Ref. [113], and using experimental data to make factorization tests and to constrain the exchange topologies, we find $\mathcal{N}_a^{(*)} \sim 1.00 \pm 0.02$ and $\mathcal{N}_E^{(*)} \sim 0.97 \pm 0.08$. The exchange contributions can be probed further in the future through the $\bar{B}_s^0 \to D^{(*)+}\pi^-$ channel, which receives only contributions from such topologies [103]. Finally, we obtain the numerical value

$$\mathcal{C}^{(*)} = 0.67 \pm 0.05. \tag{4.72}$$

Using now (4.57) and (4.66), we arrive at

$$x_s = y_s \cos\delta_s \cos(\phi_s + \gamma) \pm \sqrt{\left[\frac{\mathcal{C}^{(*)}}{\epsilon}\right]\left[\frac{\overline{\rm BR}(B_s \to D_s^{(*)\pm}K^\mp)}{\overline{\rm BR}(B_s \to D_s^{(*)\pm}\pi^\mp)}\right] - 1 + y_s^2 \cos^2\delta_s \cos^2(\phi_s+\gamma)}, \tag{4.73}$$

where x_s was defined as a positive parameter [103]. For the numerical values of ϕ_s and γ in (3.48) and (4.26), respectively, the CDF result in (4.54) gives $x_s = 0.46 \pm 0.27\,({\rm BR}) \pm 0.11\,(\mathcal{C}) \pm 0.04\,(\delta_s)$. This value for x_s is consistent with theoretical expectations [103] and the picture discussed in the next section. On the other hand, the central values of the LHCb and Belle results in (4.54) do not give real solutions for x_s. The requirement that the argument of the square-root in (4.73) is positive can be converted into the following lower bound:

$$\frac{\overline{\rm BR}(B_s \to D_s^{(*)\pm}K^\mp)}{\overline{\rm BR}(B_s \to D_s^{(*)\pm}\pi^\mp)} \geq \frac{\epsilon}{\mathcal{C}^{(*)}}\left[1 - y_s^2 \cos^2\delta_s \cos^2(\phi_s+\gamma)\right] = 0.080 \pm 0.007, \tag{4.74}$$

which is shown in Figure 4.11. We observe that the LHCb result for the ratio of branching ratios would need to increase by about two standard deviations to satisfy this bound and to give a real solution for x_s.

In the next section, we shall use data from the B factories to obtain a sharper picture of the hadronic parameters, including the CP-conserving strong phases δ_s.

4.3.2 Estimating the hadronic parameters

Using the U-spin flavour symmetry of strong interactions, the hadronic parameters x_s and δ_s of the $B_s \to D_s^{(*)\pm}K^\mp$ channels can be related to their counterparts x_d and δ_d of the $B_d \to D^{(*)\pm}\pi^\mp$ decays as follows [103]:

$$x_s = -\frac{x_d}{\epsilon}, \quad \delta_s = \delta_d. \tag{4.75}$$

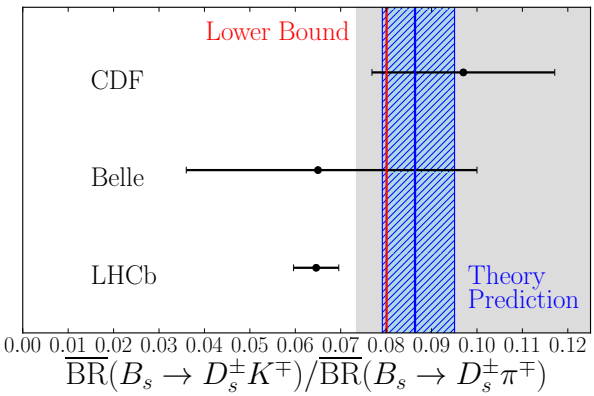

Figure 4.11: Compilation of measurements of the ratio of branching ratios as given in (4.54) and comparison with the lower bound in (4.74). The theoretical prediction indicated by the vertical band corresponds to (4.108) as given in Section 4.3.4.

These relations assume exact U-spin symmetry; the impact of possible corrections will be addressed below.

The BaBar [115, 116] and Belle [117, 118] collaborations have performed measurements which allow us to constrain the hadronic parameters $|x_d|$ and δ_s. For the $B_d \to D^{\pm}\pi^{\mp}$ system the following constraints have been extracted from studies of CP-violating effects [73]:

$$a^{D\pi} \equiv -2|x_d| \sin(\phi_d + \gamma) \cos(\delta_d) = -0.03 \pm 0.017, \tag{4.76}$$
$$c_{\mathrm{lep}}^{D\pi} \equiv -2|x_d| \cos(\phi_d + \gamma) \sin(\delta_d) = -0.022 \pm 0.021. \tag{4.77}$$

A corresponding analysis of the $B_d \to D^{*\pm}\pi^{\mp}$ decays (for which $L = 1$) yields [73]

$$a^{D^*\pi} \equiv 2|x_d^V| \sin(\phi_d + \gamma) \cos(\delta_d^V) = -0.039 \pm 0.010, \tag{4.78}$$
$$c_{\mathrm{lep}}^{D^*\pi} \equiv 2|x_d^V| \cos(\phi_d + \gamma) \sin(\delta_d^V) = -0.010 \pm 0.013, \tag{4.79}$$

where we have used the label V to distinguish the vector D^* system. In order to convert these experimental results into $|x_d|$ and δ_d, we assume the value for γ in (4.26) with the B_d^0–$\bar{B}_d^0$ mixing phase taken to be $\phi_d = (42.8 \pm 1.6)^\circ$ [73], which yields $\phi_d + \gamma = (111 \pm 7)^\circ$.

Let us first extract $|x_d|$ by determining the doubly Cabibbo-suppressed branching ratio $\mathrm{BR}(\bar{B}_d^0 \to D^-\pi^+)$ from $\mathrm{BR}(\bar{B}_d^0 \to D_s^-\pi^+)$ with the help of the $SU(3)$ flavour symmetry [119]. Using the notation of Ref. [113], we write

$$\mathrm{BR}(\bar{B}_d^0 \to D^-\pi^+) = \left(\frac{\epsilon}{\mathcal{C}'}\right) \mathrm{BR}(\bar{B}_d^0 \to D_s^-\pi^+), \tag{4.80}$$

where

$$\mathcal{C}' \equiv \frac{\Phi_{D_s\pi}}{\Phi_{D\pi}} \mathcal{N}_F' \mathcal{N}_a' \mathcal{N}_E'. \tag{4.81}$$

In analogy to (4.68), the Φ are are phase-space factors, while

$$\mathcal{N}'_F \equiv \left[\frac{f_{D_s}}{f_D}\,\frac{F_1^{\bar{B}^0_d\pi^+}(m^2_{D_s})}{F_1^{\bar{B}^0_d\pi^+}(m^2_D)}\right]^2 \tag{4.82}$$

and

$$\mathcal{N}'_a \equiv \left|\frac{a_1(D_s^+\pi^-)}{a_1(D^+\pi^-)}\right|^2 \tag{4.83}$$

describe factorizable and non-factorizable $SU(3)$-breaking effects, respectively. The $\mathcal{N}'_E$ factor takes into account that $\bar{B}^0_d \to D^-\pi^+$ has a contribution from an exchange topology, which does not have a counterpart in the $\bar{B}^0_d \to D_s^-\pi^+$ channel:

$$\mathcal{N}'_E \equiv \left|\frac{T_{D^-\pi^+}}{T_{D^-\pi^+} + E_{D^-\pi^+}}\right|^2. \tag{4.84}$$

We then obtain the following additional constraint for x_d:

$$|x_d| = \sqrt{\left(\frac{\epsilon}{\mathcal{C}'}\right)\left[\frac{\mathrm{BR}(\bar{B}^0_d \to D_s^-\pi^+)}{\mathrm{BR}(\bar{B}^0_d \to D^+\pi^-)}\right]}. \tag{4.85}$$

For the numerical analysis, we use the ratio of decay constants $f_{D_s}/f_D = 1.25 \pm 0.06$ [17] and the form-factor ratio $F_1^{\bar{B}^0_d\pi^+}(m^2_D)/F_1^{\bar{B}^0_d\pi^+}(m^2_{D_s}) = 0.9771 \pm 0.0009$, where we have applied the evolution equation for the $\bar{B}^0_d \to \pi^+$ form factor given in Ref. [120]. For the decays entering (4.80), factorization is not expected to work well. Indeed, following the approach discussed in Ref. [113], we extract $|a_1(D_s^+\pi^-)| = 0.68 \pm 0.12$ from the experimental data, while factorization would correspond to a value around one. Unfortunately, an analogous factorization test for $\bar{B}^0_d \to D^-\pi^+$ cannot be performed[4]. We allow for 20% $SU(3)$-breaking effects for the non-factorizable contributions, i.e. for the deviation of $|a_1|$ from one, leading to $\mathcal{N}'_a = 1.0 \pm 0.2$.

In order to estimate the importance of the exchange contribution, we apply the $SU(3)$ flavour symmetry and use experimental information on $\mathrm{BR}(\bar{B}^0_d \to D_s^+K^-) = (2.2 \pm 0.5) \times 10^{-5}$ [17], which receives only contributions from exchange topologies. Comparing it to the contribution from tree topologies, which we fix again through $\mathrm{BR}(\bar{B}^0_d \to D_s^-\pi^+) = (2.16 \pm 0.26) \times 10^{-5}$ [121, 122], we obtain:

$$\left|\frac{E_{D^-\pi^+}}{T_{D^-\pi^+}}\right| \sim \frac{f_\pi}{f_K}\left|\frac{V_{ub}}{V_{cb}}\right|\sqrt{\frac{\mathrm{BR}(\bar{B}^0_d \to D_s^+K^-)}{\mathrm{BR}(\bar{B}^0_d \to D_s^-\pi^+)}} \sim 0.1. \tag{4.86}$$

Consequently, we estimate $\mathcal{N}'_E \sim 1.0 \pm 0.2$. In comparison with the value of $\mathcal{N}_E \sim 0.97 \pm 0.08$ given after (4.71), this range is larger. Although the exchange topologies entering

[4]The branching ratio quoted by the Particle Data Group [17] is constructed from (4.85), so using this would create a circular argument.

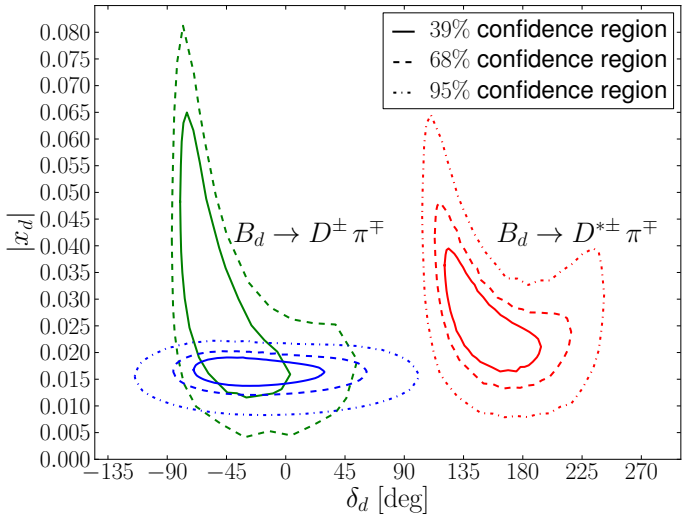

Figure 4.12: The confidence level contours for the χ^2 fit of the hadronic parameters $|x_d|$ and δ_d as discussed in the text, illustrating also the impact of the $|x_d|$ constraint in (4.88).

both quantities are estimated to have similar absolute size, the analysis performed in Ref. [113] indicates a large angle between the E and T amplitudes, which reduces the impact of E on the amplitude ratio in $\mathcal{N}_E$.

Using finally also the experimental branching ratio [17]

$$\mathrm{BR}(\bar{B}_d^0 \to D^+\pi^-) = (2.68 \pm 0.13) \times 10^{-3}, \tag{4.87}$$

the relation in (4.85) gives

$$|x_d| = 0.0163 \pm 0.0011|_{\mathrm{BR}} \pm 0.0026|_{SU(3)} = 0.0163 \pm 0.0028. \tag{4.88}$$

This value is consistent with the results for x_d given in Ref. [121, 122]. Combining (4.88) with (4.76) and (4.77) allows, in principle, the determination of $\phi_d + \gamma$ and δ_d up to discrete ambiguities. Unfortunately, a corresponding numerical fit leaves these parameters still largely unconstrained.

We proceed to extract the parameters $|x_d|, \delta_d$ and $|x_d^V|, \delta_d^V$ from the constraints in (4.76)–(4.79) using a χ^2 fit. For the former parameter set we also include the constraint in (4.88). The fit gives the following results:

$$|x_d| = 0.0166^{+0.0025}_{-0.0029}, \qquad \delta_d = \left(-35^{+65}_{-35}\right)^\circ, \tag{4.89}$$

$$|x_d^V| = 0.025^{+0.014}_{-0.008}, \qquad \delta_d^V = \left(146^{+48}_{-25}\right)^\circ, \tag{4.90}$$

where the errors give the 68% confidence level for each parameter. The χ^2/n_{dof} is 0.53 and 0.00 for the non-vector and vector decays, respectively. In Figure 4.12, we show the

corresponding 39%, 68% and 95% confidence level regions in the δ_d–$|x_d|$ plane. Note that the constraint in (4.88) considerably reduces the uncertainty of the $|x_d|$ parameter for the non-vector decay.

Using (4.75), we hereby find

$$x_s = 0.311^{+0.046}_{-0.053}\big|_{\rm input} \pm 0.06\big|_{SU(3)}, \qquad \delta_s = \left[-35^{+69}_{-40}\big|_{\rm input} \pm 20\big|_{SU(3)}\right]^\circ, \tag{4.91}$$

$$x_s^V = 0.47^{+0.26}_{-0.15}\big|_{\rm input} \pm 0.09\big|_{SU(3)}, \qquad \delta_s^V = \left[146^{+48}_{-25}\big|_{\rm input} \pm 20\big|_{SU(3)}\right]^\circ, \tag{4.92}$$

where we allow for $SU(3)$-breaking effects of 20% for the $x_s^{(V)}$ parameters and $\pm 20^\circ$ for the strong phases. In later applications of these results, the uncertainties associated with the $x_d^{(V)}$, $\delta_d^{(V)}$ parameters and the $SU(3)$-breaking effects will be combined in quadrature.

Before using the hadronic parameters given above to predict the observables of the $B_s \to D_s^{(*)\pm} K^\mp$ decays in Section 4.3.4, which serve as input for an experimental study, let us first discuss the extraction of $\phi_s + \gamma$ from these channels, with a special emphasis on multiple discrete ambiguities and their resolution.

4.3.3 Extraction of $\phi_s + \gamma$ and discrete ambiguities

For the extraction of $\phi_s + \gamma$ from the $B_s \to D_s^{(*)\pm} K^\mp$ system, it is necessary to measure the CP asymmetries described in Section 3.72:

$$\begin{aligned} A_{\rm CP}(B_s(t) \to D_s^{(*)+} K^-) &\equiv \frac{\Gamma(B_s^0(t) \to D_s^{(*)+} K^-) - \Gamma(\bar{B}_s^0(t) \to D_s^{(*)+} K^-)}{\Gamma(B_s^0(t) \to D_s^{(*)+} K^-) + \Gamma(\bar{B}_s^0(t) \to D_s^{(*)+} K^-)} \\ &= \frac{C\,\cos(\Delta M_s\, t) + S\,\sin(\Delta M_s\, t)}{\cosh(y_s\, t/\tau_{B_s}) + \mathcal{A}_{\Delta\Gamma}\,\sinh(y_s\, t/\tau_{B_s})}. \end{aligned} \tag{4.93}$$

An analogous expression holds for the CP-conjugate $D_s^{(*)-} K^+$ final states, where C, S and $\mathcal{A}_{\Delta\Gamma}$ are simply replaced by $\overline{C}$, $\overline{S}$ and $\overline{\mathcal{A}}_{\Delta\Gamma}$, respectively. The observables take the following form [103]:

$$C = -\left[\frac{1-x_s^2}{1+x_s^2}\right], \quad \overline{C} = +\left[\frac{1-x_s^2}{1+x_s^2}\right] \tag{4.94}$$

$$S = (-1)^L \frac{2\,x_s}{1+x_s^2}\,\sin(\phi_s + \gamma + \delta_s), \quad \overline{S} = (-1)^L \frac{2\,x_s}{1+x_s^2}\,\sin(\phi_s + \gamma - \delta_s), \tag{4.95}$$

which complement the expressions for $\mathcal{A}_{\Delta\Gamma}$ and $\overline{\mathcal{A}}_{\Delta\Gamma}$ in (4.57).

The mixing time-dependent observables $\overset{(-)}{C}$, $\overset{(-)}{S}$ and $\overset{(-)}{\mathcal{A}}_{\Delta\Gamma}$ are not independent of each other, but rather satisfy the relations

$$C^2 + S^2 + \mathcal{A}_{\Delta\Gamma}^2 = 1 = \overline{C}^2 + \overline{S}^2 + \overline{\mathcal{A}}_{\Delta\Gamma}^2 \tag{4.96}$$

The extraction of the weak phase $\phi_s + \gamma$ is intuitively understood if we express the above observables in terms of two polar vectors:[5]

$$\mathcal{A}_{\Delta\Gamma} + i\, S = -(-1)^L \sqrt{1 - C^2}\, e^{-i(\phi_s + \gamma + \delta_s)}, \tag{4.97}$$

$$\overline{\mathcal{A}}_{\Delta\Gamma} + i\, \overline{S} = -(-1)^L \sqrt{1 - \overline{C}^2}\, e^{-i(\phi_s + \gamma - \delta_s)}, \tag{4.98}$$

where, because $C = -\overline{C}$, both vectors have the same absolute value

$$\sqrt{1 - \overset{(-)}{C}{}^2} = \frac{2\, x_s}{1 + x_s^2}, \tag{4.99}$$

and thus span the same circle on the complex plane. As illustrated in the left panel of Fig. 4.13, the weak phase $\phi_s + \gamma$ then corresponds to the polar angle of a vector that lies halfway between the two observable vectors, (4.97) and (4.98), with an equal angular distance of δ_s to both.

From the relations (4.96) it follows that only two of the three observables for each of the final states in the $B_s \to D_s^{(*)\pm} K^{\mp}$ system are needed to determine the magnitude of the angle $\phi_s + \gamma$. However, to also resolve the discrete ambiguities of this angle, the optimal two sets are S, $\mathcal{A}_{\Delta\Gamma}$ and $\overline{S}$, $\overline{\mathcal{A}}_{\Delta\Gamma}$. To see this, consider, as in the $B_d \to D^{(*)\pm}\pi^{\mp}$ system, that we neglect the untagged observables $\mathcal{A}_{\Delta\Gamma}$ and $\overline{\mathcal{A}}_{\Delta\Gamma}$. The direct CP violation observable $|C| = |\overline{C}|$ then fixes the radius in the complex plane, and the mixing CP observables S and $\overline{S}$ the component in the imaginary direction. As illustrated in the right panel of Fig. 4.13, this results in an 8-fold discrete ambiguity for $\phi_s + \gamma$. We will refer to this as the "conventional" extraction method [102, 103]. On the contrary, as shown in the left panel of Fig. 4.13, if the observables S and $\overline{S}$ are measured together with the untagged observables $\mathcal{A}_{\Delta\Gamma}$ and $\overline{\mathcal{A}}_{\Delta\Gamma}$, the discrete ambiguity is reduced to a two-fold one.

To extract the weak phase $\phi_s + \gamma$ we proceed to find the polar vectors offset by this angle in the complex plane. We define, as in Ref. [103], the combination of observables

$$\langle \mathcal{A}_{\Delta\Gamma} \rangle_{\pm} \equiv \frac{\overline{\mathcal{A}}_{\Delta\Gamma} \pm \mathcal{A}_{\Delta\Gamma}}{2}, \quad \langle S \rangle_{\pm} \equiv \frac{\overline{S} \pm S}{2}. \tag{4.100}$$

The average sum and difference of the two vectors, (4.97) and (4.98), are then:

$$\langle \mathcal{A}_{\Delta\Gamma} \rangle_{+} + i\, \langle S \rangle_{+} = \left[(-1)^L \sqrt{1 - C^2}\, \cos\delta_s \right] e^{i[\pi - (\phi_s + \gamma)]}, \tag{4.101}$$

$$\langle \mathcal{A}_{\Delta\Gamma} \rangle_{-} + i\, \langle S \rangle_{-} = \left[(-1)^L \sqrt{1 - C^2}\, \sin\delta_s \right] e^{i[\pi/2 - (\phi_s + \gamma)]}, \tag{4.102}$$

which vanish in magnitude for the limits $\cos\delta_s \to 0$ or $\sin\delta_s \to 0$, respectively. It then follows that the weak phase combination $\phi_s + \gamma$ is given by

$$\tan(\phi_s + \gamma) = \frac{\langle S \rangle_{+}}{-\langle \mathcal{A}_{\Delta\Gamma} \rangle_{+}} = \frac{\langle \mathcal{A}_{\Delta\Gamma} \rangle_{-}}{\langle S \rangle_{-}}. \tag{4.103}$$

[5] Their relation to the complex observables ξ and $\overline{\xi}$ defined in Ref. [103] is given by $2\,\xi/(1 + |\xi|^2) = \mathcal{A}_{\Delta\Gamma} + i\, S$ and $2\,\overline{\xi}/(1 + |\overline{\xi}|^2) = \overline{\mathcal{A}}_{\Delta\Gamma} + i\, \overline{S}$, respectively.

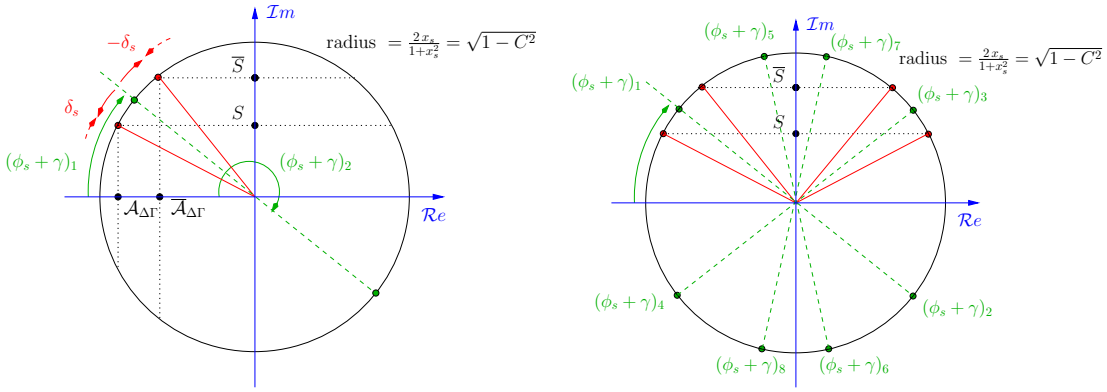

Figure 4.13: Illustration of the complex numbers $(\mathcal{A}_{\Delta\Gamma} + iS)$ and $(\overline{\mathcal{A}}_{\Delta\Gamma} + i\,\overline{S})$ with lengths $\sqrt{1-C^2}$ in the complex plane. Left panel: illustration of the reduction of the discrete ambiguity to a twofold one through the untagged observables $\mathcal{A}_{\Delta\Gamma}$ and $\overline{\mathcal{A}}_{\Delta\Gamma}$ (see (4.103)). Right panel: illustration of the conventional extraction of $\phi_s + \gamma$ and the associated eightfold discrete ambiguity.

The two-fold ambiguity inherent in the tangent function is resolvable with the sign information of the real and imaginary components. The real and imaginary components themselves have a global sign ambiguity related to the sign of $\cos\delta$ or $\sin\delta$. As discussed in Ref. [103], this remaining ambiguity can be resolved from factorization arguments, where we expect:

$$\cos\delta_s > 0, \quad \cos\delta_s^V < 0, \tag{4.104}$$

This agrees well with the results of the U-spin analysis presented Section 4.3.2, where the results for the strong phases in (4.91) and (4.92) give

$$\cos\delta_s = 0.82^{+0.18}_{-0.56}, \quad \cos\delta_s^V = -0.83^{+0.43}_{-0.17}. \tag{4.105}$$

Thus, under reasonable assumptions, the extraction of $\phi_s + \gamma$ is unambiguous.

The advantage of the optimal set of observables S, $\overline{S}$ and $\mathcal{A}_{\Delta\Gamma}$, $\overline{\mathcal{A}}_{\Delta\Gamma}$ is not only that they depend linearly on x_s – in contrast to C, $\overline{C}$ – but that x_s drops out in (4.103). Interestingly, as we will see in the next section, both observable sets can be accessed with similar precision at LHCb: the extraction of the untagged $\mathcal{A}_{\Delta\Gamma}$, $\overline{\mathcal{A}}_{\Delta\Gamma}$ observables relies on the B_s decay width parameter y_s, while the measurement of the S, $\overline{S}$ observables requires the tagging of the flavour of the initially produced B_s^0 or $\bar{B}_s^0$ mesons.

4.3.4 Experimental prospects

The hadronic parameters determined in Section 4.3.2, together with estimates for the phases ϕ_s and γ given in (3.48) and (4.26), allow us to make predictions of the observables

Table 4.1: Experimental uncertainties on the weak phase $\phi_s + \gamma$, strong phase δ_s and hadronic parameter x_s for various data samples as determined from the toy Monte Carlo simulation performed in Ref [86]. Results for the "conventional method", which excludes the untagged observables, are also shown. The errors correspond to the central values $\phi_s + \gamma = 65.5°$, $\delta_s = -35°$ and $x_s = 0.31$.

	With $\mathcal{A}_{\Delta\Gamma}$ and $\overline{\mathcal{A}}_{\Delta\Gamma}$			"Conventional Method"		
Scenario	$\phi_s + \gamma$	δ_s	x_s	$\phi_s + \gamma$	δ_s	x_s
LHCb 2012	$[\pm 17]°$	$[\pm 17]°$	± 0.080	-	-	± 0.11
LHCb 2018	$[\pm 7.3]°$	$[\pm 7.3]°$	± 0.035	$[^{+16}_{-26}]°$	$[^{+26}_{-16}]°$	± 0.048
LHCb Upgrade	$[\pm 3.0]°$	$[\pm 3.0]°$	± 0.015	$[^{+8.8}_{-19}]°$	$[^{+19}_{-8.8}]°$	± 0.021

of the $B_s \to D_s^{\pm} K^{\mp}$ decays:

$$\begin{aligned} \tau_{\text{eff}} &= 0.971^{+0.053}_{-0.012}\ \tau_{B_s}, \quad \mathcal{A}_{\Delta\Gamma} = -0.49^{+0.58}_{-0.13}, \quad C = -0.824^{+0.086}_{-0.077}, \quad S = 0.29^{+0.30}_{-0.40}, \\ \bar{\tau}_{\text{eff}} &= 1.025^{+0.030}_{-0.054}\ \tau_{B_s}, \quad \overline{\mathcal{A}}_{\Delta\Gamma} = 0.11^{+0.34}_{-0.59}, \quad \overline{C} = 0.824^{+0.077}_{-0.086}, \quad \overline{S} = 0.55^{+0.11}_{-0.28}. \end{aligned} \tag{4.106}$$

And analogously for the $B_s \to D_s^{*\pm} K^{\mp}$ decays:

$$\begin{aligned} \tau^V_{\text{eff}} &= 0.954^{+0.057}_{-0.021}\ \tau_{B_s}, \quad \mathcal{A}^V_{\Delta\Gamma} = -0.66^{+0.60}_{-0.21}, \quad C^V = -0.64^{+0.36}_{-0.20}, \quad S^V = 0.40^{+0.39}_{-0.44}, \\ \bar{\tau}^V_{\text{eff}} &= 1.027^{+0.034}_{-0.060}\ \tau_{B_s}, \quad \overline{\mathcal{A}}^V_{\Delta\Gamma} = 0.13^{+0.40}_{-0.66}, \quad \overline{C}^V = 0.64^{+0.20}_{-0.36}, \quad \overline{S}^V = 0.76^{+0.19}_{-0.30}. \end{aligned} \tag{4.107}$$

Furthermore, our predictions for the branching ratio observables (4.54) and (4.62) are

$$\left.\frac{\overline{\text{BR}}(B_s \to D_s^{\pm} K^{\mp})}{\overline{\text{BR}}(B_s \to D_s^{\pm} \pi^{\mp})}\right|_{SU(3)} = 0.0864^{+0.0087}_{-0.0072}, \tag{4.108}$$

$$\left.\frac{\overline{\text{BR}}(B_s \to D_s^{+} K^{-}) - \overline{\text{BR}}(B_s \to D_s^{-} K^{+})}{\overline{\text{BR}}(B_s \to D_s^{+} K^{-}) + \overline{\text{BR}}(B_s \to D_s^{-} K^{+})}\right|_{SU(3)} = -0.027^{+0.052}_{-0.019}, \tag{4.109}$$

respectively. The prediction in (4.108) is compared to the current experimental results in Figure 4.11. Similarly, we predict for the vector decays:

$$\left.\frac{\overline{\text{BR}}(B_s \to D_s^{*\pm} K^{\mp})}{\overline{\text{BR}}(B_s \to D_s^{*\pm} \pi^{\mp})}\right|_{SU(3)} = 0.099^{+0.030}_{-0.036}, \tag{4.110}$$

$$\left.\frac{\overline{\text{BR}}(B_s \to D_s^{*+} K^{-}) - \overline{\text{BR}}(B_s \to D_s^{*-} K^{+})}{\overline{\text{BR}}(B_s \to D_s^{*+} K^{-}) + \overline{\text{BR}}(B_s \to D_s^{*-} K^{+})}\right|_{SU(3)} = -0.035^{+0.056}_{-0.024}. \tag{4.111}$$

The LHCb experiment has performed a first measurement of the CP observables for the $B_s \to D_s^{\pm} K^{\mp}$ decays [107]. In our notation these results are given by:

$$\begin{aligned} \mathcal{A}_{\Delta\Gamma} &= -1.33 \pm 0.60 \pm 0.26, \quad C = -1.01 \pm 0.50 \pm 0.23, \quad S = -1.25 \pm 0.56 \pm 0.24, \\ \overline{\mathcal{A}}_{\Delta\Gamma} &= -0.81 \pm 0.56 \pm 0.26, \quad \overline{C} = 1.01 \pm 0.50 \pm 0.23, \quad \overline{S} = -0.08 \pm 0.68 \pm 0.28. \end{aligned} \tag{4.112}$$

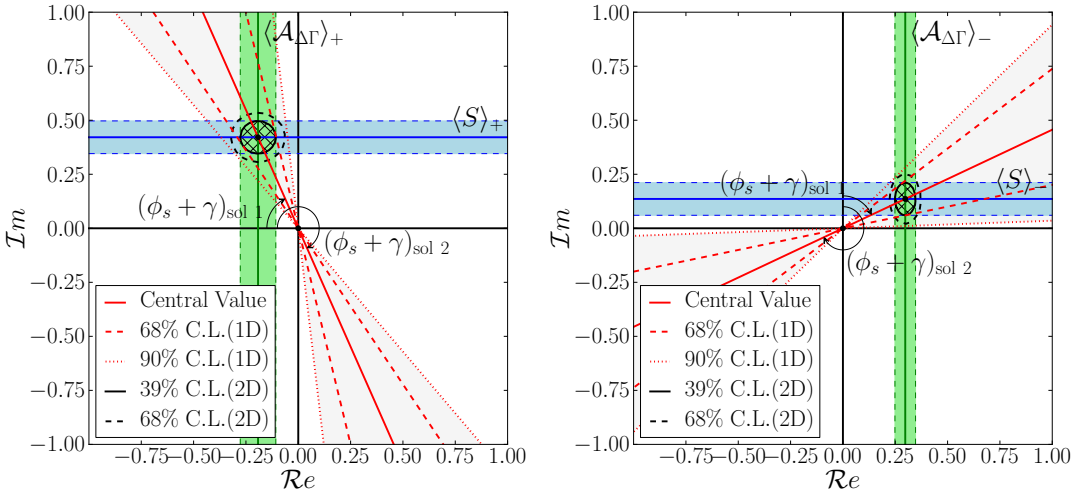

Figure 4.14: Illustration of the determination of $\phi_s + \gamma$ from the separate observable combinations $\langle \mathcal{A}_{\Delta\Gamma} \rangle_+$ and $\langle S \rangle_+$ (left) and $\langle \mathcal{A}_{\Delta\Gamma} \rangle_-$ and $\langle S \rangle_-$ (right); see (4.101) and (4.102). The errors bands correspond to the expected experimental sensitivity of LHCb before by the end of the second run in 2018, which is based on the toy study performed in Ref [86].

where $C = -\overline{C}$ has been assumed. We observe, however, that the errors are still too large for a meaningful comparison to be made with the predictions given in (4.106).

To estimate the future experimental sensitivity for the above observables, toy Monte Carlo simulations were performed in Ref. [86]. The data samples used in these simulations were chosen to represent the number of events expected by the end of the 2012 LHC run, end of the second LHC run (estimated to be in 2018), and by the end of the LHCb upgrade. Global fits for the parameters $\phi_s + \gamma$, x_s and δ_s resulting from these simulations are summarised in Table 4.1. In particular, we have also compared the analysis involving the untagged observables with the "conventional method" as discussed in Section 4.3.3. As expected, the inclusion of untagged information greatly improves our sensitivity to our parameters of interest.

Aside from a global fit, it is also possible to use the observable pairs defined in (4.101) and (4.102) separately to extract $\phi_s + \gamma$. This method is illustrated in Figure 4.14. Similarly, in the left panel of Figure 4.15, we illustrate the extraction of $\gamma + \phi_s$ from $\langle S \rangle_+$ and $\langle \mathcal{A}_{\Delta\Gamma} \rangle_+$ using the first relation in (4.103). And finally, in the right panel of Figure 4.15 we illustrate the extraction of this angle from a combination of all the observables, i.e. $\mathcal{A}_{\Delta\Gamma}$, S and C with their CP conjugates. In each of these figures we have used the results from toy simulation discussed above with a data sample corresponding to the end of the second LHC run.

The magnitude of $\mathcal{A}_{\Delta\Gamma} + iS$ can be further constrained through the $SU(3)$ flavour symmetry, i.e. through (4.73) or by means of (4.75) with (4.85). However, we find that this input, which would introduce the $SU(3)$ flavour symmetry into a theoretically clean

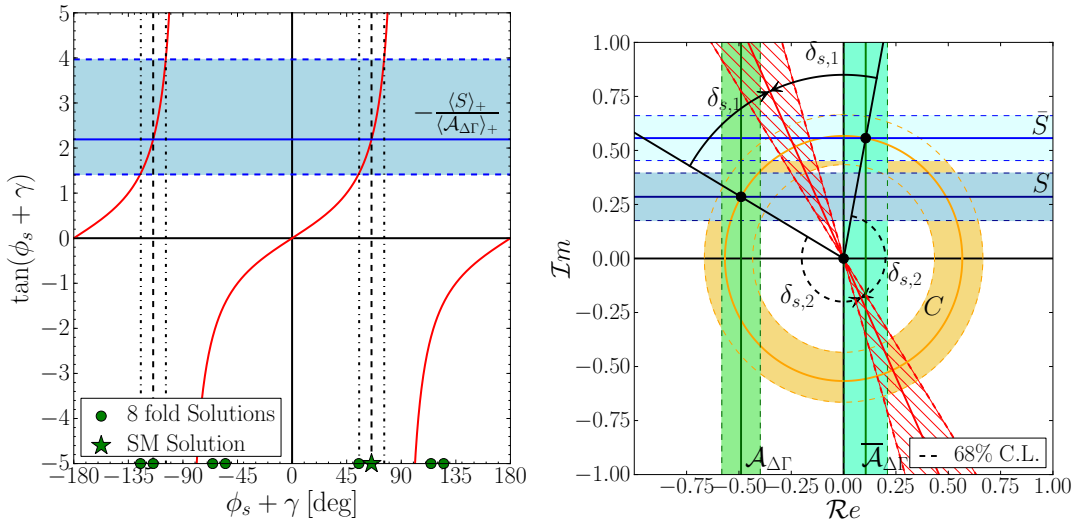

Figure 4.15: Illustration of the determination of $\phi_s+\gamma$ from two different methods. *Left panel:* using $\langle \mathcal{A}_{\Delta\Gamma}\rangle_+$ and $\langle S\rangle_+$ by means of (4.103). We also show the eightfold solution resulting from the "conventional" method as discussed in the text. *Right panel:* from a simultaneous fit to $\mathcal{A}_{\Delta\Gamma}$, S, C and their CP conjugates in the complex plane (see also Figure 4.13). The errors bands correspond to the expected experimental sensitivity of LHCb before by the end of the second run in 2018, which is based on the toy study performed in Ref [86].

strategy, does not significantly improve the precision for $\gamma+\phi_s$. If also decays of the type $B_s\to D_s^{*\pm}K^{\mp}$ can be reconstructed, the precision could be further enhanced in a theoretically clean way. However, these channels require the reconstruction of a radiative photon in the decay $D_s^{*\pm}\to D_s^{\pm}\gamma$ and as such are experimentally more challenging.

4.4 Conclusions

In this chapter we have considered strategies to determine the CKM angles γ and ϕ_s using the QCD penguin dominated transition $B_s\to K^+K^-$ and the tree-level transitions $B_s\to D_s^{(*)}K$. For both decay modes the optimal strategies for determining γ are still awaiting precise experimental data. Nonetheless, we have performed interesting first analyses for both modes and given Standard Model predictions using existing experimental measurements together with $SU(3)$ flavour symmetry assumptions. It will be very interesting to eventually compare the value of γ extracted from pure tree topologies, specifically the theoretically clean time-dependent $B_s\to D_s^{(*)}K$ analysis discussed here, with the extraction involving penguin topologies, namely the $B_s\to K^+K^-$ strategy, as the latter are potentially sensitive to New Physics effects.

Regarding the U-spin-related $B_s^0\to K^+K^-$, $B_d^0\to\pi^+\pi^-$ pair of decays, we have performed a first determination of the angle γ using alternative inputs from those of

the optimal strategy. We obtained the value $\gamma = (67.7^{+4.5}_{-5.0}|_{\rm input}{}^{+5.0}_{-3.7}|_{\xi}{}^{+0.1}_{-0.2}|_{\Delta\theta})^\circ$, which is very competitive with other determinations of this angle. Furthermore, it agrees very well with fits of the unitarity triangle. As a result we conclude that large New Physics effects in the decay amplitudes of these decays must be absent.

Assuming no New Physics in the decay amplitudes, which lets us fix the value of γ, we proceeded to analyse the potential of extracting the B_s mixing parameters from the time-dependent observables of $B_s \to K^+K^-$. A particularly interesting observable to this end is the mass-eigenstate rate asymmetry $\mathcal{A}_{\Delta\Gamma}^{K^+K^-}$, which can be probed by an effective lifetime fit to the untagged time-dependent sample. Also interesting is the mixing-induced CP asymmetry available from a tagged analysis. The Standard Model predictions of both observables are robust under the current errors of the input quantities as well as with respect to U-spin-breaking estimates. We further found both observables to be sensitive to New Physics effects in B_s mixing, and thereby complement the standard $B_s^0 \to J/\psi\phi$ analysis for determining these parameters, as well as the general $B_s^0 \to J/\psi s\bar{s}$ modes to be discussed in Chapter 5.

Finally, we illustrated the optimal strategy for extracting γ using the $B_s^0 \to K^+K^-$ decay. This strategy is still awaiting more accurate experimental results from the LHCb experiment. Once available, it will not only allow a theoretically cleaner determination of γ but will also allow an internal consistency check of the U-spin symmetry assumption. Using existing data, the current picture points towards a favourable situation with respect to possible U-spin-breaking effects.

Also for the decays $B_s \to D_s^{(*)\pm}K^\mp$ we have performed a detailed analysis of their observables. We addressed in particular their dependence on the B_s decay width difference y_s, which affects the utility of their branching ratio measurements in a subtle way. We derived a lower bound for the ratio of the experimental $B_s \to D_s^\pm K^\mp$ and $B_s \to D_s^\pm \pi^\mp$ branching ratios given in (4.54), and observed that the central value for the LHCb result is too small by about two standard deviations.

The width difference y_s offers the untagged observables $\mathcal{A}_{\Delta\Gamma}$ and $\overline{\mathcal{A}}_{\Delta\Gamma}$ for the final states $D_s^{(*)+}K^-$ and $D_s^{(*)-}K^+$, respectively, which can nicely be combined with the corresponding mixing-induced CP asymmetries S and $\overline{S}$ to determine $\phi_s + \gamma$ in an unambiguous way. We have illustrated this strategy and also given predictions for the $B_s \to D_s^{(*)\pm}K^\mp$ observables from an $SU(3)$ analysis of the B-factory data for $B_d \to D^{(*)\pm}\pi^\mp$, $B_d \to D_s^\pm\pi^\mp$ decays. Using data available from a toy experimental simulation we have illustrated that the interplay between the untagged observables $\mathcal{A}_{\Delta\Gamma}$, $\overline{\mathcal{A}}_{\Delta\Gamma}$ and the tagged CP asymmetries S, $\overline{S}$ is actually the key feature for being able to measure $\phi_s + \gamma$ through the $B_s \to D_s^{(*)\pm}K^\mp$ decays at LHCb.

Chapter 5

An exploration of $B_s \to J/\psi s\bar{s}$

5.1 Introduction

Measurements of the B_s^0–$\bar{B}_s^0$ mixing phase ϕ_s appear to be converging towards the SM prediction, suggesting that contributions from New Physics, if present, are small. The analysis driving this convergence is that of the decay mode $B_s \to J/\psi\phi$, for which the determination of ϕ_s by the LHCb experiment was given in (3.48). The presence of the ϕ vector meson in the final state helps the prominence of this decay in two ways. Firstly, the ϕ decays favourably to two charged kaons, which gives a clear signal at hadron collider experiments. And, secondly, the ϕ is believed to be almost completely an $s\bar{s}$ state. Thus the decay mode $B_s \to J/\psi\phi$ is driven by the tree-level $b \to sc\bar{c}$ transition, which does not receive a large CKM suppression and also carries no CP violating phases (in our convention). The only obvious price we must pay for picking two vector mesons in the final state is that a time-dependent angular analysis is required to disentangle the various CP-even and CP-odd polarization states [123, 79].

As precision improves, however, corrections from additional decay mode topologies will also need to be accounted for. Specifically, doubly Cabibbo suppressed penguin topologies contributing with CP violating phases can shift the value of ϕ_s that is extracted. In the formalism introduced in Section 3.2.2, this amounts to measuring a separate angle $\phi_s + \Delta\phi^{\lambda}_{J/\psi\phi}$ for each of the basis components λ constituting the angular analysis of the $B_s \to J/\psi\phi$ decay mode (see Section 3.4 for a brief discussion of this basis). In order to estimate these $\Delta\phi^{\lambda}_{J/\psi\phi}$ phase shifts, which are subject to theoretical hadronic uncertainties, it is possible to use information from decay modes whose topologies are related by $SU(3)_{\mathrm{F}}$ flavour symmetry but where the penguin topologies are not doubly Cabibbo suppressed. Two examples of such control channels are $B_s \to J/\psi\overline{K}^{0*}$ and $B_d \to J/\psi\rho^0$ [81].

Estimating the phase shifts $\Delta\phi^{\lambda}_{J/\psi\phi}$ is not the topic of this chapter, however. Instead, we seek to reduce the uncertainty of ϕ_s by overconstraining it using different independent analyses, each with their own strategies for controlling the hadronic uncertainties. In

particular we will focus on decay modes of the form $B_s \to J/\psi s\bar{s}$ with the $s\bar{s}$ bound state taken to form a spin-0 meson. In this case the experimental measurement is simplified by not requiring an angular analysis. In Section 5.2 we will consider the scalar meson state $f_0(980)$ as the $s\bar{s}$ candidate, giving the final state $B_s^0 \to J/\psi f_0(980)$. Note that from here on we will abbreviate this mode as $B_s^0 \to J/\psi f_0$ throughout the rest of this chapter. In Section 5.3 we similarly consider the pseudoscalar states η and η', giving the final states $B_s^0 \to J/\psi \eta^{(\prime)}$. The challenging feature of both these choices is that the amount of $s\bar{s}$ present in these mesons relative to other isospin singlet states is not yet settled. Furthermore, the nature of the $f_0(980)$, namely whether it is a conventional quark-antiquark state, tetraquark or something more exotic, is still under dispute. In both analyses we will therefore attempt to include these uncertainties into the expressions for the relevant observables and their SM predictions.

We may also consider completely different analysis strategies. In Chapter 4 for example we discussed how the U-spin related pair of decays $B_s \to K^+K^-$ and $B_d \to \pi^+\pi^-$ may be used to measure ϕ_s provided the angle γ is fixed by a different means. In that chapter we also converted the effective lifetime measurement of the mode $B_s \to K^+K^-$, which has a CP-even final state, into a contour in the ϕ_s–$\Delta\Gamma_s$ plane. In Section 5.2 we will do the same for the $B_s^0 \to J/\psi f_0$ effective lifetime measurement. With this pair of CP-odd and CP-even B_s final states it is thus possible to carry out the strategy for determining the B_s mixing parameters outlined in Section (3.3.2). We will do precisely this in Section 5.4 of this chapter. Finally in Section 5.5 we summarise our results.

5.2 The $f_0(980)$ as an $s\bar{s}$ state

As mentioned in the introduction, the advantage of choosing the $f_0(980)$ for the $s\bar{s}$ bound state in $B_s \to J/\psi s\bar{s}$ is that it is not a vector meson [124]. Specifically, it is a scalar state with quantum numbers $J^{PC} = 0^{++}$ [17]. Therefore the final state of $B_s^0 \to J/\psi f_0$ is a P-wave state, with the CP eigenvalue -1, and thus an angular analysis is not needed [124]. Unfortunately, besides from being a scalar state, few other properties of the $f_0(980)$ are known with certainty. Furthermore, as we will discuss in this section, its nature as a conventional quark-antiquark meson, tetraquark or a more exotic combination is still under dispute. This section as a whole is based on the work of Ref. [125].

In Table 5.1, we list the branching ratio measurements of $B_s^0 \to J/\psi f_0$ with $f_0 \to \pi^+\pi^-$, the dominant decay mode of the $f_0(980)$[1]. We observe that the number of events for $B_s^0 \to J/\psi f_0$ with $f_0 \to \pi^+\pi^-$ is about four times smaller than for $B_s^0 \to J/\psi\phi$ with $\phi \to K^+K^-$. Fewer events is a trade-off we must accept for avoiding the angular analysis of the $B_s^0 \to J/\psi\phi$ analysis. Nevertheless, the LHCb experiment has recently measured an effective lifetime and performed an early analysis of CP violation for the $B_s^0 \to J/\psi f_0$ decay mode, which we will present and discuss in this section.

[1]The LHCb, DØ and CDF experiment do not report the branching ratio directly, but instead its fraction, $R_{f_0/\phi}$, with respect to the branching ratio for $B_s^0 \to J/\psi\phi$ with $\phi \to K^+K^-$.

Experiment	$R_{f_0/\phi}$	$\overline{\text{BR}}(B_s \to J/\psi f_0; f_0 \to \pi^+\pi^-)$ $[10^{-4}]$
LHCb [126]	$0.284^{+0.053\star}_{-0.028}$	$1.39^{+0.47\star}_{-0.35}$
Belle [127]		$1.16^{+0.31+0.30}_{-0.19-0.25}$
DØ [128]	$0.275 \pm 0.041 \pm 0.061$	$1.83 \pm 0.83^\star$
CDF [129]	$0.257 \pm 0.020 \pm 0.014$	$1.71 \pm 0.65^\star$

Table 5.1: Compilation of branching ratio measurements involving $B_s^0 \to J/\psi f_0$. Here $R_{f_0/\phi} \equiv \overline{\text{BR}}(B_s \to J/\psi f_0; f_0 \to \pi^+\pi^-)/\overline{\text{BR}}(B_s \to J/\psi\phi; \phi \to K^+K^-)$, and a $\star$ indicates that this result was calculated by us, for comparison, using the additional inputs $\overline{\text{BR}}(B_s \to J/\psi\phi) = (1.00^{+0.28}_{-0.23}) \times 10^{-3}$ and $\text{BR}(\phi \to K^+K^-) = (48.9 \pm 0.5) \times 10^{-2}$ [17]. The reported errors are either the statistical and systematic uncertainties, respectively, or everything combined in quadrature.

In view of these promising developments, we briefly summarize the current knowledge about the $f_0(980)$ in Section 5.2.1, and have a closer look at the $B_s^0 \to J/\psi f_0$ amplitude structure in Section 5.2.2. In Section 5.2.3, we discuss the effective $B_s^0 \to J/\psi f_0$ lifetime $\tau_{J/\psi f_0}$, which can be determined from untagged B_s data samples and show the dependence on the CP-violating B_s^0–$\bar{B}_s^0$ mixing phase ϕ_s. The mixing phase also plays a key role for the time-dependent CP asymmetry of $B_s^0 \to J/\psi f_0$, which we address in Section 5.2.4. The theoretical predictions given in Sections 5.2.3 and 5.2.4 are limited by doubly Cabibbo-suppressed hadronic contributions. In Section 5.2.5, we point out that these effects can be constrained by an analysis of the $B_d^0 \to J/\psi f_0(980)$ channel, which has not yet been observed.

5.2.1 The hadronic structure of the $f_0(980)$

5.2.1.1 Preliminaries

Contrary to the recent discovery of a possible elementary scalar particle, a variety of scalar hadronic bound states have long been observed. These states are often categorized according to whether their mass falls above or below 1 GeV. Those belonging to the former category are expected to be composed predominantly of quark–antiquark states and among them a $SU(3)_{\text{F}}$ flavour nonet can be identified. Unfortunately, the $f_0(980)$ belongs to the latter category, where, as we will see, the interpretation is far from being straightforward. The $f_0(980)$ is an isospin singlet with a mass of (990 ± 20) MeV, just below the $K\bar{K}$ threshold, and a full width between 40 MeV and 100 MeV, which reflects the fact that the width determination is very model-dependent [17].

In the literature, the hadronic structure of the $f_0(980)$ state has been discussed for decades and there are many different interpretations, from the conventional quark–antiquark picture [130] to multiquark [131, 132] or $K\bar{K}$ bound states [133] (for a review, see, for instance, Ref. [17] and references within). As the goal is to use the $B_s^0 \to$

$J/\psi f_0$ decay for precision tests of the CP-violating sector of the SM, it is a natural and important question to explore how the hadronic structure of the $f_0(980)$ affects the corresponding observables. In this section, we have a closer look at popular descriptions of the $f_0(980)$, setting the stage for the discussion of the $B_s^0 \to J/\psi f_0$ observables. We will focus on two specific frameworks: the quark–antiquark and tetraquark pictures.

5.2.1.2 The $f_0(980)$ as a quark–antiquark state

In the conventional quark model, the scalar hadronic states are interpreted as mesons, i.e. quark–antiquark ($q\bar{q}$) bound states, with an orbital angular momentum of $L = 1$ and a spin of $S = 1$ coupled to give a total angular momentum of $J = 0$. In analogy to the pseudo-scalar mesons, it is suggestive to group the observed scalar states into nonets of the $SU(3)_{\rm F}$ flavour symmetry of strong interactions.

For the scalar states with masses $\lesssim 1$ GeV, we can identify an isotriplet $a_0(980)$, two strange isodoublets, κ or $K_0^\star(800)$, and two isosinglets $\sigma(600)$ and $f_0(980)$. In the naïve quark model, assuming ideal mixing between the heaviest and lightest members of the $SU(3)_{\rm F}$ nonet, the $f_0(980)$ and $\sigma(600)$, respectively, their quark-flavour composition would simply be given by

$$|f_0(980)\rangle = |s\bar{s}\rangle, \quad |\sigma(600)\rangle = \frac{1}{\sqrt{2}}\left(|u\bar{u}\rangle + |d\bar{d}\rangle\right). \tag{5.1}$$

However, there is also experimental evidence for a non-strange component of the $f_0(980)$, which could be interpreted as evidence for the following mixing structure:

$$\begin{pmatrix} |f_0(980)\rangle \\ |\sigma(600)\rangle \end{pmatrix} = \begin{pmatrix} \cos\varphi_{\rm M} & \sin\varphi_{\rm M} \\ -\sin\varphi_{\rm M} & \cos\varphi_{\rm M} \end{pmatrix} \cdot \begin{pmatrix} |s\bar{s}\rangle \\ \frac{1}{\sqrt{2}}\left(|u\bar{u}\rangle + |d\bar{d}\rangle\right) \end{pmatrix}. \tag{5.2}$$

Here the mixing angle $\varphi_{\rm M}$ is the counterpart of the η–η' mixing angle in the standard pseudo-scalar nonet, which will be discussed in Section 5.3.

The determination of $\varphi_{\rm M}$ is affected by large errors and appears process and model dependent. For instance:

- Using $D_s^+ \to \pi^+\pi^+\pi^-$ transitions caused dominantly by $D_s^+ \to \pi^+\bar{s}s$ processes, the range $35^\circ \leq |\varphi_{\rm M}| \leq 55^\circ$ was estimated in Ref. [134].
- By making a simultaneous calculation of radiative decays of the kind $f_0(980) \to \gamma\gamma$ and $\phi(1020) \to \gamma f_0(980)$, $\varphi_{\rm M} = (4 \pm 3)^\circ$ or $\varphi_{\rm M} = (138 \pm 6)^\circ$ were obtained in Ref. [135].
- In Ref. [136], it was found that a value of $\varphi_{\rm M} \simeq 20^\circ$ is consistent with the resonance data from $\phi(1020) \to \gamma\pi^0\pi^0$ and $J/\psi \to \omega\pi\pi$ decays.
- Using two different methods to fit the $D_{(s)} \to f_0(980)\{\pi, K\}$ branching ratios, covariant light-front dynamics and dispersion relations, $\varphi_{\rm M} = (31.5 \pm 5.0)^\circ$ and $\varphi_{\rm M} = (41.6 \pm 7.1)^\circ$ were obtained in Ref. [137].

Despite this unsatisfactory picture for the mixing angle, these studies indicate that the $f_0(980)$ has a significant $s\bar{s}$ component. This feature is also supported by the recent observation of the $B_s^0 \to J/\psi f_0$ channel, with measurements as summarized in Table 5.1.

Due to their non-zero orbital angular momentum, the scalar mesons are expected to be heavier than the pseudo-scalar and vector mesons in the naïve quark picture. This is not, however, the case for the light scalars that have masses below 1 GeV. Furthermore, the light scalar mass spectrum bears little resemblance with that of a standard nonet. An attractive framework to overcome these phenomenological problems is offered by the tetraquark model.

5.2.1.3 The $f_0(980)$ as a tetraquark

In the tetraquark picture, scalar states with quantum numbers $J^{PC} = 0^{++}$ are formed by the binding of diquark and anti-diquark configurations. A diquark, denoted by $[qq']$, transforms as $\bar{\mathbf{3}}$ under $SU(3)_{\rm C}$ colour symmetry, has spin $S = 0$, and transforms as $\bar{\mathbf{3}}$ under $SU(3)_{\rm F}$ flavour symmetry. Anti-diquarks, denoted by $[\bar{q}\bar{q}']$, are in the corresponding conjugate representations. The bound scalar states of diquarks and anti-diquarks, which do not require a non-vanishing angular momentum L in contrast to the $q\bar{q}$ interpretation, can reproduce the $SU(3)_{\rm F}$ nonet structure and mass ordering in a natural way [131, 132]. The physical $f_0(980)$ and $\sigma(600)$ states are given in terms of the ideally mixed states

$$|f_0^{[0]}(980)\rangle \equiv \frac{[su][\bar{s}\bar{u}] + [sd][\bar{s}\bar{d}]}{\sqrt{2}}, \quad |\sigma^{[0]}(600)\rangle \equiv [ud][\bar{u}\bar{d}] \tag{5.3}$$

as

$$\begin{pmatrix} |f_0(980)\rangle \\ |\sigma(600)\rangle \end{pmatrix} = \begin{pmatrix} \cos\omega & -\sin\omega \\ \sin\omega & \cos\omega \end{pmatrix} \cdot \begin{pmatrix} |f_0^{[0]}(980)\rangle \\ |\sigma^{[0]}(600)\rangle \end{pmatrix}. \tag{5.4}$$

An analysis of the measured scalar masses points to a small deviation from ideal mixing, with an upper bound of $|\omega| < 5^\circ$ [132, 138, 139], which we shall neglect in the following discussion.

In Ref. [132], it was pointed out that a coherent picture of the scalar mesons can be obtained through mixing between tetraquark and $q\bar{q}$ states due to instanton effects. Here the light scalar mesons $\lesssim 1$ GeV are predominantly tetraquark states while their heavier counterparts, with masses $\gtrsim 1$ GeV, are predominantly $q\bar{q}$ states. A fit of this model to data adequately describes the mass spectrum.

5.2.1.4 Further probes of the $f_0(980)$

In lattice QCD there is an ongoing effort to calculate the spectrum of the low-lying scalars and to study observables that will allow us to distinguish between exotic and conventional states (see for example Ref. [140]). From a phenomenological perspective, several processes are under scrutiny to probe the structure of the $f_0(980)$. Particularly

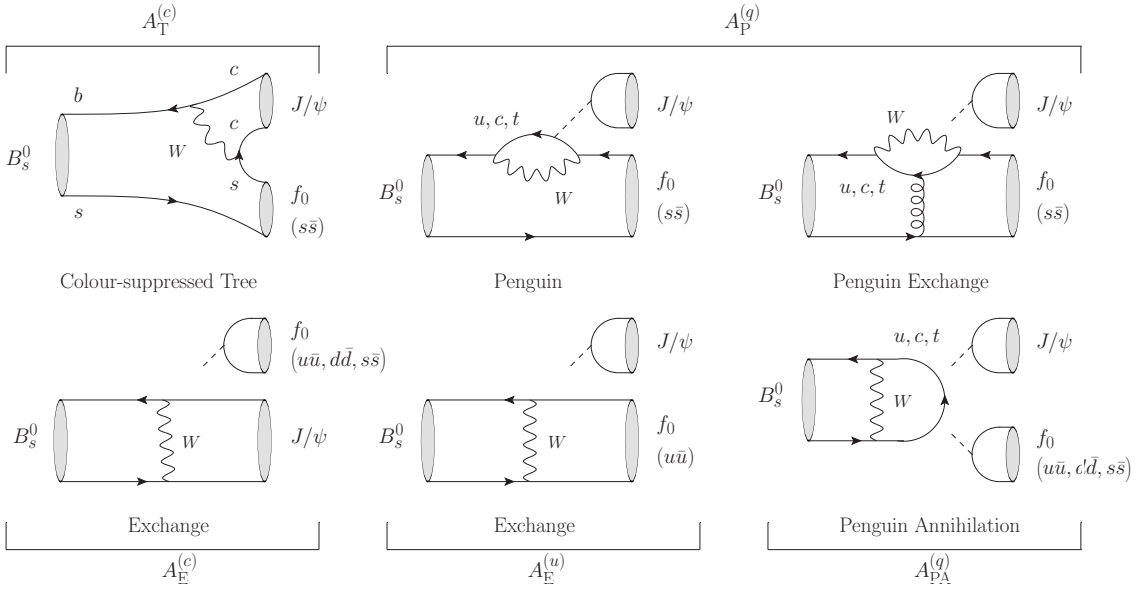

Figure 5.1: Decay topologies contributing to the $B_s^0 \to J/\psi f_0$ channel as discussed in the text. The penguin topologies implicitly include QCD and electroweak penguins. The dashed lines denote a colour-singlet exchange, which can in general connect to the quark lines of the main B_s^0 decay diagram in a number of ways.

interesting are radiative $\phi \to f_0\gamma$ decays, which were proposed to distinguish between the standard $q\bar{q}$ and tetraquark interpretation. One evident difference is that the radiative transition of the $\phi \sim s\bar{s}$ to a non-strange $q\bar{q}$ state would require the annihilation and creation of an additional quark–antiquark pair in the $q\bar{q}$ picture, which is suppressed by the Okubo–Zweig–Iizuka (OZI) rule. On the other hand, the transition to a $qq\bar{q}\bar{q}$ state containing a $s\bar{s}$ pair requires only the creation of an additional $q\bar{q}$ pair, which is not OZI-suppressed. Also here the data seem to favour a tetraquark picture, although alternative interpretations involving model-dependent assumptions are possible as well [141, 136].

The $f_0(980)$ has also been observed in hadronic decays of Z^0 bosons, where its production properties are found to be similar to those of a ϕ meson. This supports the $q\bar{q}$ picture although there are currently no predictions for the production rates of the tetraquark or the even more exotic $K\bar{K}$ molecule picture available [142].

Over the last decade, a large amount of data for decays of heavy mesons has become available, paving the way for new studies to reveal the hadronic structure of the $f_0(980)$. Decays of D_s mesons have received a lot of attention, and also charmless hadronic B decays offer a nice laboratory to shed further light on the nature of the scalar mesons [143, 144].

A more comprehensive overview of the hadronic structure of the $f_0(980)$ is beyond the scope of this section. In the following discussion of the $B_s^0 \to J/\psi f_0$ decay, we shall consider the quark–antiquark and tetraquark pictures of the $f_0(980)$ as theoretical benchmarks.

5.2.2 Amplitude structure

5.2.2.1 Decay topologies

In Figure 5.1, we show the decay topologies contributing to $B_s^0 \to J/\psi f_0$ in the SM. The structure of the corresponding decay amplitude is given as follows:

$$A(B_s^0 \to J/\psi f_0) = \lambda_c^{(s)} \left[A_{\rm T}^{(c)} + A_{\rm P}^{(c)} + A_{\rm E}^{(c)} + A_{\rm PA}^{(c)}\right] + \lambda_u^{(s)} \left[A_{\rm P}^{(u)} + A_{\rm E}^{(u)} + A_{\rm PA}^{(u)}\right] + \lambda_t^{(s)} \left[A_{\rm P}^{(t)} + A_{\rm PA}^{(t)}\right], \tag{5.5}$$

where $\lambda_q^{(s)} \equiv V_{qs}V_{qb}^*$ are CKM factors and $A_{\rm topology}^{(q)}$ generically denotes the corresponding CP-conserving strong amplitudes. Specifically, $A_{\rm T}^{(c)}$ is the colour-suppressed tree contribution, $A_{\rm P}^{(q)}$ are the penguin and penguin exchange topologies with a q-quark running in the loop, $A_{\rm E}^{(c)}$ and $A_{\rm E}^{(u)}$ describe exchange topologies with $c\bar{c}$ and $u\bar{u}$ pairs created by the W exchange, respectively, while the $A_{\rm PA}^{(q)}$ denote the penguin annihilation topologies with internal q-quarks.

The penguin topologies implicitly include QCD and electroweak penguins. In analogy to $B_d^0 \to J/\psi K_{\rm S}$ or $B_s^0 \to J/\psi\phi$, the QCD penguin topologies require a colour-singlet exchange and are OZI-suppressed. However, this comment does not apply to the electroweak penguin diagrams, which can contribute in colour-allowed form and are hence expected to have a significant impact on the $B_s^0 \to J/\psi f_0$ penguin sector [145]. It is not evident that the OZI suppression is effective for the QCD penguin topologies and that it cannot be reduced by long-distance effects. Let us also note that data on non-leptonic B-meson decays of the kind $B \to \pi\pi$ and $B \to D\pi$ indicate that colour suppression is not effective in nature [146, 113].

Using the unitarity of the CKM matrix to eliminate the $\lambda_t^{(s)}$ factor, we obtain

$$A(B_s^0 \to J/\psi f_0) = \left(1 - \frac{\lambda^2}{2}\right) \mathcal{A} \left[1 + \epsilon b e^{i\vartheta} e^{i\gamma}\right], \tag{5.6}$$

where we have introduced the CP-conserving "hadronic" parameters

$$\mathcal{A} \equiv \lambda^2 A \left[A_{\rm T}^{(c)} + A_{\rm P}^{(ct)} + A_{\rm E}^{(c)} + A_{\rm PA}^{(ct)}\right] \tag{5.7}$$

and

$$b e^{i\vartheta} \equiv R_b \left[\frac{A_{\rm P}^{(ut)} + A_{\rm E}^{(u)} + A_{\rm PA}^{(ut)}}{A_{\rm T}^{(c)} + A_{\rm P}^{(ct)} + A_{\rm E}^{(c)} + A_{\rm PA}^{(ct)}}\right], \tag{5.8}$$

using the shorthand notation

$$A_{\rm topology}^{(qt)} \equiv A_{\rm topology}^{(q)} - A_{\rm topology}^{(t)}, \tag{5.9}$$

with $q \in \{u, c\}$. These CP-conserving amplitudes can be expressed in terms of hadronic matrix elements of four-quark operators appearing in the relevant low-energy effective

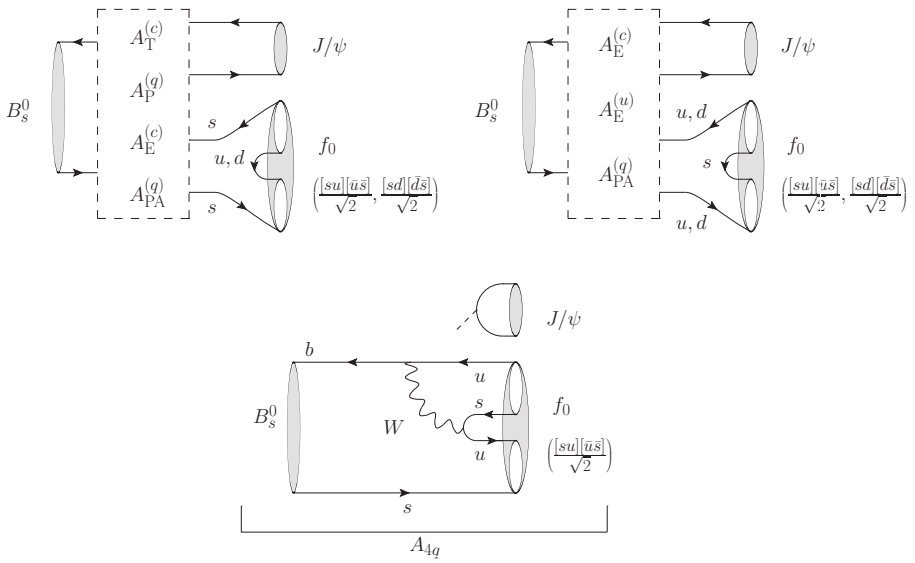

Figure 5.2: Illustration of how the topologies shown in Figure 5.1 are extended in the case where the $f_0(980)$ is a tetraquark. Also shown is the additional topology A_{4q}.

Hamiltonian (see Section 2.2). In the above expression we have used the definition $\epsilon \equiv \lambda^2/(1-\lambda^2)$. The parameters λ and A are part of the Wolfenstein parameterization defined in (2.14). The phase γ is the usual angle of the unitarity triangle defined in (2.19), and R_b is one side of the sides of this triangle as given in (2.18).

The form of the $B_s^0 \to J/\psi f_0$ amplitude is similar to that of $B_d^0 \to J/\psi K^0$ [147, 100, 148, 149, 78] and $B_s^0 \to J/\psi\phi$ [81]. In analogy to these channels, the hadronic parameters b and ϑ cannot be calculated reliably and suffer from large theoretical uncertainties. In the case of the $B_s^0 \to J/\psi f_0$ channel the situation is even worse because the details of the hadronic composition of the $f_0(980)$ affects the value of $be^{i\vartheta}$. However, the crucial feature is that this parameter enters the decay amplitude with the tiny ϵ factor, i.e. it is doubly Cabibbo-suppressed.

5.2.2.2 Specific assumptions about the $f_0(980)$

In order to obtain insights into the parameter $be^{i\vartheta}$, we have to make assumptions about the hadronic composition of the $f_0(980)$. In the case where the $f_0(980)$ adheres to the $q\bar{q}$ model as described by (5.2), we may split the strong amplitudes into separate terms, projecting out on the different quark flavours. This gives

$$\begin{aligned}
A_T^{(c)} &= \cos\varphi_M \tilde{A}_{T,s\bar{s}}^{(c)}, & A_P^{(qt)} &= \cos\varphi_M \tilde{A}_{P,s\bar{s}}^{(qt)},\\
A_E^{(c)} &= \cos\varphi_M \tilde{A}_{E,s\bar{s}}^{(c)} + \frac{1}{\sqrt{2}}\sin\varphi_M\left[\tilde{A}_{E,u\bar{u}}^{(c)} + \tilde{A}_{E,d\bar{d}}^{(c)}\right], & A_E^{(u)} &= \frac{1}{\sqrt{2}}\sin\varphi_M \tilde{A}_{E,u\bar{u}}^{(u)},\\
A_{PA}^{(qt)} &= \cos\varphi_M \tilde{A}_{PA,s\bar{s}}^{(qt)} + \frac{1}{\sqrt{2}}\sin\varphi_M\left[\tilde{A}_{PA,u\bar{u}}^{(qt)} + \tilde{A}_{PA,d\bar{d}}^{(qt)}\right], & & \qquad (5.10)
\end{aligned}$$

where $\tilde{A}^{(q')}_{\text{topology},q\bar{q}}$ denotes a CP-conserving strong amplitude contributing to the $q\bar{q}$ flavour component of the $f_0(980)$. This decomposition is analogous to $SU(3)_\text{F}$ analyses of non-leptonic B decays involving η or η' mesons, where we have to deal with η–η' mixing [150, 151, 152]. By assuming $SU(3)_\text{F}$ flavour symmetry for the strong dynamics producing the $f_0(980)$, we can, for convenience, drop the $q\bar{q}$ subscripts without further loss of generality. The hadronic parameter defined in (5.8) then takes the following form:

$$be^{i\vartheta}\big|_{q\bar{q}} = R_b \left[\frac{\cos\varphi_\text{M} \left\{ \tilde{A}^{(ut)}_\text{P} + \tilde{A}^{(ut)}_\text{PA} \right\} + \frac{1}{\sqrt{2}} \sin\varphi_\text{M} \left\{ \tilde{A}^{(u)}_\text{E} + 2\tilde{A}^{(ut)}_\text{PA} \right\}}{\cos\varphi_\text{M} \left\{ \tilde{A}^{(c)}_\text{T} + \tilde{A}^{(ct)}_\text{P} + \tilde{A}^{(c)}_\text{E} + \tilde{A}^{(ct)}_\text{PA} \right\} + \frac{1}{\sqrt{2}} \sin\varphi_\text{M} \left\{ 2\tilde{A}^{(c)}_\text{E} + 2\tilde{A}^{(ct)}_\text{PA} \right\}} \right]. \tag{5.11}$$

If, instead, the $f_0(980)$ is a tetraquark, the $u\bar{u}$, $d\bar{d}$ and $s\bar{s}$ final states of the topologies in Figure 5.1 are modified by the creation of an extra quark–antiquark pair as shown in Figure 5.2. Moreover, there is an additional topology A_{4q}, which is specific to the tetraquark description of the $f_0(980)$. Another example of a weak B-meson decay with an additional topology in the tetraquark interpretation of the light scalars that is not present in the $q\bar{q}$ picture is the $B^0_d \to \kappa^+ K^-$ channel, as was pointed out in Ref. [144].

In order to simplify the discussion, we assume $\omega = 0$ in (5.4). The strong amplitudes can then be written as follows:

$$\begin{aligned}
A^{(c)}_\text{T} &= \frac{1}{\sqrt{2}} \left(\tilde{A}^{(c)}_{\text{T},su\bar{u}\bar{s}} + \tilde{A}^{(c)}_{\text{T},sd\bar{d}\bar{s}} \right) \overset{\text{isospin}}{=} \sqrt{2}\tilde{A}^{(c)}_\text{T}, \\
A^{(qt)}_\text{P} &= \frac{1}{\sqrt{2}} \left(\tilde{A}^{(qt)}_{\text{P},su\bar{u}\bar{s}} + \tilde{A}^{(qt)}_{\text{P},sd\bar{d}\bar{s}} \right) \overset{\text{isospin}}{=} \sqrt{2}\tilde{A}^{(qt)}_\text{P}, \\
A^{(c)}_\text{E} &= \frac{1}{\sqrt{2}} \left(\tilde{A}^{(c)}_{\text{E},su\bar{u}\bar{s}} + \tilde{A}^{(c)}_{\text{E},sd\bar{d}\bar{s}} + \tilde{A}^{(c)}_{\text{E},us\bar{s}\bar{u}} + \tilde{A}^{(c)}_{\text{E},ds\bar{s}\bar{d}} \right) \overset{SU(3)_\text{F}}{=} 2\sqrt{2}\tilde{A}^{(c)}_\text{E}, \\
A^{(u)}_\text{E} &= \frac{1}{\sqrt{2}} \tilde{A}^{(u)}_{\text{E},us\bar{s}\bar{u}} = \frac{1}{\sqrt{2}} \tilde{A}^{(u)}_\text{E}, \\
A^{(qt)}_\text{PA} &= \frac{1}{\sqrt{2}} \left(\tilde{A}^{(c)}_{\text{PA},su\bar{u}\bar{s}} + \tilde{A}^{(c)}_{\text{PA},sd\bar{d}\bar{s}} + \tilde{A}^{(c)}_{\text{PA},us\bar{s}\bar{u}} + \tilde{A}^{(c)}_{\text{PA},ds\bar{s}\bar{d}} \right) \overset{SU(3)_\text{F}}{=} 2\sqrt{2}\tilde{A}^{(qt)}_\text{PA},
\end{aligned} \tag{5.12}$$

where $\tilde{A}^{(q')}_{\text{topology},qq'\bar{q}'\bar{q}}$ denotes a strong amplitude of which the $f_0(980)$ tetraquark was formed by a $q\bar{q}$ final state (from the corresponding topology in Figure 5.1) combining with a $q'\bar{q}'$ pair. In the last equalities of the expressions in (5.12) we have assumed – as indicated – isospin or $SU(3)_\text{F}$ symmetry in order to simplify them. The additional topology A_{4q} in Figure 5.2 can be written correspondingly as

$$A_{4q} = \frac{1}{\sqrt{2}} \tilde{A}_{4q,us\bar{u}\bar{s}} = \frac{1}{\sqrt{2}} \tilde{A}_{4q}, \tag{5.13}$$

and contributes with the CKM factor $\lambda^{(s)}_u$. We finally arrive at the following expression for the hadronic parameter defined in (5.8):

$$be^{i\vartheta}\big|_{4\text{q}} = R_b \left[\frac{\tilde{A}^{(ut)}_\text{P} + \frac{1}{2}\tilde{A}^{(u)}_\text{E} + 2\tilde{A}^{(ut)}_\text{PA} + \frac{1}{2}\tilde{A}_{4q}}{\tilde{A}^{(c)}_\text{T} + \tilde{A}^{(ct)}_\text{P} + 2\tilde{A}^{(c)}_\text{E} + 2\tilde{A}^{(ct)}_\text{PA}} \right]. \tag{5.14}$$

It is interesting to observe that in the absence of the A_{4q} contribution $be^{i\vartheta}\big|_{q\bar{q}}$ takes the same form as $be^{i\vartheta}\big|_{4\mathrm{q}}$ for

$$\cos\varphi_{\mathrm{M}} = \sqrt{\frac{2}{3}}, \quad \sin\varphi_{\mathrm{M}} = \sqrt{\frac{1}{3}}, \tag{5.15}$$

i.e. for a mixing angle of $\varphi_{\mathrm{M}} = 35^\circ$, which corresponds to

$$|f_0(980)\rangle = \frac{1}{\sqrt{6}}\left[|u\bar{u}\rangle + |d\bar{d}\rangle + 2|s\bar{s}\rangle\right], \tag{5.16}$$

with a flavour structure similar to that of the η' meson (see Section 5.3 and Refs [153, 150]). The individual topological amplitudes would, however, still take different values in the quark–antiquark and tetraquark descriptions of the $f_0(980)$. Unfortunately, we cannot easily calculate these amplitudes as they are non-perturbative quantities.

For the discussion of the $B_s^0 \to J/\psi f_0$ observables in Sections 5.2.3 and 5.2.4, we will consider the following range for the relevant hadronic parameters:

$$0 \le b \le 0.5, \quad 0^\circ \le \vartheta \le 360^\circ. \tag{5.17}$$

Because of $R_b \sim 0.5$, the value of $b \sim 0.5$ would correspond to strong amplitudes in the numerator and denominator of (5.8) of the same order of magnitude. In view of the still unsettled hadronic structure of the $f_0(980)$ and the complex – and essentially unknown – hadronization dynamics of the $B_s^0 \to J/\psi f_0$ channel we cannot exclude such a scenario. For example, using experimental data on $B_d^0 \to J/\psi\pi^0$ and the $SU(3)_{\mathrm{F}}$ flavour symmetry, the counterparts of b and ϑ in $B_d^0 \to J/\psi K^0$ are found at the $1\,\sigma$ level to be in the ranges $[0.15, 0.67]$ and $[174, 212]^\circ$, respectively [78]. We shall return to the hierarchy of the different decay topologies in Section 5.2.5.4.

The expressions for $be^{i\vartheta}$ in the $q\bar{q}$ and tetraquark pictures will be useful when discussing the $B_d^0 \to J/\psi f_0(980)$ channel in Section 5.2.5.

5.2.2.3 Estimate of the branching ratio in factorization

It is instructive to estimate the branching ratio of $B_s^0 \to J/\psi f_0$ from the measured $B_d^0 \to J/\psi K^0$ branching ratio. To this end, we assume that the $f_0(980)$ is a quark–antiquark state satisfying (5.2). In the factorization approximation (see Section 2.3), the hadronic matrix element takes the following form [154, 155]:

$$\begin{aligned}\langle f_0(p')|\bar{s}\gamma^\mu\gamma_5 b|B_s^0(p)\rangle &= \cos\varphi_{\mathrm{M}} F_{1,s\bar{s}}^{B_s^0 f_0}(q^2)\left[(p+p')^\mu - \left(\frac{M_{B_s^0}^2 - M_{f_0}^2}{q^2}\right)q^\mu\right] \\ &\quad + \cos\varphi_{\mathrm{M}} F_{0,s\bar{s}}^{B_s^0 f_0}(q^2)\left(\frac{M_{B_s^0}^2 - M_{f_0}^2}{q^2}\right)q^\mu,\end{aligned} \tag{5.18}$$

where $q \equiv p - p'$ is the transfered momentum and M denotes a particles mass. Here the $F_{k,s\bar{s}}^{B_s^0 f_0}$, with $k \in \{1, 2\}$, are form factors that describe the transition of the B_s^0 meson to the $s\bar{s}$ component of the $f_0(980)$. Since the $f_0(980)$ is a scalar particle, Lorentz invariance implies that only the axial-vector part of the $V - A$ current contributes to the matrix element with the pseudo-scalar B_s^0 meson.

If we use the factorization approximation and take only the colour-suppressed tree-diagram-like topology $A_{\mathrm{T}}^{(c)}$ into account, we obtain

$$\left.\frac{\mathrm{BR}(B_s \to J/\psi f_0)}{\mathrm{BR}(B_d \to J/\psi K^0)}\right|_{\mathrm{fact.}} = \frac{\tau_{B_s^0}}{\tau_{B_d^0}} \left(\frac{M_{B_s^0}\Phi_s}{M_{B_d^0}\Phi_d}\right)^3 \left[\frac{F_{1,s\bar{s}}^{B_s^0 f_0}(M_{J/\psi}^2)}{F_1^{B_d^0 K^0}(M_{J/\psi}^2)}\right]^2 \cos^2\varphi_{\mathrm{M}}, \tag{5.19}$$

where

$$\Phi_s \equiv \Phi(M_{J/\psi}/M_{B_s^0}, M_{f_0}/M_{B_s^0}), \quad \Phi_d \equiv \Phi(M_{J/\psi}/M_{B_d^0}, M_{K^0}/M_{B_d^0}) \tag{5.20}$$

with

$$\Phi(x, y) \equiv \sqrt{\left[1 - (x+y)^2\right]\left[1 - (x-y)^2\right]} \tag{5.21}$$

are phase-space factors. The B_s branching ratio defined here corresponds to the theoretical definition of a branching ratio given in (3.105).

To calculate the $B_d^0 \to K^0$ form factor we use the leading-order light-cone QCD sum-rule analysis of Ref. [156] and extrapolate to the scale of interest, $M_{J/\psi}^2$, by using the analytic evolution equations in q^2 provided. The resulting value is very similar to the one that can be inferred from the plots of Ref. [93]; we obtain

$$F_1^{B_d^0 K^0}(M_{J/\psi}^2) = 0.615 \pm 0.076. \tag{5.22}$$

The $B_s^0 \to f_0(980)$ form factor of the axial-vector current is more problematic due to the uncertain mixing angle φ_{M}. The authors of Ref. [154, 155] perform a leading order light-cone QCD sum-rule calculation with the assumption that the $f_0(980)$ is entirely an $s\bar{s}$ state, i.e. that $\varphi_{\mathrm{M}} = 0°$. Using the evolution equation in q^2 that they provide, we obtain

$$\left[\cos\varphi_{\mathrm{M}} F_{1,s\bar{s}}^{B_s^0 f_0}(M_{J/\psi}^2)\right]_{\varphi_{\mathrm{M}}=0°} = 0.32^{+0.06}_{-0.05}. \tag{5.23}$$

On the other hand, the authors of Ref. [137] determine the mixing angle φ_{M} by performing a fit of the $D_{(s)} \to f_0(980)\{\pi, K\}$ branching ratios with the help of two approaches: covariant light-front dynamics and dispersion relations. The latter method gives a fitted mixing angle of $\varphi_{\mathrm{M}} = 41.6°$ and is better behaved for the large momentum transfer $M_{J/\psi}^2$; we read off from their plot:

$$\left[\cos\varphi_{\mathrm{M}} F_{1,s\bar{s}}^{B_s^0 f_0}(M_{J/\psi}^2)\right]_{\varphi_{\mathrm{M}}=41.6°} \simeq 0.5. \tag{5.24}$$

Due to the wide variance in results for the different methods and mixing angles, we will not include error estimates for the corresponding branching ratio calculation.

By combining the form factors in (5.22), (5.23) and (5.24) with the measured value $\mathrm{BR}(B_d \to J/\psi K^0) = (8.71 \pm 0.32) \times 10^{-4}$, as well as the lifetimes and mass values listed in Ref. [17], we find

$$\mathrm{BR}(B_s \to J/\psi f_0)|_{\varphi_\mathrm{M}=0^\circ} \simeq 1.9 \times 10^{-4} \tag{5.25}$$

and

$$\mathrm{BR}(B_s \to J/\psi f_0)|_{\varphi_\mathrm{M}=41.6^\circ} \simeq 4.8 \times 10^{-4}, \tag{5.26}$$

for the branching ratios (using the theoretical definition). Let us emphasize that these estimates assume that the $f_0(980)$ is described in the $q\bar{q}$ picture by (5.2), include only tree topologies, and take only factorizable $SU(3)$-breaking effects through the form-factor calculations listed above into account.

5.2.2.4 Estimate of the branching ratio from experiment

We proceed to compare the results obtained in the previous subsection with the data listed in Table 5.1. Combining errors in quadrature and taking a weighted average gives

$$\overline{\mathrm{BR}}(B_s \to J/\psi f_0; f_0 \to \pi^+\pi^-)\big|_\mathrm{avg} = \left(1.27^{+0.22}_{-0.17}\right) \times 10^{-4}. \tag{5.27}$$

The missing ingredient is $\mathrm{BR}(f_0 \to \pi^+\pi^-)$, which has not been adequately measured. However, measurements do exist for the ratios

$$R \equiv \frac{\Gamma(f_0 \to \pi\pi)}{\Gamma(f_0 \to \pi\pi) + \Gamma(f_0 \to KK)} \quad \text{and} \quad R' \equiv \frac{\Gamma(f_0 \to K^+K^-)}{\Gamma(f_0 \to \pi^+\pi^-)}. \tag{5.28}$$

Under the assumption that all other decay channels (such as $\gamma\gamma$) are neglegible and that the $\pi\pi$ and KK channels adhere to isospin symmetry, we expect

$$\mathrm{BR}(f_0 \to \pi^+\pi^-) = \frac{2R}{3} = \frac{2}{4R'+3} \tag{5.29}$$

as well as

$$\mathrm{BR}(f_0 \to K^+K^-) = \frac{1}{2}(1-R) = \frac{2R'}{4R'+3}, \tag{5.30}$$

which we include for completeness. We note, however, that the isospin assumption $\Gamma(f_0 \to K^+K^-) = \Gamma(f_0 \to K^0\bar{K}^0)$ on which (5.30) and the expressions involving R' depend, could be spoiled by phase-space effects. Specifically, because the decay thresholds of both the $f_0 \to K^+K^-$ and $f_0 \to K^0\bar{K}^0$ channels are beyond the f_0 mass peak, the slope of its wide resonance could significantly break the isospin assumption. As the $\pi\pi$ final states have a much lower threshold and thus access to a large phase space, we expect the equality in (5.29) involving R to be stable under the above considerations.

Using the measurement $R = 0.75^{+0.11}_{-0.13}$, which was reported by BES2 in 2005 [157], the authors of Ref. [137] have used the above relations to extract

$$\mathrm{BR}(f_0 \to \pi^+\pi^-) = 0.50^{+0.07}_{-0.09} \tag{5.31}$$

and $\mathrm{BR}(f_0 \to K^+K^-) = 0.125^{+0.055}_{-0.065}$. Using the 2006 BaBar result $R' = 0.69 \pm 0.32$ [158], we find $\mathrm{BR}(f_0 \to \pi^+\pi^-) = 0.35 \pm 0.08$ and $\mathrm{BR}(f_0 \to K^+K^-) = 0.24 \pm 0.06$. Because of the near $1\,\sigma$ discrepancy of these results and the preceding discussion concerning the possible $f_0 \to K\bar{K}$ isospin-breaking effects, we do not use the latter result.

By naïvely assuming a narrow width for the f_0, we can combine the average in (5.27) with (5.31) to obtain

$$\overline{\mathrm{BR}}(B_s \to J/\psi f_0)\big|_{\mathrm{avg}} = \left(2.55^{+0.62}_{-0.51}\right) \times 10^{-4}. \tag{5.32}$$

To compare with the estimates given in (5.25) and (5.26) it is necessary to express this *experimental* branching ratio, as defined in (3.104), in terms of a theoretical branching ratio as defined in (3.105). To this end, we may employ the experimentally measured effective lifetime [159]

$$\tau_{J/\psi f_0} = [1.700 \pm 0.040\,(\mathrm{stat}) \pm 0.026\,(\mathrm{syst})]\,\mathrm{ps}, \tag{5.33}$$

together with the dictionary given in (3.107). This gives

$$\mathrm{BR}(B_s \to J/\psi f_0)\big|_{\mathrm{avg}} = \left(2.25^{+0.56}_{-0.46}\right) \times 10^{-4}. \tag{5.34}$$

Thus the colour-suppressed tree topologies by themselves account for the correct order of magnitude of the measured $B_s^0 \to J/\psi f_0$ branching ratio in the quark–antiquark picture. However, in view of the large errors, we cannot draw further conclusions about the hadronic structure of the $f_0(980)$ from this exercise.

5.2.3 The effective lifetime

5.2.3.1 Mass-eigenstate rate asymmetry

As introduced in Section 3.2.1, an untagged time-dependent analysis of B_s mesons decaying to the CP eigenstate $J/\psi f_0$ allows us to probe the mass-eigenstate rate asymmetry of this decay mode. This final state dependent asymmetry is sensitive to CP violation both in B_s^0–$\overline{B}_s^0$ mixing and in the decay mode. Being an untagged observable, it is unaffected by tagging related experimental considerations such as the associated efficiency and systematics. Hereby its extraction also requires less events and it is available sooner.

As the final state $J/\psi f_0$ is a CP eigenstate, with CP eigenvalue $\eta_{J/\psi f_0} = -1$, we may compute its time-dependent observables using the formalism presented in Section (3.2.2). To that end we will adopt the parameterization for the SM decay amplitude in (5.6), thereby making the plausible assumption that there is no significant NP contribution at

the decay amplitude level. Experimental evidence in support of this assumption is given by the absence of large direct CP violation in the $B_d^0 \to J/\psi K^0$ and $B^+ \to J/\psi K^+$ channels [73, 17]. Putting exchange and penguin annihilation topologies aside, these channels emerge from the same quark-level transitions as $B_s^0 \to J/\psi f_0$.

To proceed with the formalism of Section (3.2.2) we make the substitutions

$$h_{J/\psi\, f_0} = \epsilon\, b, \qquad \delta_{J/\psi\, f_0} = \vartheta, \qquad \varphi_1^{J/\psi\, f_0} = 0, \qquad \varphi_2^{J/\psi\, f_0} = \gamma. \tag{5.35}$$

We then find that the direct CP violation in the decay mode is given by

$$C \equiv C(B_s \to J/\psi f_0) = \frac{-2\epsilon b \sin\vartheta \sin\gamma}{1 + 2\epsilon b \cos\vartheta \cos\gamma + \epsilon^2 b^2}. \tag{5.36}$$

And, likewise, the hadronic phase shift by

$$\tan\Delta\phi = \frac{2\epsilon b \cos\vartheta \sin\gamma + \epsilon^2 b^2 \sin 2\gamma}{1 + 2\epsilon b \cos\vartheta \cos\gamma + \epsilon^2 b^2 \cos 2\gamma}. \tag{5.37}$$

Using only this expression would result in a two-fold ambiguity for $\Delta\phi$. However, this can be lifted using sign information from $\sin\Delta\phi$ and $\cos\Delta\phi$, which can be computed using (3.85) and (3.86), respectively.

We may now write the mass-eigenstate rate asymmetry as

$$\mathcal{A}_{\Delta\Gamma} \equiv \mathcal{A}_{\Delta\Gamma}(B_s \to J/\psi f_0) = \sqrt{1 - C^2}\cos(\phi_s + \Delta\phi), \tag{5.38}$$

where ϕ_s is the B_s^0–$\overline{B}_s^0$ mixing phase given in (3.46).

As discussed in Section 3.3, one way to experimentally probe the mass-eigenstate rate asymmetry is with an effective lifetime measurement of the untagged decay rate. The dependence of the effective lifetime on $\mathcal{A}_{\Delta\Gamma}$ is given by

$$\frac{\tau_{J/\psi f_0}}{\tau_{B_s}} = \frac{1}{1 - y_s^2}\left[\frac{1 + 2\mathcal{A}_{\Delta\Gamma}\, y_s + y_s^2}{1 + \mathcal{A}_{\Delta\Gamma}\, y_s}\right]. \tag{5.39}$$

In (5.33) we already gave the latest experimental determination of the $B_s \to J/\psi f_0$ effective lifetime by the LHCb experiment.

5.2.3.2 Numerical analysis

In order to estimate the effective lifetime, as well as illustrate the impact of the hadronic corrections to it, we will assume

$$\gamma = (68 \pm 7)^\circ, \tag{5.40}$$

which is in agreement with the determination of this angle in Chapter 4 and fits of the UT [75, 101]. For the hadronic parameters we use the conservative ranges given in

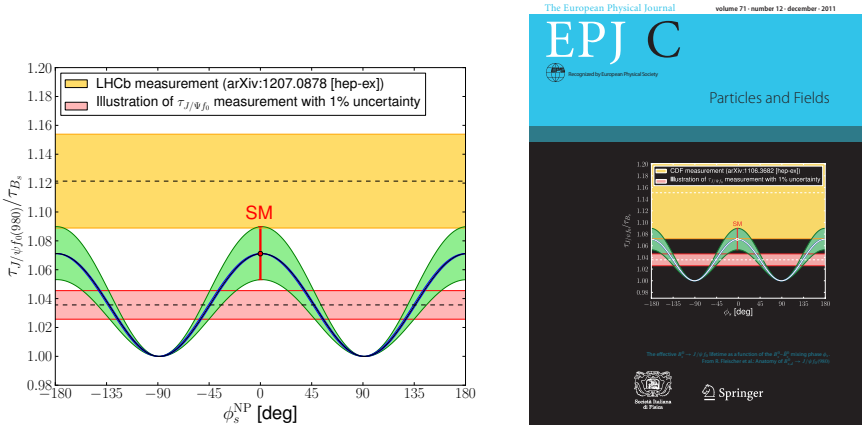

Figure 5.3: The effective $B_s^0 \to J/\psi f_0$ lifetime as a function of the B_s^0–$\bar{B}_s^0$ mixing phase ϕ_s. Assuming $\gamma = (68 \pm 7)^\circ$ with $0 \leq b \leq 0.5$ and $0^\circ \leq \vartheta \leq 360^\circ$ results in the narrow band in the centre of the curve. The major source of the theoretical error comes from the value of $y_s^{\rm Th} = 0.067 \pm 0.016$, as illustrated by the wide band of the curve. This plot made it onto the cover of the European Physical Journal C (right image).

(5.17). Although these ranges are indeed very large, they enter the observables of the decay mode with a double Cabibbo suppression. Therefore, to leading order in ϵ we find

$$\Delta\phi = 2\,\epsilon\,b \sin\gamma \cos\theta + \mathcal{O}(\epsilon^2) \approx [6^\circ]\, b \sin\gamma \cos\theta \tag{5.41}$$

$$C = -2\,\epsilon\,b \sin\gamma \sin\theta + \mathcal{O}(\epsilon^2) \approx [-0.1]\, b \sin\gamma \sin\theta \tag{5.42}$$

We thus conclude that at a $1\,\sigma$ confidence level the observables lie in the ranges:

$$\Delta\phi_{J/\psi f_0} \in [-2.9^\circ, 2.8^\circ], \quad |C_{J/\psi f_0}| \lesssim 0.05. \tag{5.43}$$

The missing ingredients for predicting the effective lifetime as parameterised by (5.39) and (5.38) are the B_s^0-$\overline{B}_s^0$ mixing parameters. For the mean B_s lifetime we will use the experimental value given in (3.53). To give a Standard Model prediction, we may use the theoretical prediction for y_s given in (3.43) together with the $\phi_s^{\rm SM}$ given in (3.47). These combine to give

$$\tau_{J/\psi f_0}\big|_{\rm SM} = (1.624 \pm 0.031)\,\text{ps}, \tag{5.44}$$

In Figure 5.3 we show the dependence of $\tau_{J/\psi f_0}/\tau_{B_s}$ on the phase $\phi_s = \phi_s^{\rm SM} + \phi_s^{\rm NP}$. Here also y_s is taken to depend on $\phi_s^{\rm NP}$ as given by the expression in (3.45) and motivated by the accompanying discussion. The LHCb measurement given in (5.33) is shown as the top horizontal band (the central value is indicated by the dashed line), which is about 1σ above the upper bound for the lifetime. Thus the measurement of $\tau_{J/\psi f_0}$ offers an interesting probe for CP-violating NP contributions to B_s^0–$\bar{B}_s^0$ mixing. The lower horizontal band in Figure 5.3 illustrates the impact of a future measurement of

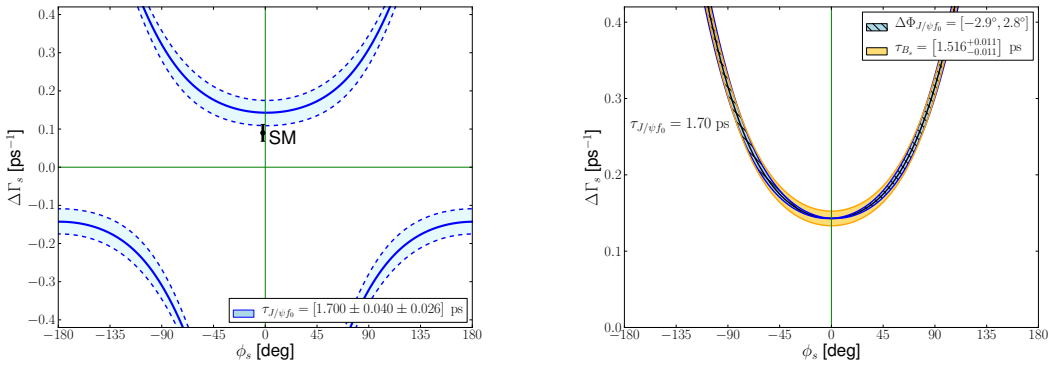

Figure 5.4: Measurement of the $B_s \to J/\psi f_0(980)$ lifetime projected onto the ϕ_s–$\Delta\Gamma_s$ plane. Error bands correspond to the effective lifetime measurement (left panel) and the hadronic phase shift and mean B_s lifetime (right panel).

$\tau_{J/\psi f_0}/\tau_{B_s}$ at the 1% level, assuming, purely for illustration, a value of $\phi_s = -45°$. It is clearly an important goal to push the measurement of the effective $B_s^0 \to J/\psi f_0$ lifetime to the 1% level.

The main source of uncertainty in the numerical analysis of the effective lifetime up to this point is the theoretical estimate $y_s^{\rm Th}$. This input can be avoided if we instead plot the effective lifetime as a contour in the ϕ_s–$\Delta\Gamma_s$ plane, as discussed in Section 3.3.2. In Figure 5.4 we do precisely this, showing also the corresponding experimental errors of the effective lifetime measurement (left panel) and the effect of the hadronic phase shift (right panel). As the final state $J/\psi f_0$ is CP-odd, this contour can be combined with a contour of an effective lifetime measurement for a CP-even decay mode to pinpoint the B_s mixing parameters. In the Chapter 4 we presented such a CP-even contour for the $B_s \to K^+K^-$ effective lifetime. In Section 5.4 we will perform this combination.

In Ref. [76] an effective lifetime measurement is given for the $B_s \to J/\psi\pi^+\pi^-$ decay mode:

$$\tau_{J/\psi\pi^+\pi^-} = 1.652 \pm 0.024 \pm 0.024 \text{ ps}. \tag{5.45}$$

The $\pi^+\pi^-$ final state is considered in the mass range 775 to 1550 MeV, and the $f_0(980)$ resonance is estimated to give a contribution of 70% in this window [160]. Although this result is more accurate than that given in (5.33), the fact it is not purely given by the $f_0(980)$ resonance only further complicates the question of which decay topologies contribute. We therefore do not use it in our numerical analysis.

5.2.4 Mixing-induced CP asymmetry

A tagged analysis, from which we can distinguish between initially present B_s^0 or $\bar{B}_s^0$ mesons, allows us to measure the time-dependent, CP-violating rate asymmetry as defined for a general final state in (3.72). The observables C and $\mathcal{A}_{\Delta\Gamma}$ for the decay mode

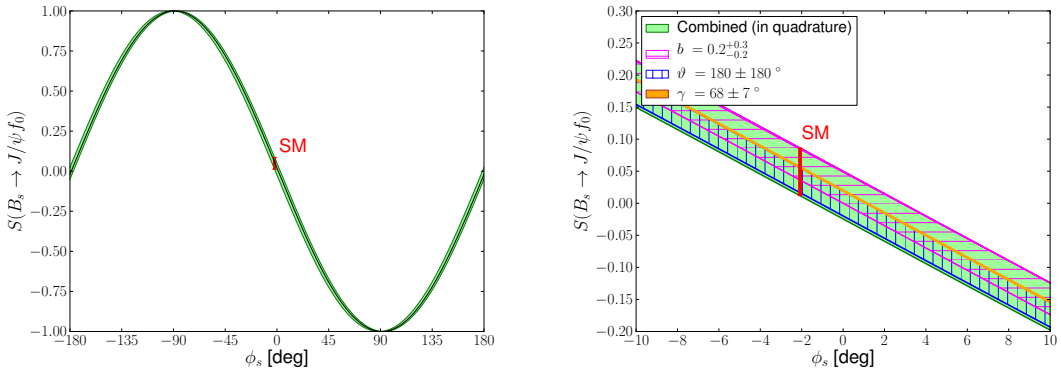

Figure 5.5: *Left panel*: the mixing-induced CP asymmetry of $B_s^0 \to J/\psi f_0$ as a function of the B_s^0–$\bar{B}_s^0$ mixing phase ϕ_s; assuming $\gamma = (68 \pm 7)°$, $0 \leq b \leq 0.5$ and $0° \leq \vartheta \leq 360°$ gives the error band. *Right panel*: individual errors associated with the input quantities, zoomed in on the region $\phi_s \in [-10°, 10°]$ close to the SM case.

under consideration have already been given in (5.36) and (5.38), respectively. The remaining mixing-induced CP-violating observable is given by

$$S \equiv S(B_s \to J/\psi f_0) = -\sqrt{1 - C^2}\,\sin(\phi_s + \Delta\phi). \tag{5.46}$$

In order to explore the impact of the hadronic effects, we assume again (5.17) with (5.40), resulting in ranges for $\Delta\phi$ and C as given in (5.43). In the left panel of Figure 5.5, we show the dependence of S on the B_s^0–$\bar{B}_s^0$ mixing phase ϕ_s, with the band showing the contributing errors added in quadrature. Our SM prediction, which is indicated by the error bar, is given by

$$S(B_s^0 \to J/\psi f_0)\big|_{\rm SM} \in [0.012, 0.086], \tag{5.47}$$

which should be compared with the naïve SM value $(\sin\phi_s)|_{\rm SM} = 0.036 \pm 0.002$, which corresponds to $b = 0$. The right panel of Figure 5.5 is a zoomed in version of the same plot, focusing on smallish phases ϕ_s. Here the individual errors associated with the input parameters have been included, revealing that b and ϑ lead to a comparable and sizable error in this ϕ_s domain, whereas the error on γ in (5.40) is negligible. These plots are complemented by Figure 5.6, where we show the dependence of S and C on (b, ϑ) and the resulting correlation between these observables for the SM central value of ϕ_s.

From these plots and the range in (5.47) we see that a large value of $|S|$ would give unambiguous evidence for NP in B_s^0–$\bar{B}_s^0$ mixing. However, such a scenario is now essentially excluded by the LHCb measurement of these mixing parameters given in (3.48) using the $B_s \to J/\psi\phi$ decay mode. Regarding the measurement of mixing-induced CP violation in $B_s^0 \to J/\psi f_0$, LHCb has performed such an analysis for the decay mode $B_s^0 \to J/\psi\,\pi^+\pi^-$ [160, 76]. As discussed in Section 5.2.3, the $\pi^+\pi^-$ final

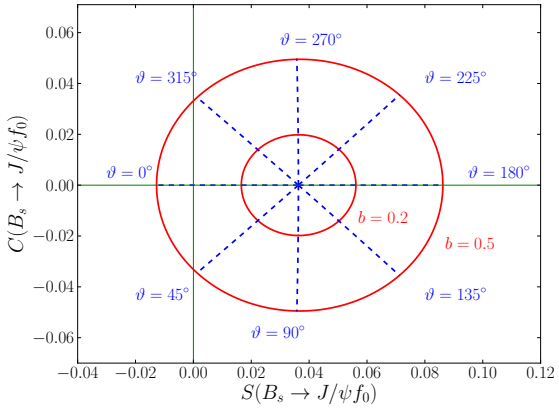

Figure 5.6: Parametric plot of the mixing-induced and direct CP asymmetries of the $B_s^0 \to J/\psi f_0$ decay, S and C, respectively, for $\gamma = 68°$ and the SM central value $\phi_s^{\rm SM} = -2.1°$. The solid rings correspond to the fixed points of $b = 0.2$ and 0.5 with ϑ allowed to vary. Likewise, the dashed lines are fixed points of ϑ with b allowed to vary.

state is considered in a mass window where the $f_0(980)$ resonance only contributes to approximately 70% of the events. In terms of addressing hadronic uncertainties in the extraction of the mixing parameters this strategy is less optimal than focusing purely on the $f_0(980)$. The result of this analysis, which assumes $S = -\sin(\phi_s)$, is [76]

$$S = 0.14^{\pm 0.16}_{-0.17}. \tag{5.48}$$

It is compatible with the SM prediction given in (5.47), however the errors are still too large to draw conclusions about the presence or absence of New Physics. In particular, should a future measurement of S fall into the range

$$0 \lesssim S \lesssim 0.1, \tag{5.49}$$

the hadronic SM effects related to the b parameter would preclude conclusions on the presence or absence of CP-violating NP contributions to B_s^0–$\bar{B}_s^0$ mixing, unless we have insights into this parameter. First constraints can be obtained through the measurement of direct CP violation in $B_s^0 \to J/\psi f_0$. However, this asymmetry takes a value of at most $\sim 5\%$ in Figure 5.6 and will be challenging to measure precisely.

5.2.5 The $B_d^0 \to J/\psi f_0(980)$ channel

5.2.5.1 Decay amplitude and observables

An interesting decay to obtain an insight into the size of the hadronic parameter $be^{i\vartheta}$ is $B_d^0 \to J/\psi f_0(980)$, which we will abbreviate from here on as $B_d^0 \to J/\psi f_0$. In order to obtain its decay topologies, we need only interchange all strange and down quarks in

Figure 5.1. The leading colour-suppressed tree-diagram-like topology emerges from the $d\bar{d}$ component of the $f_0(980)$ state.

A key feature of the $B_d^0 \to J/\psi f_0$ mode is that the CKM factors $\lambda_q^{(d)} \equiv V_{qd}V_{qb}^*$ enter the expression for the decay amplitude. If we assume the SM and apply the unitarity of the CKM matrix, we arrive at

$$A(B_d^0 \to J/\psi f_0) = -\lambda \mathcal{A}' \left[1 - b' e^{i\vartheta'} e^{i\gamma}\right], \tag{5.50}$$

where $\mathcal{A}'$ and $b'e^{i\vartheta'}$ take the same form as (5.7) and (5.8), respectively. In contrast to the $B_s^0 \to J/\psi f_0$ amplitude (5.6), the hadronic parameter $b'e^{i\vartheta'}$ is *not* suppressed by ϵ. Consequently, its impact is effectively *magnified* in $B_d^0 \to J/\psi f_0$ with respect to $B_s^0 \to J/\psi f_0$.

In contrast to the B_s meson system, the B_d meson system has a negligibly small decay width difference: $y_d \approx 0$ as given in (3.54). Therefore no interesting information, specifically no mass-eigenstate rate asymmetry, is extractable from an untagged time-dependent measurement. However, a CP violating rate asymmetry can be extracted for $B_d^0 \to J/\psi f_0$ analogous to the B_s case, and is given by

$$\frac{\Gamma(B_d(t) \to J/\psi f_0) - \Gamma(\bar{B}_d(t) \to J/\psi f_0)}{\Gamma(B_d(t) \to J/\psi f_0) + \Gamma(\bar{B}_d(t) \to J/\psi f_0)} = C' \cos(\Delta M_d t) + S' \sin(\Delta M_d t). \tag{5.51}$$

We can apply the same formalism presented in Section 3.2.2 for B_s decay modes to CP eigenstates to find expressions for the observables C' and S' of the B_d decay mode. To this end we make the substitutions

$$h'_{J/\psi\, f_0} = -b, \qquad \delta'_{J/\psi\, f_0} = \theta', \qquad \varphi_1'^{J/\psi\, f_0} = 0, \qquad \varphi_2'^{J/\psi\, f_0} = \gamma. \tag{5.52}$$

For the direct CP violating observable we thus find

$$C' \equiv C(B_d \to J/\psi f_0) = \frac{2b' \sin\vartheta' \sin\gamma}{1 - 2b' \cos\vartheta' \cos\gamma + b'^2}. \tag{5.53}$$

And for the phase shift of the decay mode we find

$$\tan\Delta\phi' = \frac{-2b' \cos\vartheta' \sin\gamma + b'^2 \sin 2\gamma}{1 - 2b' \cos\vartheta' \cos\gamma + b'^2 \cos 2\gamma}. \tag{5.54}$$

These two parameter allow us to define the mixing-induced CP violation as

$$S' \equiv S(B_d \to J/\psi f_0) = -\sqrt{1 - C'^2}\, \sin(\phi_d + \Delta\phi'), \tag{5.55}$$

where ϕ_d is the B_d^0–$\bar{B}_d^0$ mixing phase given in (3.56). A measurement of C' and S' would allow us to determine b' and θ', with the corresponding expressions given in Ref. [78].

5.2.5.2 Specific assumptions about the $f_0(980)$

As we did for $B_s \to J/\psi f_0$ in Section 5.2.2.2, let us now discuss the forms of the hadronic parameter $b' e^{i\theta'}$ in the quark–antiquark and tetraquark frameworks. In the quark–antiquark case, in analogy to the flavour decomposition for the $B_s^0 \to J/\psi f_0$ channel in (5.10), we obtain for the $B_d \to J/\psi f_0$ decay:

$$A_{\rm T}^{\prime(c)} = \frac{\sin\varphi_{\rm M}}{\sqrt{2}} \tilde{A}_{{\rm T},d\bar{d}}^{\prime(c)}, \quad A_{\rm P}^{\prime(qt)} = \frac{\sin\varphi_{\rm M}}{\sqrt{2}} \tilde{A}_{{\rm P},d\bar{d}}^{\prime(qt)}, \tag{5.56}$$

where the amplitudes $A_{\rm E}^{\prime(c)}$, $A_{\rm E}^{\prime(u)}$ and $A_{\rm PA}^{\prime(qt)}$ take the same forms as their $B_s^0 \to J/\psi f_0$ counterparts. Using $SU(3)_{\rm F}$ flavour symmetry, we can drop the $q\bar{q}$ subscripts. Moreover, we can then also identify the $B_d^0 \to J/\psi f_0$ amplitudes with their $B_s^0 \to J/\psi f_0$ partners, i.e. can simply drop the primes. This results in the following expression for the hadronic $B_d^0 \to J/\psi f_0$ parameter:

$$b' e^{i\vartheta'}\Big|_{q\bar{q}} = R_b \left[\frac{\cos\varphi_{\rm M} \left\{ \tilde{A}_{\rm PA}^{(ut)} \right\} + \frac{1}{\sqrt{2}} \sin\varphi_{\rm M} \left\{ \tilde{A}_{\rm P}^{(ut)} + \tilde{A}_{\rm E}^{(u)} + 2\tilde{A}_{\rm PA}^{(ut)} \right\}}{\cos\varphi_{\rm M} \left\{ \tilde{A}_{\rm E}^{(c)} + \tilde{A}_{\rm PA}^{(ct)} \right\} + \frac{1}{\sqrt{2}} \sin\varphi_{\rm M} \left\{ \tilde{A}_{\rm T}^{(c)} + \tilde{A}_{\rm P}^{(ct)} + 2\tilde{A}_{\rm E}^{(c)} + 2\tilde{A}_{\rm PA}^{(ct)} \right\}} \right], \tag{5.57}$$

which can be compared with (5.11).

In contrast to the conventional $SU(3)_{\rm F}$ strategies involving decays of $B_{(s,d)}$ mesons into pions and kaons, there is a complication due to the presence of the mixing angle $\varphi_{\rm M}$, as reflected in the expressions (5.11) and (5.57). A particularly interesting situation arises when

$$\cos\varphi_{\rm M} = \frac{1}{\sqrt{2}} \sin\varphi_{\rm M}, \tag{5.58}$$

which is satisfied for $\varphi_{\rm M} = 55^\circ$. In this case, we have

$$|f_0(980)\rangle = \frac{1}{\sqrt{3}} \left[|u\bar{u}\rangle + |d\bar{d}\rangle + |s\bar{s}\rangle \right], \tag{5.59}$$

which gives

$$b e^{i\vartheta}\Big|_{q\bar{q}} = R_b \left[\frac{\tilde{A}_{\rm P}^{(ut)} + \tilde{A}_{\rm E}^{(u)} + 3\tilde{A}_{\rm PA}^{(ut)}}{\tilde{A}_{\rm T}^{(c)} + \tilde{A}_{\rm P}^{(ct)} + 3\tilde{A}_{\rm E}^{(c)} + 3\tilde{A}_{\rm PA}^{(ct)}} \right] = b' e^{i\vartheta'}\Big|_{q\bar{q}}. \tag{5.60}$$

We could then simply identify the $b e^{i\theta}$ of the $B_s^0 \to J/\psi f_0$ channel with the $b' e^{i\theta'}$ of the $B_d^0 \to J/\psi f_0$ mode. Looking at the current ranges of $\varphi_{\rm M}$ summarized in Section 5.2.1.2, this scenario – or a situation close to it – may actually be realized in nature. It is interesting to note that the flavour structure of (5.58) corresponds to an $SU(3)_{\rm F}$ singlet, in analogy to the η_1 state of the η–η' system of the pseudo-scalar mesons.

On the contrary, as we discussed in Section 5.2.1, the tetraquark interpretation of

the $f_0(980)$ appears to be more favourable. In this picture, we obtain

$$\begin{aligned}
A_{\rm T}^{\prime(c)} &= \frac{1}{\sqrt{2}}\tilde{A}_{{\rm T},sd\bar{d}\bar{s}}^{\prime(c)}\\
A_{\rm P}^{\prime(qt)} &= \frac{1}{\sqrt{2}}\tilde{A}_{{\rm P},sd\bar{d}\bar{s}}^{\prime(qt)}\\
A_{\rm E}^{\prime(c)} &= \frac{1}{\sqrt{2}}\left[\tilde{A}_{{\rm E},su\bar{u}\bar{s}}^{\prime(c)}+\tilde{A}_{{\rm E},sd\bar{d}\bar{s}}^{\prime(c)}+\tilde{A}_{{\rm E},us\bar{s}\bar{u}}^{\prime(c)}+\tilde{A}_{{\rm E},ds\bar{s}\bar{d}}^{\prime(c)}\right]\stackrel{SU(3)_{\rm F}}{=}2\sqrt{2}\tilde{A}_{\rm E}^{\prime(c)},\\
A_{\rm E}^{\prime(u)} &= \frac{1}{\sqrt{2}}\tilde{A}_{{\rm E},us\bar{s}\bar{u}}^{\prime(u)}=\frac{1}{\sqrt{2}}\tilde{A}_{\rm E}^{\prime(u)},\\
A_{\rm PA}^{\prime(qt)} &= \frac{1}{\sqrt{2}}\left[\tilde{A}_{{\rm PA},su\bar{u}\bar{s}}^{\prime(c)}+\tilde{A}_{{\rm PA},sd\bar{d}\bar{s}}^{\prime(c)}+\tilde{A}_{{\rm PA},us\bar{s}\bar{u}}^{\prime(c)}+\tilde{A}_{{\rm PA},ds\bar{s}\bar{d}}^{\prime(c)}\right]\stackrel{SU(3)_{\rm F}}{=}2\sqrt{2}\tilde{A}_{\rm PA}^{\prime(qt)},
\end{aligned}\tag{5.61}$$

in analogy to (5.12). The A_{4q} topology shown in Figure 5.2 does not have a counterpart in $B_d^0\to J/\psi f_0$ for $\omega=0$ in (5.4), which was assumed in the expressions given above. For a non-vanishing value of this angle, it would be suppressed by $\sin\omega<0.1$. Assuming again the $SU(3)_{\rm F}$ flavour symmetry to identify the topological amplitudes in $B_d^0\to J/\psi f_0$ and $B_s^0\to J/\psi f_0$, we arrive at

$$b^\prime e^{i\vartheta^\prime}\Big|_{\rm 4q}=R_b\left[\frac{\tilde{A}_{\rm P}^{(ut)}+\tilde{A}_{\rm E}^{(u)}+4\tilde{A}_{\rm PA}^{(ut)}}{\tilde{A}_{\rm T}^{(c)}+\tilde{A}_{\rm P}^{(ct)}+4\tilde{A}_{\rm E}^{(c)}+4\tilde{A}_{\rm PA}^{(ct)}}\right].\tag{5.62}$$

5.2.5.3 Estimate of the $B_d^0\to J/\psi f_0$ branching ratio

For experimental studies, it is useful to estimate the branching ratio of the $B_d^0\to J/\psi f_0$ decay. Using (5.6) and (5.50), we obtain the following expression for the ratio of the CP-averaged decay amplitudes:

$$\left|\frac{\langle A(B_d\to J/\psi f_0)\rangle}{\langle A(B_s\to J/\psi f_0)\rangle}\right|^2=\epsilon\left[\frac{1-2b^\prime\cos\vartheta^\prime\cos\gamma+b^{\prime 2}}{1+2\epsilon b\cos\vartheta\cos\gamma+\epsilon^2b^2}\right]\left|\frac{\mathcal{A}^\prime}{\mathcal{A}}\right|^2,\tag{5.63}$$

where (5.7) gives

$$\left|\frac{\mathcal{A}^\prime}{\mathcal{A}}\right|=\left|\frac{A_{\rm T}^{\prime(c)}+A_{\rm P}^{\prime(ct)}+A_{\rm E}^{\prime(c)}+A_{\rm PA}^{\prime(ct)}}{A_{\rm T}^{(c)}+A_{\rm P}^{(ct)}+A_{\rm E}^{(c)}+A_{\rm PA}^{(ct)}}\right|.\tag{5.64}$$

Keeping only the tree and penguin contributions and using the $SU(3)_{\rm F}$ symmetry yields

$$\left|\frac{\mathcal{A}^\prime}{\mathcal{A}}\right|_{\rm q\bar{q}}=\frac{\tan\varphi_{\rm M}}{\sqrt{2}}\quad\text{and}\quad\left|\frac{\mathcal{A}^\prime}{\mathcal{A}}\right|_{4q}=\frac{1}{2}\tag{5.65}$$

for the quark–antiquark and tetraquark descriptions of the $f_0(980)$, respectively. For the former case, the result

$$\left|\frac{\mathcal{A}^\prime}{\mathcal{A}}\right|_{q\bar{q}}\sim\left[\frac{F_1^{B_d^0f_0}(M_{J/\psi}^2)}{F_1^{B_s^0f_0}(M_{J/\psi}^2)}\right]_{\varphi_{\rm M}=41.6^\circ}\sim 0.44,\tag{5.66}$$

which was obtained in Ref. [137] for the $q\bar{q}$ framework (using dispersion relations, see Section 5.2.2.3), is in the same ball-park as

$$\left.\frac{\tan\varphi_{\rm M}}{\sqrt{2}}\right|_{\varphi_{\rm M}=41.6^\circ} = 0.63. \tag{5.67}$$

If we introduce the quantity

$$H_{f_0} \equiv \frac{1-2b'\cos\vartheta'\cos\gamma+b'^2}{1+2\epsilon b\cos\vartheta\cos\gamma+\epsilon^2 b^2}, \tag{5.68}$$

we can write the branching ratio as

$$\mathrm{BR}(B_d\to J/\psi f_0) = H_{f_0}\times \mathrm{BR}(B_d\to J/\psi f_0)_0, \tag{5.69}$$

where

$$\begin{aligned}\mathrm{BR}(B_d\to J/\psi f_0)_0 = \epsilon\left|\frac{\mathcal{A}'}{\mathcal{A}}\right|^2\left(\frac{M_{B_d^0}\Phi'_d}{M_{B_s^0}\Phi_s}\right)^3\frac{\tau_{B_d^0}}{\tau_{B_s^0}}\\ \times\overline{\mathrm{BR}}(B_s\to J/\psi f_0)\left[2-(1-y_s^2)\frac{\tau_{J/\psi f_0}}{\tau_{B_s}}\right]\end{aligned} \tag{5.70}$$

is the branching ratio in the limit $b'=0$; Φ'_d denotes the $B_d^0\to J/\psi f_0$ phase-space factor. This relation holds correspondingly for the branching ratios with $f_0\to\pi^+\pi^-$. Using (5.27) yields

$$\mathrm{BR}(B_d\to J/\psi f_0; f_0\to\pi^+\pi^-)_0 = \left(1.32^{+0.18}_{-0.23}\right)\times 10^{-6}, \tag{5.71}$$

where we have used the tetraquark value in (5.65), which is also in the ball-park of (5.66). In this estimate, the error is essentially due to (5.27) and does not take (unknown) theoretical uncertainties into account. As we will see in Section 5.2.5.5, the range $0\le b'\lesssim 0.5$ corresponds to $0.8\lesssim H_{f_0}\lesssim 1.6$, so that (5.69) yields for the central value in (5.71) the following range:

$$\mathrm{BR}(B_d\to J/\psi f_0; f_0\to\pi^+\pi^-)\sim (1\text{–}3)\times 10^{-6}. \tag{5.72}$$

Since the tetraquark picture corresponds to (5.15) with $\varphi_{\rm M}=35^\circ$, it gives a more predictive estimate of the $B_d^0\to J/\psi f_0$ branching ratio than the quark–antiquark picture. As we discussed in Section 5.2.1.2, in the latter case, the mixing angle suffers from large uncertainties. Because the leading contribution to $B_d^0\to J/\psi f_0$ is caused by the $d\bar{d}$ component of the $f_0(980)$, a mixing angle close to 0° or 180° would strongly suppress the decay. Therefore an observation of $B_d^0\to J/\psi f_0$ in the 10^{-6} regime would imply a significant $d\bar{d}$ component of the $f_0(980)$.

The LHCb experiment has recently placed the following upper bound on this decay [161]

$$\mathrm{BR}(B_d\to J/\psi f_0; f_0\to\pi^+\pi^-) < 1.1\times 10^{-6} \tag{5.73}$$

at a confidence level of 90%. We may therefore soon know whether the tetraquark picture holds, or if in the quark–antiquark picture the $f_0(980)$ has a significant $d\bar{d}$ component. Finally we note that the $B_d^0\to J/\psi f_0$ will also be an interesting topic for the e^+e^- Belle-II project.

5.2.5.4 Hierarchy of topological amplitudes

So far, we have not assumed any hierarchy for the different topologies contributing to the decays at hand. The dominant contribution is expected to be given by the colour-suppressed tree amplitude $A_{\rm T}^{(c)}$. Should all other topologies give negligible contributions, we would simply have $b' = b = 0$, and the observables discussed in Sections 5.2.3 and 5.2.4 would not be affected by hadronic uncertainties and the structure of the $f_0(980)$.

Should, in addition to $A_{\rm T}^{(c)}$, only the penguin topologies described by the $A_{\rm P}^{(q)}$ amplitudes have a significant impact, thereby resulting in a sizable value of b, the situation would be given in the $SU(3)_{\rm F}$ limit as follows:

$$be^{i\vartheta} = R_b \left[\frac{A_{\rm P}^{(ut)}}{A_{\rm T}^{(c)} + A_{\rm P}^{(ct)}}\right] = b' e^{i\vartheta'}, \tag{5.74}$$

both in the tetraquark and $q\bar{q}$ descriptions of the $f_0(980)$. In the latter case, however, we have to assume that the mixing angle $\varphi_{\rm M}$ is significantly different from 0° or 180°, as is evident from (5.56) and (5.57). The hadronic corrections to the mixing-induced CP violation in $B_s^0 \to J/\psi f_0$ could then be constrained by the $B_d^0 \to J/\psi f_0$ mode.

In addition to $SU(3)_{\rm F}$-breaking effects, the relation in (5.74) is affected by additional topologies. The exchange and penguin annihilation topologies, which involve the spectator quarks, are usually neglected in the literature (see, for instance, Refs. [150, 151, 152]). In the case of B decays involving the $f_0(980)$, there is an interesting argument that supports their suppression that is related to the decay constant of this state. Namely, the $f_0(980)$ decay constant is defined by

$$\langle f_0(p)|\bar{q}\gamma^\mu(1-\gamma_5)q|0\rangle = \langle f_0(p)|\bar{q}\gamma^\mu q|0\rangle \equiv f_{f_0} p^\mu, \tag{5.75}$$

where the axial-vector current does not contribute because of Lorentz symmetry ($q \in \{s, d, u\}$). Using the CP transformation

$$(\mathcal{CP})\,[\bar{q}\gamma^\mu(1-\gamma_5)q]\,(\mathcal{CP})^\dagger = -\,[\bar{q}\gamma_\mu(1-\gamma_5)q] \tag{5.76}$$

with $(\mathcal{CP})^\dagger(\mathcal{CP}) = \hat{1}$ and $(\mathcal{CP})|f_0\rangle = +|f_0\rangle$ in (5.75) as well as the CP invariance of strong interactions, it follows straightforwardly that the decay constant has to vanish, i.e. $f_{f_0} = 0$. The same argument in fact applies to all CP-eigenstate scalar states. Consequently, the exchange and penguin annihilation topologies will vanish in the factorization picture as, in this framework, they are proportional to the product $f_{B_{s,d}} f_{J/\psi} f_{f_0}$ of the decay constants. This feature suggests that these topologies play an even less pronounced role than they do in B decays into pseudo-scalar/vector mesons. Moreover, it is plausible to assume that they are suppressed significantly with respect to the penguin contributions $A_{\rm P}^{(qt)}$ of the $B_{s,d}^0 \to J/\psi f_0$ decays.

Experimental insights into this issue for B decays into conventional mesons can be obtained through the $B_d^0 \to J/\psi\phi$ [81] and $B_s^0 \to J/\psi\pi^0$ modes [78], which can only

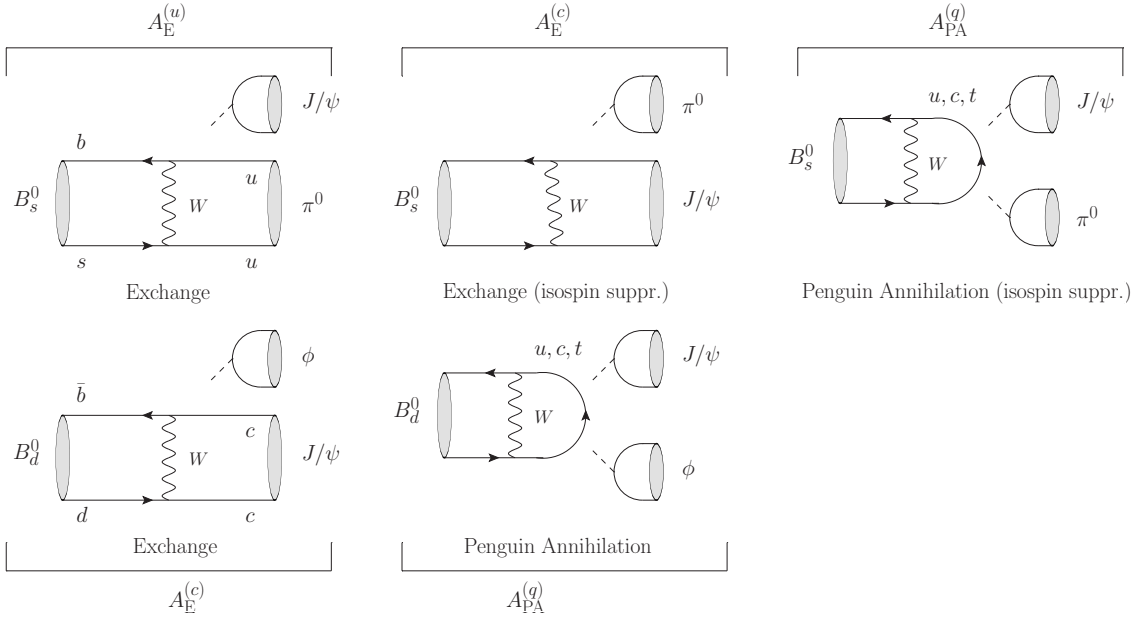

Figure 5.7: Decay topologies contributing to the $B_s^0 \to J/\psi\pi^0$ (top row) and $B_d^0 \to J/\psi\phi$ (bottom row) decays. The creation of a π^0 from a colourless state is forbidden by isospin symmetry (QED effects and electroweak penguin annihilation topologies can circumvent this argument).

emerge from exchange and penguin annihilation topologies. As shown in Figure 5.7, the $B_d^0 \to J/\psi\phi$ and $B_s^0 \to J/\psi\pi^0$ decays probe the counterparts of the $A_{\rm E}^{(c)} + A_{\rm PA}^{(ct)}$ and $A_{\rm E}^{(u)} + A_{\rm PA}^{(ct)}$ amplitudes, respectively. The current experimental 90% confidence level upper bounds on the branching ratios can are:

$$\begin{aligned} {\rm BR}(B_d \to J/\psi\phi) &< 9.4 \times 10^{-7}\,[162], & (5.77)\\ \overline{\rm BR}(B_s \to J/\psi\pi^0) &< 1.2 \times 10^{-3}\,[163]. & (5.78) \end{aligned}$$

If we use ${\rm BR}(B_d \to J/\psi K^{*0}) = (1.33\pm0.06)\times10^{-3}$ [17] and the $SU(3)$ flavour symmetry, the upper bound in (5.77) allows us to obtain the following constraint:

$$\left|\frac{A_{\rm E}^{(c)} + A_{\rm PA}^{(ct)}}{A_{\rm T}^{(c)}}\right| \sim \left(\frac{1-\lambda^2/2}{\lambda}\right)\sqrt{\frac{{\rm BR}(B_d \to J/\psi\phi)}{{\rm BR}(B_d \to J/\psi K^{*0})}} \lesssim 0.1. \qquad (5.79)$$

Here $A_{\rm E}^{(c)}$, $A_{\rm PA}^{(ct)}$ and $A_{\rm T}^{(c)}$ denote exchange, penguin annihilation and colour-suppressed tree amplitudes in these decays, which are the counterparts of those contributing to $B_{s,d}^0 \to J/\psi f_0$. Since we have two vector mesons in the final state, angular distributions should be used to disentangle the different final-state configurations. For simplicity, we have just assumed generic sizes for the topological amplitudes. The upper bound in (5.79) supports the expectation that the exchange and penguin annihilation topologies are strongly suppressed. It would be important to further improve the upper bound in

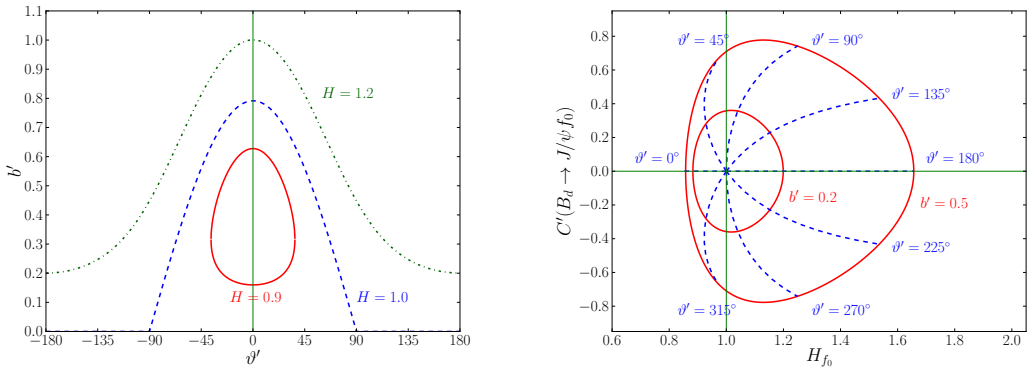

Figure 5.8: *Left panel:* Correlation between b' and ϑ' for $H_{f_0} = 0.9$, 1.0, 1.2 and 1.6. *Right panel:* Correlation between H_{f_0} and the direct CP asymmetry C' of $B_d^0 \to J/\psi f_0$, assuming $\gamma = 68°$. The solid rings correspond to $b' = 0.2$ and 0.5 with ϑ' allowed to vary. Likewise, the dashed lines are fixed points of ϑ' with b' allowed to vary.

(5.77) and to put constraints on the $B_s^0 \to J/\psi\pi^0$ branching ratio that are much more stringent than the one in (5.78), which was published by L3 in 1997.

The scalar meson counterpart of $B_s^0 \to J/\psi\pi^0$ is given by the $B_s^0 \to J/\psi\, a_0^0(980)$ channel, where

$$a_0^0(980) = \frac{1}{\sqrt{2}}\left(u\bar{u} - d\bar{d}\right) \quad \text{and} \quad a_0^0(980) = \frac{1}{\sqrt{2}}\left([su][\bar{s}\bar{u}] - [sd][\bar{s}\bar{d}]\right) \tag{5.80}$$

in the quark–antiquark and tetraquark pictures, respectively. If we neglect the isospin-suppressed topologies corresponding to those in Figure 5.7, we only get a contribution from the exchange topology in the quark–antiquark description of the $a_0^0(980)$. On the other hand, in the tetraquark picture, we get an additional contribution from the counterpart of the A_{4q} topology in Figure 5.2. Upper bounds on the branching ratio of the $B_s^0 \to J/\psi a_0^0$ channel and their comparison with $B_s^0 \to J/\psi\pi^0$ would therefore allow us to put some constraints on the A_{4q} contribution.

Another interesting decay in this context is $B_s^0 \to J/\psi\bar{\kappa}^0(800)$, which receives only contributions from colour-suppressed tree and penguin topologies in the quark–antiquark picture of the scalar state $\bar{\kappa}^0(800) = s\bar{d}$. On the other hand, in the tetraquark description, $\bar{\kappa}^0 = [su][\bar{u}\bar{d}]$, we get an additional contribution from the counterpart of the A_{4q} topology. However, the properties of the κ meson, which appears to have a very large width around of 500 MeV and sits close to the $K\pi$ threshold, are essentially unknown [17].

5.2.5.5 Control of the hadronic effects in $B_s^0 \to J/\psi f_0$

Once the branching ratio of $B_d^0 \to J/\psi f_0$ has been measured, we can determine H_{f_0} introduced in (5.68) by rewriting expressions (5.69) and (5.70) as follows:

$$H_{f_0} = \frac{1}{\epsilon}\left|\frac{\mathcal{A}}{\mathcal{A}'}\right|^2 \left(\frac{M_{B_s^0}\Phi_s}{M_{B_d^0}\Phi'_d}\right)^3 \frac{\tau_{B_s^0}}{\tau_{B_d^0}} \frac{\mathrm{BR}(B_d \to J/\psi f_0)}{\mathrm{BR}(B_s \to J/\psi f_0)}. \tag{5.81}$$

In the left panel of Figure 5.8, we show the correlation between the hadronic parameters for various values of H_{f_0}, assuming $b = b'$ and $\vartheta = \vartheta'$ in (5.68); even dramatic corrections to these relations would have a small impact because of the ϵ suppression in (5.68). Under the same assumption, we also show in the right panel of Figure 5.8 the correlation between H_{f_0} and the direct CP asymmetry C' of the $B_d^0 \to J/\psi f_0$ channel. First constraints on b' can be obtained from H_{f_0} from

$$(b')^{\mathrm{max}}_{\mathrm{min}} = \left|\left(\frac{1+\epsilon H_{f_0}}{1-\epsilon^2 H_{f_0}}\right)\cos\gamma \pm \sqrt{\left[\left(\frac{1+\epsilon H_{f_0}}{1-\epsilon^2 H_{f_0}}\right)\cos\gamma\right]^2 + \frac{H_{f_0}-1}{1-\epsilon^2 H_{f_0}}}\right|, \tag{5.82}$$

which, for $\epsilon = 0$, corresponds to the bounds derived in Ref. [164]. This constrained will be significantly sharpened via the measurement of C'. Once the mixing-induced CP asymmetry S' of $B_d^0 \to J/\psi f_0$ is measured, the quantity H_{f_0} will no longer be needed for the determination of b' and θ'.

As we have seen in the previous section, we expect the exchange and penguin annihilation topologies to play a minor role in the $B_{s,d}^0 \to J/\psi f_0$ decays. In the quark–antiquark picture, assuming that the mixing angle φ_{M} is significantly different from 0° or 180°, we would then have (5.74) in the $SU(3)_{\mathrm{F}}$ limit, and could control the hadronic effects in the mixing-induced CP asymmetry of the $B_s^0 \to J/\psi f_0$ decay.[2] The theoretical uncertainties are governed by $SU(3)_{\mathrm{F}}$-breaking corrections and the situation would be similar to $B_s^0 \to J/\psi\phi$, as discussed in Ref. [81].

As we have seen in Section 5.2.1, the tetraquark description of the $f_0(980)$ has a variety of phenomenological advantages. But in this framework we have to deal with the additional topology A_{4q} shown in Figure 5.2, which contributes to $B_s^0 \to J/\psi f_0$ but does not have a counterpart in $B_d^0 \to J/\psi f_0$. Can we make quantitative statements about the A_{4q} topology? The topology contributes also in the *spectator* approximation and arises at the tree level, i.e. is not loop-suppressed like the penguin contributions. On the other hand, it involves the production of the J/ψ through a colour-singlet exchange, in analogy to the penguin and exchange topologies in Figure 5.1. Furthermore, the us diquark and the $\bar{u}\bar{s}$ anti-diquark have to be produced in the decay of the b quark in such a way as to form the $f_0(980)$ bound state, which suggests a possible suppression. Presumably strong attractive forces are at work between these quark correlations, but the hadronization mechanism itself is essentially unknown.

[2] In the case of φ_{M} close to 0° or 180°, the $B_d^0 \to J/\psi a_0^0(980)$ channel offers an alternative to $B_d^0 \to J/\psi f_0$. It is the "scalar-meson" counterpart of the $B_d^0 \to J/\psi\pi^0$ decay [148, 149, 78].

The central question for the analysis of the $B^0_{s,d} \to J/\psi f_0$ system is the competition between the $4q$ and penguin topologies in (5.14). Should the former give a contribution at the same – or even larger – level as the penguins, which would be reflected by a sizeable value of b, we could not control the hadronic effects through the $B^0_d \to J/\psi f_0$ channel. In view of this situation, more detailed studies of the b parameter in the tetraquark description of the $f_0(980)$ would be very important.

5.3 η and η' as $s\bar{s}$ states

We will now consider the final state $B_s \to J/\psi s\bar{s}$ when the bound state $s\bar{s}$ is assumed to hadronise into a pseudoscalar η or η' meson. The key complication in this analysis is due to imprecise experimental knowledge of the mixing angle between these two isospin singlet states, and also to what extent a gluonic component contributes. This analysis is therefore very similar to that of $B_s \to J/\psi f_0$ discussed in Section 5.2 with the $f_0(980)$ assumed be a conventional quark-antiquark state. In particular, we will estimate the hadronic uncertainties for the untagged and tagged observables of these decay modes and propose strategies to constrain them using the B_d decays to the same final states, which are related by $SU(3)_{\rm F}$ flavour symmetry. This section follows closely the work presented in Ref. [165].

In Ref. [151] the $SU(3)_{\rm F}$ flavour symmetry related decay modes $B_d \to J/\psi\eta^{(\prime)}$ and $B_s \to J/\psi\eta^{(\prime)}$ were used in a strategy to determine the angle γ. This method is a variant of the $B_{s,d} \to J/\psi K_{\rm S}$ strategy proposed in Ref. [147, 100]. However, neither strategy is as competitive for determining γ as other more conventional methods, including those discussed in Chapter 4. In this section we will therefore assume γ is fixed by some other means in the same way as we did in Section 5.2.

Unfortunately the $B_{s,d} \to J/\psi\eta^{(\prime)}$ decay modes are challenging to measure at hadron colliders because the $\eta^{(\prime)}$ mesons decay prominently to photons and neutral pions. Currently the branching ratios of all but $B_d \to J/\psi\eta'$ have been measured by the Belle collaboration, which we will present in this section. These measurements will allow us to place constraints on the η–η' mixing angles and the relative contribution of a possible gluonic component. An optimal determination will be possible once the $B_d \to J/\psi\eta^{(\prime)}$ branching ratio is also measured. Measuring the observables of these modes, including time-dependent tagged and untagged analyses, will be particularly suited to future e^+e^- colliders such as the upcoming Belle-II experiment.

The outline is as follows: in Section 5.3.1, we give a brief overview of η–η' mixing and discuss how it is implemented in the $B^0_s \to J/\psi\eta^{(\prime)}$ decay amplitudes. In Section 5.3.2, we turn to the effective lifetimes and the CP-violating observables of the $B^0_s \to J/\psi\eta^{(\prime)}$ transitions. In Section 5.3.3, we focus on the $B^0_d \to J/\psi\eta^{(\prime)}$ decays and their role as control channels. Finally, in Section 5.3.4 we discuss the determination of the mixing angles between the isospin singlet states contributing to η and η' using current and future branching ratio measurements.

5.3.1 η–η' mixing

Before focusing on the $B_s \to J/\psi\eta^{(\prime)}$ decays, we will first give a brief overview of η–η' mixing. The physical $|\eta\rangle$ and $|\eta'\rangle$ states are mixtures of the octet and singlet states $|\eta_8\rangle$ and $|\eta_1\rangle$, respectively, and can be written as follows [17]:

$$\begin{pmatrix} |\eta\rangle \\ |\eta'\rangle \end{pmatrix} = \begin{pmatrix} \cos\theta_P & -\sin\theta_P \\ \sin\theta_P & \cos\theta_P \end{pmatrix} \cdot \begin{pmatrix} |\eta_8\rangle \\ |\eta_1\rangle \end{pmatrix}, \tag{5.83}$$

where

$$|\eta_8\rangle = \frac{1}{\sqrt{6}}\left(|u\bar{u}\rangle + |d\bar{d}\rangle - 2|s\bar{s}\rangle\right), \quad |\eta_1\rangle = \frac{1}{\sqrt{3}}\left(|u\bar{u}\rangle + |d\bar{d}\rangle + |s\bar{s}\rangle\right). \tag{5.84}$$

The mixing between the octet and singlet states is a manifestation of the breaking of the $SU(3)_{\rm F}$ flavour symmetry of strong interactions. Alternatively, η–η' mixing can be described in terms of the isospin singlet states

$$|\eta_q\rangle \equiv \frac{1}{\sqrt{2}}\left(|u\bar{u}\rangle + |d\bar{d}\rangle\right), \quad |\eta_s\rangle \equiv |s\bar{s}\rangle. \tag{5.85}$$

By also taking the possible mixing with a purely gluonic component $|gg\rangle$ into account, we can write the following expressions (for a recent detailed discussion, see Ref. [153]):

$$|\eta\rangle = \cos\phi_P|\eta_q\rangle - \sin\phi_P|\eta_s\rangle, \tag{5.86}$$

$$|\eta'\rangle = \cos\phi_G\sin\phi_P|\eta_q\rangle + \cos\phi_G\cos\phi_P|\eta_s\rangle + \sin\phi_G|gg\rangle. \tag{5.87}$$

Here it has been assumed, for simplicity, that the heavier η' contains a larger gluonic admixture than the lighter η and that the coupling of the latter state to $|gg\rangle$ is negligible. Estimates give $\sin^2\phi_G \sim 0.1$ [166], i.e. $|\phi_G| \sim 20^\circ$, which indicates that the impact of this contribution is suppressed.

The mixing angle ϕ_P is still subject of ongoing studies, using data for processes such as $D_s^+ \to \eta^{(\prime)}\ell^+\nu_\ell$ decays and the two-photon width of the $\eta^{(\prime)}$ mesons (see Ref. [153] and references therein). The full spectrum of results correspond to $30^\circ \lesssim \phi_P \lesssim 45^\circ$, with the majority of analyses converging at values of ϕ_P around 40°. Consequently, the relations

$$\cos\phi_P \approx \sqrt{\frac{2}{3}}, \quad \sin\phi_P \approx \sqrt{\frac{1}{3}}, \tag{5.88}$$

where the numerical values correspond to $\phi_P = 35^\circ$, are affected by uncertainties of $\mathcal{O}(20\%)$. These approximate relations result in the simple expressions

$$|\eta\rangle \approx \frac{1}{\sqrt{3}}\left(|u\bar{u}\rangle + |d\bar{d}\rangle - |s\bar{s}\rangle\right) \tag{5.89}$$

$$|\eta'\rangle \approx \frac{1}{\sqrt{6}}\left(|u\bar{u}\rangle + |d\bar{d}\rangle + 2|s\bar{s}\rangle\right)\cos\phi_G + \sin\phi_G|gg\rangle, \tag{5.90}$$

which are useful for $SU(3)_{\rm F}$ analyses of non-leptonic B-meson decays with $\eta^{(\prime)}$ mesons in the final states [150, 152]. In our study we shall follow a similar conceptual avenue, keeping, however, ϕ_P as a free parameter.

The decay amplitudes for the $B_s^0 \to J/\psi\eta^{(\prime)}$ decay modes can similarly be described by the amplitude formalism given in (5.6) for the $B_s^0 \to J/\psi f_0$ mode. We will label the associated hadronic parameters accordingly by $\mathcal{A}_{\eta^{(\prime)}}$ and $b_{\eta^{(\prime)}} e^{i\vartheta_{\eta^{(\prime)}}}$. Furthermore, both decay modes have dynamics very similar to the $B_s^0 \to J/\psi f_0$ with a quark–antiquark description assumed for the f_0 as given in Section 5.2.1. For the $B_s^0 \to J/\psi\eta$ the decay topology structure is in fact the same. To obtain the transition amplitude in this case we only need to make the substitution $\varphi_M \to \varphi_P + 90^\circ$ in the relevant formula.

For the $B_s^0 \to J/\psi\eta'$ mode we may similarly make the substitution $\varphi_M \to \varphi_P$. We find in particular that if we apply the angle relations given in (5.88) the amplitude structure is analogous to that of the $B_s^0 \to J/\psi f_0$ with a tetraquark interpretation for the f_0. However, in this case there is an additional topology that is specific to the f_0 tetraquark state. On the other hand, the $B_s^0 \to J/\psi\eta'$ mode has an additional contribution from the gluonic component of the η'. This component can only contribute through exchange and penguin annihilation topologies, which are expected to be small in comparison to the tree and penguin topologies, respectively.

5.3.2 Observables

Since 2012 the Belle collaboration now has observations for both the $B_s^0 \to J/\psi\eta$ and $B_s^0 \to J/\psi\eta'$ decays, with the following branching ratio measurements [167]:

$$\overline{\rm BR}(B_s \to J/\psi\eta) = \left[5.10 \pm 0.50\,({\rm stat.}) \pm 0.25\,({\rm syst.})^{+1.14}_{-0.79}\,(f_s)\right] \times 10^{-4} \tag{5.91}$$

$$\overline{\rm BR}(B_s \to J/\psi\eta') = \left[3.71 \pm 0.61\,({\rm stat.}) \pm 0.18\,({\rm syst.})^{+0.83}_{-0.57}\,(f_s)\right] \times 10^{-4}. \tag{5.92}$$

Here the latter errors refer to the B_s fragmentation function f_s.

Using the $SU(3)_{\rm F}$ flavour symmetry the theoretically defined $B_s^0 \to J/\psi\eta^{(\prime)}$ branching ratios (see Section 3.4) can be related to the $B_d^0 \to J/\psi K^0$ branching ratio. Taking factorizable $SU(3)_{\rm F}$-breaking corrections into account yields

$$\left.\frac{{\rm BR}(B_s \to J/\psi\eta^{(\prime)})}{{\rm BR}(B_d \to J/\psi K^0)}\right|_{\rm fact.} = \frac{\tau_{B_s^0}}{\tau_{B_d^0}} \left[\frac{M_{B_s^0}\Phi_s^{\eta^{(\prime)}}}{M_{B_d^0}\Phi_d^{K^0}}\right]^3 \left[\frac{F_1^{B_s^0\eta^{(\prime)}}(M^2_{J/\psi})}{F_1^{B_d^0 K^0}(M^2_{J/\psi})}\right]^2, \tag{5.93}$$

where the $\tau_{B_q^0}$ and $M_{B_q^0}$ are the B_q^0 lifetimes and masses, respectively,

$$\Phi_q^P \equiv \sqrt{\left[1 - \left(\frac{M_P + M_{J/\psi}}{M_{B_q}}\right)^2\right]\left[1 - \left(\frac{M_P - M_{J/\psi}}{M_{B_q}}\right)^2\right]} \tag{5.94}$$

denotes the phase-space factor for $B_q^0 \to J/\psi P$ decays, and the $F_1^{B_q^0 P}(M^2_{J/\psi})$ are hadronic form factors of quark currents. These relations have been used previously to predict the $B_s^0 \to J/\psi\eta^{(\prime)}$ branching ratios [151, 155].

Now that the branching ratios have been measured, it is possible to probe the non-factorizable $SU(3)_{\rm F}$-breaking corrections. To this end we define the quantities

$$K_{SU(3)}^{\eta^{(\prime)}} \equiv \frac{\tau_{B_d^0}}{\tau_{B_s^0}} \left[\frac{M_{B_d^0}\Phi_d^{K^0}}{M_{B_s^0}\Phi_s^{\eta^{(\prime)}}}\right]^3 \left[\frac{F_1^{B_d^0 K^0}(M_{J/\psi}^2)}{F_1^{B_s^0\eta^{(\prime)}}(M_{J/\psi}^2)}\right]^2 \times \frac{\overline{\rm BR}(B_s \to J/\psi\eta^{(\prime)})}{\rm BR(B_d \to J/\psi K^0)} \left[\frac{1-y_s^2}{1+y_s\,\mathcal{A}_{\Delta\Gamma}^{J/\psi\eta^{(\prime)}}}\right], \tag{5.95}$$

where $K_{SU(3)}^{\eta^{(\prime)}} = 1$ in the case of vanishing non-factorizable $SU(3)_{\rm F}$-breaking corrections. Since non-perturbative calculations of the $F_1^{B_s^0\eta^{(\prime)}}(M_{J/\psi}^2)$ form factors are not yet available, we project out on the $|\eta_s\rangle$ component in (5.86) and write

$$F_1^{B_s^0\eta}(M_{J/\psi}^2) = -\sin\phi_P F_1^{B_d^0 K^0}(M_{J/\psi}^2) \tag{5.96}$$

$$F_1^{B_s^0\eta'}(M_{J/\psi}^2) = \cos\phi_G\cos\phi_P F_1^{B_d^0 K^0}(M_{J/\psi}^2), \tag{5.97}$$

where we neglect $SU(3)_{\rm F}$-breaking corrections originating from the down and strange spectator quarks. Because the effective lifetimes of $B_s^0 \to J/\psi\eta^{(\prime)}$ have not yet been measured, we do not have an experimental handle on the mass-eigenstate rate asymmetries $\mathcal{A}_{\Delta\Gamma}^{J/\psi\eta^{(\prime)}}$.

In Section 5.2 the evaluation of $\mathcal{A}_{\Delta\Gamma}$ has been discussed in detail for the $B_s^0 \to J/\psi f_0$ channel. Since the $\eta^{(\prime)}$ are pseudoscalar mesons with quantum numbers $J^{PC} = 0^{-+}$, the final states of $B_{s,d}^0 \to J/\psi\eta^{(\prime)}$ are CP-even. This sign difference results in

$$\mathcal{A}_{\Delta\Gamma}^{J/\psi\eta^{(\prime)}} = -\sqrt{1-C_{J/\psi\eta^{(\prime)}}^2}\cos(\phi_s + \Delta\phi_{J/\psi\eta^{(\prime)}}). \tag{5.98}$$

Here $C_{J/\psi\eta^{(\prime)}}$ describes direct CP violation of these decay modes. The quantity $\Delta\phi_{J/\psi\eta^{(\prime)}}$ is the hadronic phase shift, which can be obtained from

$$\tan\Delta\phi_{J/\psi\eta^{(\prime)}} = \frac{2\,\epsilon\,b_{\eta^{(\prime)}}\cos\vartheta_{\eta^{(\prime)}}\sin\gamma + \epsilon^2\,b_{\eta^{(\prime)}}^2\sin 2\gamma}{1 + 2\,\epsilon\,b_{\eta^{(\prime)}}\cos\vartheta_{\eta^{(\prime)}}\cos\gamma + \epsilon^2\,b_{\eta^{(\prime)}}^2\cos 2\gamma}. \tag{5.99}$$

We observe that the hadronic parameters, which are poorly known, enter $\Delta\phi_{J/\psi\eta^{(\prime)}}$ in a doubly Cabibbo-suppressed way. Therefore the effective lifetimes turn out to be very robust with respect to the hadronic corrections, in analogy to the situation in $B_s^0 \to J/\psi f_0$. As in Section 5.2, we use $\gamma = (68 \pm 7)^\circ$ in order to illustrate the hadronic effects. As far as the hadronic parameters are concerned, we consider the ranges

$$0 \le b_{\eta^{(\prime)}} \le 0.5, \quad 90^\circ \le \vartheta_{\eta^{(\prime)}} \le 270^\circ. \tag{5.100}$$

Due to the factor $R_b \sim 0.5$ in (5.11), which has an analogous form for the $\eta^{(\prime)}$ case, the range for $b_{\eta^{(\prime)}}$ is conservative. The range for the strong phase is motivated by the

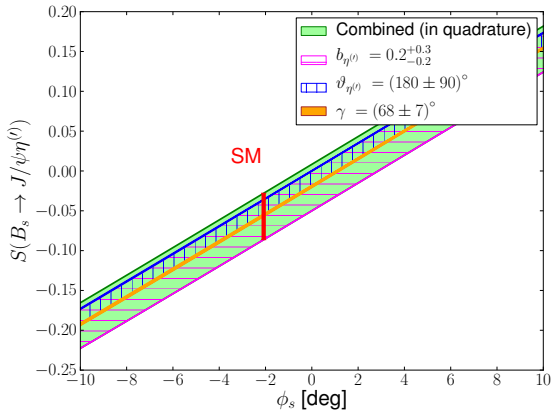

Figure 5.9: The mixing-induced CP asymmetry of $B_s^0 \to J/\psi\eta^{(\prime)}$ as a function of ϕ_s, assuming $\gamma = (68 \pm 7)^\circ$, $0 \leq b_{\eta^{(\prime)}} \leq 0.5$ and $90^\circ \leq \vartheta_{\eta^{(\prime)}} \leq 270^\circ$ for the calculation of the error band. We show only the region close to the SM case.

topological structure entering $b_{\eta^{(\prime)}}$.. For the ranges given in (5.100) the hadronic phase shift takes values in the interval

$$\Delta\phi_{J/\psi\eta^{(\prime)}} \in [-3^\circ, 0^\circ]. \tag{5.101}$$

Likewise, the direct CP asymmetry satisfies $|C_{J/\psi\eta^{(\prime)}}| \lesssim 0.05$ under these assumptions and thereby has a negligible impact on $\mathcal{A}_{\Delta\Gamma}^{J/\psi\eta^{(\prime)}}$.

To give estimates for $K_{SU(3)}^{\eta^{(\prime)}}$ we set, for simplicity, $\mathcal{A}_{\Delta\Gamma}^{J/\psi\eta^{(\prime)}} = -1$, which corresponds to no mixing-induced or direct CP violation for these decay modes. Using $\mathrm{BR}(B_d \to J/\psi K^0) = (8.71 \pm 0.32) \times 10^{-4}$ [17] then yields

$$\begin{aligned} K_{SU(3)}^{\eta}\Big|_{\mathcal{A}_{\Delta\Gamma}^{J/\psi\eta}=-1} &= \left[\frac{\sin 40^\circ}{\sin\phi_P}\right]^2 \times \left(1.4^{+0.4}_{-0.3}\right), \\ K_{SU(3)}^{\eta'}\Big|_{\mathcal{A}_{\Delta\Gamma}^{J/\psi\eta'}=-1} &= \left[\frac{\cos 20^\circ}{\cos\phi_G}\right]^2 \left[\frac{\cos 40^\circ}{\cos\phi_P}\right]^2 \times \left(1.0^{+0.3}_{-0.2}\right). \end{aligned} \tag{5.102}$$

These numbers indicate a sizable $SU(3)_{\mathrm{F}}$-breaking correction for $B_s^0 \to J/\psi\eta$, although the currently large errors preclude us from drawing stronger conclusions. In Section 5.3.4, we will return to the $B_s^0 \to J/\psi\eta^{(\prime)}$ branching ratios, using them to extract the mixing angles ϕ_P and ϕ_G.

Once the $B_s^0 \to J/\psi\eta^{(\prime)}$ effective lifetimes have been measured they can be converted into contours in the ϕ_s–$\Delta\Gamma_s$ plane, as discussed in Section 3.3.2. Furthermore, using complementary information from a second CP-odd final state, such as $B_s^0 \to J/\psi f_0$, the mixing parameters ϕ_s and $\Delta\Gamma_s$ can be extracted. The corresponding theoretical SM prediction for the effective lifetimes is

$$\tau_{J/\psi\eta^{(\prime)}}\big|_{\mathrm{SM}} = (1.422 \pm 0.024)\ \text{ps}, \tag{5.103}$$

where we have used τ_{B_s} as given in (3.53).

A tagged analysis of $B_s^0 \to J/\psi\eta^{(\prime)}$ decays allows the extraction of the mixing-induced CP observable

$$S_{J/\psi\eta^{(\prime)}} = \sqrt{1 - C^2_{J/\psi\eta^{(\prime)}}}\,\sin(\phi_s + \Delta\phi_{J/\psi\eta^{(\prime)}}). \tag{5.104}$$

The minus sign differs from the mixing-induced CP asymmetry of the $B_s^0 \to J/\psi f_0$ channel (5.46) because of the opposite CP eigenvalues of the final states. In the right panel of Figure 5.9, we show the dependence of $S_{J/\psi\eta^{(\prime)}}$ on the mixing phase ϕ_s and illustrate how the hadronic SM uncertainties as well as the uncertainties on γ propagate through. We observe that a future measurement of the mixing-induced CP asymmetry in the range

$$-0.09 \lesssim S_{J/\psi\eta^{(\prime)}} \lesssim -0.03 \tag{5.105}$$

would not allow us to distinguish the SM from CP-violating NP contributions to B_s^0–$\bar{B}_s^0$ mixing. Should we encounter such a situation, more information would be required to accomplish this task.

5.3.3 Control channels

The leading contributions to the $B_d^0 \to J/\psi\eta$ decay originate from $\bar{b} \to \bar{c}c\bar{d}$ quark-level processes. It is the formal counterpart of the $B_d^0 \to J/\psi f_0$ mode discussed in Section 5.2.5. Thus the transition amplitude given in (5.50) applies, and we may label the corresponding hadronic parameters as $\mathcal{A}'_\eta$ and $b'_\eta e^{i\vartheta'_\eta}$. Again, the key difference of the $B_d^0 \to J/\psi\eta$ decay with respect to its $B_s^0 \to J/\psi\eta$ counterpart is that the hadronic parameter $b'_\eta e^{i\vartheta'_\eta}$ does not enter the amplitude in a doubly Cabibbo-suppressed way. Consequently, its impact is magnified in the $B_d^0 \to J/\psi\eta$ observables. On the other hand, the branching ratio does suffer from a λ^2 suppression.

As discussed in detail in Section 5.2.5.4, the exchange and penguin amplitudes play a minor role and can be probed through the $B_d^0 \to J/\psi\phi$ and $B_s^0 \to J/\psi\pi^0$ decays. Neglecting these contributions and using the $SU(3)_{\rm F}$ symmetry, we obtain

$$b_\eta e^{i\vartheta_\eta} \overset{SU(3)_{\rm F}}{=} R_b \left[\frac{\tilde{A}_{\rm P}^{(ut)}}{\tilde{A}_{\rm T}^{(c)} + \tilde{A}_{\rm P}^{(ct)}}\right] \overset{SU(3)_{\rm F}}{=} b'_\eta e^{i\vartheta'_\eta}. \tag{5.106}$$

Interestingly, the dependence on ϕ_P drops out if the exchange and penguin annihilation contributions are neglected. Since the parameters b'_η and ϑ'_η can be determined from the $B_d^0 \to J/\psi\eta$ observables in a clean way, we can control the penguin effects in the $B_s^0 \to J/\psi\eta$ observables.

As the $b_\eta^{(\prime)} e^{i\vartheta_\eta^{(\prime)}}$ are ratios of hadronic amplitudes, we expect (5.106) to be robust with respect to $SU(3)_{\rm F}$ breaking corrections. Should the $B_d^0 \to J/\psi\eta$ data favour a small value of b'_η, the exchange and penguin annihilation amplitudes could contribute significant uncertainties in relating b'_η to b_η. However, the doubly Cabibbo-suppressed

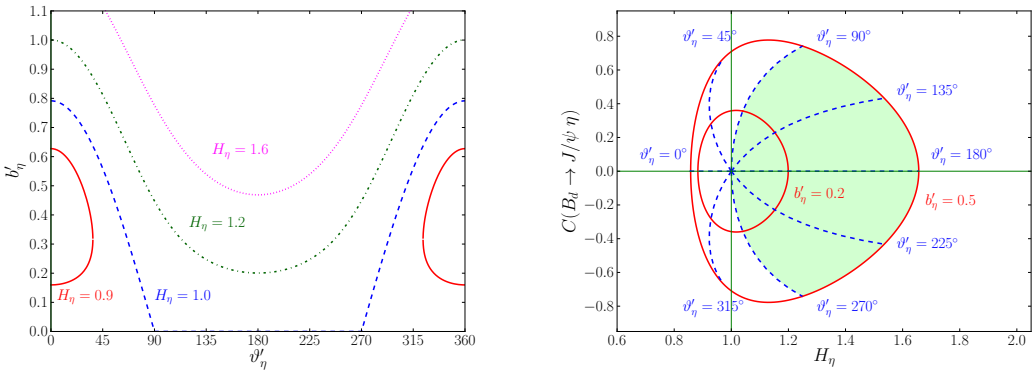

Figure 5.10: *Left panel:* constraints in the ϑ'_η–b'_η plane for various values of H_η. *Right panel:* correlation between H_η and the direct CP asymmetry of $B^0_d \to J/\psi\eta$, where the solid rings correspond to $b'_\eta = 0.2$ and 0.5 with ϑ'_η allowed to vary; likewise, the dashed lines are fixed points of ϑ'_η with b'_η allowed to vary. In both plots, we have assumed $\gamma = 68°$.

corrections to the mixing-induced CP violation in $B^0_s \to J/\psi\eta$ would then be tiny anyway.

The $B^0_d \to J/\psi\eta$ decay was observed by the Belle collaboration [168], with

$$\mathrm{BR}(B_d \to J/\psi\eta) = [12.3^{+1.8}_{-1.7}(\mathrm{stat.}) \pm 0.7(\mathrm{syst.})] \times 10^{-6}, \tag{5.107}$$

which is consistent with the estimates given in Ref. [151]. We can use this measurement to obtain a first constraint on the hadronic parameters with the help of

$$H_\eta \equiv \frac{1}{\epsilon}\left|\frac{\mathcal{A}_\eta}{\mathcal{A}'_\eta}\right|^2 \left(\frac{M_{B^0_s}\Phi^\eta_s}{M_{B^0_d}\Phi^\eta_d}\right)^3 \frac{\tau_{B^0_s}}{\tau_{B^0_d}}\,\frac{\mathrm{BR}(B_d \to J/\psi\eta)}{\overline{\mathrm{BR}}(B_s \to J/\psi\eta)}\cdot\left[\frac{1}{2-(1-y_s^2)\,\tau_{J/\psi\eta}/\tau_{B_s}}\right], \tag{5.108}$$

which is the counterpart of H_{f_0} defined in Section 5.2.5.3. Similarly, it depends on γ and the hadronic parameters in the following way

$$H_\eta = \frac{1 - 2b'_\eta\cos\vartheta'_\eta\cos\gamma + b'^2_\eta}{1 + 2\epsilon b_\eta\cos\vartheta_\eta\cos\gamma + \epsilon^2 b^2_\eta}. \tag{5.109}$$

In order to extract H_η from the branching ratios, we have to calculate the $SU(3)$-breaking ratio of the $\mathcal{A}_\eta$ and $\mathcal{A}'_\eta$ amplitudes. Using the factorization approximation and keeping only the leading tree contributions gives

$$\left|\frac{\mathcal{A}_\eta}{\mathcal{A}'_\eta}\right|_{\mathrm{fact.}} = -\sqrt{2}\tan\phi_P\left[\frac{F_1^{B^0_d K^0}(M^2_{J/\psi})}{F_1^{B^0_d\pi^-}(M^2_{J/\psi})}\right], \tag{5.110}$$

where we have, as in (5.96), also neglected $SU(3)_{\mathrm{F}}$-breaking corrections that originate from the down and strange spectator quarks. Using the leading-order light-cone QCD

sum-rule results of Ref. [156], we find for the form factors

$$F_1^{B_d^0 K^0}(M_{J/\psi}^2) = 0.615 \pm 0.076, \quad F_1^{B_d^0 \pi^-}(M_{J/\psi}^2) = 0.49 \pm 0.06. \tag{5.111}$$

Because the $B_{s,d}^0 \to J/\psi\eta$ effective lifetime has not yet been measured we will use the SM estimate given in (5.103) to correct for the experimental branching ratio (see Section 3.4). Including the $B_{s,d}^0 \to J/\psi\eta$ branching ratio measurements given earlier, we finally arrive at

$$H_\eta \times \left[\frac{\tan 40^\circ}{\tan\phi_P}\right]^2 = 1.04^{+0.29}_{-0.26}\big|_{\rm BR}{}^{+0.40}_{-0.32}\big|_{\rm FF} = 1.04^{+0.50}_{-0.41}. \tag{5.112}$$

The errors reflect only the experimental and form-factor uncertainties and do not take non-factorizable $SU(3)$-breaking corrections into account. Using the factorization tests in (5.102), a future measurement of the $B_s^0 \to J/\psi\eta$ branching ratio should give us better quantitative insights into these effects. In Figure 5.10, we convert this result into contours in the ϑ'_η–b'_η plane (see Section 5.2.5.5 for details).

As soon as measurements of the CP asymmetries for $B_d^0 \to J/\psi\eta$ become available we will be able to determine b'_η and θ'_η in a clean way. Subsequently, we can determine H_η through (5.109). Using information from the branching ratios and (5.108) and (5.110), we can then determine $|\tan\phi_P|$. Alternatively, assuming that we will have a sharp picture of ϕ_P by the time these measurements become available (see also Section 5.3.4), we can perform a test of non-factorizable $SU(3)_{\rm F}$-breaking corrections.

Neglecting the exchange and penguin annihilation topologies, the control of the hadronic parameters in the $B_s^0 \to J/\psi\eta'$ observables by means of the $B_d^0 \to J/\psi\eta'$ mode is analogous to the case of the $B_{s,d}^0 \to J/\psi\eta$ channels.

5.3.4 Determining the η–η' mixing parameters

Let us finally discuss determinations of the η–η' mixing parameters through measurements of the $B_{s,d}^0 \to J/\psi\eta^{(\prime)}$ branching ratios. If we project out on the singlet states in (5.86) and (5.87) and assume that the exchange and penguin annihilation topologies give negligible contributions, we obtain the relation

$$R_s \equiv \frac{\overline{\rm BR}(B_s \to J/\psi\eta')}{\overline{\rm BR}(B_s \to J/\psi\eta)} \left(\frac{\Phi_s^\eta}{\Phi_s^{\eta'}}\right)^3 = \frac{\cos^2\phi_G}{\tan^2\phi_P}, \tag{5.113}$$

which does not assume $SU(3)_{\rm F}$ or factorization. The same expression with $\phi_G = 0$ has already been given in Ref. [169]. Both the Belle and LHCb collaborations have measurements of the branching ratio fraction

$$\left.\frac{\overline{\rm BR}(B_s \to J/\psi\eta')}{\overline{\rm BR}(B_s \to J/\psi\eta)}\right|_{\rm exp} = \begin{cases} 0.73 \pm 0.14\,({\rm stat.}) \pm 0.02\,({\rm syst.}) & : \text{ Belle [167]} \\ 0.90 \pm 0.09\,({\rm stat.})^{+0.06}_{-0.02}\,({\rm syst.}) & : \text{ LHCb [170]} \end{cases}. \tag{5.114}$$

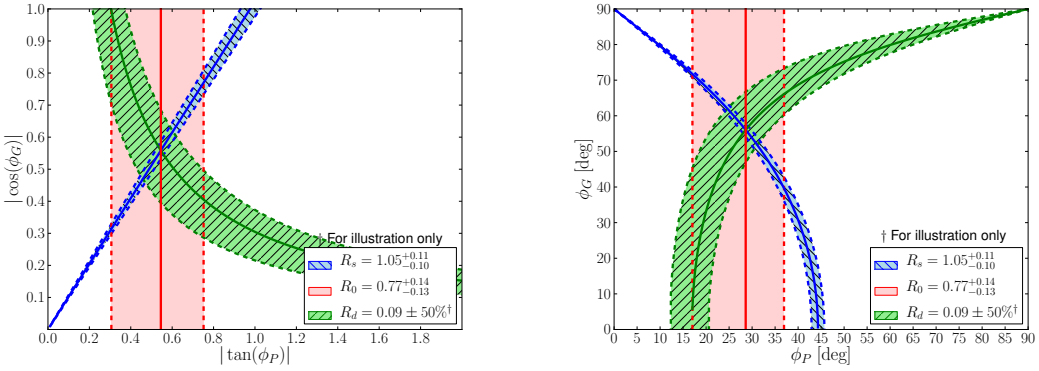

Figure 5.11: Constraints on the η–η' mixing parameters from the $B^0_{s,d} \to J/\psi\eta^{(\prime)}$ and $B^0_d \to J/\psi\pi^0$ branching ratios as discussed in the text. Note that the right panel does not show all the discrete angular ambiguities.

Using these experimental results we find

$$R_s = \begin{cases} 0.91 \pm 0.18 & : \text{ Belle} \\ 1.12^{+0.13}_{-0.11} & : \text{ LHCb} \end{cases} = 1.05^{+0.11}_{-0.10} \quad \text{(weighted average)}. \tag{5.115}$$

In analogy to (5.113), we introduce the following ratio for the B_d decays:

$$R_d \equiv \frac{\text{BR}(B_d \to J/\psi\eta')}{\text{BR}(B_d \to J/\psi\eta)} \left(\frac{\Phi_d^\eta}{\Phi_d^{\eta'}}\right)^3 = \cos^2\phi_G \, \tan^2\phi_P. \tag{5.116}$$

Using the experimental value in (5.107), this expression results in the prediction

$$\text{BR}(B_d \to J/\psi\eta') = \left[\frac{\cos\phi_G}{\cos 20^\circ}\right]^2 \left[\frac{\tan\phi_P}{\tan 40^\circ}\right]^2 \times \left(6.0^{+1.0}_{-0.9}\right) \times 10^{-6}. \tag{5.117}$$

Only the upper bound

$$\text{BR}(B_d \to J/\psi\eta') < 7.4 \times 10^{-6} \ (90\%\text{C.L.}) \tag{5.118}$$

is currently available from the Belle collaboration [168].

Once the $B^0_d \to J/\psi\eta'$ branching ratio has been measured, we can use

$$\frac{R_d}{R_s} = \tan^4\phi_P, \quad R_s R_d = \cos^4\phi_G \tag{5.119}$$

to determine the mixing angles up to fourfold discrete ambiguities. It is interesting to note that the 4th powers in these expressions result in precise determinations of $|\tan\phi_P|$ and $|\cos\phi_G|$ even for branching ratio measurements with significant errors. If we assume,

for illustration, a future measurements of $R_d = 0.09 \pm 0.05$, i.e. with precisions of 50%, we would obtain $\phi_P = (28.6^{+2.6}_{-4.0})^\circ$ and $|\phi_G| \in [52^\circ, 62^\circ]$.

In Figure 5.11, we have illustrated this method, showing the contours for the current experimental value of R_s in (5.113) and our illustrative value of $R_d = 0.6 \pm 0.2$. It is interesting to include also the constraint from the following ratio [171]:

$$R_0 \equiv \frac{\mathrm{BR}(B_d \to J/\psi\eta)}{\mathrm{BR}(B_d \to J/\psi\pi^0)} \left(\frac{\Phi_d^{\pi^0}}{\Phi_d^{\eta}}\right)^3 = \cos^2\phi_P. \tag{5.120}$$

Here penguin annihilation and exchange topologies were again neglected. The penguin parameters of the $B_d^0 \to J/\psi\pi^0$ decay [78, 148, 149] are then the same as in the $B_d^0 \to J/\psi\eta^{(\prime)}$ modes. In particular, we also expect the same direct and mixing-induced CP asymmetries. As (5.120) does not depend on ϕ_G, we can straightforwardly convert the Belle result in (5.107) with $\mathrm{BR}(B_d \to J/\psi\pi^0) = (1.76 \pm 0.16) \times 10^{-5}$ [17] into

$$\phi_P|_{R_0} = \left(29^{+8}_{-12}\right)^\circ. \tag{5.121}$$

The intersection of the corresponding band in Figure 5.11 with the R_s contour gives $\phi_G = 55^\circ$ for the central values. These results are in good agreement with those discussed at the beginning of Section 5.3.1. Using these central values for the angles gives the following prediction

$$\mathrm{BR}(B_d \to J/\psi\eta') = \left[\frac{\cos\phi_G}{\cos 55^\circ}\right]^2 \left[\frac{\tan\phi_P}{\tan 29^\circ}\right]^2 \times \left(9.0^{+8.2}_{-6.3}\right) \times 10^{-7}. \tag{5.122}$$

which is in better agreement with the upper bound given in (5.118).

5.4 Effective lifetime constraints

5.4.1 Constraints from current and future data

In Section 3.3.2 we discussed how a pair of B_s effective lifetime measurements of CP eigenstate final states, one CP-odd and one CP-even, can be used to pinpoint the B_s mixing parameters ϕ_s and $\Delta\Gamma_s$. It so happen that such a pair of effective lifetimes has already been accurately measured by LHCb. In this chapter we have analysed in detail the effective lifetime of the CP-odd final state $J/\psi f_0(980)$, with the latest LHCb measurement given in (5.33). In Figure 5.4 this effective lifetime measurement is shown in the ϕ_s–$\Delta\Gamma_s$ plane. Furthermore, in Chapter 4 we addressed the effective lifetime of the CP-even final state K^+K^-. Its LHCb measurement is given in (4.17), and estimates for the hadronic parameters entering its decay mode in (4.49). In Figure 4.5 effective lifetime measurement of this CP-even final state is shown in the ϕ_s–$\Delta\Gamma_s$ plane. Thus we have all the ingredients that we need available to perform this analysis.

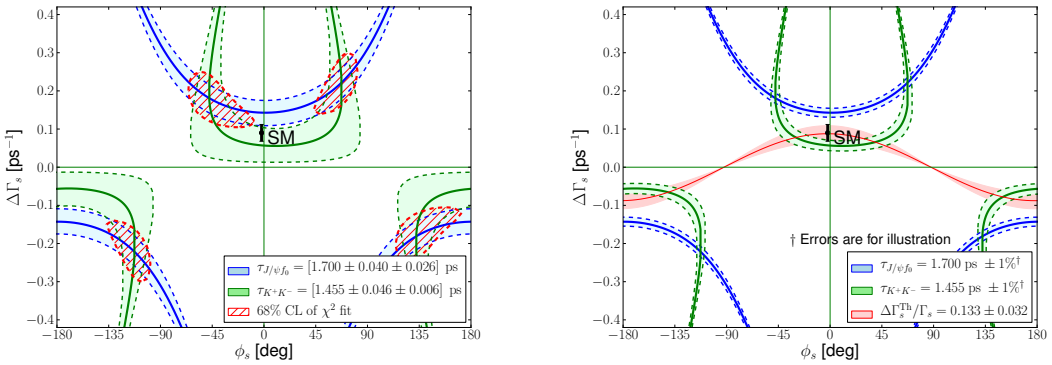

Figure 5.12: The measurements of the effective $B_s^0 \to K^+K^-$ and $B_s^0 \to J/\psi f_0$ lifetimes projected onto the ϕ_s–$\Delta\Gamma_s$ plane. *Left panel:* analysis of the current data, where the shaded bands give the $1\,\sigma$ uncertainties of the lifetimes; the 68% confidence regions originating from a χ^2 fit are also shown. *Right panel*: illustration of how the situation improves for unchanged central values if the uncertainties were improved to 1% accuracy, including also the constraint from the theoretical value of $\Delta\Gamma_s^{\rm Th}/\Gamma_s$.

In the left panel of Figure 5.12, we show the combined effective lifetime contours of the $B_s^0 \to K^+K^-$ and $B_s^0 \to J/\psi f_0(980)$ decays on the ϕ_s–$\Delta\Gamma_s$ plane. The coloured bands correspond to the $1\,\sigma$ measurement errors. We also show the 68% confidence level region resulting from a χ^2 fit of these two results. The corresponding individual 68% confidence level χ^2 fitted values for the ϕ_s and $\Delta\Gamma_s$ parameters are as follows:

$$\phi_s = -\left(47^{+11}_{-20}\right)^\circ, \quad \Delta\Gamma_s = \left(0.18^{+0.04}_{-0.05}\right) \text{ps}^{-1} \tag{5.123}$$

and

$$\phi_s = \left(68^{+8}_{-13}\right)^\circ, \quad \Delta\Gamma_s = \left(0.23^{+0.04}_{-0.06}\right) \text{ps}^{-1}. \tag{5.124}$$

As can be seen from the left panel of Figure 5.12, each solution has a two-fold ambiguity given by the transformation

$$\phi_s \to \phi_s + 180^\circ, \quad \Delta\Gamma_s \to -\Delta\Gamma_s. \tag{5.125}$$

Both lifetime measurements currently have an error of approximately 3%. In the right panel of Figure 5.12, we show for illustration the impact of measurements of the $B_s^0 \to K^+K^-$ and $B_s^0 \to J/\psi f_0$ effective lifetimes with 1% uncertainty, assuming no change in the central values. Clearly, at this level of accuracy, the lifetime measurements could strongly constrain ϕ_s and $\Delta\Gamma_s$.

Using the relation in (3.45), we also include the band corresponding to the theoretical value of $y_s^{\rm Th}$ given in (3.43). We observe, as also noted in Section 5.2.3, that the central value of the $\tau_{J/\psi f_0}$ measurement is too large in comparison with this constraint. As discussed in Section 3.1, this relation relies on the well motivated assumption that NP effects to Γ_{12} are negligible. Therefore, should this discrepancy continue to hold, it may

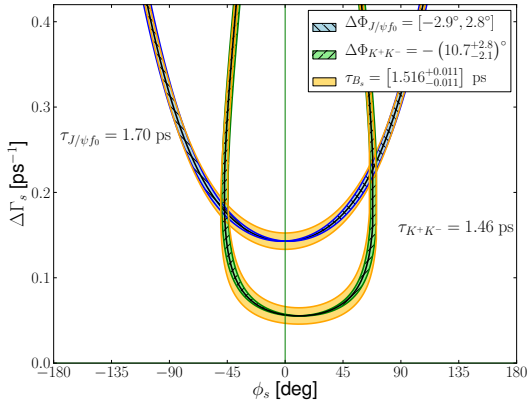

Figure 5.13: Illustration of the errors of the hadronic phase shifts $\Delta\phi_{K^+K^-}$ and $\Delta\phi_{J/\psi f_0}$ on the contours in the ϕ_s–$\Delta\Gamma_s$ plane for the central values of the lifetime measurements. We also shown the impact of the present error of the B_s lifetime.

be that the theoretical calculation of $y_s^{\rm Th}$ is too low due to unaccounted for long distance hadronic effects or a failure of the heavy quark expansion. The $B_s^0 \to J/\psi f_0$ effective lifetime predicted by this theoretical calculation is given in (5.44).

The uncertainties of the hadronic phase shifts given in (5.43) and (4.49) as well as the error of the B_s mean lifetime were not included in Figure 5.12 or in the fit results in (5.123) and (5.124). In Figure 5.13, we illustrate the impact of these uncertainties on the lifetime contours in the ϕ_s–$\Delta\Gamma_s$ plane. Comparing with the error bands in Figure 5.12, we observe that the effects of these uncertainties are marginal with respect to the current errors of the effective lifetime measurement. More sophisticated fits should take these uncertainties into account as well.

It is interesting to compare our fitted results to recent measurements of CP violation using the full-tagged analysis of the $B_s \to J/\psi\phi$ channel. In Figure 5.14 we have combined the effective lifetime contours and fit results of our analysis described above with the latest $B_s \to J/\psi\phi$ analysis results from DØ [172], CDF [173], LHCb [76] and ATLAS [174, 175]. The fitted region from the effective lifetimes is seen to agree best with the DØ result. However, the tagged analysis from LHCb is considerably more accurate. This reflects the fact that a tagged analysis is more sensitive to a small mixing-induced CP violating phase, which can be be seen from the expression for S_f given in (3.80). Nonetheless, because the effective lifetime curves are flat close to the Standard Model point, as shown in Figure 3.3.2, $\Delta\Gamma_s$ could still be determined accurately in this case. Furthermore, the effective lifetime analysis is sensitive to different experimental systematics and the hadronic uncertainties involved can be theoretically controlled in an independent way. It therefore offers an important cross check to the conventional methods of extracting the B_s^0–$\overline{B}_s^0$ mixing parameters.

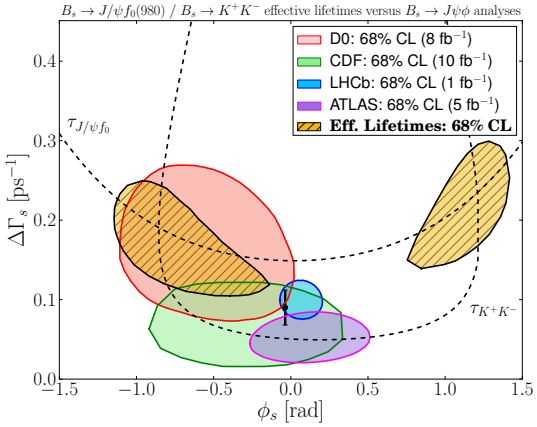

Figure 5.14: The fitted lifetime regions in the ϕ_s–$\Delta\Gamma_s$ plane from the left panel of Figure 5.12 added to a compilation of measurements as discussed in the text. The ATLAS, DØ, CDF and LHCb allowed regions refer to tagged analyses of $B_s^0 \to J/\psi\phi$.

5.4.2 Further promising B_s decays

So far we have discussed the effective lifetimes for the $B_s^0 \to K^+K^-$ and $B_s^0 \to J/\psi f_0$ channels, which have both been measured to an accuracy of 3% by the LHCb collaboration. Recently also the effective lifetime of the $B_s^0 \to J/\psi K_S$ mode has been measured to an accuracy of 8% [176]:

$$\tau_{J/\psi K_S} = 1.75 \pm 0.12 \pm 0.07 \text{ ps}. \tag{5.126}$$

This channel has a CP-odd final state and is caused by $\bar{b} \to \bar{c}c\bar{d}$ quark-level processes, i.e. it has a CKM structure that is different from the decays considered above [147, 100]. In particular, the relevant hadronic parameter does not enter in a doubly Cabibbo-suppressed way. However, the uncertainties can be controlled through $B_d^0 \to J/\psi\pi^0$ and are found to have a moderate impact on the effective $B_s^0 \to J/\psi K_S$ lifetime [177].

Another promising CP-even final state is $B_s^0 \to D_s^+ D_s^-$. Here the hadronic corrections are again doubly Cabibbo-suppressed and can be controlled with the help of the U-spin-related $B_d^0 \to D^+D^-$ decay [147]. A theoretical analysis of the effective lifetime of $B_s^0 \to D_s^+ D_s^-$ was performed in Ref. [178].

Decays of B_s mesons into CP-eigenstate final states with two vector mesons offer another laboratory for lifetime analyses. Such final states are mixtures of CP-even and CP-odd eigenstates and can be disentangled by means of angular analyses. It would be interesting to perform measurements of the lifetimes for the CP-even and CP-odd final-state configurations and to add them as contours to the ϕ_s–$\Delta\Gamma_s$ plane along the lines of the strategy proposed above. Examples of two such vector final states are $B_s^0 \to \phi\phi$ and $B_s^0 \to K^{*0}\bar{K}^{*0}$, which are both driven by penguin topologies. Another example is the decay mode $B_s \to J/\psi\phi$, which is already subject to a full tagged angular analysis. Also here it would be desirable to have measurements of the individual lifetimes for the CP-

even and CP-odd final-state angular configurations separately. This can, for instance, be achieved with the moment analysis proposed in Ref. [123]. The hadronic uncertainties of the $B_s^0 \to J/\psi\phi$ channel can be controlled by channels such as $B_s^0 \to J/\psi\bar{K}^{*0}$ and $B_d^0 \to J/\psi\rho^0$ [81].

Also decays with final states that are not CP-eigenstates can be added to the agenda to further constrain ϕ_s and $\Delta\Gamma_s$, provided both a B_s^0 and a $\bar{B}_s^0$ meson can decay into the same final state. Prime examples are the $B_s \to D_s^{\pm}K^{(*)\mp}$ channels that are studied in Section 4.3. The difference in orbital angular momentum L between the D_sK and $D_sK^{(*)}$ final states can discriminate their curves on the $(\phi_s+\gamma)$–$\Delta\Gamma_s$ plane in analogy to the CP eigenvalue η_f of a CP-eigenstate final state.

5.5 Conclusions

The conventional strategy for extracting the B_s^0–$\overline{B}_s^0$ mixing parameters involves a flavour-tagged time-dependent angular analysis of the decay mode $B_s \to J/\psi\phi$. An assumption that is usually implicit in this analysis is that the vector meson ϕ is purely an $s\bar{s}$ state. As such, penguin topologies, which introduce theoretical hadronic uncertainties into the extraction, are doubly Cabibbo suppressed as well as OZI suppressed. In this chapter we have explored the possibilities of performing the same extraction with other hadronic states in place of the ϕ that are also believed to have a sizable $s\bar{s}$ component. Namely, we considered the scalar meson $f_0(980)$ and the pseudoscalar mesons η and η'. Our motivation for studying these modes is to eventually be able to overconstrain the extraction of the B_s mixing parameters using many different analysis strategies.

The advantage of picking a non-vector meson for the $s\bar{s}$ bound state in the $B_s \to J/\psi s\bar{s}$ transition is that the angular analysis can be avoided. The challenging feature is that for both $f_0(980)$ and $\eta^{(\prime)}$ the exact composition in terms of $s\bar{s}$ has not been settled. Regarding the $f_0(980)$, even its classification as a conventional quark-antiquark meson, a tetraquark or some other exotic combination is not yet certain. This leads to an a priori unknown contribution from CP-violating topologies and consequently significant theoretical uncertainties.

To get a handle on these uncertainties we have proposed control channels for the decay modes in question based on $SU(3)_{\mathrm{F}}$ flavour symmetry. These control channels are the B_d counterparts to the same final state hadronic particles, although the charmless isospin singlet state is typically created from a $d\bar{d}$ rather than a $s\bar{s}$ combination. The prominence of these control channels is therefore dependent on the relative fraction of $d\bar{d}$ present; so far only $B_d \to J/\psi\eta$ has been observed. Their key feature is that the contributing CP violating topologies are not doubly Cabibbo suppressed and thereby the relative dynamics of these topologies can be probed. The flavour symmetry strategy is applicable if we may assume that exchange and penguin annihilation topologies are negligible. To this end, improved upper bounds on the branching ratios of $B_d^0 \to J/\psi\phi$ and $B_s^0 \to J/\psi\pi^0$, which are dominated by such topologies, would be very useful.

Concerning specifically the decay $B_s^0 \to J/\psi f_0$, the advantage of not having to perform an angular analysis is offset by having approximately a factor of four less events. Nonetheless, this decay mode is being taken seriously by the LHCb experiment, and early time-dependent untagged and tagged measurements have been performed. In this chapter we focused on the hadronic uncertainties present in these observables and gave their corresponding SM predictions. We found significant differences in the contributing CP violating topologies depending on whether the conventional quark-antiquark or tetraquark picture for the $f_0(980)$ is subscribed to. In the tetraquark picture we also pointed out the existence of an additional topology which is not obviously suppressed. We have predicted the branching ratio of the control channel $B_s \to J/\psi f_0$ to be of the order 10^{-6} in the tetraquark picture or in the quark-antiquark picture with a sizable $d\bar{d}$ component. LHCb has recently placed an upper bound in this ballpark, which promises interesting future developments.

The decay modes $B_s^0 \to J/\psi\eta^{(\prime)}$ are challenging to measure at hadron colliders because the $\eta^{(\prime)}$ mesons dominantly decay to photons and neutral pions. Currently only branching ratio measurements exist from the Belle collaboration. The hadronic uncertainties present in this decay are fueled by the experimentally still unsettled mixing angle between the two isospin singlet states η and η' and the relative contribution of a possible gluonic component. By making branching ratio *ratios* with the control channels $B_d \to J/\psi\eta^{(\prime)}$, it is possible to estimate these mixing angles. We found that if the ratios of these two pairs of modes are known to a moderate accuracy then the η–η' mixing angle can be determined with to a very good precision. Because the control channel $B_d^0 \to J/\psi\eta'$ has not yet been observed, an alternative ratio strategy using $B_d \to J/\psi\pi^0$ and flavour symmetry was considered and found to so far give consistent results. The study of the $B_{s,d}^0 \to J/\psi\eta^{(\prime)}$ modes will be particularly suited for the future e^+e^- Belle-II experiment.

In this chapter the effective lifetime observable of the $B_s \to J/\psi f_0$, which has a CP-odd final state, was analysed in detail. Specifically, its hadronic errors were estimated, which allowed us to plot the LHCb measurement of this observable as a contour on the plane of the B_s^0–$\overline{B}_s^0$ mixing parameters ϕ_s and $\Delta\Gamma_s$. In Chapter 4 a similar analysis was performed for the effective lifetime of the $B_s \to K^+K^-$, which has a CP-even final state. As discussed in Chapter 3, we have combined the contours for this pair of CP-even and CP-odd final states in order to pinpoint the location of the mixing parameters. The result is found to deviate by $1\,\sigma$ from the Standard Model. However, for a small mixing phase it is not competitive with the full tagged analysis of $B_s \to J/\psi\phi$, the results of which suggest that this is indeed the case. Nonetheless, it provides an interesting cross-check that is subject to different experimental systematics and has no tagging efficiency. It will be interesting to overconstrain the ϕ_s–$\Delta\Gamma_s$ plane with both tagged and untagged measurements in the future, in analogy to the determination of the apex of the unitarity triangle.

Chapter 6

Decay-time profile of a rare decay

6.1 Introduction

The decay $B_s \to \mu^+\mu^-$ is famous among its peers for being very suppressed in the SM, very sensitive to New Physics and theoretically relatively clean [179]. Indeed, it was long hoped that New Physics would induce a branching ratio orders of magnitude larger than its tiny SM prediction. To be precise, the latest Standard Model prediction for the branching ratio is [180]

$$\overline{\mathrm{BR}}(B_s \to \mu^+\mu^-)_{\mathrm{SM}} = (3.65 \pm 0.23) \times 10^{-9}, \tag{6.1}$$

which now includes NLO electroweak effects [181] and NNLO QCD matching corrections [182]. Thus, within the Standard Model, only about one in every 300 million B_s^0 mesons is predicted to decay to a pair of muons. In order to express this result as a time-integrated branching ratio (see Section 3.4) it was assumed that in the Standard Model only the heavy mass-eigenstate contributes to this decay, giving a maximal mass-eigenstate rate asymmetry [183]. Using the dictionary given in (3.106), the same result given in terms of the theoretically defined branching ratio is

$$\mathrm{BR}(B_s \to \mu^+\mu^-)_{\mathrm{SM}} = (3.38 \pm 0.22) \times 10^{-9}. \tag{6.2}$$

This prediction supersedes the prediction given in Ref. [184]. Comparing (6.2) with (6.1) we thus observe that the Standard Model prediction this branching ratio requires a maximal correction of $\sim 8\%$ due to the non-zero B_s decay width difference.

Over the last decade upper bounds for the $B_s \to \mu^+\mu^-$ branching ratio have continuously move down thanks to the CDF and DØ collaborations at the Tevatron and the ATLAS, CMS and LHCb experiments at the LHC (for a review, see Ref. [185]). Finally, in 2012, the LHCb collaboration reported the first evidence for the $B_s \to \mu^+\mu^-$ decay with a signal significance of 3.5σ above the background. In 2013 the LHCb and CMS experiments reported the following results with signal significances of 4σ and 4.3σ,

respectively:

$$\overline{\mathrm{BR}}(B_s \to \mu^+\mu^-)_{\rm exp} = \begin{cases} \left(2.9^{+1.1}_{-1.0}\right) \times 10^{-9} & \text{LHCb [186]} \\ \left(3.0^{+1.0}_{-0.9}\right) \times 10^{-9} & \text{CMS [187]} \end{cases} = (2.9 \pm 0.7) \times 10^{-9} \quad (6.3)$$

The last equality is the averaged combination given in Ref. [188]. The agreement with (6.1) is certainly remarkable. Nonetheless, the experimental errors still allow for sizable NP contributions, although this will now be a more challenging endeavour.

This chapter is based on the work presented in Refs [184, 183, 189]. In the presence of a non-zero decay width difference, the decay-time profile of the $B_s \to \mu^+\mu^-$ transition allows us to probe the mass-eigenstate rate asymmetry $\mathcal{A}^{\mu\mu}_{\Delta\Gamma}$. This asymmetry is sensitive to New Physics and gives complementary information to the branching ratio. If flavour-tagging is also included in a study of the decays time profile, a third observable $\mathcal{S}_{\mu\mu}$, which is sensitive to mixing-induced CP violation, also becomes accessible. Because measurements of these time-dependent observables must wait for the era of the LHCb upgrade, we can assume that ϕ_s will be known precisely once data for these observables become available. Our goal in this chapter is therefore to investigate as well as illustrate how combinations of the three observables

$$\overline{\mathrm{BR}}(B_s \to \mu^+\mu^-), \qquad \mathcal{A}^{\mu\mu}_{\Delta\Gamma}, \qquad \mathcal{S}_{\mu\mu}, \quad (6.4)$$

can shed light on the possible presence of New Physics in this decay.

This chapter is organized as follows. In Section 6.2 we define the observables in (6.4) and discuss their properties. In Section 6.3 we introduce various scenarios for New Physics, classifying them in terms of four general parameters which can in principle be calculated in any fundamental model and are directly related to the physics of $B_s \to \mu^+\mu^-$. In this context we classify a selection of popular NP models into the considered scenarios. In Section 6.4 we perform a numerical analysis for three classes of specific NP models, including current constraints from B_s mixing. In particular we demonstrate how the measurements of the observables in (6.4) can distinguish between these three classes. In Section 6.5 we conclude.

6.2 Observables of $B_s \to \mu^+\mu^-$

6.2.1 Decay amplitudes

The two muons arising from the decay of a spinless B_s^0 particle can be in two possible partial wave states. If the spins of the muons are anti-aligned along some quantization axis, so that the total spin $S = 0$, then they form a S-wave state. The S-wave configuration, with an orbital angular momentum of $L = 0$, is CP-odd. On the other hand if the spins are aligned so that $S = 1$, then $L = 1$, giving a CP-even P-wave state. In Figure 6.1 we have illustrated these two configurations. As we will soon show, in the language of a low-energy effective Hamiltonian a P-wave state requires the presence of

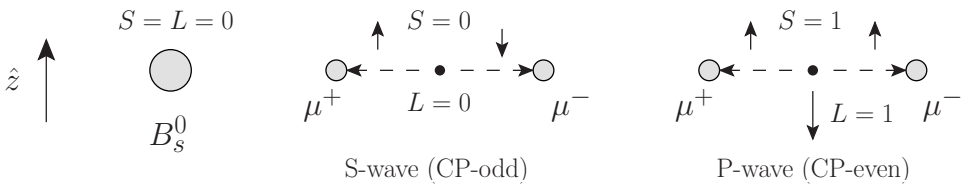

Figure 6.1: The two possible partial wave states for the pair of muons arising from a $B_s \to \mu^+\mu^-$ transition.

scalar operators. In the Standard Model such operators are strongly suppressed due to the weak coupling of the Higgs boson to muons. Also the CP-violating phase present in the S-wave decay cancels against the B_s^0-$\overline{B}_s^0$ mixing phase in the Standard Model. As a result only the heavy mass-eigenstate contributes to this decay. Detecting the light mass-eigenstate decaying to two muons could therefore indicate New Physics in the form of new scalar particles, new CP violation, or both.

Although the partial waves give an intuitive understanding of the final state, it will be more convenient to proceed in a helicity basis. Once we have established amplitudes in this basis we will return to their interpretation in terms of partial waves. In the discussion that follows we will for generality refer to muons with the generic lepton label ℓ. The helicity final states that give nonzero contributions are $|\ell_{\rm L}^+\ell_{\rm L}^-\rangle$ and $|\ell_{\rm R}^+\ell_{\rm R}^-\rangle$, which behave under a CP transformation as

$$\mathcal{CP}|\ell_{\rm R}^+\ell_{\rm R}^-\rangle = e^{i\xi_{\ell\ell}}|\ell_{\rm L}^+\ell_{\rm L}^-\rangle, \qquad \mathcal{CP}|\ell_{\rm L}^+\ell_{\rm L}^-\rangle = e^{-i\xi_{\ell\ell}}|\ell_{\rm R}^+\ell_{\rm R}^-\rangle, \tag{6.5}$$

with $\xi_{\ell\ell}$ an unphysical convention-dependent phase. The eigenstates of the CP operator are thus

$$|(\ell^+\ell^-)_\pm\rangle \equiv \frac{1}{\sqrt{2}}\left(|\ell_{\rm R}^+\ell_{\rm R}^-\rangle \pm e^{i\xi_{\ell\ell}}|\ell_{\rm L}^+\ell_{\rm L}^-\rangle\right), \tag{6.6}$$

corresponding to the CP-even (P-wave) and CP-odd (S-wave) states discussed earlier, respectively.

Let us now consider the decay amplitudes. In the Standard Model the contributing topologies are given in Figure 6.2. Beyond the Standard Model it's possible that new heavy gauge bosons or scalar particles with effective FCNC couplings also contribute to the decay, as shown in Figure 6.3. In order to discuss this decay in a model-independent way, we will make use of a low-energy effective Hamiltonian formalism, as introduced in Chapter 2. The Wilson coefficients and operators relevant for the decay in question are [190, 191]

$$\mathcal{H}_{\rm eff} = -\frac{G_F\,\alpha}{\sqrt{2}\pi}\left\{V_{ts}^*V_{tb}\sum_i^{10,S,P}\left(C_i\,\mathcal{O}_i + C_i'\,\mathcal{O}_i'\right) + \text{h.c}\right\}, \tag{6.7}$$

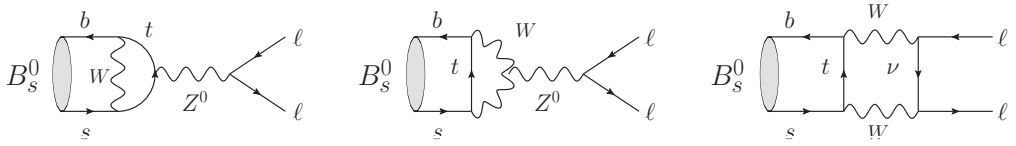

Figure 6.2: Feynman diagrams contributing to $B_s^0 \to \ell^+\ell^-$ in the Standard Model.

Figure 6.3: Examples of amplitudes that could contribute to $B_s^0 \to \ell^+\ell^-$ beyond the Standard Model. *Left panel:* a Z' gauge boson with effective tree-level FCNC coupling $\Delta^{bs}_{L,R}(Z')$ to quarks. *Right panel:* same as before but with the Z' replaced by a scalar or pseudoscalar boson H.

with the operators[1]

$$\begin{aligned} \mathcal{O}_{10} &= (\bar{s}\gamma_\mu P_L b)(\bar{\ell}\gamma^\mu\gamma_5\ell), & \mathcal{O}'_{10} &= (\bar{s}\gamma_\mu P_R b)(\bar{\ell}\gamma^\mu\gamma_5\ell), \\ \mathcal{O}_S &= m_b(\bar{s}P_R b)(\bar{\ell}\ell), & \mathcal{O}'_S &= m_b(\bar{s}P_L b)(\bar{\ell}\ell), \\ \mathcal{O}_P &= m_b(\bar{s}P_R b)(\bar{\ell}\gamma_5\ell), & \mathcal{O}'_P &= m_b(\bar{s}P_L b)(\bar{\ell}\gamma_5\ell). \end{aligned} \tag{6.8}$$

In the Standard Model C'_{10}, $C_S^{(\prime)}$ and $C_P^{(\prime)}$ are all negligibly small. The Wilson coefficient C_{10}, driven by the topologies in Figure 6.2, is given by [192]

$$C_{10}^{\rm SM} = -\eta_Y \sin^{-2}\theta_W\, Y_0(x_t) = -4.134, \tag{6.9}$$

where

$$Y_0(x_t) = \frac{x_t}{8}\left[\frac{x_t-4}{x_t-1} + \frac{3\,x_t}{(x_t-1)^2}\ln x_t\right] \tag{6.10}$$

describes the loop dynamics with $x_t = m_t^2/M_W^2$. The coefficient η_Y is a QCD factor that for $m_t = m_t(m_t)$ is close to unity: $\eta_Y = 1.012$ [193, 194]. Note that while C_{10} and C'_{10} are dimensionless, the coefficients $C_S^{(\prime)}$ and $C_P^{(\prime)}$ have dimension GeV^{-1}.

In principle, corrections to the above formalism can arise from loop topologies with internal charm and up quark exchanges. However, these are both doubly Cabibbo suppressed and suppressed by the $B_s \to \mu^+\mu^-$ dynamics. They can thereby be neglected.

[1]The operator $\mathcal{O}_{10}$ defined here is different to the four quark $\Delta B = 1$ operator of the same name given in Section 2.2.

Using the low-energy effective Hamiltonian given above, the $\overline{B}{}^0_s \to \ell^+_\lambda \ell^-_\lambda$ decay amplitude can be expressed as

$$\begin{aligned}\langle l^+_{\lambda_1} l^-_{\lambda_2}|\mathcal{H}_{\rm eff}|\overline{B}{}^0_q\rangle = -\frac{G_F\,\alpha}{2\sqrt{2}\pi}V^*_{ts}V_{tb}\Big\{ & \\ -(C_{10}-C'_{10})\,\bar u(p_2,\lambda_2)\,\gamma^\mu\gamma_5 v(p_1,\lambda_1)\langle 0|\bar s\,\gamma_\mu(1-\gamma_5)\,b|\overline{B}{}^0_s\rangle & \\ +(C_S-C'_S)\,\bar u(p_2,\lambda_2)\,v(p_1,\lambda_1)\langle 0|\bar s\,(1-\gamma_5)\,b|\overline{B}{}^0_s\rangle & \\ +(C_P-C'_P)\,\bar u(p_2,\lambda_2)\,\gamma_5\,v(p_1,\lambda_1)\langle 0|\bar s\,(1-\gamma_5)\,b|\overline{B}{}^0_s\rangle\Big\}, & \end{aligned} \tag{6.11}$$

where $\bar u(p_2,\lambda_2)$ and $v(p_1,\lambda_1)$ are the Dirac spinors for the outgoing leptons. We will denote the decay constant for the pseudoscalar meson $\overline{B}{}^0_s$, which is defined for a generic pseudoscalar in (2.42), as f_{B_s}. The conservation of parity symmetry in the strong force implies that the vector current $\langle 0|\bar s\gamma_\mu\, b|\overline{B}{}^0_s(p)\rangle$ vanishes. Contracting the above expressions with p^μ and applying the Dirac equation then gives

$$\langle 0|\bar s\gamma_5 b|\overline{B}{}^0_s(p)\rangle = -i\frac{M^2_{B_s}}{m_b+m_s}f_{B_s}, \qquad \langle 0|\bar s\,b|\overline{B}{}^0_s(p)\rangle = 0, \tag{6.12}$$

where $p_\mu = p_{b,\mu} + p_{s,\mu}$ and $p^2 = M^2_{B_s}$. The Dirac spinor products can be contracted for individual helicities to give

$$\bar u_{\left(\begin{smallmatrix}\rm R\\ \rm L\end{smallmatrix}\right)}\, v_{\left(\begin{smallmatrix}\rm R\\ \rm L\end{smallmatrix}\right)} = -M_{B_s}\sqrt{1-4\frac{m^2_\ell}{M^2_{B_s}}}, \qquad \bar u_{\left(\begin{smallmatrix}\rm R\\ \rm L\end{smallmatrix}\right)}\gamma_5\, v_{\left(\begin{smallmatrix}\rm R\\ \rm L\end{smallmatrix}\right)} = \pm M_{B_s}, \tag{6.13}$$

with the other combinations zero. Inserting the decay constants and spinor products into (6.11) then gives

$$\begin{aligned}\langle \ell^+_{\rm R}\ell^-_{\rm R}|\mathcal{H}_{\rm eff}|\overline{B}{}^0_s\rangle &= -\,i\frac{G_F\,\alpha\,f_{B_s}}{\sqrt{2}\pi}\,C^{\rm SM}_{10}\,M_{B_s}m_\ell\,V^*_{ts}V_{tb}\,\{-P+S\}\,,\\ \langle \ell^+_{\rm L}\ell^-_{\rm L}|\mathcal{H}_{\rm eff}|\overline{B}{}^0_s\rangle &= -\,i\frac{G_F\,\alpha\,f_{B_s}}{\sqrt{2}\pi}\,C^{\rm SM}_{10}\,M_{B_s}m_\ell\,V^*_{ts}V_{tb}\,e^{i\xi_{\ell\ell}}\,\{P+S\}\,,\end{aligned} \tag{6.14}$$

where

$$P \equiv \frac{C_{10}-C'_{10}}{C^{\rm SM}_{10}} + \frac{M^2_{B_s}}{2\,m_\ell}\left(\frac{m_b}{m_b+m_s}\right)\left(\frac{C_P-C'_P}{C^{\rm SM}_{10}}\right) \equiv |P|e^{i\varphi_P}, \tag{6.15}$$

$$S \equiv \sqrt{1-\frac{4\,m^2_\ell}{M^2_{B_s}}}\,\frac{m^2_{B_s}}{2\,m_\ell}\left(\frac{m_b}{m_b+m_s}\right)\left(\frac{C_S-C'_S}{C^{\rm SM}_{10}}\right) \equiv |S|e^{i\varphi_S}, \tag{6.16}$$

arise from the scalar and pseudoscalar lepton densities, respectively. We observe that the contributions to the amplitude from the operators $C^{(\prime)}_{10}$ are proportional to the lepton mass m_ℓ. The axial-vector coupling produces a lepton–anti-lepton pair with opposite

chirality. Because the leptons must have equal helicity to conserve angular momentum, one of the leptons has a helicity opposite to its chirality, which is only possible for a massive fermion. This dependence on a nonzero lepton mass is reflected by the factor m_ℓ/M_{B_s} relative to the scalar operators, which can couple to lepton pairs with the same chirality, is known as *helicity suppression*.

Similarly for $B_s^0 \to \ell_\lambda^+\ell_\lambda^-$ we find

$$\langle \ell_{\rm R}^+\ell_{\rm R}^-|\mathcal{H}_{\rm eff}|B_s^0\rangle = -\,i\frac{G_F\,\alpha\,f_{B_s}}{\sqrt{2}\pi}\,C_{10}^{\rm SM}\,M_{B_s}m_\ell\,V_{ts}V_{tb}^*\,e^{i(\xi_{B_s}-\xi_b+\xi_s)}\,\{P^*+S^*\}\,, \tag{6.17}$$

$$\langle \ell_{\rm L}^+\ell_{\rm L}^-|\mathcal{H}_{\rm eff}|B_s^0\rangle = -\,i\frac{G_F\,\alpha\,f_{B_s}}{\sqrt{2}\pi}\,C_{10}^{\rm SM}\,M_{B_s}m_\ell\,V_{ts}V_{tb}^*\,e^{i(\xi_{B_s}-\xi_b+\xi_s+\xi_{\ell\ell})}\,\{-P^*+S^*\}\,, \tag{6.18}$$

where the * denotes that the weak phases φ_P and φ_S have been conjugated. Long-distance contributions, via intermediate off-shell photons in the case of $K_{\rm L}\to\mu^+\mu^-$ for example [195], are assumed to be completely negligible for these decays. Therefore we can neglect CP conserving strong phases in these amplitudes.

The helicity amplitudes can be expressed in terms of partial waves amplitudes, $\langle(\ell^+\ell^-)_{L,S}\,|\mathcal{H}_{\rm eff}|\overset{(-)}{B}{}_s^0\rangle$, using the dictionary

$$\langle \ell_\lambda^+\ell_\lambda^-|\mathcal{H}_{\rm eff}|\overset{(-)}{B}{}_s^0\rangle = \sum_{L,S}\sqrt{2\,L+1}\,C_{\frac12\,\frac12}(S\,0;\lambda\,(-\lambda))\,C_{L\,S}(0\,0;0\,0)\,\langle\big(\ell^+\ell^-\big)_{L,S}\,|\mathcal{H}_{\rm eff}|\overset{(-)}{B}{}_s^0\rangle, \tag{6.19}$$

where $C_{j_1\,j_2}(J\,M;\,m_1\,m_2)$ are Clebsch-Gordon coefficients and $\lambda\in\{\mathrm{R}:1/2;\,\mathrm{L}:-1/2\}$. As shown in Figure 6.1, the relevant partial wave amplitudes are $L=0$, $S=0$ and $L=1$, $S=1$, which correspond to the CP-odd S-wave and CP-even P-wave discussed earlier, respectively. We indeed find that

$$\begin{aligned}
\langle\big(\ell^+\ell^-\big)_{0,0}\,|\mathcal{H}_{\rm eff}|\overset{(-)}{B}{}_s^0\rangle &= \frac{1}{\sqrt{2}}\Big[\langle\ell_{\rm R}^+\ell_{\rm R}^-|\mathcal{H}_{\rm eff}|\overset{(-)}{B}{}_s^0\rangle - \langle\ell_{\rm L}^+\ell_{\rm L}^-|\mathcal{H}_{\rm eff}|\overset{(-)}{B}{}_s^0\rangle\Big] = \langle(\ell^+\ell^-)_-|\mathcal{H}_{\rm eff}|\overset{(-)}{B}{}_s^0\rangle,\\
\langle\big(\ell^+\ell^-\big)_{1,1}\,|\mathcal{H}_{\rm eff}|\overset{(-)}{B}{}_s^0\rangle &= -\frac{1}{\sqrt{2}}\Big[\langle\ell_{\rm R}^+\ell_{\rm R}^-|\mathcal{H}_{\rm eff}|\overset{(-)}{B}{}_s^0\rangle + \langle\ell_{\rm L}^+\ell_{\rm L}^-|\mathcal{H}_{\rm eff}|\overset{(-)}{B}{}_s^0\rangle\Big] = -\langle(\ell^+\ell^-)_+|\mathcal{H}_{\rm eff}|\overset{(-)}{B}{}_s^0\rangle.
\end{aligned} \tag{6.20}$$

We are now in a position to consider the decays of the mass-eigenstates in terms of the partial waves. These are

$$\begin{aligned}
\langle(\ell^+\ell^-)_-|\mathcal{H}_{\rm eff}|B_{s,\rm H}\rangle &= 2\,N\,|P|\cos\left(\varphi_P-\phi_s^{\rm NP}/2\right),\\
\langle(\ell^+\ell^-)_-|\mathcal{H}_{\rm eff}|B_{s,\rm L}\rangle &= -2\,i\,N\,|P|\sin\left(\varphi_P-\phi_s^{\rm NP}/2\right),\\
\langle(\ell^+\ell^-)_+|\mathcal{H}_{\rm eff}|B_{s,\rm H}\rangle &= -2\,i\,N\,|S|\sin\left(\varphi_S-\phi_s^{\rm NP}/2\right),\\
\langle(\ell^+\ell^-)_+|\mathcal{H}_{\rm eff}|B_{s,\rm L}\rangle &= 2\,N\,|S|\cos\left(\varphi_S-\phi_s^{\rm NP}/2\right),
\end{aligned} \tag{6.21}$$

where

$$N \equiv -i\frac{G_F\,\alpha\,f_{B_s}}{\sqrt{2}\pi}\,C_{10}^{\rm SM}\,M_{B_s}m_\ell\,V_{ts}V_{tb}^*\,e^{i(\xi_{B_s}-\xi_b+\xi_s)}\,e^{-i\phi_s^{\rm NP}/2} \tag{6.22}$$

The phase $\phi_s^{\rm NP}$ represents the CP-violating New Physics contributions to B_s^0–$\bar{B}_s^0$ mixing, as defined in (3.46). In the Standard Model only C_{10} is non-negligible, thus from (6.16) we see that $P^{\rm SM} = 1$ and $S^{\rm SM} = 0$. It follows that in the Standard Model only the heavy mass-eigenstate can decay to two muons. A contribution from the lighter mass-eigenstate would require New Physics in the form of either new CP-violating phases (φ_P, φ_S or $\phi_s^{\rm NP}$ nonzero) or scalar operators $\mathcal{O}_{\rm S}^{(\prime)}$. Therefore the mass-eigenstate rate asymmetry, defined in (3.70), which can be probed with an untagged measurement, is an ideal observable for this decay.

In principle it is experimentally possible to measure the helicities of the outgoing lepton pair. However, if no attempt is made to disentangle them, then we measure their sum:

$$|\langle \ell^+\ell^-|\mathcal{H}_{\rm eff}|B_{s,\left({\rm H \atop L}\right)}\rangle|^2 \equiv \sum_{\lambda\in\{L,R\}} |\langle \ell^+_\lambda \ell^-_\lambda|\mathcal{H}_{\rm eff}|B_{s,\left({\rm H \atop L}\right)}\rangle|^2 = \sum_{L,S} |\langle \left(\ell^+\ell^-\right)_{L,S}|\mathcal{H}_{\rm eff}|B_{s,\left({\rm H \atop L}\right)}\rangle|^2. \tag{6.23}$$

The squared amplitudes for the B_s mass eigenstates to a specific helicity final state are independent of helicity:

$$\begin{aligned}
|\langle \ell^+_\lambda \ell^-_\lambda|\mathcal{H}_{\rm eff}|B_{s,\rm H}\rangle|^2 &= 2|N|^2\left\{|P|^2\cos^2\left(\varphi_P - \phi_s^{\rm NP}/2\right) + |S|^2\sin^2\left(\varphi_S - \phi_s^{\rm NP}/2\right)\right\},\\
|\langle \ell^+_\lambda \ell^-_\lambda|\mathcal{H}_{\rm eff}|B_{s,\rm L}\rangle|^2 &= 2|N|^2\left\{|P|^2\sin^2\left(\varphi_P - \phi_s^{\rm NP}/2\right) + |S|^2\cos^2\left(\varphi_S - \phi_s^{\rm NP}/2\right)\right\},
\end{aligned} \tag{6.24}$$

Thus for the mass-eigenstate rate asymmetry we find [183]

$$\begin{aligned}
\mathcal{A}^{\ell\ell}_{\Delta\Gamma} &\equiv \frac{\Gamma(B_{s,\rm H}\to\ell^+\ell^-) - \Gamma(B_{s,\rm L}\to\ell^+\ell^-)}{\Gamma(B_{s,\rm H}\to\ell^+\ell^-) + \Gamma(B_{s,\rm L}\to\ell^+\ell^-)}\\
&= \frac{|P|^2\cos(2\varphi_P - \phi_s^{\rm NP}) - |S|^2\cos(2\varphi_S - \phi_s^{\rm NP})}{|P|^2 + |S|^2}.
\end{aligned} \tag{6.25}$$

If the lepton helicities are separably measurable, then a mass-eigenstate rate asymmetry $\mathcal{A}^{\ell\ell,\lambda}_{\Delta\Gamma}$ can be measured for each helicity. However, because the mass eigenstate decay rates are not dependent on helicity, the seperable rate asymmetries are equal: $\mathcal{A}^{\ell\ell,\lambda}_{\Delta\Gamma} = \mathcal{A}^{\ell\ell}_{\Delta\Gamma}$. Because in the SM $P = 1$ and $S = 0$, as we discussed earlier, we have that

$$\mathcal{A}^{\ell\ell}_{\Delta\Gamma}\big|_{\rm SM} = 1, \tag{6.26}$$

a maximal asymmetry that reflects the complete dominance of the heavy mass-eigenstate.

For untagged measurements of $B_s \to \ell^+\ell^-$, the ability to distinguish between the helicity final states would be interesting if there were CP conserving strong phases present in the amplitude. In that case we should redefine the parameters P and S as $P = |P|e^{i(\varphi_P+\delta_P)}$ and $S = |S|e^{i(\varphi_S+\delta_S)}$ for strong phases δ_P and δ_S. Then the *longitudinal polarization* asymmetry is given by

$$\begin{aligned}
\mathcal{A}^{\ell\ell}_{\rm hel} &\equiv \frac{\left[\Gamma(B_{s,\rm H}\to\ell^+_{\rm L}\ell^-_{\rm L}) + \Gamma(B_{s,\rm L}\to\ell^+_{\rm L}\ell^-_{\rm L})\right] - \left[\Gamma(B_{s,\rm H}\to\ell^+_{\rm R}\ell^-_{\rm R}) + \Gamma(B_{s,\rm L}\to\ell^+_{\rm R}\ell^-_{\rm R})\right]}{\left[\Gamma(B_{s,\rm H}\to\ell^+_{\rm L}\ell^-_{\rm L}) + \Gamma(B_{s,\rm L}\to\ell^+_{\rm L}\ell^-_{\rm L})\right] + \left[\Gamma(B_{s,\rm H}\to\ell^+_{\rm R}\ell^-_{\rm R}) + \Gamma(B_{s,\rm L}\to\ell^+_{\rm R}\ell^-_{\rm R})\right]}\\
&= \frac{2|P||S|\sin(\varphi_P + \varphi_S - \phi_s^{\rm NP})\sin(\delta_P - \delta_S)}{|P|^2 + |S|^2},
\end{aligned} \tag{6.27}$$

which can only be non-vanishing if there is a strong phase difference. However, as already mentioned earlier, strong phases are assumed to be negligible for these processes, let alone a strong phase difference. Because this asymmetry is also experimentally challenging to measure, we will not consider it further.

6.2.2 Time-dependent rates

We now specialize to the case of two final state muons. The time-dependent rate for a B_s^0 meson decaying to two muons with a specific helicity $\lambda = L, R$ is given by

$$\begin{aligned}\Gamma(B_s^0(t) \to \mu_\lambda^+ \mu_\lambda^-) =& \frac{G_F^4\, M_W^4 \sin^4\theta_W}{16\pi^5} \left|C_{10}^{\rm SM} V_{ts} V_{tb}^*\right|^2 f_{B_s}^2 m_{B_s} m_\mu^2 \sqrt{1-\frac{4m_\mu^2}{m_{B_s}^2}} \times \left(|P|^2+|S|^2\right) \\ & \times \Bigg\{ \mathcal{C}_{\mu\mu}^\lambda \cos(\Delta M_s\, t) + \mathcal{S}_{\mu\mu} \sin(\Delta M_s\, t) \\ & \quad + \cosh\left(\frac{y_s\, t}{\tau_{B_s}}\right) + \mathcal{A}_{\Delta\Gamma}^{\mu\mu} \sinh\left(\frac{y_s\, t}{\tau_{B_s}}\right) \Bigg\} \times\, e^{-t/\tau_{B_s}}, \end{aligned} \tag{6.28}$$

where $\tau_{B_s} \equiv 2/(\Gamma_{\rm H} + \Gamma_{\rm L})$ is the B_s mean lifetime and y_s is defined in (3.19). The time-dependent rate for a $\bar{B}_s^0$ meson is obtained from the above expression by replacing $\mathcal{C}_{\mu\mu}^\lambda \to -\mathcal{C}_{\mu\mu}^\lambda$ and $\mathcal{S}_{\mu\mu} \to -\mathcal{S}_{\mu\mu}$. The time-dependent observables for both rates can be expressed in terms of the parameters defined in (6.16) as [183, 196]

$$\mathcal{C}_{\mu\mu}^\lambda = -\eta_\lambda \left[\frac{2|PS|\cos(\varphi_P - \varphi_S)}{|P|^2+|S|^2}\right], \tag{6.29}$$

$$\mathcal{S}_{\mu\mu} = \frac{|P|^2 \sin(2\varphi_P - \phi_s^{\rm NP}) - |S|^2 \sin(2\varphi_S - \phi_s^{\rm NP})}{|P|^2+|S|^2}, \tag{6.30}$$

and $\mathcal{A}_{\Delta\Gamma}^{\mu\mu}$ as given in (6.25). Only the observable $\mathcal{C}_{\mu\mu}^\lambda$ is dependent on the helicity of the final state i.e. it depends on the parameter $\eta_\lambda \equiv \{+1\colon L; -1\colon R\}$. We see explicitly that the presence of the observable $\mathcal{A}_{\Delta\Gamma}^{\mu\mu}$ is a consequence of the sizable B_s decay width difference $\Delta\Gamma_s$.

As we already noted earlier, in practice the sum of the muon helicities λ is measured:

$$\begin{aligned}\Gamma(B_s^0(t) \to \mu^+\mu^-) &\equiv \sum_{\lambda=L,R} \Gamma(B_s^0(t) \to \mu_\lambda^+ \mu_\lambda^-), \\ \Gamma(\bar{B}_s^0(t) \to \mu^+\mu^-) &\equiv \sum_{\lambda=L,R} \Gamma(\bar{B}_s^0(t) \to \mu_\lambda^+ \mu_\lambda^-). \end{aligned} \tag{6.31}$$

We observe from equations (6.28) and (6.29) that $\mathcal{C}_{\mu\mu}^\lambda$, which was dependent on the muon helicity, cancels in both sums [183].

The $B_s \to \mu^+\mu^-$ helicity-summed time-dependent untagged rate is then given by

$$\begin{aligned}\langle\Gamma(B_s(t) \to \mu^+\mu^-)\rangle &\equiv \Gamma(B_s^0(t) \to \mu^+\mu^-) + \Gamma(\bar{B}_s^0(t) \to \mu^+\mu^-) \\ &= \frac{G_F^4\, M_W^4 \sin^4\theta_W}{4\pi^5} \left|C_{10}^{\rm SM} V_{ts} V_{tb}^*\right|^2 f_{B_s}^2 m_{B_s} m_\mu^2 \sqrt{1 - \frac{4m_\mu^2}{m_{B_s}^2}} \\ &\quad \times \left(|P|^2 + |S|^2\right) \\ &\quad \times e^{-t/\tau_{B_s}} \left[\cosh\left(y_s\, t/\tau_{B_s}\right) + \mathcal{A}_{\Delta\Gamma}^{\mu\mu} \sinh\left(y_s\, t/\tau_{B_s}\right)\right]. \end{aligned} \tag{6.32}$$

Similarly, the helicity-summed time-dependent tagged rate asymmetry is

$$\frac{\Gamma(B_s^0(t) \to \mu^+\mu^-) - \Gamma(\bar{B}_s^0(t) \to \mu^+\mu^-)}{\Gamma(B_s^0(t) \to \mu^+\mu^-) + \Gamma(\bar{B}_s^0(t) \to \mu^+\mu^-)} = \frac{\mathcal{S}_{\mu\mu} \sin(\Delta M_s t)}{\cosh(y_s t/\tau_{B_s}) + \mathcal{A}_{\Delta\Gamma}^{\mu\mu} \sinh(y_s t/\tau_{B_s})}. \tag{6.33}$$

It is important to clarify that although there is no explicit term for direct CP violation in the rate asymmetry, this does not mean that the absolute values squared of $\mathcal{S}_{\mu\mu}$ and $\mathcal{A}_{\Delta\Gamma}^{\mu\mu}$ necessarily sum to one, as could be inferred from the relation given in (3.74). These two observables also have an implicit dependence on $\mathcal{C}_{\mu\mu}^{\lambda}$, the rate asymmetry for B_s^0 and $\bar{B}_s^0$ decays to the specific helicity muon final states. This gives the relation

$$|\mathcal{S}_{\mu\mu}|^2 + |\mathcal{A}_{\Delta\Gamma}^{\mu\mu}|^2 = 1 - |\mathcal{C}_{\mu\mu}^{\lambda}|^2 = 1 - \left[\frac{2|PS|\cos(\varphi_P - \varphi_S)}{|P|^2 + |S|^2}\right]^2. \tag{6.34}$$

Thus if there are no new CP-violating phases in the mixing or decay amplitudes, $\varphi_P = \varphi_S = \phi_s^{\rm NP} = 0$ such that $\mathcal{S}_{\mu\mu} = 0$, $\mathcal{A}_{\Delta\Gamma}^{\mu\mu}$ does not have to take its SM value of 1. The presence of a non-negligible scalar operator $\mathcal{O}_S^{(\prime)}$, so that $|S| \neq 0$, is sufficient to ensure that $\mathcal{A}_{\Delta\Gamma}^{\mu\mu} \neq 1$, as can also be seen from (6.25).

In contrast to the branching ratio, the dependence on f_{B_s} cancels in both $\mathcal{A}_{\Delta\Gamma}^{\mu\mu}$ and $\mathcal{S}_{\mu\mu}$. Consequently, they are effectively theoretically clean. Moreover, these observables are also not affected by the ratio f_d/f_s of fragmentation functions, which are the major limitation of the precision of the $B_s \to \mu^+\mu^-$ branching ratio measurement at hadron colliders [197]. As $\mathcal{A}_{\Delta\Gamma}^{\mu\mu}$ does not rely on flavour tagging, which is especially challenging for a rare decay, it can be determined sooner. As discussed in Section 3.2, with enough statistics a full fit to the time-dependent untagged rate will give $\mathcal{A}_{\Delta\Gamma}^{\mu\mu}$. With limited statistics, an *effective lifetime* measurement may be easier, which corresponds to fitting a single exponential to this rate as defined in Section 3.3.

6.2.3 The branching ratio

As discussed in Section 3.4, a $B_s \to \mu^+\mu^-$ branching ratio measurement amounts to counting all events over all (accessible) time, and is thus defined as the time integral of the untagged rate given in (6.32):

$$\overline{\rm BR}(B_s \to \mu^+\mu^-) \equiv \frac{1}{2}\int_0^\infty \langle\Gamma(B_s(t) \to \mu^+\mu^-)\rangle\, dt. \tag{6.35}$$

Therefore the combined LHCb and CMS branching ratio results given in (6.3) are more precisely described as a measurement of the $B_s \to \mu^+\mu^-$ *time-integrated* decay rate. In contrast, the SM prediction for the $B_s \to \mu^+\mu^-$ branching ratio given in (6.2) is computed theoretically for one instant in time, namely at $t = 0$ i.e. it neglects the effects of B_s^0–$\bar{B}_s^0$ mixing. Specifically, in this case the branching ratio definition from (3.105) is used, giving

$$\begin{aligned}\mathrm{BR}(B_s \to \mu^+\mu^-)_{\mathrm{SM}} &= \frac{\tau_{B_s}}{2}\langle\Gamma(B_s(t) \to \mu^+\mu^-)\rangle\Big|_{t=0,\,P=1,\,S=0} \\ &= \frac{\tau_{B_s}\, G_F^4\, M_W^4 \sin^4\theta_W}{8\pi^5}\left|C_{10}^{\mathrm{SM}} V_{ts}V_{tb}^*\right|^2 f_{B_s}^2 m_{B_s} m_\mu^2 \sqrt{1-\frac{4m_\mu^2}{m_{B_s}^2}}, \quad (6.36)\end{aligned}$$

An updated numerical estimate of this quantity is given in (6.2).

As also discussed in Section 3.4, the differing branching ratio definitions in (6.35) and (6.36) are related by the dictionary given in (3.106), which depends on the mass-eigenstate rate asymmetry, defined in (6.25) for this decay, and the B_s decay width difference y_s. In the Standard Model this asymmetry takes a maximal value of $+1$ (see (6.26) and the surrounding discussion), which results in a maximal discrepancy between the two definitions of $\sim 8\%$ [183]. The $B_s \to \mu^+\mu^-$ decay is therefore a prime example of a decay for which it is important to include this correction.

Beyond the Standard Model, where the parameters P and S can take arbitrary values, it is straightforward to derive the expression

$$\frac{\mathrm{BR}(B_s \to \mu^+\mu^-)}{\mathrm{BR}(B_s \to \mu^+\mu^-)_{\mathrm{SM}}} = |P|^2 + |S|^2. \quad (6.37)$$

However, because it is not the theoretical but the experimental branching ratio that is measured, the following ratio serves as a more useful observable [183]:

$$\begin{aligned}\overline{R} &\equiv \frac{\overline{\mathrm{BR}}(B_s \to \mu^+\mu^-)}{\overline{\mathrm{BR}}(B_s \to \mu^+\mu^-)_{\mathrm{SM}}} = \left[\frac{1+\mathcal{A}_{\Delta\Gamma}^{\mu\mu}\, y_s}{1+y_s}\right] \times (|P|^2 + |S|^2) \\ &= \left[\frac{1+y_s\cos(2\varphi_P - \phi_s^{\mathrm{NP}})}{1+y_s}\right]|P|^2 + \left[\frac{1-y_s\cos(2\varphi_S - \phi_s^{\mathrm{NP}})}{1+y_s}\right]|S|^2, \quad (6.38)\end{aligned}$$

where the sizable decay width difference y_s enters. The parameter $\overline{R}$ is related to R defined in Ref. [183] by $\overline{R} = (1-y_s)R$. Combining the theoretical SM prediction in (6.1) with the experimental result in (6.3) gives

$$\overline{R} = 0.79 \pm 0.20 \quad (6.39)$$

This range should be compared with the SM value $\overline{R}_{\mathrm{SM}} = 1$.

6.3 Constrained scenarios and their phenomenology

6.3.1 Preliminaries

As discussed in the introduction to this chapter, experiments have begun honing in on the $B_s \to \mu^+\mu^-$ time-integrated rate, or branching ratio, for which the observable $\overline{R}$ parameterises possible NP contributions. Next in line will be a time-dependent analysis, first without tagging, giving $\mathcal{A}_{\Delta\Gamma}^{\mu\mu}$, and then with tagging, giving $\mathcal{S}_{\mu\mu}$. The end result will be three experimental observables, which, if there are scalar operators contributing to the decay mode, can each contain independent information (see the discussion around (6.34)).

With the phase $\phi_s^{\rm NP}$ already significantly constrained by the current data, see (3.48), these three observables will essentially depend on four unknowns:

$$|P|, \qquad \varphi_P, \qquad |S|, \qquad \varphi_S. \tag{6.40}$$

Therefore we cannot in general solve for all of these model-independent NP parameters by considering the decay $B_s \to \mu^+\mu^-$ alone. One solution is to invoke other $b \to s\mu^+\mu^-$ transitions like the decays $B \to K\mu^+\mu^-$ and $B \to K^*\mu^+\mu^-$. In particular, as emphasized in Ref. [198], observables in $B \to K\mu^+\mu^-$ are sensitive to $C_{S,P} + C'_{S,P}$, rather than differences of these coefficients, thereby allowing additional complementary tests and in principle the determination of all Wilson coefficients. However, present form factor uncertainties in these decays do not yet provide significant new constraints on scalar operators relative to the ones obtained from $B_s \to \mu^+\mu^-$.

We will consider various scenarios for S and P that will allow us to reduce the number of free NP parameters and eventually, with the help of future data, uniquely determine them. Our scenarios are motivated by generic features of NP models and, as we will show, result in a distinct phenomenology for the observables $\overline{R}$, $\mathcal{A}_{\Delta\Gamma}^{\mu\mu}$ and $\mathcal{S}_{\mu\mu}$. In the present section our analysis is dominantly phenomenological, although we do discuss the motivation behind each scenario and the characteristic features of its phenomenology. Moreover we indicate what kind of fundamental physics could be at the basis of each scenario considered and we survey specific models of NP and categorise them into the scenarios that we will list now.

The four scenarios to be considered are as follows:

A: $S = 0$

B: $P = 1$

C: $P \pm S = 1$

D: $\varphi_P, \varphi_S \in \{0, \pi\}$

The scenarios are intended to be limiting cases, i.e. although we are not aware of a model that exactly predicts $P \pm S = 1$, $P \pm S \approx 1$ is conceivable and the resulting phenomenology will be approximately the same.

6.3.2 Scenario A: $S = 0$

6.3.2.1 General formulation

This scenario is realised if $C_S - C'_S = 0$, leaving $C_{10}^{(\prime)}$ and $C_P^{(\prime)}$ free to take non-SM values as well as CP-violating phases. Thus models with only new gauge bosons or pseudoscalars naturally fall into this category and consequently, as we will see below, this scenario includes a number of popular BSM models. Also models with scalars can qualify, provided the scalars couple left-right symmetrically to quarks so that $C_S = C'_S$.

In this scenario the rate asymmetry between B_s^0 and $\bar{B}_s^0$ decays to the individual muon helicities vanishes: $\mathcal{C}_{\mu\mu}^{\lambda} = 0$. Therefore the two time-dependent observables do not carry independent information, being bound by the constraint

$$|\mathcal{S}_{\mu\mu}|^2 + |\mathcal{A}_{\Delta\Gamma}^{\mu\mu}|^2 = 1. \tag{6.41}$$

Specifically,

$$\mathcal{A}_{\Delta\Gamma}^{\mu\mu} = \cos(2\varphi_P - \phi_s^{\rm NP}), \quad \mathcal{S}_{\mu\mu} = \sin(2\varphi_P - \phi_s^{\rm NP}), \tag{6.42}$$

while the branching ratio observable is given by

$$\overline{R} = |P|^2 \left[\frac{1 + y_s \cos(2\varphi_P - \phi_s^{\rm NP})}{1 + y_s}\right]. \tag{6.43}$$

The three observables in (6.42) and (6.43) are given in terms of two unknowns: $|P|$ and φ_P. As we assume that $\phi_s^{\rm NP}$ will already be determined once time-dependent measurements for this decay are possible, $\mathcal{A}_{\Delta\Gamma}^{\mu\mu}$ and $\mathcal{S}_{\mu\mu}$ will allow an unambiguous extraction of the phase $2\varphi_P$. In turn, with the help of $\overline{R}$, also $|P|$ can be determined.

The P parameter can also conveniently be expressed as $P = 1 + \tilde{P}$ with

$$\tilde{P} = |\tilde{P}|e^{i\tilde{\varphi}_P} \equiv \frac{\delta C_{10} - C'_{10}}{C_{10}^{\rm SM}} + \frac{m_{B_s}^2}{2m_\mu}\left(\frac{m_b}{m_b + m_s}\right)\left(\frac{C_P - C'_P}{C_{10}^{\rm SM}}\right). \tag{6.44}$$

where

$$\delta C_{10} \equiv C_{10} - C_{10}^{\rm SM}. \tag{6.45}$$

In this notation all NP effects are contained in the parameter $\tilde{P}$. In the left panel of Figure 6.4 we show the correlations between $\overline{R}$ and $\mathcal{A}_{\Delta\Gamma}^{\mu\mu}$ in *Scenario A* using this notation. We have varied $\tilde{P} \in [0, 1]$, and most importantly show the dependence on the phase $\tilde{\varphi}_P$. As will be discussed in detail in Section 6.4, the requirement for new gauge bosons or pseudoscalars to satisfy our B_s mixing constraints implies that $\tilde{\varphi}_P \sim \pi/2$ or $\tilde{\varphi}_P \sim 0, \pi$, respectively.

Note that in the case of no new phases, $\varphi_P \in \{0, \pi\}$, and $\phi_s^{\rm NP} = 0$,

$$\mathcal{A}_{\Delta\Gamma}^{\mu\mu} = 1, \qquad \mathcal{S}_{\mu\mu} = 0, \qquad \overline{R} = |P|^2. \tag{6.46}$$

While the first two results coincide with the SM, NP effects can still arise in $\overline{R}$.

6.3.2.2 Examples of models

Essentially all models of New Physics in which no scalar particles contribute to the $B_s \to \mu^+\mu^-$ transition qualify for *Scenario A*. To give a general impression we will give some examples.

The simplest example is Constrained Minimal Flavour Violation (CMFV). In CMFV it is assumed that new low-energy effective operators beyond those present in the SM are very strongly suppressed and that flavour violation and CP violation are governed by the CKM matrix [199, 200]. Therefore only the Wilson coefficient C_{10} is non-zero, and it is restricted to be real. This gives *Scenario A* with the added restrictions that $\varphi_P = \phi_s^{\rm NP} = 0$. Consequently the expression in (6.46) applies and NP enters only through the ratio $\overline{R}$.

Beyond CMFV there is the class of NP models that have the same operator structure as the SM but allow for new CP-violating phases. In this case the general expressions in (6.42) and (6.43) apply. Examples of such models are the Littlest Higgs Model with T-Parity (LHT) and 331 models. In these models new physics effects to the branching ratio and CP observables are expected to be moderate at best [201, 202].

Finally there is the class of models that allow for a new operator structure beyond that of the SM i.e. beyond the operator C_{10}. A specific example is the Randall–Sundrum model with custodial protection, in which NP contributions to $B_s \to \mu^+\mu^-$ are governed by right-handed flavour-violating Z couplings to quarks [203]. In general Z' models with tree-level FCNC couplings can have new operators and CP-violating structure as analysed in Ref. [204]. We will discuss such a model further in Section 6.4. Also a model with NP dominated by the tree-level FCNC contributions of a pseudoscalar belongs to this class. It has been analysed recently in Ref. [189], and we will also present complementary implications of this model in Section 6.4.

6.3.3 Scenario B: $P = 1$

6.3.3.1 General formulation

The simplest realisation of this scenario is $C_{10} = C_{10}^{\rm SM}$ and $C'_{10} = C_P^{(\prime)} = 0$. However, pseudoscalars that couple left-right symmetrically to quarks, so that $C_P = C'_P$, or a conspiracy of the form $C_{10} - C'_{10} = C_{10}^{\rm SM}$ are also allowed. The point is that in this scenario only scalar operators $\mathcal{O}_S^{(\prime)}$ drive new physics effects in $B_s \to \mu^+\mu^-$. In this sense this case is complementary to *Scenario A*.

As there are scalar operators present, there is a rate asymmetry in the B_s^0 and $\bar{B}_s^0$ decays to the individual muon helicities. Therefore the two time-dependent observables

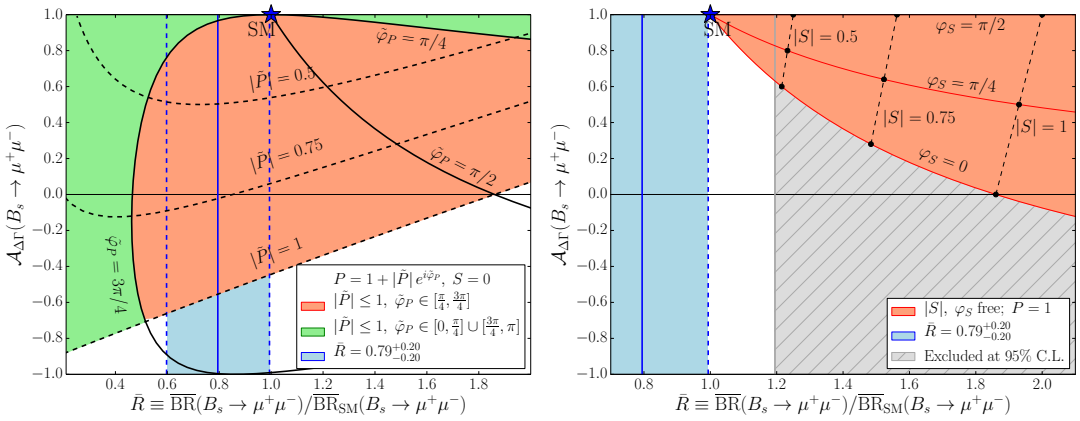

Figure 6.4: The correlation between the $\overline{R}$ and $\mathcal{A}^{\mu\mu}_{\Delta\Gamma}$ observables in *Scenario A* (left panel) and *Scenario B* (right panel). In *Scenario A* we have set $P = 1 + \tilde{P}$ and $S = 0$ with $\tilde{P}$ free to vary. In *Scenario B* $P = 1$ and S is free to vary.

do carry independent information. In this scenario the observables are given by

$$\begin{aligned}
\mathcal{A}^{\mu\mu}_{\Delta\Gamma} &= \frac{\cos\phi_s^{\rm NP} - |S|^2\cos(2\varphi_S - \phi_s^{\rm NP})}{1 + |S|^2}, \\
\mathcal{S}_{\mu\mu} &= \frac{-\sin\phi_s^{\rm NP} - |S|^2\sin(2\varphi_S - \phi_s^{\rm NP})}{1 + |S|^2}, \\
\overline{R} &= \frac{1 + y_s\cos\phi_s^{\rm NP}}{1 + y_s} + |S|^2\left[\frac{1 - y_s\cos(2\varphi_S - \phi_s^{\rm NP})}{1 + y_s}\right].
\end{aligned} \tag{6.47}$$

Again, with precise value of $\phi_s^{\rm NP}$ to be determined first, these three observables are in principle sufficient to determine the two NP unknowns, $2\varphi_S$ and $|S|$. Consequently the untagged observables $\overline{R}$ and $\mathcal{A}^{\mu\mu}_{\Delta\Gamma}$ are already sufficient to determine $2\varphi_S$ and $|S|$. Moreover, if all three observables are considered, correlations between them will result that depend on the precise value of $\phi_s^{\rm NP}$ [189].

In the right panel of Figure 6.4 we show the correlation between $\overline{R}$ and $\mathcal{A}^{\mu\mu}_{\Delta\Gamma}$ for different values of S [183]. An interesting feature is that for no CP-violating phase, $\varphi_S = \{0, \pi\}$, an increase of $|S|$ pushes $\mathcal{A}^{\mu\mu}_{\Delta\Gamma} \to 0$. But within current experimental bounds we have the prediction that $\mathcal{A}^{\mu\mu}_{\Delta\Gamma}$ cannot take a negative value. Moreover in this scenario $|S| \leq 0.5$ is favoured.

6.3.3.2 Examples of models

Models in which only a scalar particle can generate the necessary quark FCNC qualify for this scenario. An example of a model where such a scalar can arise is a two-Higgs doublet model (2HDM) in which the heavier scalar particle H^0 is considerably lighter than the pseudoscalar A^0. A pseudoscalar with a similar mass and FCNCs to quarks will

give *Scenario C*, as we will discuss in Section 6.3.4. Also models with NP dominated by the tree-level FCNC contributions of a scalar, as recently analysed in Ref. [189], belong to this class. We will discuss the specific of such models in more detail in Section 6.4.

6.3.4 Scenario C: $P \pm S = 1$

6.3.4.1 General formulation

The meaning of this scenario is clearer if we let $P = 1 + \tilde{P}$, with $\tilde{P}$ defined in (6.44). Then the condition $P \pm S = 1$ is equivalent to $\tilde{P} = \mp S$ i.e. in this scenario NP effects to S and P are on the same footing. If we neglect contributions to $C_{10}^{(\prime)}$ and m_μ with respect to m_{B_s}, this scenario is realised if $C_S^{(\prime)} = \pm C_P^{(\prime)}$.

Letting $\tilde{P} = -\kappa S$ for $\kappa = \pm 1$, the time-dependent observables are

$$\begin{aligned} \mathcal{A}_{\Delta\Gamma}^{\mu\mu} &= \frac{\cos\phi_s^{\rm NP} - 2\,\kappa|S|\cos(\varphi_S - \phi_s^{\rm NP})}{1 - 2\kappa|S|\cos\varphi_S + 2|S|^2}, \\ \mathcal{S}_{\mu\mu} &= \frac{-\sin\phi_s^{\rm NP} - 2\,\kappa|S|\sin(\varphi_S - \phi_s^{\rm NP})}{1 - 2\kappa|S|\cos\varphi_S + 2|S|^2}, \end{aligned} \tag{6.48}$$

which are in general independent. The branching ratio observable is

$$\overline{R} = \frac{1 - 2\kappa|S|\cos\varphi_S + 2|S|^2 + y_s[\cos\phi_s^{\rm NP} - 2\kappa|S|\cos(\varphi_S - \phi_s^{\rm NP})]}{1 + y_s}. \tag{6.49}$$

If $\phi_s^{\rm NP}$ is known, then $\overline{R}$ in combination with $\mathcal{A}_{\Delta\Gamma}^{\mu\mu}$ or $\mathcal{S}_{\mu\mu}$ is sufficient to determine the two NP unknowns φ_S and $|S|$ up to discrete ambiguities. An optimal determination would involve all three observables, which can resolve the discrete ambiguities.

The observable $\overline{R}$ is minimised by $S_{\rm crit} = \kappa(1 + y_s)/2$ and $\phi_s^{\rm NP} = 0$, giving the lower bound

$$\overline{R} \geq \frac{1 - y_s}{2}. \tag{6.50}$$

This lower bound, without the y_s and phase considerations, was first observed in Ref. [205]. A branching ratio measurement below this bound would thereby rule out this scenario.

If we assume the new physics phase $\phi_s^{\rm NP}$ in B_s mixing is known, then the purely untagged observables $\mathcal{A}_{\Delta\Gamma}^{\mu\mu}$ and $\overline{R}$ can solve for S and φ_S. Setting $\phi_s^{\rm NP} = 0$ for simplicity, we have the expressions

$$\begin{aligned} |S| = |P - 1| &= \sqrt{\frac{\overline{R}\,(1 + y_s)(1 - \mathcal{A}_{\Delta\Gamma}^{\mu\mu})}{2(1 + y_s\,\mathcal{A}_{\Delta\Gamma}^{\mu\mu})}}, \\ \cos\varphi_S = -\kappa\cos(\tilde{\varphi}_P) &= \sqrt{\frac{(1 + y_s\,\mathcal{A}_{\Delta\Gamma}^{\mu\mu})}{2\,\overline{R}\,(1 + y_s)(1 - \mathcal{A}_{\Delta\Gamma}^{\mu\mu})}}\left[1 - \frac{\overline{R}\,(1 + y_s)\mathcal{A}_{\Delta\Gamma}^{\mu\mu}}{1 + y_s\mathcal{A}_{\Delta\Gamma}^{\mu\mu}}\right]. \end{aligned} \tag{6.51}$$

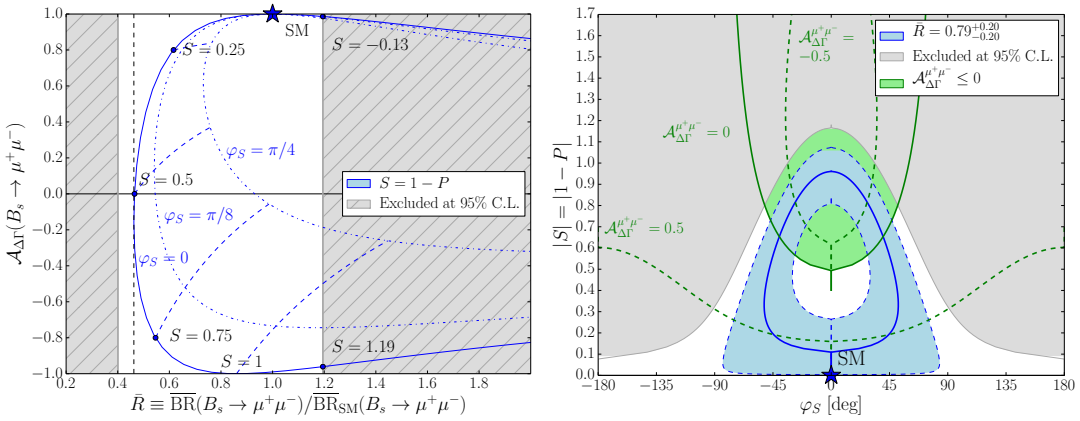

Figure 6.5: Scenario C: $P \pm S = 1$. *Left panel:* the correlation between the $\overline{R}$ and $\mathcal{A}^{\mu\mu}_{\Delta\Gamma}$ observables. *Right panel:* correlation between the $|S| = |P-1|$ and $\varphi_S = \tilde{\varphi_P} + (1+\kappa)\pi/2$ NP parameters (see text).

In the left panel of Figure 6.5 we show the correlation between $\overline{R}$ and $\mathcal{A}^{\mu\mu}_{\Delta\Gamma}$ in the limit $\phi_s^{\mathrm{NP}} = 0$. Observe the lower bound on $\overline{R}$ specified in (6.50). If, furthermore, $\tilde{\varphi_P} = \varphi_S = \{0, \pi\}$ we observe that $\mathcal{A}^{\mu\mu}_{\Delta\Gamma}$ can help to resolve the two possible solutions for S coming from a branching ratio measurement $\overline{R}$.

In the right panel of Figure 6.5 we show the correlation between φ_S and $|S|$. Observe that the current measurement of $\overline{R}$ still allows a large range for both NP parameters. If $\mathcal{A}^{\mu\mu}_{\Delta\Gamma}$ were measured with a negative sign it would indicate large contributions from NP. Moreover in this case the $\mathcal{A}^{\mu\mu}_{\Delta\Gamma}$ sharply cuts the $\overline{R}$ contour, so that a measurement of $\mathcal{A}^{\mu\mu}_{\Delta\Gamma}$ would distinguish between the magnitude and the phase of S up to the twofold ambiguity in φ_S.

6.3.4.2 Examples of models

A 2HDM in the decoupling regime, such that $M_{H^0} \simeq M_{A^0} \simeq M_{H^\pm} \gg M_h$ (see Appendix A), has the generic feature that

$$C_S = -C_P, \quad C'_S = C'_P. \tag{6.52}$$

If the couplings of the heavy Higgs bosons are not left-right symmetric, so that either $C_{S,P}$ or $C'_{S,P}$ are dominant[2], this corresponds to *Scenario C*. Thus the branching ratio has a lower bound and a significant scalar NP contribution is indicated by negative values of $\mathcal{A}^{\mu\mu}_{\Delta\Gamma}$. A precise measurement of the untagged observable $\mathcal{A}^{\mu\mu}_{\Delta\Gamma}$ can distinguish the phase and magnitude of the NP Wilson coefficients. We will analyse a similar scenario in more detail in Section 6.4.

[2]In MFV this is the case. Namely $C'_{S,P}/C_{S,P} \sim m_s/m_b$.

The above is true also for the MSSM, provided that NP contributions to vector-axial operators, C'_{10}, are negligible. The MSSM has the added advantage that large $\tan\beta$ effects, which are one way to realise the decoupling regime, can give a significant boost to the scalar operators [206, 207, 208].

If the 2HDM is not in a decoupling regime, then either the physical scalar H^0 or pseudoscalar A^0 may be considerably lighter than the other. If this solo particle can generate the required FCNC, then we are in *Scenario B* or *Scenario A* respectively.

6.3.5 Scenario D: $\varphi_P, \varphi_S \in \{0, \pi\}$

6.3.5.1 General formulation

In this scenario we assume no CP-violating phases in the $B_s \to \mu^+\mu^-$ decay mode: $\varphi_P, \varphi_S \in \{0, \pi\}$ [183]. This is equivalent to all of the Wilson coefficients taking real values. Clearly this constraint can also be applied to the other scenarios discussed in this section, but this scenario is distinct in that S and P are allowed to remain arbitrary *real* values. Yet, in the presence of a non-vanishing NP phase $\phi_s^{\rm NP}$, the CP-asymmetry $\mathcal{S}_{\mu\mu}$ could be non-vanishing.

The resulting time dependent observables in this scenario are

$$\mathcal{A}_{\Delta\Gamma}^{\mu\mu} = \cos\phi_s^{\rm NP}\left[\frac{|P|^2-|S|^2}{|P|^2+|S|^2}\right], \quad \mathcal{S}_{\mu\mu} = -\sin\phi_s^{\rm NP}\left[\frac{|P|^2-|S|^2}{|P|^2+|S|^2}\right], \tag{6.53}$$

and the branching ratio observable is given by

$$\overline{R} = |P|^2\left[\frac{1+y_s\cos\phi_s^{\rm NP}}{1+y_s}\right] + |S|^2\left[\frac{1-y_s\cos\phi_s^{\rm NP}}{1+y_s}\right]. \tag{6.54}$$

Importantly, whereas the branching ratio observable $\overline{R}$ gives their squared sum, the $\mathcal{A}_{\Delta\Gamma}^{\mu\mu}$ is sensitive to the difference. With known $\phi_s^{\rm NP}$ these three observables are sufficient to determine the two NP unknowns $|P|$ and $|S|$. As $\sin\phi_s^{\rm NP}$ is already known to be small, $\mathcal{S}_{\mu\mu}$ is also small in this scenario. Consequently $\mathcal{A}_{\Delta\Gamma}^{\mu\mu}$ and $\overline{R}$ will be the relevant observables in this determination. With $\cos\phi_s^{\rm NP}$ very close to unity one then finds

$$|P|^2 = (1+y_s)\frac{\overline{R}}{2}\left[\frac{1+\mathcal{A}_{\Delta\Gamma}^{\mu\mu}}{1+y_s\mathcal{A}_{\Delta\Gamma}^{\mu\mu}}\right], \qquad |S|^2 = (1+y_s)\frac{\overline{R}}{2}\left[\frac{1-\mathcal{A}_{\Delta\Gamma}^{\mu\mu}}{1+y_s\mathcal{A}_{\Delta\Gamma}^{\mu\mu}}\right]. \tag{6.55}$$

Finally a measurement of $\mathcal{S}_{\mu\mu}$ incompatible with the known value of $\phi_s^{\rm NP}$ would exclude this scenario and indicate new CP-violating phases in the decay.

In Figure 6.6 we illustrate how measurements of $\overline{R}$ and $\mathcal{A}_{\Delta\Gamma}^{\mu\mu}$ can be used to pinpoint the parameters $|S|$ and $|P|$ (we have taken $\phi_s^{\rm NP} = 0$).

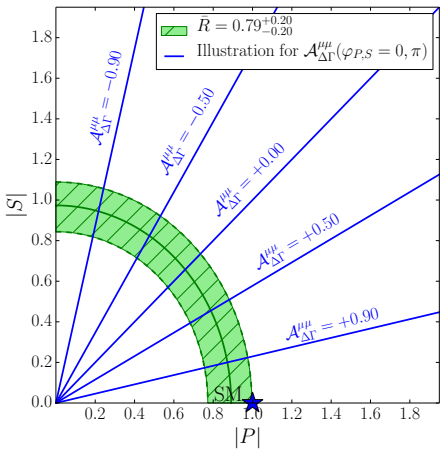

Figure 6.6: Scenario D: $\varphi_P, \varphi_S \in \{0, \pi\}$. The correlation between the $|P|$ and $|S|$ parameters for varying values of $\mathcal{A}^{\mu\mu}_{\Delta\Gamma}$. Also shown is the current measurement of $\overline{R}$.

6.3.5.2 Example of models

Models with Minimal Flavour Violation (MFV), but without flavour blind phases, as formulated as an effective field theory in Ref. [209], belong naturally to this class. MFV protects against any additional flavour structure or CP violation beyond what is already present in the CKM matrix, while still allowing for additional, higher-dimensional, operators [209]. MFV therefore falls into *Scenario D*, with the added restriction that also $\phi_s^{\rm NP}$ is zero. Thus in models with MFV, as seen in (6.55), the time-dependent untagged observable $\mathcal{A}^{\mu\mu}_{\Delta\Gamma}$ together with the branching ratio observable $\overline{R}$ are sufficient to disentangle the scalar contribution S from P. A measurement of $\mathcal{S}_{\mu\mu} \neq 0$ would falsify MFV. Typical examples in this class are MSSM with MFV and 2HDM with MFV.

An exception are models with MFV and flavour-blind phases, like the 2HDM with such phases, also known as 2HDM$_{\overline{\rm MFV}}$ [210]. In this case model specific details are necessary in order for the time-dependent observables to distinguish between the operators and phases.

6.3.6 Summary

In Table 6.1 we have collected the properties of the selected models discussed above with respect to the basic phenomenological parameters listed in (6.40) together with the scenarios they belong to. We also indicate whether the phase $\phi_s^{\rm NP}$ can be non-zero in these models. In all cases $|P|$ is generally different from zero as it contains the SM contributions. In order to distinguish between different models in each row of this table a more detailed analysis has to be performed taking all existing constraints into account. However, already identifying which of these four rows has been chosen by nature would be a tremendous step forward.

Model	Scenario	$\lvert P\rvert$	φ_P	$\lvert S\rvert$	φ_S	$\phi_s^{\rm NP}$
CMFV	A	$\lvert P\rvert$	0	0	0	0
MFV	D	$\lvert P\rvert$	0	$\lvert S\rvert$	0	0
LHT, 4G, RSc, Z'	A	$\lvert P\rvert$	φ_P	0	0	$\phi_s^{\rm NP}$
2HDM (Decoupling)	C	$\lvert 1\mp S\rvert$	$\arg(1\mp S)$	$\lvert S\rvert$	φ_S	$\phi_s^{\rm NP}$
2HDM (A Dominance)	A	$\lvert P\rvert$	φ_P	0	0	$\phi_s^{\rm NP}$
2HDM (H Dominance)	B	1	0	$\lvert S\rvert$	φ_S	$\phi_s^{\rm NP}$

Table 6.1: General structure of basic variables in different NP models. The last three cases apply also to the MSSM.

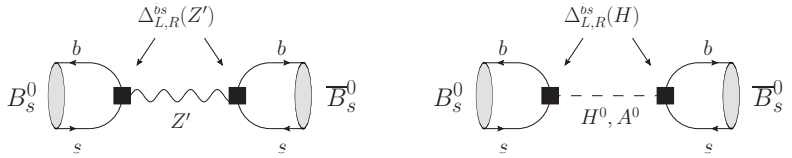

Figure 6.7: Tree-level exchange diagrams that contribute to B_s^0–$\overline{B}_s^0$ mixing in models containing a heavy colourless particle with FCNC couplings to quarks. *Left panel:* a heavy Z' gauge boson with effective couplings $\Delta^{bs}_{L,R}(Z')$. *Right panel:* a heavy scalar H^0 or pseudoscalar A^0 boson with effective couplings $\Delta^{bs}_{L,R}(H)$.

6.4 Specific models and constraints from B_s mixing

6.4.1 Constraints from B_s mixing

In this section we will consider New Physics in the form of new heavy colourless particles with effective tree-level FCNC couplings to quarks. Specifically, we will consider a heavy neutral gauge boson, as found for example in Z' models, and a heavy neutral (pseudo)scalar, as found for example in two-Higgs doublet models. We are interested in the phenomenology of such particles for the $\Delta B = 1$ $B_s \to \mu^+\mu-$ transition, as illustrated in Figure 6.3. However, New Physics of this nature will naturally also contribute to $\Delta B = 2$ processes and thereby affect B_s^0–$\overline{B}_s^0$ mixing as shown in Figure 6.7. Thus we first present a general framework within which we can take constraints from B_s mixing in account.

We define the flavour-violating couplings of neutral gauge boson Z' to quarks as follows [204]

$$\mathcal{L}_{\rm FCNC}(Z') = \left[\Delta_L^{sb}(Z')(\bar{s}\gamma_\mu P_L b) + \Delta_R^{sb}(Z')(\bar{s}\gamma_\mu P_R b)\right] Z'^\mu, \tag{6.56}$$

where $\Delta^{sb}_{L,R}(Z')$ are generally complex. Similarly, the flavour violating couplings of a

neutral scalar boson H as [189]

$$\mathcal{L}_{\rm FCNC}(H) = \left[\Delta_L^{sb}(H)(\bar{s}P_L b) + \Delta_R^{sb}(H)(\bar{s}P_R b)\right] H \tag{6.57}$$

with also $\Delta_{L,R}^{sb}(H)$ generally complex. We will denote by H any spin 0 particle, and will refer specifically to a scalar or pseudoscalar as H^0 or A^0, respectively. The conjugates are defined as follows:

$$\Delta_{L,R}^{sb}(Z') = [\Delta_{L,R}^{bs}(Z')]^*, \qquad \Delta_{L,R}^{sb}(H) = [\Delta_{R,L}^{bs}(H)]^*. \tag{6.58}$$

In a general New Physics scenario the B_s mixing parameters are given by

$$\Delta M_s = \frac{G_F^2}{6\pi^2} M_W^2 \, M_{B_s} |V_{ts}V_{tb}^*|^2 f_{B_s}^2 B_1^{\rm VLL} \hat{\eta}_B |S(B_s)|, \tag{6.59}$$

$$\phi_s = \phi_s^{\rm SM} - \arg[S(B_s)]. \tag{6.60}$$

Here $S(B_s)$ is a generalization of the $S_0(x_t)$ function defined in (3.24). Specifically

$$S(B_s) = S_0(x_t) + \sum_a \left[\Delta S(B_s)\right]_a, \tag{6.61}$$

where the label $a \in \{\rm VLL, VRR, RL, SLL, SRR\}$ refers to the operator basis [211]

$$\begin{aligned}
\mathcal{O}_1^{\rm VLL} &= (\bar{b}\gamma_\mu P_L s)\,(\bar{b}\gamma^\mu P_L s),\\
\mathcal{O}_1^{\rm LR} &= (\bar{b}\gamma_\mu P_L s)\,(\bar{b}\gamma^\mu P_R s),\\
\mathcal{O}_2^{\rm LR} &= (\bar{b}P_L s)\,(\bar{b}P_R s),\\
\mathcal{O}_1^{\rm SLL} &= (\bar{b}P_L s)\,(\bar{b}P_L s),\\
\mathcal{O}_2^{\rm SLL} &= (\bar{b}\sigma_{\mu\nu}P_L s)\,(\bar{b}\sigma_{\mu\nu}P_L s),
\end{aligned} \tag{6.62}$$

with the VRR and SRR operators given by interchanging L $\to$ R for VLL and SLL, respectively. The associated Wilson coefficients, and their NLO corrections, depend on the type of particle exchanged. In general we may write [189]

$$[\Delta S(B_s)]_{(X)AB} = \sum_P \frac{r_P^{(X)AB}(M_P)}{M_P^2} \frac{\Delta_A^{bs}(P)\Delta_B^{bs}(P)}{(V_{ts}V_{tb}{}^*)^2} \tag{6.63}$$

where we have summed over the contributing New Physics particles denoted by P. Once the type and quantity of the new particles are fixed, the remaining model-dependence is set by the couplings $\Delta_{L,R}^{bs}(P)$ and the masses M_P. The parameters $r_P^{(X)AB}$ are given by

$$\begin{aligned}
r_P^{(X)AB}(M_P) = &\left[\frac{12\pi^2}{G_F^2 f_{B_s}^2 \hat{\eta}_B B_1^{\rm VLL} M_{B_s} M_W^2}\right] \times \frac{1}{1+\delta_{AB}} \times \left\{ \begin{array}{lcl} +1 & : & P = Z' \\ -1 & : & P = H \end{array} \right\} \\
&\times \sum_i C_{P,i}^{(X)AB}(\mu)\, \langle \mathcal{O}_i^{(X)AB}(\mu)\rangle,
\end{aligned} \tag{6.64}$$

where $i = 1$ for $X = V$ and $i \in \{1, 2\}$ otherwise. A key ingredient in this parameterisation are the hadronic matrix elements

$$\begin{aligned}\langle \mathcal{O}_i^{(X)AB}(\mu)\rangle &\equiv \hat{U}(\mu_b,\mu)_{ji}\,\langle \overline{B}_0|\mathcal{O}_j^{(X)AB}(\mu_b)|B_s^0\rangle \\ &= \frac{M_{B_s} f_{B_s}^2}{3} P_i^{(X)AB}(\mu),\end{aligned} \tag{6.65}$$

which are evaluated at the high energy matching scale μ. We have expressed them in terms of the universal QCD factors $P_i^{(X)AB}(\mu)$ as defined in Ref. [211]. For example,

$$P_1^{\rm VLL}(\mu) = [\eta(\mu_b,\mu)]_{\rm VLL}\, B_1^{\rm VLL}(\mu_b) \tag{6.66}$$

describes the evolution of the bag parameter dominant in the Standard Model. By setting the high energy matching scale to the top quark mass $\mu = \mu_t \equiv m_t(m_t)$ we recover the familiar combination

$$P_1^{\rm VLL}(\mu_t) = \hat{\eta}_B B_1^{\rm VLL}(\mu_b) = \eta_B \hat{B}_{B_s}, \tag{6.67}$$

from Section 3.1, where we used $\hat{\eta}_B = [\eta(\mu_b,\mu_t)]_{\rm VLL}$.

The current most precise lattice calculations for the bag parameters corresponding to the operators listed in (6.62) are given in Ref. [72]. The resulting hadronic matrix elements are given in Table 6.2 at matching scales of 1 TeV and $m_t(m_t)$. We note, however, that the lattice value for the operator $\mathcal{O}_1^{\rm VLL}$, dominant in the Standard Model, does not currently agree perfectly with the lattice world average that we used in (3.39) (which has yet to include this value). In summary, we have

$$f_{B_s}\sqrt{B_1^{\rm VLL}} = \begin{cases} 211 \pm 8 \text{ MeV} & : \text{ tmQCD [72]} \\ 237 \pm 14 \text{ MeV} & : \text{ Fermilab Lattice/MILC [212]} \\ 226 \pm 12 \text{ MeV} & : \text{ Lattice averages (not incl. tmQCD) [27]} \end{cases} \tag{6.68}$$

at a common scale $\mu_b = m_b$. The Standard Model value of ΔM_s given in (3.40) uses the lattice world average of Ref. [27], which we will continue to use throughout this chapter. It is also the value used by Refs [184, 189] on which this chapter is based. However, contrary to these papers, we will use the more recent results of Ref. [72] for the full $B_i^{(X)AB}$ operator basis.

The other important ingredient in the evaluation of $r_P^{(X)AB}$ are the Wilson coefficients, which are dependent on the type of (effective) tree-level particle exchanged. In Ref. [213] these coefficients have been calculated for neutral scalars and gauge bosons at NLO using the $\overline{\rm MS}$–NDR scheme.

Combining these ingredients, we can calculate values of $r_P^{(X)AB}$ for specific particle masses. In Table 6.3 we list values corresponding to exchanged scalars and gauge bosons with masses of 100 GeV, 500 GeV and 1 TeV. Thus once we fix the new tree-level particle content and their masses, the only freedom that remains is in choosing the FCNC couplings $\Delta_{\rm L,R}^{bs}$. In the following sections we will consider scenarios in which

μ	$\langle\mathcal{O}_1^{\rm VLL}(\mu)\rangle$	$\langle\mathcal{O}_1^{\rm LR}(\mu)\rangle$	$\langle\mathcal{O}_2^{\rm LR}(\mu)\rangle$	$\langle\mathcal{O}_1^{\rm SLL}(\mu)\rangle$	$\langle\mathcal{O}_2^{\rm SLL}(\mu)\rangle$
1 TeV	0.063	-0.15	0.19	-0.08	-0.15
$m_t(m_t)$	0.067	-0.12	0.15	-0.07	-0.13

Table 6.2: Hadronic matrix elements $\langle\mathcal{O}_i^{\rm (X)AB}(\mu)\rangle$, evaluated at $\mu = 1\,\text{TeV}$ and $\mu = m_t(m_t)$, in units of GeV^3 using the lattice calculations of Ref. [72].

M	$r_{Z'}^{\rm VLL}(M)$	$r_{Z'}^{\rm LR}(M)$	$r_H^{\rm LR}(M)$	$r_H^{\rm SLL}(M)$
1 TeV	22	-104	-130	28
500 GeV	23	-96	-120	27
100 GeV	24	-85	-102	25

Table 6.3: $r_P^{(X)AB}(M)$ in units of TeV^2 as defined in (6.64) using the lattice calculations of Ref. [72]. The matching scale is set to $\mu = M$.

these couplings are described in terms of a single complex parameter. The allowed values of this parameter are then constrained by the experimental measurements of ΔM_s and ϕ_s, as given in (3.41) and (3.48), respectively.

We will enforce the following constraints on the specific models we consider

$$-5.4^\circ \leq \phi_s \leq 14.4^\circ, \qquad 16.9\ \text{ps}^{-1} \leq \Delta M_s \leq 18.7\ \text{ps}^{-1}. \tag{6.69}$$

The bounds on ϕ_s are the $\pm 2\sigma$ experimental uncertainties as given in (3.48). The bounds on ΔM_s correspond to the experimental value $\pm 5\%$ to account for hadronic uncertainties, corresponding to the 1σ errors on lattice average given in (6.68). Considering the current disagreement between the values listed in (6.68), this range is a bit aggressive ($\pm 10\%$ would be more conservative). The advantage of taking an aggresive range is that it better illustrates how different scenarios of New Physics may be distinguished between in the future. Namely, using the lattice average value of Ref. [27] gives a Standard Model prediction for ΔM_s above this range, which requires certain models of New Physics to resolve this tension via new CP-violating phases. Had we instead used the tmQCD [27] value, the Standard Model prediction would be below this range, and the necessary resolutions from New Physics would be different. This latter case is not studied numerically, but the change in conclusions can be inferred from the theoretical discussion given in Section 6.3.

6.4.2 Gauge boson exchange

6.4.2.1 Basic formulae

We begin by considering Z' models in which NP contributions to FCNC observables are dominated by tree-level Z' exchanges. A detailed analysis of these models has recently been presented in Ref. [204]. Also there the three observables in (6.4) have been

considered but the emphasis has been put on the correlations of them with $\Delta B = 2$ observables, in particular ϕ_s. Here we will complement this study by computing the correlations among $\overline{R}$, $\mathcal{A}_{\Delta\Gamma}^{\mu\mu}$, and $\mathcal{S}_{\mu\mu}$.

The flavour-violating couplings of Z' are defined in (6.56). We also define the Z' couplings to muons

$$\mathcal{L}_{\ell\bar{\ell}}(Z') = \left[\Delta_L^{\ell\ell}(Z')(\bar{\ell}\gamma_\mu P_L \ell) + \Delta_R^{\ell\ell}(Z')(\bar{\ell}\gamma_\mu P_R \ell)\right] Z'^{\mu} \tag{6.70}$$

and introduce

$$\Delta_A^{\mu\bar{\mu}}(Z') = \Delta_R^{\mu\bar{\mu}}(Z') - \Delta_L^{\mu\bar{\mu}}(Z'). \tag{6.71}$$

Then the non-vanishing Wilson coefficients contributing to $B_s \to \mu^+\mu^-$ are given as follows:

$$\sin^2\theta_W C_{10} = -\eta_Y Y_0(x_t) - \frac{1}{g_{\rm SM}^2}\frac{1}{M_{Z'}^2}\frac{\Delta_L^{sb}(Z')\Delta_A^{\mu\bar{\mu}}(Z')}{V_{ts}^* V_{tb}}, \tag{6.72}$$

$$\sin^2\theta_W C'_{10} = -\frac{1}{g_{\rm SM}^2}\frac{1}{M_{Z'}^2}\frac{\Delta_R^{sb}(Z')\Delta_A^{\mu\bar{\mu}}(Z')}{V_{ts}^* V_{tb}}, \tag{6.73}$$

where

$$g_{\rm SM}^2 = 4\frac{G_F}{\sqrt{2}}\frac{\alpha}{2\pi\sin^2\theta_W}\,. \tag{6.74}$$

As only the coefficients C_{10} and C'_{10} are non-vanishing this NP scenario is governed by the formulae (6.42) and (6.43). Indeed this scenario is an example of *Scenario A* in which, in addition to $S = 0$, also the pseudoscalar contributions vanish. Yet, as P can differ from unity and have a nontrivial phase, a rich phenomenology is found [204].

6.4.2.2 Numerical analysis

As in the analyses in Refs. [204, 189] it will be instructive to consider the following four schemes for the gauge boson couplings and in the next subsection for scalar couplings:

1. Left-handed Scheme (LHS) with complex $\Delta_L^{bs} \neq 0$ and $\Delta_R^{bs} = 0$,
2. Right-handed Scheme (RHS) with complex $\Delta_R^{bs} \neq 0$ and $\Delta_L^{bs} = 0$,
3. Left-Right symmetric Scheme (LRS) with complex $\Delta_L^{bs} = \Delta_R^{bs} \neq 0$,
4. Left-Right asymmetric Scheme (ALRS) with complex $\Delta_L^{bs} = -\Delta_R^{bs} \neq 0$.

Note that the ordering in flavour indices in the couplings in these schemes is governed by the operator structure in B_s^0–$\bar{B}_s^0$ mixing [204, 189] and differs from the one in (6.56) and (6.57). In this context one should recall the relations given in (6.58) giving the conjugate couplings, where the scalar coupling has a chirality flip.

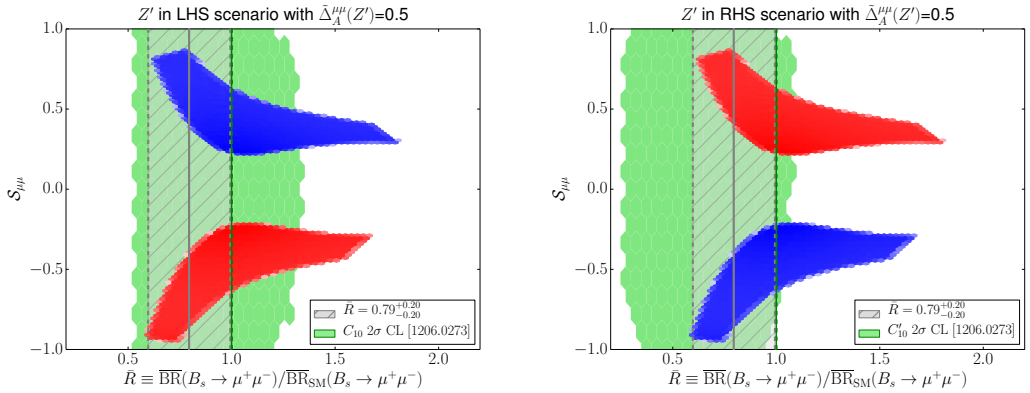

Figure 6.8: $\mathcal{S}_{\mu\mu}$ versus $\overline{R}$ for LHS (left) and RHS (right), assuming $M_{Z'} = 1$ TeV and $\Delta_A^{\mu\mu}(Z') = 0.5$. Gray region: exp 1σ range for $\overline{R}$. The $2\,\sigma$ CL combined fit region for the Wilson coefficients $C_{10}^{(\prime)}$ come from a general $b \to s l^+ l^-$ analysis given in Ref. [215].

The ranges for B_s mixing given in (6.69) result in two allowed regions for the magnitudes and phases of the quark couplings $\Delta_{L,R}^{sb}$ depending on the scheme chosen above. These regions in parameter space are dubbed *oases*. The oases for each scheme have a two fold degeneracy in the complex phase of the coupling. Where it is relevant we will distinguish between these two different oases using the colours blue and red.

Concerning the direct lower bounds on $M_{Z'}$ from collider experiments, the most stringent bounds are provided by the CMS experiment [214]. However, these constraints are most sensitive to the couplings of the Z' to the light quarks,which do not play any role in our analysis. Moreover, the collider bounds on $M_{Z'}$ are generally model dependent. While for the so-called sequential Z' the lower bound for $M_{Z'}$ is in the ballpark of 2.5 TeV, in other models values as low as 1 TeV are still possible. In order to cover large set of models, we will choose as our nominal value $M_{Z'} = 1$ TeV. With the help of the formalism given in Ref. [204] it is possible to estimate how our results would change for $1\,\mathrm{TeV} \leq M_{Z'} \leq 3\,\mathrm{TeV}$.

In order to perform the present analysis we assign $\Delta_A^{\mu\bar{\mu}}(Z') = 0.5$, as was done in Ref. [204]. In Section 6.4.3.3 and beyond, where we compare Z' exchange with various (pseudo)scalar exchanges, this coupling will be allowed to vary. The sign of this coupling is crucial for the identification of various enhancements and suppressions with respect to SM branching ratio and CP asymmetries and impacts the search for successful oases in the space of parameters that has been performed in Ref. [204]. In Figure 6.8 we show the correlation between $\mathcal{S}_{\mu\mu}$ and $\overline{R}$ for LHS (left) and RHS (right) schemes. Corresponding correlations between $\mathcal{A}_{\Delta\Gamma}^{\mu\mu}$ and $\overline{R}$ and between $\mathcal{A}_{\Delta\Gamma}^{\mu\mu}$ and $\mathcal{S}_{\mu\mu}$ are given in Figure 6.9 for LHS only. As we mentioned above, the two colours correspond to two parameter oases consistent with the ΔM_s and ϕ_s constraints given in (6.69).

We observe in analogy with findings of Ref. [204] that the correlations in the LHS and RHS schemes have the same shape except the oases and consequently the colours in

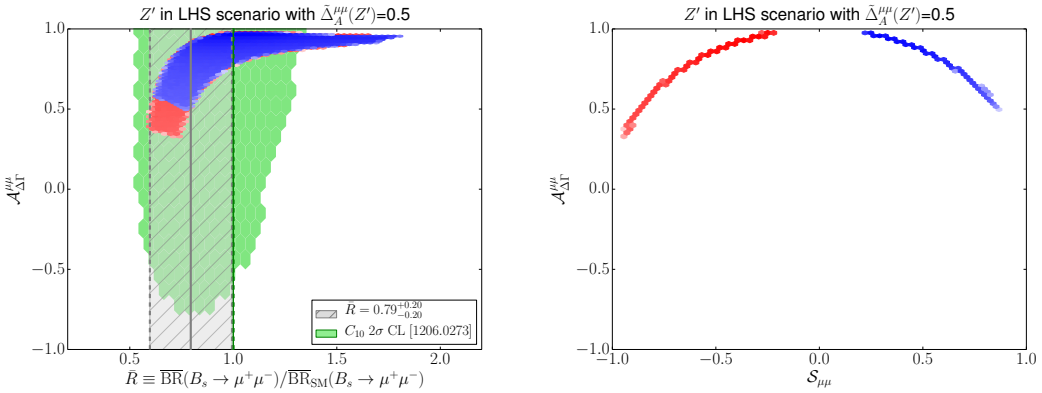

Figure 6.9: $\mathcal{A}_{\Delta\Gamma}^{\mu\mu}$ versus $\overline{R}$ (left) and $\mathcal{A}_{\Delta\Gamma}^{\mu\mu}$ versus $\mathcal{S}_{\mu\mu}$ (right) for LHS, assuming $M_{Z'} = 1$ TeV and $\Delta_A^{\mu\mu}(Z') = 0.5$. Gray region in left panel: exp 1σ range for $\overline{R}$. The $2\,\sigma$ CL combined fit region for the Wilson coefficient C_{10} comes from a general $b \to s l^+ l^-$ analysis given in Ref. [215].

Figure 6.8 have to be interchanged. We therefore conclude that on the basis of the three observables that we consider it is not possible to distinguish between LHS and RHS schemes because in the RHS scheme one can simply interchange the oases to obtain the same physical results as in LHS scheme. Consequently if one day we will have precise measurements of $\mathcal{A}_{\Delta\Gamma}^{\mu\mu}$, $S_{\mu^+\mu^-}$ and $\mathrm{BR}(B_s \to \mu^+\mu^-)$ we will still not be able to distinguish for instance whether we deal with LHS scheme in the blue oasis or RHS scheme in the red oasis.

As pointed out in Ref. [204], in order to make this distinction one has to consider simultaneously $B \to K^*\mu^+\mu^-$, $B \to K\mu^+\mu^-$ and $b \to s\nu\bar{\nu}$ transitions, which is beyond the scope of this chapter. However, we do include regions corresponding to the $2\,\sigma$ CL combined fits of Ref. [215] for the Wilson coefficients C_{10} and C'_{10}, which result from these transitions, in Figures 6.8 and 6.9 where relevant. The combination of our oases and these additional constraints gives us valuable information. The allowed values for the three observables considered are, in this NP scenario,

$$0.4 \leq \mathcal{A}_{\Delta\Gamma}^{\mu\mu} \leq 1.0, \quad 0.2 \leq |\mathcal{S}_{\mu^+\mu^-}| \leq 0.9, \quad 0.5 \leq \overline{R} \leq \begin{cases} 1.3 & : \text{ LHS scheme} \\ 1.0 & : \text{ RHS scheme} \end{cases} . \tag{6.75}$$

Moreover, the smallest values of $\mathcal{A}_{\Delta\Gamma}^{\mu\mu}$ and largest values of $|\mathcal{S}_{\mu^+\mu^-}|$ are obtained for smallest values of $\overline{R}$. The non-zero values of $\mathcal{S}_{\mu^+\mu^-}$ originate in Z' models from requiring that ΔM_s is suppressed with respect to its SM value in order to achieve a better agreement with data. As we will see below for models with scalar or pseudoscalar exchanges, this requirement can also be satisfied for a vanishing $\mathcal{S}_{\mu^+\mu^-}$.

If both LH and RH currents are present in NP contributions with symmetric couplings to quarks, the LRS scheme, then NP contributions to $B_s \to \mu^+\mu^-$ vanish. Specifically, in this case $P = 1$, and we from (6.42) and (6.43) that

$$\mathcal{A}_{\Delta\Gamma}^{\mu\mu} = \cos(\phi_s^{\mathrm{NP}}), \quad \mathcal{S}_{\mu\mu} = -\sin(\phi_s^{\mathrm{NP}}), \tag{6.76}$$

and a branching ratio observable given by

$$\overline{R} = \left[\frac{1 + y_s \cos(\phi_s^{\rm NP})}{1 + y_s}\right]. \tag{6.77}$$

In view of the smallness of $\phi_s^{\rm NP}$ the results for the three observables are very close to the SM values. This example shows that even if no departures from SM expectation will be found in $B_s \to \mu^+\mu^-$, this does not necessarily mean that there is no NP present. This physics could then be seen in $B \to K^*\mu^+\mu^-$ and $B \to K\mu^+\mu^-$ and $b \to s\nu\bar{\nu}$ transitions as demonstrated in Ref. [204].

In the ALRS scheme NP contributions to $B_s \to \mu^+\mu^-$ enter again with full power. Therefore the three observables in (6.4) offer, as in the LHS and RHS schemes, a good test of NP. In fact, as found in Ref. [204], after the $\Delta B = 2$ constraints are taken into account, the pattern of NP contributions is similar to LHS scheme except that the effects are smaller. This is because the relevant couplings have to be smaller in the presence of LR operators in $\Delta B = 2$ in order to agree with the data on ΔM_s.

6.4.3 (Pseudo)Scalar exchange

6.4.3.1 Basic formulae

We will next consider tree-level pseudoscalar or scalar exchanges that one encounters in various models either at the fundamental level or in an effective theory. It could in principle be the SM Higgs boson, but as the recent analysis in Ref. [189] shows, once the constraints from $\Delta F = 2$ processes are taken into account, NP effects in $B_s \to \mu^+\mu^-$ via a tree-level SM Higgs exchange are at most 8% of the usual SM contribution and thus hardly measurable. The SM Higgs coupling to muons is simply too small. Therefore, what we have in mind here is a new heavy scalar or pseudoscalar boson encountered in 2HDM or supersymmetric models. Yet, in this subsection we will make the working assumption that either a neutral scalar or pseudoscalar tree-level exchange dominates NP contributions. A general analysis of FCNC processes within such scenarios has been recently presented in Ref. [189], with a focus on correlation between the observables given in (6.4) with the B_s mixing phase ϕ_s. Here we will complement this study by computing the correlations among $\overline{R}$, $\mathcal{A}_{\Delta\Gamma}^{\mu\mu}$, and $\mathcal{S}_{\mu\mu}$.

The flavour violating couplings of H are given in (6.57). Muon couplings $\Delta_{L,R}^{\mu\bar{\mu}}(H)$ are defined in a similar way. Due to the relation between left and right handed scalar couplings given in (6.58), only $\Delta_R^{sb}(H)$ and $\Delta_L^{sb}(H)$ are non-vanishing in the LHS and RHS schemes, respectively. The relevant non-vanishing Wilson coefficients are then

given as follows

$$m_b(M_H)\sin^2\theta_W C_S = \frac{1}{g_{\rm SM}^2}\frac{1}{M_H^2}\frac{\Delta_R^{sb}(H)\Delta_S^{\mu\bar{\mu}}(H)}{V_{ts}^*V_{tb}}, \tag{6.78}$$

$$m_b(M_H)\sin^2\theta_W C'_S = \frac{1}{g_{\rm SM}^2}\frac{1}{M_H^2}\frac{\Delta_L^{sb}(H)\Delta_S^{\mu\bar{\mu}}(H)}{V_{ts}^*V_{tb}}, \tag{6.79}$$

$$m_b(M_H)\sin^2\theta_W C_P = \frac{1}{g_{\rm SM}^2}\frac{1}{M_H^2}\frac{\Delta_R^{sb}(H)\Delta_P^{\mu\bar{\mu}}(H)}{V_{ts}^*V_{tb}}, \tag{6.80}$$

$$m_b(M_H)\sin^2\theta_W C'_P = \frac{1}{g_{\rm SM}^2}\frac{1}{M_H^2}\frac{\Delta_L^{sb}(H)\Delta_P^{\mu\bar{\mu}}(H)}{V_{ts}^*V_{tb}}, \tag{6.81}$$

where we have introduced

$$\begin{aligned}\Delta_S^{\mu\bar{\mu}}(H) &= \Delta_R^{\mu\bar{\mu}}(H) + \Delta_L^{\mu\bar{\mu}}(H),\\ \Delta_P^{\mu\bar{\mu}}(H) &= \Delta_R^{\mu\bar{\mu}}(H) - \Delta_L^{\mu\bar{\mu}}(H).\end{aligned} \tag{6.82}$$

Note that m_b has to be evaluated at $\mu = M_H$.

From the hermiticity of the relevant Hamiltonian one can show that $\Delta_S^{\mu\bar{\mu}}(H)$ is real and $\Delta_P^{\mu\bar{\mu}}(H)$ purely imaginary. For convenience we define

$$\Delta_P^{\mu\bar{\mu}}(H) \equiv i\tilde{\Delta}_P^{\mu\bar{\mu}}(H), \tag{6.83}$$

so that $\tilde{\Delta}_P^{\mu\bar{\mu}}(H)$ is real. *Scenario A* can be realised by setting $\Delta_S^{\mu\bar{\mu}}(H) = 0$. Similarly, *Scenario B* follows from setting $\Delta_P^{\mu\bar{\mu}}(H) = 0$. The case of a mixed scalar and pseudoscalar combination will be addressed in Section 6.4.4, which more naturally give the intended usage cases of *Scenarios C and D*.

6.4.3.2 Numerical analysis

Analogous to the case of tree-level Z' exchanges, we will use the general B_s mixing formalism discussed in Section 6.4.1 and the conditions in (6.69) to constrain the quark-scalar couplings in the schemes LHS, RHS, LRS and ALRS. The first step is to set values for the scalar and pseudoscalar muon couplings. For a single scalar particle H^0, the parameter $|S|$ driving NP (*Scenario B*) is directly proportional to the muon coupling $|\Delta_S^{\mu\mu}(H^0)|$. However, for a single pseudoscalar particle A^0, the muon coupling $\Delta_P^{\mu\mu}(A^0)$ is not directly proportional to P, and the resulting NP observables thereby have a more involved dependence on it. In Figure 6.10 we show the dependence of the observables $\overline{R}$ (left panel) and $\mathcal{A}_{\Delta\Gamma}^{\mu\mu}$ (right panel) with respect to muon coupling $\tilde{\Delta}_P^{\mu\mu}(A^0)$ defined in (6.83) satisfying the B_s mixing constraints for the LHS case. We observe that the parameter space of the NP physics observables is very dependent on whether we pick a large or small coupling, and that a fixed coupling cannot do it justice. We further observe that the oases become indistinguishable if the sign of the coupling is not fixed.

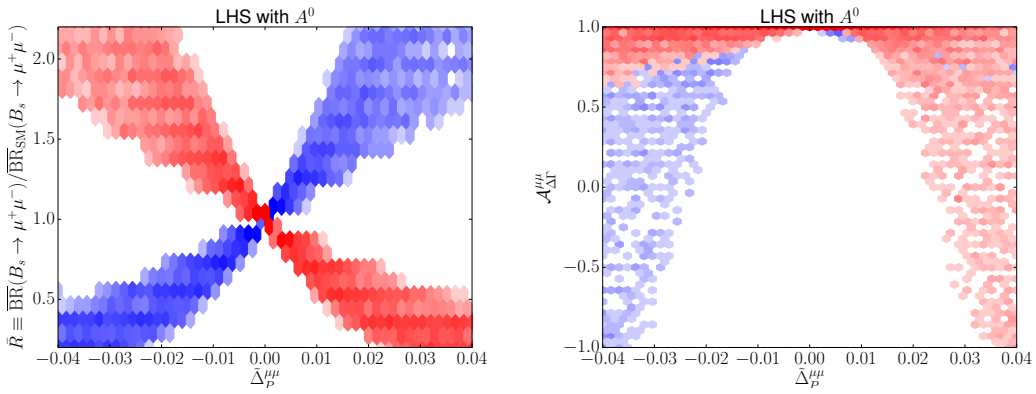

Figure 6.10: The dependence of the observables $\overline{R}$ (left) and $\mathcal{A}_{\Delta\Gamma}^{\mu\mu}$ (right) on the pseudoscalar lepton coupling $\tilde{\Delta}_P^{\mu\bar{\mu}}(H)$ satisfying the B_s mixing constraints in the LHS case. For a pseudoscalar with mass $M_{A^0} = 1\,\mathrm{TeV}$.

In order to compare the oases behaviour of the scalar and pseudoscalar we begin by fixing the muon couplings to

$$\Delta_S^{\mu\bar{\mu}}(H^0) = 0.024, \qquad \Delta_P^{\mu\bar{\mu}}(A^0) = i\ 0.012, \tag{6.84}$$

and $\Delta_P^{\mu\bar{\mu}}(H^0) = \Delta_S^{\mu\bar{\mu}}(A^0) = 0$. These values are consistent with the allowed range for $\mathrm{BR}(B_s \to \mu^+\mu^-)$ when the constraints on the quark couplings from $B_s^0 - \bar{B}_s^0$ are taken into account and $M = 1\,\mathrm{TeV}$. The reason the scalar couplings are chosen to be larger than the pseudoscalar ones is because scalars do not interfere with SM contributions and thereby more weakly constrained. The constraints from $b \to s\ell^+\ell^-$ transitions do not have any impact in the (pseudo) scalar case, as shown in Ref. [189].

In Figure 6.11 we show the correlations of $\mathcal{S}_{\mu\mu}$ versus $\overline{R}$ satisfying B_s mixing constraints for a single tree-level scalar (left) and pseudoscalar (right) exchange in the LHS scheme. For the scalar case the blue and red oases overlap. The red oases in the pseudoscalar case corresponds to $\overline{R} < 1$ and is therefore clearly distinguishable from the scalar case, where $\overline{R} > 1$ for both oases. In Section 6.4.3.3 we will compare these correlation with Z' exchange.

As we stated earlier, fixing the pseudoscalar muon couplings to one value does not reveal the full structure of the NP parameter space. We therefore now consider the muon couplings varied over the following range:

$$|\Delta_S^{\mu\bar{\mu}}(H^0)|,\ |\Delta_P^{\mu\bar{\mu}}(A^0)| \in [0.012, 0.024]. \tag{6.85}$$

From here on we will ignore the sign of the lepton couplings, but again note that this degeneracy can be resolved in the pseudoscalar case if the blue or red oasis from the B_s mixing constraints can be singled out. We thus also stop distinguishing between the two oases.

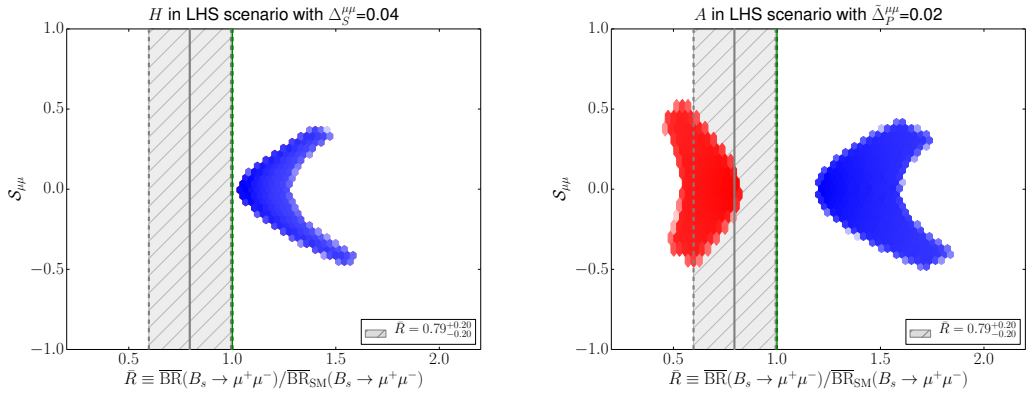

Figure 6.11: $\mathcal{S}_{\mu\mu}$ versus $\overline{R}$ for for LHS scheme with a scalar (left) and pseudoscalar (right) for $M_{H^0} = M_{A^0} = 1\,\mathrm{TeV}$. Gray region: exp 1σ range for $\overline{R}$.

In Figure 6.12, $\overline{R}$ is plotted against $\mathcal{A}_{\Delta\Gamma}^{\mu\mu}$ (left panel) and $\mathcal{S}_{\mu\mu}$ (right panel) with the regions allowed by the B_s mixing constraints overlayed for the various specific tree-level models discussed in this section. The scalar and pseudoscalar muon couplings have been varied as just discussed, and also the Z' muon couplings have been varied: $\Delta_A^{\mu\mu}(Z') \in [0.3, 0.7]$. These three models are shown for the LHS scheme. For the Z' model the allowed region has also been constrained by a $2\,\sigma$ CL combined fit of the Wilson coefficient C_{10} from $b \to s l^+ l^-$ transitions [215]. For the scalar (H^0) case the branching ratio observable $\overline{R}$ can only be enhanced as there is no interference with the SM contribution. On the other hand, for the pseudoscalar (A^0) case it can be suppressed or enhanced depending on which parameter oasis is chosen. The values of $\mathcal{A}_{\Delta\Gamma}^{\mu\mu}$ are seen to be positive for both H^0 and A^0 and for $\overline{R}$ within one σ experimental value close to unity. $\mathcal{S}_{\mu\mu}$ can reach ± 0.50 in both cases.

We have not shown the corresponding results in the RHS scheme because, similar to the gauge boson case, the correlations in question have an identical structure. In the scalar case the two correlations are exactly equal, whereas in the pseudoscalar case the oases should be interchanged for the RHS scheme. In the LRS case, as expected, NP effects are very small as scalar and pseudoscalar contributions are absent and (6.76) applies.

6.4.3.3 Comparison with a gauge boson exchange

It is worthwhile to also include the exchange of a gauge boson, as presented in Section 6.4.2, to our discussion of how the $B_s \to \mu + \mu^-$ observables allow us to distinguish between different models. Indeed in the left panel of Figure 6.8 we see that the correlation between $\mathcal{S}_{\mu\mu}$ and $\overline{R}$ has a very different structure from the case of pseudoscalar or scalar exchanges shown in Figure 6.11. In the right panel of Figure 6.12 an overlay of these regions is shown for LHS schemes, with the lepton couplings varied as given

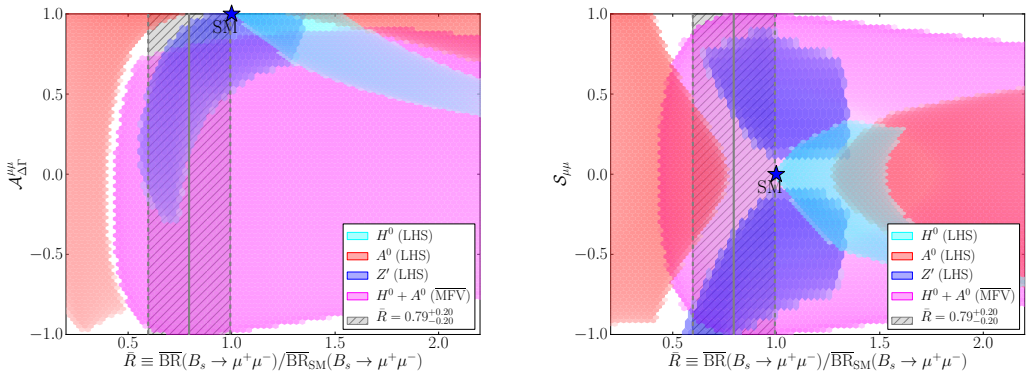

Figure 6.12: Overlay of the correlations for $\overline{R}$ versus $\mathcal{A}^{\mu\mu}_{\Delta\Gamma}$ (left) and $\mathcal{S}_{\mu\mu}$ (right) for the various specific models considered. The lepton couplings are varied in the ranges $|\Delta^{\mu\mu}_{S,P}(H)| \in [0.012, 0.024]$ and $\Delta^{\mu\mu}_{A}(Z') \in [0.3, 0.7]$. All particles are taken to have a mass of 1 TeV.

in (6.85). Similarly, in the left panel of Figure 6.12 we show the correlation between $\mathcal{A}^{\mu\mu}_{\Delta\Gamma}$ and $\overline{R}$, where strong contrasts between the allowed regions also emerge. The difference between the gauge boson and pseudoscalar exchange is interesting because both particles generate *Scenario A*.

The difference in phenomenology of the A^0 and Z' models in question can be traced back to a difference in phase for the NP correction $\tilde{P}$, which was defined in (6.44). As we have defined the couplings $\Delta^{bs}_{L}(A^0, Z')$ in the same way for both models, the difference enters through the muon couplings, which are imaginary in the case of the A^0 but real for the Z'. Specifically, by defining

$$\tilde{P}(Z') = r_{Z'} e^{i\delta_{Z'}}, \qquad \tilde{P}(A^0) = r_{A^0} e^{i\delta_{A^0}} \tag{6.86}$$

we find that

$$r_{Z'} \approx r_{A^0}, \qquad \delta_{A^0} = \delta_{Z'} - \frac{\pi}{2}. \tag{6.87}$$

The B_s mixing constraints we have taken force $\delta_{Z'}$ to be in the ballpark of 90° and 270° for the blue and red oasis, respectively [204, 189]. This results in positive and negative value of $\mathcal{S}_{\mu\mu}$ for the blue and red oasis, respectively, as shown in Figure 6.8. Concerning $\overline{R}$, where NP is governed by $\cos\delta_{Z'}$, we find that it can be enhanced or suppressed in each oasis. On the other hand, (6.87) implies that the phase δ_{A^0} is in the ballpark of 0° and 180^0 for the blue and red oasis, respectively. Therefore the asymmetry $\mathcal{S}_{\mu\mu}$ can vanish in both oases, while this was not possible in the Z' case. As NP in $\overline{R}$ is governed by $\cos\delta_{A^0}$, this enhances and suppresses $\overline{R}$ for blue and red oasis, respectively as clearly seen in Figure 6.11. In particular, $\overline{R}$ differs from its SM value, while this is not the case in the Z' scenario.

What is particularly interesting is that these differences are directly related to the difference in the fundamental properties of the particles involved: their spin and CP-

parity. As far as the last property is concerned, also differences between the implications of the pseudoscalar and scalar exchanges have been identified as discussed in detail above. They are related to the fact that the scalar contribution, being CP-even, cannot interfere with the SM contribution.

6.4.4 Scalar and pseudoscalar exchange

6.4.4.1 Basic formulae

In this model we assume the presence of a scalar H^0 and pseudoscalar A^0 with equal (or nearly degenerate) mass M_H. This is, for example, effectively realised in 2HDMs in a decoupling regime, where H^0 and A^0 are much heavier than the SM Higgs h^0 and almost degenerate in mass (see Appendix A). We will show that under specific assumptions this setup can reproduce *Scenarios C* or *D*.

The couplings of the scalar and pseudoscalar to quarks are given in general by the following flavour-violating Lagrangian:

$$\begin{aligned}\mathcal{L}_{\text{FCNC}}(H^0, A^0) = &\left[\Delta_L^{sb}(H^0)(\bar{s}P_L b) + \Delta_R^{sb}(H^0)(\bar{s}P_R b)\right] H^0 \\ &+ \left[\Delta_L^{sb}(A^0)(\bar{s}P_L b) + \Delta_R^{sb}(A^0)(\bar{s}P_R b)\right] A^0. \end{aligned} \tag{6.88}$$

We will assume that the scalar and pseudoscalar couple with equal strength to quarks:

$$\mathcal{L} \ni \bar{D}_L \tilde{\Delta} D_R (H^0 + iA^0) + \text{h.c}, \tag{6.89}$$

where $D = (d, s, b)$ and $\tilde{\Delta}$ is a matrix in flavour space. Then

$$\begin{aligned} \Delta_R^{sb}(H^0) &= \tilde{\Delta}^{sb}, & \Delta_L^{sb}(H^0) &= \left[\tilde{\Delta}^{bs}\right]^*, \\ \Delta_R^{sb}(A^0) &= i\tilde{\Delta}^{sb}, & \Delta_L^{sb}(A^0) &= -i\left[\tilde{\Delta}^{bs}\right]^*. \end{aligned} \tag{6.90}$$

where in general $\tilde{\Delta}^{sb}, \tilde{\Delta}^{bs} \in \mathbb{C}$.

Scenario C:

To reproduce this scenario we set the pseudoscalar and scalar masses to be exactly equal: $M_{H^0} = M_{A^0} = M_H$. Further relating the lepton couplings by a single real parameter $\tilde{\Delta}^{\mu\bar{\mu}}$:

$$\Delta^{\mu\bar{\mu}}(H^0) = \tilde{\Delta}^{\mu\bar{\mu}}, \qquad \Delta^{\mu\bar{\mu}}(A^0) = i\,\tilde{\Delta}^{\mu\bar{\mu}} \tag{6.91}$$

and inserting the lepton and quark couplings into formulae (6.78)–(6.81) we find:

$$C_S = -C_P = \frac{1}{g_{SM}^2\, M_H^2\, m_b \sin^2\theta_W} \frac{\tilde{\Delta}^{sb}\tilde{\Delta}^{\mu\mu}}{V_{ts}^* V_{tb}} \tag{6.92}$$

$$C_S' = C_P' = \frac{1}{g_{SM}^2\, M_H^2\, m_b \sin^2\theta_W} \frac{\left[\tilde{\Delta}^{bs}\right]^* \tilde{\Delta}^{\mu\mu}}{V_{ts}^* V_{tb}}. \tag{6.93}$$

This simple model satisfies the relations in (6.52) and thereby belongs to *Scenario C*. These relations are in fact valid for all the quark coupling schemes: LHS, RHS, LRS and ALRS. However, the physics implications depend on the scheme considered: In the LHS and RHS schemes NP contributions to B_s^0–$\bar{B}_s^0$ mixing from scalar and pseudoscalar with the same mass cancel each other, therefore there is no constraint from B_s^0–$\bar{B}_s^0$ mixing. In this case NP effects in $B_s \to \mu^+\mu^-$ can only be constrained by the decay itself or other $b \to s\ell^+\ell^-$ transitions. In LRS and ALRS schemes non-vanishing contributions from LR operators to B_s^0–$\bar{B}_s^0$ mixing are present. Moreover we find

$$C_S = C_S', \qquad C_P = -C_P' \qquad \text{(LRS)}, \tag{6.94}$$

$$C_S = -C_S', \qquad C_P = C_P' \qquad \text{(ALRS)}. \tag{6.95}$$

Therefore in the LRS case only pseudoscalar contributes to $B_s \to \mu^+\mu^-$ (*Scenario A*), while in the ALRS case only scalar contributes (*Scenario B*).

We conclude therefore that in order to have an example of *Scenario C* that differs from *Scenario A* and *B* and moreover in which NP contributions to B_s^0–$\bar{B}_s^0$ mixing are present, we need both L and R couplings that are not equal to each other or do not differ only by a sign.

An option to reproduce *Scenario C* with non-trivial constraints from mixing is given by Minimal Flavour Violation (MFV). In the MFV formalism (see Appendix A) $\tilde{\Delta}$ is constructed out of the spurion matrices Y_U and Y_D [209]. In principle the following constructions can contribute to the $b \to s$ FCNCs at leading order in the off-diagonal structure:

$$Y_U Y_U^\dagger Y_D, \quad Y_D Y_D^\dagger Y_U Y_U^\dagger Y_D, \quad Y_U Y_U^\dagger Y_D Y_D^\dagger Y_D. \tag{6.96}$$

However, the last two will in general receive dynamical (loop) suppressions. Thus, for simplicity, we assume the first construction to be dominant. In the notation of Ref. [210], where MFV is discussed in the context of a general 2HDM with flavour blind phases (2HDM$_{\overline{\text{MFV}}}$), this is equivalent to assuming $|a_0| \gg |a_1|, |a_2|$. As a result we find

$$\tilde{\Delta}^{sb} = \epsilon\, y_b\, y_t^2\, V_{ts}^* V_{tb}, \qquad \left[\tilde{\Delta}^{bs}\right]^* = \epsilon^*\, y_s\, y_t^2\, V_{ts}^* V_{tb} = \frac{m_s}{m_b}\frac{\epsilon^*}{\epsilon}\tilde{\Delta}^{sb}. \tag{6.97}$$

Thus under the above assumptions all of the quark couplings in (6.88) can be expressed in terms of a single NP parameter ϵ[3].

The parameter ϵ is real in pure MFV but may be complex in 2HDM$_{\overline{\text{MFV}}}$ [210]. Inserting relation (6.97) into (6.93) we find

$$C_S' = \frac{m_s}{m_b}\frac{\epsilon^*}{\epsilon} C_S \qquad\qquad C_P' = -\frac{m_s}{m_b}\frac{\epsilon^*}{\epsilon} C_P, \tag{6.98}$$

and observe a m_s/m_b suppression of the primed operators. In pure MFV, where ϵ is real, the parameters $C_{S,P}^{(\prime)}$ are also all real.

[3] It should be emphasized that in general this is not the case for 2HDM$_{\overline{\text{MFV}}}$ [210, 216]. See additional comments below.

Scenario D:

In *Scenario D* the parameters P and S are arbitrary but do not carry new CP-violating phases. The pure MFV model with a scalar and pseudoscalar that we just discussed is therefore a natural candidate. However, because this model was defined to satisfy *Scenario C*, as it stands we have $P \pm S = 1$. If we continue to insist that the scalar and pseudoscalar should couple with equal strengths and phases to quarks as in (6.89), then there are two choices for making P and S arbitrary.

One choice is to allow different couplings to leptons for the scalar and pseudoscalar i.e. $|\Delta^{\mu\bar{\mu}}(H^0)| \neq |\Delta^{\mu\bar{\mu}}(A^0)|$. In this case the constraints from B_s mixing (discussed below) do not change, and only the current bounds on $\overline{R}$ must be satisfied.

Alternatively, a non-trivial difference between the scalar mass M_{H^0} and the pseudoscalar mass M_{A^0} can be introduced. In this case the lepton couplings can remain equal as defined in (6.91). The catch, however, is that now the LL and (to a much lesser extent in MFV) RR contributions to B_s mixing no longer vanish. Thus the allowed mass difference, and thereby the arbitrariness of P and S is constrained by mixing.

6.4.4.2 Numerical analysis

Our numerical analysis for this model will focus on the above mentioned assumptions that produce *Scenario C*. Specifically, we begin by assuming an exactly degenerate scalar mass M_H, equal scalar and pseudoscalar lepton couplings and MFV. At the end of this section we also briefly address the consequences of a scalar–pseudoscalar mass difference, which could produce *Scenarios D*.

By imposing MFV on the flavour matrix $\tilde{\Delta}$ introduced in (6.89), it follows that the analogues of $\tilde{\Delta}^{sb}$ in the B_d and K systems are related to it by

$$\tilde{\Delta}^{db} = -\frac{V_{td}^*}{V_{ts}^*}\tilde{\Delta}^{sb}, \qquad \tilde{\Delta}^{ds} = -\frac{m_s}{m_b}\frac{V_{td}^*}{V_{tb}^*}\left[\tilde{\Delta}^{sb}\right]^*. \tag{6.99}$$

Therefore the value taken by $\tilde{\Delta}^{sb}$ should in principle not only satisfy the experimental B_s mixing constraints, but also those of the B_d and K systems. In practice, however, NP contributions in this model to B_d mixing are suppressed by a factor of m_d/m_s relative to B_s mixing and thereby very small. As a result, this model with MFV cannot relieve the current tensions in B_d mixing between theory and experiment [217, 218]. Contributions to neutral Kaon mixing are totally negligible. We therefore proceed to only consider constraints from B_s mixing.

The only contribution that survives in B_s mixing is the LR one and this introduces the following shift in $S(B_s)$ (defined in (6.61)):

$$[\Delta S(B_s)]_{LR} = 2\, r^{LR}\frac{[\tilde{\Delta}^{sb}]^*\tilde{\Delta}^{bs}}{M_H^2\,(V_{ts}V_{tb}^*)^2} = 2\, r_H^{LR}\left(\frac{m_s}{m_b}\right)\frac{|\epsilon|^2\, y_b^2\, y_t^4}{M_H^2}. \tag{6.100}$$

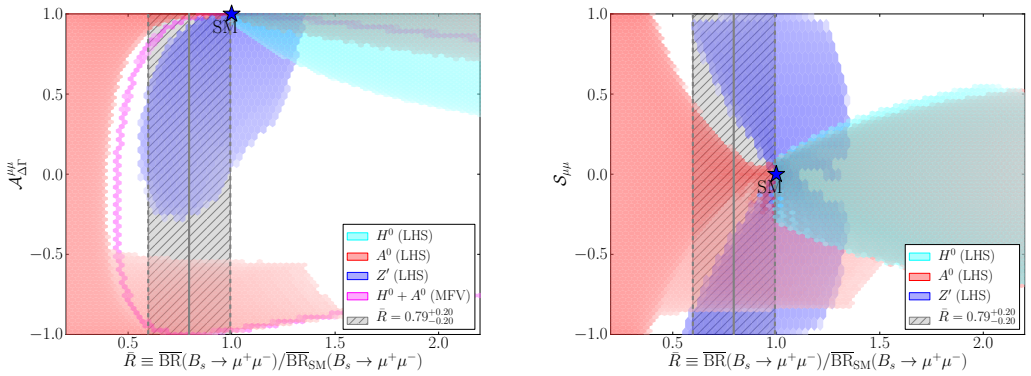

Figure 6.13: Overlay of the correlations for $\overline{R}$ versus $\mathcal{A}^{\mu\mu}_{\Delta\Gamma}$ (left) and $\mathcal{S}_{\mu\mu}$ (right) for the various specific models considered. The lepton couplings are varied in the ranges $|\Delta^{\mu\mu}_{S,P}(H)| \in [0.00, 0.035]$ and $\Delta^{\mu\mu}_{A}(Z') \in [0.0, 1.0]$. All particles are taken to have a mass of 1 TeV.

with r^{LR}_H given in Table 6.3. Although new flavour blind phases are possible in the $\overline{\mathrm{MFV}}$ scenario, wee see that they do not show up in B_s mixing. Therefore the B_s mixing phase ϕ_s remains at its SM value, and is thereby consistent with experiment. In Ref. [210] the $\Delta B = 2$ operator for a 2HDM with MFV is also found to leave flavour-blind phases unconstrained in the limit $|a_0| \gg |a_1|, |a_2|$. In general this is not the case for 2HDM$_{\overline{\mathrm{MFV}}}$ and, as analysed in Refs. [210, 216], ϕ_s can receive NP contributions. Contrary to the mixing phase, ΔM_s does receive a small negative contribution, which is suppressed by m_s/m_b. This suppression due to LR operators within a MFV framework was first pointed out for the MSSM with MFV in Ref. [208]. As we will soon see, the fact that the flavour-blind phases are unconstrained by B_s mixing allows for significant effects in $B_s \to \mu^+\mu^-$ observables.

For both MFV and $\overline{\mathrm{MFV}}$ we find the range:

$$|\tilde{\Delta}^{sb}| \in [0.00196, 0.00530], \tag{6.101}$$

for $M_H = 1\,\mathrm{TeV}$, which, as seen in (6.97), is consistent with the implicit assumption that ϵ should be small. To proceed with numerics for the $B_s \to \mu^+\mu^-$ observables we must set the coupling of H^0 and A^0 to muons. For *Scenario C* this means setting $\tilde{\Delta}^{\mu\mu}$ as defined in (6.91). In order to compare with the single tree-level scalar and pseudoscalar models discussed in the previous section we begin by varying the coupling between $[0.012, 0.024]$ as also done in (6.85).

The left panel of Figure 6.12 shows $\mathcal{A}^{\mu\mu}_{\Delta\Gamma}$ plotted versus $\overline{R}$ for $\overline{\mathrm{MFV}}$ with $M_H = 1\,\mathrm{TeV}$. The allowed region from B_s mixing constraints shown in this plot should be compared with the theoretical situation sketched for *Scenario C* in the left panel of Figure 6.5. By inspection of the theoretical plot one observes that the pure MFV model (with no flavour blind phases) corresponds to the outer border of the $\overline{\mathrm{MFV}}$ region shown. It is

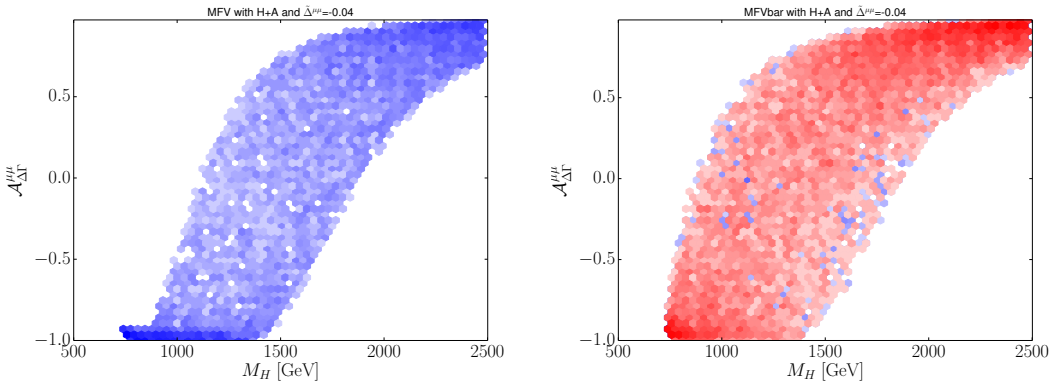

Figure 6.14: The allowed region of $\mathcal{A}_{\Delta\Gamma}^{\mu\mu}$ versus the heavy scalar mass M_H in MFV (left panel) and $\overline{\text{MFV}}$ (right panel). The allowed region satisfies the B_s mixing constraints and falls with the $2\,\sigma$ C.L region of $\overline{R}$: $\overline{R} \in [0.30, 1.80]$.

interesting to observe that in both models a negative $\mathcal{A}_{\Delta\Gamma}^{\mu\mu}$ is possible within the B_s constraints mixing, in contrast to the tree-level models considered above with a single (pseudo)scalar or gauge boson. Because the flavour-blind phase in $\overline{\text{MFV}}$ is completely unconstrained, almost the entire experimentally allowed region is left unconstrained by B_s mixing in this model.

In the right panel of Figure 6.12 we similarly show $\mathcal{S}_{\mu\mu}$ versus $\overline{R}$ in the $\overline{\text{MFV}}$ model for $M_H = 1\,\text{TeV}$. In the pure MFV model $\mathcal{S}_{\mu\mu} = 0$ and therefore these plots are not interesting.

In a 2HDM with large $\tan\beta$, which can generate a decoupled heavy scalar and pseudoscalar as discussed here, the muon coupling is given by

$$\tilde{\Delta}^{\mu\mu} = -2\left(\frac{\sqrt{2}\,m_\mu}{v}\tan\beta\right) = -0.03\left[\frac{\tan\beta}{25}\right], \tag{6.102}$$

which demonstrates that the (pseudo)scalar muon couplings can be larger than what we have assumed so far. In Figure 6.13 we repeat the plots we have shown in Figure 6.12, but now with the muon couplings varied over much larger ranges:

$$|\Delta_{S,P}^{\mu\bar{\mu}}(H^0, A^0)| \in [0.00, 0.035], \qquad |\Delta_{A}^{\mu\bar{\mu}}(Z')| \in [0.0, 1.0]. \tag{6.103}$$

This range of couplings gives a better impression of the full allowed parameter space, at the cost of hiding some of the characteristic differences between the considered models. We do not again show the large allowed region of $H^0 + A^0$ model with $\overline{\text{MFV}}$, but we do show it with pure MFV in the $\mathcal{A}_{\Delta\Gamma}^{\mu\mu}$ versus $\overline{R}$ case (left panel).

In Figure 6.14 we show the allowed range of $\mathcal{A}_{\Delta\Gamma}^{\mu\mu}$ with respect to the heavy scalar mass M_H in the MFV (left panel) and $\overline{\text{MFV}}$ (right panel). In these plots we have fixed the muon couplings to $\tilde{\Delta}^{\mu\bar{\mu}} = -0.03$. The allowed range takes the B_s mixing constraints

into account and falls within the $2\,\sigma$ C.L of $\overline{R}$ as defined in (6.39). We observe that for $M_H \leq 0.75\,\text{TeV}$ negative values of $\mathcal{A}^{\mu\mu}_{\Delta\Gamma}$ are predicted in this scenario, while for $M_H \geq 2.5\,\text{TeV}$ its SM value is approached.

Let us now briefly consider a mass difference between the scalar and pseudoscalar:

$$M_{H^0} \neq M_{A^0}. \tag{6.104}$$

A small mass difference is still consistent with a 2HDM in a decoupling regime, and will still approximately reproduce *Scenario C*. In the presence of a non-zero mass difference the following contribution to the general SM box (see (6.61)) in MFV or a LHS model no longer vanishes:

$$[\Delta S(B_s)]_{LL} = \left(\frac{[\tilde{\Delta}^{sb}]^*}{V_{ts}V_{tb}^*}\right)^2 \left[\frac{r_H^{LL}(M_{H^0})}{M_{H^0}^2} - \frac{r_H^{LL}(M_{A^0})}{M_{A^0}^2}\right] \tag{6.105}$$

and an analogous expression for a RHS model after the replacement $[\tilde{\Delta}^{sb}]^* \to \tilde{\Delta}^{bs}$ and L with $\overline{R}$. In MFV we therefore find:

$$[\Delta S(B_s)]_{LL} = \left(\frac{m_b}{m_s}\right)^2 ([\Delta S(B_s)]_{RR})^* = (\epsilon^*)^2\, y_b^2\, y_t^4 \left[\frac{r_H^{LL}(M_{H^0})}{M_{H^0}^2} - \frac{r_H^{LL}(M_{A^0})}{M_{A^0}^2}\right]. \tag{6.106}$$

We observe that the LL contribution does not suffer from m_s/m_b suppression, although it is suppressed relative to the LR contribution due to a smaller hadronic matrix element (Table 6.2 gives $|r^{LR}| \approx 6|r^{LL}|$) and the splitting between scalar and pseudoscalar masses. Thus whether the SLL contribution or LR dominates depends sensitively on the size of the mass splitting in question. The SRR contribution on the other hand is negligible. Furthermore, the SLL contribution now in principle contains a new flavour-blind phase in ϵ allowing for new CP-violating effects in B_s mixing. The expressions in (6.100) and (6.106) are also valid in a non-MFV framework in which new flavour and CP-violating phases are present in ϵ.

Finally, it is interesting to consider the possibility that the interference between the SM and the pseudoscalar is such that P vanishes in this model. Because the scalar and pseudoscalar couple in the same way to quarks (see (6.89)), there would be no new CP-violating phases in the decay. However, the NP mixing phase ϕ_s^{NP} can still contribute (unless we assume MFV), and we find for $P = 0$ the time-dependent observables:

$$\mathcal{A}^{\mu\mu}_{\Delta\Gamma} = -\cos(\phi_s^{\text{NP}}), \qquad \mathcal{S}_{\mu\mu} = \sin(\phi_s^{\text{NP}}). \tag{6.107}$$

This change in sign for these observables with respect to the SM is a smoking gun signal of scalars dominating in the $B_s \to \mu^+\mu^-$ decay.

6.5 Conclusions

The most immediately relevant result presented in this chapter is the correction of the Standard Model prediction for the $B_s \to \mu^+\mu^-$ branching ratio due to the B_s decay width

difference. Namely, we discussed how in the Standard Model the decay $B_s \to \mu^+\mu^-$ only receives contributions from the heavy mass-eigenstate, which results in a maximal mass-eigenstate rate asymmetry and therefore a maximal correction of $\sim 8\%$. A correction of this size is particularly important because the $B_s \to \mu^+\mu^-$ branching ratio has recently been measured by the LHCb and CMS experiments, and found to lie in the ballpark of the Standard Model prediction.

Aside from addressing the branching ratio correction, we have also performed a detailed phenomenological analysis of the decay-time profile of the $B_s \to \mu^+\mu^-$ decay. Early on in such a time-dependent analysis, when flavour tagging is not experimentally feasible, the mass-eigenstate rate asymmetry $\mathcal{A}^{\mu\mu}_{\Delta\Gamma}$ can be extracted from an effective lifetime measurement. Once flavour tagging is included, also the observable $\mathcal{S}_{\mu\mu}$ becomes available. These two observables complement the branching ratio measurement of this decay, and combinations of the three allow various scenarios of New Physics to be disentangled. Specifically, the presence of new scalar, pseudoscalar or gauge boson particles can potentially be identified, which is not possible on the basis of the branching ratio alone.

The effect of New Physics on the three observables we consider can be described by two the complex parameters S and P, representing amplitudes with a scalar or pseudoscalar lepton density, respectively. These two parameters can in turn be described by the fundamental parameters of a given model. Under plausible model specific assumptions, which we refer to as phenomenological scenarios, combinations of the considered observables allow us to determine S and P, and thereby probe New Physics, in a theoretically clean way. To illustrate the usefulness of this approach, we have grouped several popular extensions of the SM into these phenomenological scenarios (see Table 6.1).

We have further presented numerical analyses for the observables in question for models with tree-level contributions to $B_s \to \mu^+\mu^-$ mediated by heavy gauge bosons, scalars, pseudoscalars and a combination of scalars with pseudoscalars. This analysis takes existing experimental constraints from B_s mixing and $b \to s\ell^+\ell^-$ processes into account. The plots in Figures 6.12 and 6.13 illustrate our general findings. We essentially found that each of the four models considered has a qualitatively different behaviour in "observable" space. In particular, for models with a single new particle with a mass of 1 TeV, be it a gauge boson, scalar or pseudoscalar, negative values of $\mathcal{A}^{\mu\mu}_{\Delta\Gamma}$ require large couplings to muons and a significant deviation of the B_s mixing phase ϕ_s from its SM value. On the contrary, a negative value of $\mathcal{A}^{\mu\mu}_{\Delta\Gamma}$ can naturally be explained in models with both a scalar and pseudoscalar and a common mass $M_H \leq 1.5\,\text{TeV}$. Furthermore, in this setup a deviation of ϕ_s from its SM value is not required, and the branching ratio has a lower bound. An example of such a model is a decoupled two-Higgs doublet model.

Chapter 7

Summary and outlook

In this thesis we have developed strategies to hunt for New Physics using B_s meson decays, which are a particularly promising hunting ground due to the LHCb, CMS and ATLAS detectors at CERN that began operating in early 2010. Our strategies are based on what is called a *bottom up* approach. Specifically, we have in general taken a model independent parameterization for the phenomena of interest with the aim of potentially observing deviations in these parameters from their Standard Model predictions. This is in contrast to a *top down* approach where one assumes a specific model of New Physics, which usually follows from the introduction of some well motivated new symmetry of Nature.

The first run of the LHC is now complete, and the data collected has not revealed any obvious signals of New Physics. Fortunately, the second run, due to start in 2015, promises to deliver an order of magnitude more data. This should translate into a significant increase in precision, with which we can hunt for less obvious New Physics effects. However, in order to identify the presense or absense of such small effects, more precise Standard Model predictions will be necessary. Therefore a key focus of the strategies that we have developed throughout this thesis has been to control the theoretical uncertainties present in the parameters to be probed by experiment. To this end we have primarily made use of the flavour symmetries of strong interactions to relate the hadronic matrix elements that appear in the B_s decay amplitudes to those appearing in their so-called *control channels*.

As we stated in the introduction, it will be important to overconstrain our parameters of interest using several different analysis strategies. Throughout this thesis we have focused in particular on strategies that utilise the mass-eigenstate rate asymmetry of a B_s decay mode. This asymmetry is available in the B_s system due to the difference in lifetimes of its mass-eigenstates, and can be extracted from an untagged time-dependent analysis. As such, it does not depend on the experimental tagging efficiency, and is available much sooner than the CP asymmetries that do rely on flavour tagging. The observable sensitive to this asymmetry that is usually quoted by experiments is the effective lifetime of a B_s decay mode. We have found that effective lifetimes can be a

sensitive probe of New Physics in several different contexts. Furthermore, they contain the missing information necessary to convert between the experimental and theoretical definitions of a B_s branching ratio.

One of the parameters whose consistency we sought to check with the Standard Model is the angle γ of the unitarity triangle. We discussed strategies for extracting this angle from two different B_s decay modes. One mode, $B_s \to D_s^{(*)}K$, involves only tree-level topologies. The other, $B_s \to K^+K^-$, is driven by QCD penguin topologies. In order to control the hadronic uncertainties in the latter mode and extract meaningful physics, it is necessary to relate it using U-spin flavour symmetry to the mode $B_d \to \pi^+\pi^-$. The former mode is theoretically clean, however we still made use of its U-spin relation to $B_d \to D^{(*)}K$ to provide early Standard Model predictions. The LHCb experiment has already published early results for the CP violating observables of both decays. However, the associated errors are still too large to perform the optimal determinations of γ. Over the lifetime of the LHCb experiment these determinations will become possible. It will be interesting to eventually be able to compare the value of γ extracted from tree and penguin topologies. If a disagreement is found it could be an indication of New Physics entering the penguin loop processes.

Another parameter we sought to overconstrain is the B_s^0–$\overline{B}_s^0$ mixing phase ϕ_s. We proposed alternative determinations of this phase that complement the conventional tagged time-dependent angular analysis of the decay mode $B_s \to J/\psi\phi$. In particular, we considered decay modes of the form $B_s \to J/\psi s\bar{s}$ where the $s\bar{s}$ state was taken to have zero spin in order to avoid an angular analysis. Taking the $f_0(980)$ as the $s\bar{s}$ state gives a promising final state for the LHCb experiment, but it introduces additional theoretical uncertainties stemming from the still unknown hadronic composition of this particle. Observing the U-spin related decay mode $B_d \to J/\psi f_0(980)$ would help a lot in solving this mystery and controlling these effects. The composition of the $\eta^{(\prime)}$ isospin singlets is more certain, however their relative ratio of $s\bar{s}$ is not yet known precisely. We discussed how the branching ratio measurements of the modes $B_s \to J/\psi\eta^{(\prime)}$ together with their U-spin related pairs $B_d \to J/\psi\eta^{(\prime)}$ can be used to accurately determine these mixing angles. Unfortunately, the $\eta^{(\prime)}$ are difficult to detect at hadron collider experiments such as LHCb, and therefore the $B_{s,d} \to J/\psi\eta^{(\prime)}$ decay modes are more suitable for future e^+e^- experiments such as Belle-II.

Aside from avoiding an angular analysis, we also explored how we may avoid the flavour tagging present in the conventional determination of the phase ϕ_s. To that end we proposed a strategy involving the effective lifetime measurements for a pair of final states where one is CP-even and the other CP-odd. Specifically, we took the pair of decay modes $B_s \to K^+K^-$ and $B_s \to J/\psi f_0(980)$, respectively. These effective lifetime measurements can be converted into contours in the ϕ_s–y_s plane, with their intersections pinpointing the possible solutions. For a small mixing phase this untagged analysis is not as sensitive as a tagged analysis. However, it still provides a useful cross-check, being sensitive to different experimental systematics and theoretical uncertainties. Furthermore, these theoretical uncertainties are quite robust in this case. It will be

interesting to watch this picture develop as the effective lifetime errors improve from their current 3% uncertainty to below 1%, and additional effective lifetimes such as $B_s \to D_s^+ D_s^-$ and $B_s \to J/\psi K_S$ are also precisely measured.

A highlight of this thesis was our discussion of the famous rare decay $B_s \to \mu^+\mu^-$, the branching ratio of which is very sensitive to New Physics. In particular, we pointed out that the theoretical prediction for its branching ratio requires an $\sim 8\%$ correction, due to B_s decay width difference, in order to be compared with experiment. Because the first measurements of this branching ratio by the LHCb and CMS experiments have found it to lie in the ballpark of the Standard Model, this correction is very relevant. We also discussed how untagged time-dependent measurements of this decay could prove useful in our hunt for New Physics. Specifically, an effective lifetime measurement offers complementary information to the branching ratio in the form of the theoretically clean mass-eigenstate rate asymmetry. Together these two observables have the potential to discriminate between various models of New Physics, which we classified into various phenomenological scenarios. Especially interesting are decoupled two-Higgs doublet models, where the mass-eigenstate rate asymmetry can be maximally different to the Standard Model but still compatible with all existing experimental bounds. A relative precision of 1% for the effective lifetime would translate into an uncertainty of approximately 10% for the mass-eigenstate rate asymmetry. Although a complete study of the experimental potential of this new observable is still pending, an early estimate is that the LHCb experiment should achieve a precision of 5% or better for the 50 fb^{-1} of data expected by the end of its lifetime [183].

Appendix A

Decoupled two-Higgs doublet models

In this appendix we consider two-Higgs doublet models (2HDMs) in the context of down-type flavour changing neutral currents, and in particular the transition $b \to s\,\ell^+\ell^-$. We will focus specifically on such models in the limit that all but the lightest physical scalar particles effectively decouple. This limit has the advantage that it is easy to reconcile with current direct bounds on scalar masses and, as we will show, leads to simpler phenomenological properties.

Consider the two Higgs doublets

$$H_1 = \begin{pmatrix} H_1^+ \\ H_1^0 \end{pmatrix}, \quad H_2 = \begin{pmatrix} H_2^0 \\ H_2^- \end{pmatrix} \tag{A.1}$$

charged under $SU(2)_L \times U(1)_Y$ with hypercharges of $1/2$ and $-1/2$, respectively. Their most general renormalizable and gauge invariant scalar potential is given by [219]

$$\begin{aligned} V = {} & \mu_1^2|H_1|^2 + \mu_2^2|H_2|^2 - (bH_1^T H_2^c + \text{h.c}) + \frac{\lambda_1}{2}|H_1|^4 + \frac{\lambda_2}{2}|H_2|^4 + \lambda_3|H_1|^2|H_2|^2 \\ & + \lambda_4|H_1 H_2|^2 + \left[\frac{\lambda_5}{2}(H_1^T H_2^c)^2 - \lambda_6|H_1|^2 H_1^T H_2^c - \lambda_7|H_2|^2 H_1^T H_2^c + \text{h.c}\right], \end{aligned} \tag{A.2}$$

where

$$H_i^c \equiv (-i)\sigma_2 H_i^*. \tag{A.3}$$

In principle the couplings b, λ_5, λ_6 and λ_7 can all be complex. However, we can always redefine the Higgs fields H_1 and H_2 so that the b coupling is real.

Upon electroweak symmetry breaking we require that the neutral components gain a vacuum expectation value: $\langle H_1^0 \rangle = v_1/\sqrt{2}$ and $\langle H_2^0 \rangle = v_2/\sqrt{2}$ with $v^2 = v_1^2 + v_2^2 = (\sqrt{2}\,G_F)^{-1}$. A useful change of basis is then given by the rotation[1]

$$\begin{pmatrix} \Phi_v \\ \Phi_H \end{pmatrix} = \begin{pmatrix} c_\beta & s_\beta \\ -s_\beta & c_\beta \end{pmatrix} \begin{pmatrix} H_1 \\ H_2^c \end{pmatrix}, \tag{A.4}$$

[1]We will use the notation of Ref. [210] throughout this appendix.

where $c_\beta \equiv \cos\beta = v_1/v$ and $s_\beta \equiv \sin\beta = v_2/v$. In this basis only Φ_v contains a non-zero vacuum expectation value, and the fields can be decomposed into neutral, charged and goldstone bosons:

$$\Phi_v = \begin{pmatrix} G^+ \\ \frac{1}{\sqrt{2}}(v + S_1 + iG^0) \end{pmatrix}, \quad \Phi_H = \begin{pmatrix} H^+ \\ \frac{1}{\sqrt{2}}(S_2 + iS_3) \end{pmatrix}. \tag{A.5}$$

The ratio of the vacuum expectation values is given by $t_\beta \equiv \tan\beta = v_2/v_1$.

The neutral scalars S_1, S_2 and S_3 pick up masses due to the spontaneous symmetry breaking and can in principle be mixed. These mixed mass terms are given by their quadratic couplings at the minimum of the potential. As the $U(1)_Q$ symmetry of quantum electrodynamics remains unbroken, we may set the charged fields $H_1^\pm$ and $H_2^\pm$ in the potential to zero at the minimum. The resulting neutral scalar potential is then

$$\begin{aligned} V_{\text{neutral}} = {} & \mu_1^2|H_1^0|^2 + \mu_2^2|H_2^0|^2 - b(H_1^0 H_2^0 + H_1^{0*} H_2^{0*}) + \frac{\lambda_1}{2}|H_1^0|^4 + \frac{\lambda_2}{2}|H_2^0|^4 \\ & + (\lambda_3 + \lambda_4)|H_1^0|^2|H_2^0|^2 + \frac{\lambda_5}{2}(H_1^0 H_2^0)^2 + \frac{\lambda_5^*}{2}(H_1^{0*} H_2^{0*})^2 \\ & - \lambda_6|H_1^0|^2 H_1^0 H_2^0 - \lambda_6^*|H_1^0|^2 H_1^{0*} H_2^{0*} - \lambda_7|H_2^0|^2 H_1^0 H_2^0 - \lambda_7^*|H_2^0|^2 H_1^{0*} H_2^{0*}. \end{aligned} \tag{A.6}$$

The critical points $\partial V_{\text{neutral}}/\partial H_1^0 = 0$ and $\partial V_{\text{neutral}}/\partial H_2^0 = 0$ give the minimisation conditions

$$\begin{aligned} \mu_1^2 &= b\, t_\beta - \frac{v^2}{2}\left\{\lambda_1 c_\beta^2 + [\lambda_3 + \lambda_4 + \text{Re}(\lambda_5)]\, s_\beta^2 - \text{Re}(\lambda_6) 3\, c_\beta\, s_\beta - \text{Re}(\lambda_7)\, t_\beta\, s_\beta^2\right\}, \\ \mu_2^2 &= b\, t_\beta^{-1} - \frac{v^2}{2}\left\{\lambda_2 s_\beta^2 + [\lambda_3 + \lambda_4 + \text{Re}(\lambda_5)]\, c_\beta^2 - \text{Re}(\lambda_6)\, t_\beta^{-1}\, c_\beta^2 - \text{Re}(\lambda_7) 3\, c_\beta\, s_\beta\right\}, \end{aligned} \tag{A.7}$$

respectively. Substituting (A.7) into (A.6) and changing to the basis in (A.4), the neutral scalars S_3 couples to S_1 and S_2 as follows:

$$\begin{aligned} V \ni {} & \frac{3}{4}v^2\left[\sin 2\beta\, \text{Im}(\lambda_5) - \cos 2\beta\, \text{Im}(\lambda_6 - \lambda_7) - \text{Im}(\lambda_6 + \lambda_7)\right] S_1\, S_3 \\ & + \frac{1}{2}v^2\left[\cos 2\beta\, \text{Im}(\lambda_5) + \sin 2\beta\, \text{Im}(\lambda_6 - \lambda_7)\right] S_2\, S_3. \end{aligned} \tag{A.8}$$

Thus we observe that in general the neutral scalars S_1, S_2 and S_3 all mix, and their diagonalisation gives three mass-eigenstates that are not CP eigenstates. If the scalar potential is CP invariant i.e. if $\text{Im}(\lambda_{5,6,7}) = 0$, then the above couplings vanish and S_3 will be a mass-eigenstate. In this case it will be a CP-odd pseusoscalar and is often denoted by A^0. The remaining scalars S_1 and S_2 are then CP-even, and in general mix to give the two mass-eigenstates H^0 and h^0.

The decoupling limit

Let us first consider the case that the scalar potential is CP invariant, so that all the couplings are real. Then, after spontaneous symmetry breaking, the physical scalar masses are given by [219]

$$M_A^2 = \frac{b}{s_\beta c_\beta} - \frac{1}{2}v^2(2\lambda_5 - \lambda_6\, t_\beta^{-1} - \lambda_7 t_\beta), \tag{A.9}$$

$$M_{H^\pm}^2 = M_A^2 + \frac{1}{2}v^2(\lambda_5 - \lambda_4), \tag{A.10}$$

$$\begin{pmatrix} M_H^2 & 0 \\ 0 & M_h^2 \end{pmatrix} = \begin{pmatrix} c_\alpha & s_\alpha \\ -s_\alpha & c_\alpha \end{pmatrix} \mathcal{M} \begin{pmatrix} c_\alpha & -s_\alpha \\ s_\alpha & c_\alpha \end{pmatrix}, \tag{A.11}$$

with

$$\begin{aligned} \mathcal{M} \equiv \quad & M_A^2 \begin{pmatrix} s_\beta^2 & -s_\beta c_\beta \\ -s_\beta c_\beta & c_\beta^2 \end{pmatrix} \\ & + v^2 \begin{pmatrix} \lambda_1 c_\beta^2 + 2\lambda_6 s_\beta c_\beta + \lambda_5 s_\beta^2 & (\lambda_3+\lambda_4) s_\beta c_\beta + \lambda_6 c_\beta^2 + \lambda_7 s_\beta^2 \\ (\lambda_3+\lambda_4) s_\beta c_\beta + \lambda_6 c_\beta^2 + \lambda_7 s_\beta^2 & \lambda_2 s_\beta^2 + 2\lambda_7 s_\beta c_\beta + \lambda_5 c_\beta^2 \end{pmatrix}. \end{aligned} \tag{A.12}$$

We observe that if $M_A^2 \gg |\lambda_i| v^2$ for $i \in \{1, \ldots, 7\}$ the contribution of the v^2 terms to $\mathcal{M}$ is very small. Assuming $|\lambda_i| \lesssim \mathcal{O}(1)$, the condition to diagonalise (A.11) in this limit is then

$$\sin(\alpha - \beta)\cos(\alpha - \beta) - \mathcal{O}\left(\frac{v^2}{M_A^2}\right) = 0, \tag{A.13}$$

and for $M_H > M_h$ (by definition) that $\sin^2(\alpha - \beta) > \cos^2(\alpha - \beta)$, implying:

$$\cos(\alpha - \beta) = \mathcal{O}\left(\frac{v^2}{M_A^2}\right), \tag{A.14}$$

$$M_h = \mathcal{O}\left(v\right), \tag{A.15}$$

$$M_H = M_A + \mathcal{O}\left(\frac{v^2}{M_A}\right), \tag{A.16}$$

$$M_{H^\pm} = M_A + \mathcal{O}\left(\frac{v^2}{M_A}\right). \tag{A.17}$$

This is the so-called *decoupling regime*. It is characterized by two separate mass scales: the electroweak scale v and a second scale $M_A \gg v$. If the particles of order M_A are integrated out, then we are left with a theory that closely resembles the one-Higgs-doublet SM i.e the lighter neutral scalar h is indistinguishable from the SM Higgs boson. Note that we can always choose the phases of the scalar Higgs doublets so that v_1 and v_2 are positive, so that $0 \leq \beta \leq \pi/2$. The decoupling limit then corresponds to:

$$\alpha \to \beta - \pi/2. \tag{A.18}$$

By inspection of the pseudoscalar mass in (A.9), we see that one way to realise the decoupling regime is to have $t_\beta \gg 1$ and $b \gtrsim \lambda_i v^2$ for $i \in \{1, \ldots, 7\}$. If $\lambda_7 < 0$ we additionally require that $\lambda_7 t_\beta = \mathcal{O}(\lambda_i)$ for $i \in \{1, \ldots, 6\}$.

To consider the case of explicit CP violation in the scalar potential, we begin by assuming that $t_\beta \gg 1$ and subsequently expand for small c_β [210]. In the basis given in (A.4), we then find the following mixing matrix for the neutral scalars:

$$V \ni \frac{1}{2} \begin{pmatrix} S_1 \\ S_2 \\ S_3 \end{pmatrix}^T \mathcal{M}_S \begin{pmatrix} S_1 \\ S_2 \\ S_3 \end{pmatrix}, \tag{A.19}$$

$$\begin{aligned} \mathcal{M}_S = & \begin{pmatrix} v^2 \lambda_2 & v^2 \operatorname{Re}(\lambda_7) & -\frac{3}{2} v^2 \operatorname{Im}(\lambda_7) \\ v^2 \operatorname{Re}(\lambda_7) & \frac{1}{c_\beta} \left[b + \frac{1}{2} v^2 \operatorname{Re}(\lambda_7) \right] & -\frac{1}{2} v^2 \operatorname{Im}(\lambda_5) \\ -\frac{3}{2} v^2 \operatorname{Im}(\lambda_7) & -\frac{1}{2} v^2 \operatorname{Im}(\lambda_5) & \frac{1}{c_\beta} \left[b + \frac{1}{2} v^2 \operatorname{Re}(\lambda_7) \right] - v^2 \operatorname{Re}(\lambda_5) \end{pmatrix} \\ & + c_\beta \begin{pmatrix} -4\, v^2 \operatorname{Re}(\lambda_7) & v^2 \left[\lambda_2 - \lambda_{345} \right] & \frac{3}{2} v^2 \operatorname{Im}(\lambda_5) \\ v^2 \left[\lambda_2 - \lambda_{345} \right] & \frac{1}{2}\, b - \frac{1}{4}\, v^2 \operatorname{Re}(6\, \lambda_6 - 7\, \lambda_7) & v^2 \operatorname{Im}(\lambda_6 - \lambda_7) \\ \frac{3}{2} v^2 \operatorname{Im}(\lambda_5) & v^2 \operatorname{Im}(\lambda_6 - \lambda_7) & \frac{1}{2}\, b - \frac{1}{4}\, v^2 \operatorname{Re}(2\, \lambda_6 - \lambda_7) \end{pmatrix} \\ & + \mathcal{O}\left(c_\beta^2\right), \end{aligned} \tag{A.20}$$

where $\lambda_{345} \equiv \lambda_3 + \lambda_4 + \operatorname{Re}(\lambda_5)$. We observe that λ_7 dominates the mixing of S_1 in the large t_β limit. Regardless, if we assume $b \gtrsim \lambda_i v^2$, S_1 effectively decouples from S_2 and S_3 and becomes the lightest mass-eigenstate h_1^0. We are then left with finding the mass-eigenstates for the mixed system S_2–S_3, which we will denote by h_2^0 and h_3^0. Diagonalising the 2×2 submatrix gives:

$$V \ni \frac{1}{2} \begin{pmatrix} S_2 \\ S_3 \end{pmatrix}^T \mathcal{M}_{S_{2,3}} \begin{pmatrix} S_2 \\ S_3 \end{pmatrix} = \frac{1}{2} \begin{pmatrix} h_2^0 \\ h_3^0 \end{pmatrix}^T \begin{pmatrix} M_{h_2^0}^2 & 0 \\ 0 & M_{h_3^0}^2 \end{pmatrix} \begin{pmatrix} h_2^0 \\ h_3^0 \end{pmatrix}, \tag{A.21}$$

where

$$\begin{pmatrix} S_2 \\ S_3 \end{pmatrix} = \begin{pmatrix} c_\chi & s_\chi \\ -s_\chi & c_\chi \end{pmatrix} \begin{pmatrix} h_2^0 \\ h_3^0 \end{pmatrix}, \tag{A.22}$$

and

$$\chi = \frac{\theta_5}{2} + c_\beta \left(\frac{|\lambda_6| \sin(\theta_5 - \theta_6) + |\lambda_7| \sin(\theta_5 - \theta_7)}{|\lambda_5|} \right) + \mathcal{O}(c_\beta^2) \quad \text{radians}, \tag{A.23}$$

Here we have defined for convenience $\lambda_i = |\lambda_i| e^{i\theta_i}$. The corresponding masses are:

$$M^2_{h^0_2} = b\left\{\frac{1}{c_\beta} + c_\beta\right\} + \frac{1}{2}\,v^2\left\{\frac{1}{c_\beta}|\lambda_7|\cos\theta_7 + |\lambda_5|\,(1-\cos\theta_5)\right\} - c_\beta\frac{1}{2}\,v^2\left\{|\lambda_6|\,[\cos\theta_6 + 2\cos(\theta_5-\theta_6)] - |\lambda_7|\left[\frac{3}{2}\cos\theta_7 + 2\cos(\theta_5-\theta_7)\right]\right\}, \tag{A.24}$$

$$M^2_{h^0_3} = b\left\{\frac{1}{c_\beta} + c_\beta\right\} + \frac{1}{2}\,v^2\left\{\frac{1}{c_\beta}|\lambda_7|\cos\theta_7 - |\lambda_5|\,(1+\cos\theta_5)\right\} - c_\beta\frac{1}{2}\,v^2\left\{|\lambda_6|\,[\cos\theta_6 - 2\cos(\theta_5-\theta_6)] - |\lambda_7|\left[\frac{3}{2}\cos\theta_7 - 2\cos(\theta_5-\theta_7)\right]\right\}. \tag{A.25}$$

Observe that in the large t_β decoupling regime $M_{h^0_2} \approx M_{h^0_3}$. In the CP conserving limit $\mathrm{Im}(\lambda_{5,6,7}) \to 0$ we recover $\chi \to 0$.

Scalar mediated $b \to s\ell^+\ell^-$ transitions

The most general quark Yukawa-term Lagrangian in a general 2HDM is [219]

$$-\mathcal{L}^{\rm gen}_{{\rm Y},q} = \bar{Q}_{\rm L} X_{d1} D_R H_1 + \bar{Q}_{\rm L} X_{d2} D_R H_2^c + \bar{Q}_{\rm L} X_{u1} U_R H_1^c + \bar{Q}_{\rm L} X_{u2} U_R H_2 + \text{h.c}, \tag{A.26}$$

with H_i^c defined in (A.3). The presence of a symmetry under which only D_R and H_1 transform, such as $U(1)_{\rm PQ}$ Peccei-Quinn symmetry or a discrete alternative, will forbid the couplings X_{d2} and X_{u1} at tree level. However, loop processes due to $U(1)_{\rm PQ}$ breaking terms, or from elsewhere, can reintroduce these couplings. Such breaking terms are necessarily present in the scalar potential, because without them the physical pseudoscalar A^0 would be massless. So even if such symmetries are present, (A.26) can be interpreted as an *effective* Lagrangian.

To emphasise the origin of the FCNCs, we change to the Higgs doublet basis given in (A.4). In this basis we have the following down-type quark couplings

$$-\mathcal{L}^{\rm gen}_{{\rm Y},d} = \bar{D}_{\rm L}\left[\frac{\sqrt{2}}{v} M_d \Phi^0_v + Z_d \Phi^0_H\right] D_R + \text{h.c}, \tag{A.27}$$

where

$$M_d = \frac{1}{\sqrt{2}}\,(v_1 X_{d1} + v_2 X_{d2})\,, \quad Z_d = c_\beta X_{d2} - s_\beta X_{d1}. \tag{A.28}$$

The main point is that for general matrices in flavour space X_{d1} and X_{d2}, it is not possible to simultaneously diagonalise the mass matrix M_d and the coupling matrix Z_d by redefining the down-type quark fields D. The residual off-diagonal terms in Z_d after

diagonalisation of M_d lead to FCNCs. We will consider only the FCNCs for down-type quarks:

$$\begin{aligned} -\mathcal{L}^{\text{eff}}_{\text{FCNC},d} &= \frac{1}{\sqrt{2}}\bar{D}_{\text{L}} Z_d D_R \left[S_2 + i\, S_3\right] + \text{h.c} \\ &= \frac{1}{\sqrt{2}}\bar{D}_{\text{L}} Z_d D_R \left[(c_\chi - i s_\chi)\, h^0_2 + (s_\chi + i c_\chi)\, h^0_3\right] + \text{h.c.} \end{aligned} \tag{A.29}$$

where in the second line we have changed to the physical basis in the large t_β decoupling regime.

We will assume that the dominant contribution to the $b \to s\, l^+ l^-$ transition is from an S-channel neutral Higgs boson. That is, we neglect box and self-energy diagrams as well as the SM contributions. This approximation of dropping box diagrams is often made in the literature to simplify the t_β discussion. For example: in supersymmetric [208] and non-supersymmetric [207] 2HDMs[2].

For the couplings of the neutral Higgs bosons to leptons we assume a flavour diagonal structure and no CP violation. These assumptions give the following leptonic couplings to the neutral scalar Higgs bosons:

$$\begin{aligned} -\mathcal{L}_{\text{Y},l} &= \bar{L}_L\, \text{diag}(y_e, y_\mu, y_\tau)\, E_R\, H_1 + \text{h.c} \\ &\ni \sum_{l=e,\mu,\tau} \frac{m_l}{v}\, \bar{l}\, \left[S_1 - t_\beta S_2 - i\gamma_5 t_\beta S_3\right]\, l \\ &= \sum_{l=e,\mu,\tau} \frac{m_l\, t_\beta}{v}\, \bar{l}\, \left[\frac{h^0_1}{t_\beta} - (c_\chi - i\gamma_5 s_\chi)\, h^0_2 - (s_\chi + i\gamma_5 c_\chi)\, h^0_3\right]\, l \end{aligned} \tag{A.30}$$

where we used $y_l = \sqrt{2}\, m_l / v\, c_\beta$, and the last line is expressed in the physical basis in the large t_β decoupling limit discussed earlier.

Combining the effective down-type quark FCNC given in (A.29) with the Higgs lepton couplings in (A.30) and integrating out the Higgs degrees of freedom gives:

$$\begin{aligned} \mathcal{H}_{\text{eff}} = \quad & \frac{m_l\, t_\beta}{\sqrt{2}v}\, (Z_d)_{ij}\, \bar{D}_i P_R D_j\, \bar{l} l \left[\frac{(c_\chi - i\, s_\chi) c_\chi}{M^2_{h^0_2}} + \frac{(s_\chi + i\, c_\chi) s_\chi}{M^2_{h^0_3}}\right] \\ & + \frac{m_l\, t_\beta}{\sqrt{2}v}\, (Z_d)_{ij}\, \bar{D}_i P_R D_j\, \bar{l}\gamma_5 l \left[\frac{(c_\chi - i\, s_\chi)(-i s_\chi)}{M^2_{h^0_2}} + \frac{(s_\chi + i\, c_\chi)(i c_\chi)}{M^2_{h^0_3}}\right] + \text{h.c.} \end{aligned} \tag{A.31}$$

As we are assuming the large t_β decoupling regime we have that $M_{h^0_2} \approx M_{h^0_3}$ and thus in this limit

$$\begin{aligned} \mathcal{H}_{\text{eff}} = & -\frac{m_l\, t_\beta}{\sqrt{2}v\, M^2_H}\, (Z_d)_{i3} \left[\bar{D}_i P_R b\, \bar{l} l - \bar{D}_j P_R b\, \bar{l}\gamma_5 l\right] \\ & - \frac{m_l\, t_\beta}{\sqrt{2}v\, M^2_H} \left(Z^\dagger_d\right)_{i3} \left[\bar{D}_i P_L b\, \bar{l} l + \bar{D}_i P_L b\, \bar{l}\gamma_5 l\right] + \text{h.c}, \end{aligned} \tag{A.32}$$

[2]Computationally they set $g = 0$ i.e. they turn off gauge interactions.

where $M_H \equiv M_{h_3^0} \approx M_{h_2^0}$. Comparing now with the low-energy effective Hamiltonian in (6.7), we find

$$C_S = -C_P = \frac{m_l\, v}{M_H^2\, m_b} \frac{\sqrt{2}\,\pi\, t_\beta}{\alpha} \left[\frac{\left(Z_d\right)_{i3}}{V_{tq}^* V_{tb}} \right],$$
$$C_S' = +C_P' = \frac{m_l\, v}{M_H^2\, m_b} \frac{\sqrt{2}\,\pi\, t_\beta}{\alpha} \left[\frac{\left(Z_d^\dagger\right)_{i3}}{V_{tq}^* V_{tb}} \right]. \tag{A.33}$$

Thus independent of the type of 2HDM, $|C_S^{(\prime)}| \approx |C_P^{(\prime)}|$ in the *decoupling regime with large* t_β. Furthermore, any CP violating phase coming from Z_d is common to both Wilson coefficients and explicit CPV phases in the Higgs potential have no effect.

Minimal Flavour Violation

Minimal Flavour Violation (MFV) is a formalism that protects against any additional flavour structure or CP violation beyond what is already present in the CKM matrix, while still allowing additional, higher-dimensional, operators [209]. This is in contrast to *Constrained Minimal Flavour Violation*, where only the existing SM operators are allowed. MFV achieves its goal by insisting that the flavour symmetry group

$$SU(3)_{Q_L} \times SU(3)_{U_R} \times SU(3)_{D_R} \tag{A.34}$$

is only broken by the background values of auxiliary *spurion* fields Y_U and Y_D, which transform as $(3, \bar{3}, 1)$ and $(3, 1, \bar{3})$ under this group. The Yukawa terms in (A.26) are then kept formally flavour group invariant as long as X_{ui} and X_{di} contain combinations of Y_U and Y_D so that they too transform as $(3, \bar{3}, 1)$ and $(3, 1, \bar{3})$, respectively. Then to lowest order, $\mathcal{O}(Y^1)$, $X_{di} = c_{di} Y_D$ and $X_{ui} = c_{ui} Y_U$ for arbitrary coefficients $c_{di}, c_{ui} \in \mathbb{C}$. This thus ensures that

$$M_d \propto Y_D \propto Z_d, \tag{A.35}$$

and therefore no tree-level down-type quark FCNCs (and similarly for up-type quarks).

We are free to re-define $Y_D \equiv X_{d1}$ and $Y_U \equiv X_{u2}$, which then gives the expansion:

$$X_{d2} = (\epsilon_0 + \epsilon_1 Y_D Y_D^\dagger + \epsilon_2 Y_U Y_U^\dagger + \ldots) Y_D. \tag{A.36}$$

We are further free to rotate the quark fields so that the background values of the spurions are

$$Y_D = \mathrm{diag}(\hat{y}_d, \hat{y}_s, \hat{y}_b) \equiv \hat{\lambda}_d, \tag{A.37}$$
$$Y_U = \hat{V}^\dagger \times \mathrm{diag}(\hat{y}_d, \hat{y}_s, \hat{y}_b) \equiv \hat{V}^\dagger \hat{\lambda}_u, \tag{A.38}$$

where the hat indicates contributions from $\epsilon_i^{(\prime)} \neq 0$ e.g. in the limit $\epsilon_i^{(\prime)} = 0$ we recover $\hat{V} = V_{\mathrm{CKM}}$. The $\epsilon_i^{(\prime)}$ parameters are assumed to be small as they are normally taken to represent the loop induced $U(1)_{\mathrm{PQ}}$ breaking.

In the large t_β limit, the smallness of the bottom quark relative to the top quark mass is attributed to this vacuum expectation value ratio and thereby the bottom Yukawa coupling can be $\hat{y}_b = \mathcal{O}(1)$. The remaining Yukawa couplings are, however, still negligible: $y_s/y_b \propto m_s/m_b$. Thus

$$Y_D Y_D^\dagger \approx \mathrm{diag}(0,0,\hat{y}_b^2), \quad \left(Y_U Y_U^\dagger\right)_{ij} \approx y_t^2 \hat{V}_{3i}^* \hat{V}_{3j}. \tag{A.39}$$

Defining

$$\Delta \equiv \frac{1}{\hat{y}_b^2} Y_D Y_D^\dagger, \quad (\hat{\lambda}_{\mathrm{FC}})_{ij} \equiv \begin{cases} (Y_U Y_U^\dagger)_{ij} & : \ i \neq j \\ 0 & : \ i = j \end{cases} \tag{A.40}$$

we have to lowest order in the off-diagonal terms:

$$X_{d2} = \left(\epsilon_0 + \epsilon_1 \Delta + \epsilon_2 \hat{\lambda}_{\mathrm{FC}} + \epsilon_3 \hat{\lambda}_{\mathrm{FC}} \Delta + \epsilon_4 \Delta \hat{\lambda}_{\mathrm{FC}}\right) \hat{\lambda}_d. \tag{A.41}$$

Now diagonalising the mass matrix for the down-type quark sector gives [209]

$$Z_d = \frac{1}{\sin\beta} \left[a_0 \lambda_{\mathrm{FC}} + a_1 \lambda_{\mathrm{FC}} \Delta + a_2 \Delta \lambda_{\mathrm{FC}}\right] \lambda_d, \tag{A.42}$$

where a_0, a_1 and a_2 depend on ϵ_i and t_β. For our purposes we only need:

$$a_0 + a_1 = \frac{t_\beta}{y_t^2} \left[\frac{\epsilon_2 + \epsilon_3}{[1 + (\epsilon_0 + \epsilon_1) t_\beta]\,[1 + (\epsilon_0 + \epsilon_1 - \epsilon_2 - \epsilon_3) t_\beta]}\right]. \tag{A.43}$$

In the large t_β limit $\epsilon_i t_\beta = \mathcal{O}(1)$ is possible, and thus these FCNC couplings can be sizable. However, processes such as $s \to d$ are now protected by the flavour structure, as it resembles that of the SM.

Consider now the scalar coefficients $C_{S,P}^{(\prime)}$ as given in (A.33) for the transition $b \to q\, l^+ l^-$ for $q \in \{d, s\}$. For $q \neq b$, we have $\bar{q}\Delta = 0$ as well as $\Delta b = b$, such that

$$(Z_d)_{i3} = \frac{1}{\sin\beta} (a_0 + a_1) y_t^2 V_{tb} V_{ti}^*\, y_b, \tag{A.44}$$

$$(Z_d^\dagger)_{i3} = \frac{1}{\sin\beta} (a_0^* + a_1^*) y_t^2 V_{tb} V_{ti}^*\, y_q. \tag{A.45}$$

This thereby gives

$$\begin{aligned} C_S = -C_P &= \frac{1}{m_b} \frac{\sqrt{2}\pi}{2 M_H^2 G_F \alpha} y_l\, y_b\, y_t^2\, (a_0 + a_1) \\ &= \frac{2\pi\, m_l}{M_H^2\, \alpha}\, t_\beta^3 \left[\frac{\epsilon_2 + \epsilon_3}{[1 + (\epsilon_0 + \epsilon_1) t_\beta]\,[1 + (\epsilon_0 + \epsilon_1 - \epsilon_2 - \epsilon_3) t_\beta]}\right], \end{aligned} \tag{A.46}$$

$$\begin{aligned} C_S' = +C_P' &= \frac{1}{m_b} \frac{\sqrt{2}\pi}{2 M_H^2 G_F \alpha} y_l\, y_q\, y_t^2\, (a_0^* + a_1^*) \\ &= \frac{m_q}{m_b} \frac{2\pi\, m_l}{M_H^2\, \alpha}\, t_\beta^3 \left[\frac{\epsilon_2^* + \epsilon_3^*}{[1 + (\epsilon_0^* + \epsilon_1^*) t_\beta]\,[1 + (\epsilon_0^* + \epsilon_1^* - \epsilon_2^* - \epsilon_3^*) t_\beta]}\right], \end{aligned} \tag{A.47}$$

$$\tag{A.48}$$

in the *decoupling regime with large* t_β. We find $C'_S = C'_P \approx 0$ in the limit $m_q/m_b \approx 0$. Note that the t_β scales with a third power.

Bibliography

[1] G. Bertone, D. Hooper, and J. Silk, *Particle dark matter: Evidence, candidates and constraints*, Phys.Rept. **405** (2005) 279–390, [hep-ph/0404175].

[2] S. P. Martin, *A Supersymmetry primer*, hep-ph/9709356.

[3] H. Baer and X. Tata, *Weak scale supersymmetry: From superfields to scattering events*, .

[4] **ATLAS** Collaboration, G. Aad et al., *Observation of a new particle in the search for the Standard Model Higgs boson with the ATLAS detector at the LHC*, Phys.Lett. **B716** (2012) 1–29, [arXiv:1207.7214].

[5] **CMS** Collaboration, S. Chatrchyan et al., *Observation of a new boson at a mass of 125 GeV with the CMS experiment at the LHC*, Phys.Lett. **B716** (2012) 30–61, [arXiv:1207.7235].

[6] **ATLAS** Collaboration. https://twiki.cern.ch/twiki/bin/view/AtlasPublic/SupersymmetryPublicResults.

[7] **CMS** Collaboration. https://twiki.cern.ch/twiki/bin/view/CMSPublic/SUSYSMSSummaryPlots8TeV.

[8] E. Bertuzzo, *SUSY after LHC8: a brief overview*, arXiv:1307.0318.

[9] A. Sakharov, *Violation of CP Invariance, c Asymmetry, and Baryon Asymmetry of the Universe*, Pisma Zh.Eksp.Teor.Fiz. **5** (1967) 32–35.

[10] J. Christenson, J. Cronin, V. Fitch, and R. Turlay, *Evidence for the 2 pi Decay of the k(2)0 Meson*, Phys.Rev.Lett. **13** (1964) 138–140.

[11] **BaBar** Collaboration, B. Aubert et al., *Observation of CP violation in the B^0 meson system*, Phys.Rev.Lett. **87** (2001) 091801, [hep-ex/0107013].

[12] **Belle** Collaboration, K. Abe et al., *Observation of large CP violation in the neutral B meson system*, Phys.Rev.Lett. **87** (2001) 091802, [hep-ex/0107061].

[13] **Tevatron B Working Group** Collaboration. http://tevbwg.fnal.gov/results/Summer2009_betas.

[14] **LHCb** Collaboration, R. Aaij et al., *Differential branching fraction and angular analysis of the decay $B^0 \to K^{*0}\mu^+\mu^-$*, JHEP **1308** (2013) 131, [arXiv:1304.6325].

[15] **LHCb** Collaboration, R. Aaij et al., *Measurement of form-factor independent observables in the decay $B^0 \to K^{*0}\mu^+\mu^-$*, arXiv:1308.1707.

[16] **LHCb** Collaboration, R. Aaij et al., *Measurement of the isospin asymmetry in $B \to K^{(*)}\mu^+\mu^-$ decays*, JHEP **1207** (2012) 133, [arXiv:1205.3422].

[17] **Particle Data Group** Collaboration, J. Beringer et al., *Review of Particle Physics (RPP)*, Phys.Rev. **D86** (2012) 010001.

[18] P. W. Higgs, *Broken Symmetries and the Masses of Gauge Bosons*, Phys.Rev.Lett. **13** (1964) 508–509.

[19] F. Englert and R. Brout, *Broken Symmetry and the Mass of Gauge Vector Mesons*, Phys.Rev.Lett. **13** (1964) 321–323.

[20] N. Cabibbo, *Unitary Symmetry and Leptonic Decays*, Phys.Rev.Lett. **10** (1963) 531–533.

[21] M. Kobayashi and T. Maskawa, *CP Violation in the Renormalizable Theory of Weak Interaction*, Prog.Theor.Phys. **49** (1973) 652–657.

[22] B. Pontecorvo, *Mesonium and anti-mesonium*, Sov.Phys.JETP **6** (1957) 429.

[23] B. Pontecorvo, *Neutrino Experiments and the Problem of Conservation of Leptonic Charge*, Sov.Phys.JETP **26** (1968) 984–988.

[24] Z. Maki, M. Nakagawa, and S. Sakata, *Remarks on the unified model of elementary particles*, Prog.Theor.Phys. **28** (1962) 870–880.

[25] M. Gonzalez-Garcia and M. Maltoni, *Phenomenology with Massive Neutrinos*, Phys.Rept. **460** (2008) 1–129, [arXiv:0704.1800].

[26] S. Glashow, J. Iliopoulos, and L. Maiani, *Weak Interactions with Lepton-Hadron Symmetry*, Phys.Rev. **D2** (1970) 1285–1292.

[27] J. Laiho, E. Lunghi, and R. S. Van de Water, *Lattice QCD inputs to the CKM unitarity triangle analysis*, Phys. Rev. **D81** (2010) 034503, [arXiv:0910.2928]. Updates available on http://latticeaverages.org/.

[28] K. Chetyrkin, J. Kuhn, A. Maier, P. Maierhofer, P. Marquard, et al., *Charm and Bottom Quark Masses: An Update*, Phys.Rev. **D80** (2009) 074010, [arXiv:0907.2110].

[29] L. Wolfenstein, *Parametrization of the Kobayashi-Maskawa Matrix*, Phys.Rev.Lett. **51** (1983) 1945.

[30] A. J. Buras, M. E. Lautenbacher, and G. Ostermaier, *Waiting for the top quark mass, K+ → pi+ neutrino anti-neutrino, B(s)0 - anti-B(s)0 mixing and CP asymmetries in B decays*, Phys.Rev. **D50** (1994) 3433–3446, [hep-ph/9403384].

[31] C. Jarlskog, *A Basis Independent Formulation of the Connection Between Quark Mass Matrices, CP Violation and Experiment*, Z.Phys. **C29** (1985) 491–497.

[32] R. Feynman and M. Gell-Mann, *Theory of Fermi interaction*, Phys.Rev. **109** (1958) 193–198.

[33] K. G. Wilson, *Nonlagrangian models of current algebra*, Phys.Rev. **179** (1969) 1499–1512.

[34] K. Wilson and W. Zimmermann, *Operator product expansions and composite field operators in the general framework of quantum field theory*, Commun.Math.Phys. **24** (1972) 87–106.

[35] G. Buchalla, A. J. Buras, and M. E. Lautenbacher, *Weak decays beyond leading logarithms*, Rev.Mod.Phys. **68** (1996) 1125–1144, [hep-ph/9512380].

[36] D. Fakirov and B. Stech, *F and D Decays*, Nucl.Phys. **B133** (1978) 315–326.

[37] N. Cabibbo and L. Maiani, *Two-Body Decays of Charmed Mesons*, Phys.Lett. **B73** (1978) 418.

[38] M. Beneke, G. Buchalla, M. Neubert, and C. T. Sachrajda, *QCD factorization for exclusive, nonleptonic B meson decays: General arguments and the case of heavy light final states*, Nucl.Phys. **B591** (2000) 313–418, [hep-ph/0006124].

[39] M. Bauer, B. Stech, and M. Wirbel, *Exclusive Nonleptonic Decays of D, D(s), and B Mesons*, Z.Phys. **C34** (1987) 103.

[40] M. Neubert, V. Rieckert, B. Stech, and Q. Xu, *Exclusive weak decays of B mesons*, .

[41] M. Neubert and B. Stech, *Nonleptonic weak decays of B mesons*, Adv.Ser.Direct.High Energy Phys. **15** (1998) 294–344, [hep-ph/9705292].

[42] B. Stech, *Hadronic B decays*, hep-ph/9706384.

[43] A. J. Buras and L. Silvestrini, *Generalized factorization in nonleptonic two-body B decays: A Critical look*, Nucl.Phys. **B548** (1999) 293–308, [hep-ph/9806278].

[44] H.-n. Li and H.-L. Yu, *Perturbative QCD analysis of B meson decays*, Phys.Rev. **D53** (1996) 2480–2490, [hep-ph/9411308].

[45] Y.-Y. Keum, H.-n. Li, and A. Sanda, *Fat penguins and imaginary penguins in perturbative QCD*, Phys.Lett. **B504** (2001) 6–14, [hep-ph/0004004].

[46] Y.-Y. Keum and H.-n. Li, *Nonleptonic charmless B decays: Factorization versus perturbative QCD*, Phys.Rev. **D63** (2001) 074006, [hep-ph/0006001].

[47] M. Beneke, G. Buchalla, M. Neubert, and C. T. Sachrajda, *QCD factorization in B -¿ pi K, pi pi decays and extraction of Wolfenstein parameters*, Nucl.Phys. **B606** (2001) 245–321, [hep-ph/0104110].

[48] M. Beneke and M. Neubert, *QCD factorization for B -¿ PP and B -¿ PV decays*, Nucl.Phys. **B675** (2003) 333–415, [hep-ph/0308039].

[49] S. Scherer, *Introduction to chiral perturbation theory*, Adv.Nucl.Phys. **27** (2003) 277, [hep-ph/0210398].

[50] S. L. Adler, *Axial vector vertex in spinor electrodynamics*, Phys.Rev. **177** (1969) 2426–2438.

[51] M. Gell-Mann, *A Schematic Model of Baryons and Mesons*, Phys.Lett. **8** (1964) 214–215.

[52] Y. Ne'eman, *Derivation of strong interactions from a gauge invariance*, Nucl.Phys. **26** (1961) 222–229.

[53] M. Gronau and D. London, *Isospin analysis of CP asymmetries in B decays*, Phys.Rev.Lett. **65** (1990) 3381–3384.

[54] G. C. Branco, L. Lavoura, and J. P. Silva, *CP Violation*, Int.Ser.Monogr.Phys. **103** (1999) 1–536.

[55] J. Donoghue, E. Golowich, and B. R. Holstein, *Dynamics of the standard model*, Camb.Monogr.Part.Phys.Nucl.Phys.Cosmol. **2** (1992) 1–540.

[56] D. Zeppenfeld, *SU(3) Relations for B Meson Decays*, Z.Phys. **C8** (1981) 77.

[57] B. Grinstein and R. F. Lebed, *SU(3) decomposition of two-body B decay amplitudes*, Phys.Rev. **D53** (1996) 6344–6360, [hep-ph/9602218].

[58] M. Gronau, O. F. Hernandez, D. London, and J. L. Rosner, *Decays of B mesons to two light pseudoscalars*, Phys.Rev. **D50** (1994) 4529–4543, [hep-ph/9404283].

[59] M. Gronau, O. F. Hernandez, D. London, and J. L. Rosner, *Broken SU(3) symmetry in two-body B decays*, Phys.Rev. **D52** (1995) 6356–6373, [hep-ph/9504326].

[60] R. Fleischer, *Flavour Physics and CP Violation: Expecting the LHC*, arXiv:0802.2882.

[61] G. C. Branco, J. I. Silva-Marcos, and M. N. Rebelo, *Universal strength for yukawa couplings*, Phys. Lett. **B237** (1990) 446–450.

[62] T. Inami and C. Lim, *Effects of Superheavy Quarks and Leptons in Low-Energy Weak Processes k(L) → mu anti-mu, K+ → pi+ Neutrino anti-neutrino and K0 – anti-K0*, Prog.Theor.Phys. **65** (1981) 297.

[63] A. J. Buras, M. Jamin, and P. H. Weisz, *Leading and next-to-leading QCD corrections to ε parameter and $B^0 - \bar{B}^0$ mixing in the presence of a heavy top quark*, Nucl. Phys. **B347** (1990) 491–536.

[64] R. Aleksan, A. Le Yaouanc, L. Oliver, O. Pene, and J. Raynal, *Estimation of Delta Gamma for the B(s) - anti-B(s) system: Exclusive decays and the parton model*, Phys.Lett. **B316** (1993) 567–577.

[65] C.-K. Chua, W.-S. Hou, and C.-H. Shen, *Long-Distance Contribution to $\Delta\Gamma_s/\Gamma_s$ of the $B_s - \bar{B}_s$ System*, Phys.Rev. **D84** (2011) 074037, [arXiv:1107.4325].

[66] M. Beneke, G. Buchalla, and I. Dunietz, *Width Difference in the $B_s - \bar{B}_s$ System*, Phys.Rev. **D54** (1996) 4419–4431, [hep-ph/9605259].

[67] A. Lenz and U. Nierste, *Theoretical update of $B_s - \bar{B}_s$ mixing*, JHEP **06** (2007) 072, [hep-ph/0612167].

[68] A. Lenz and U. Nierste, *Numerical Updates of Lifetimes and Mixing Parameters of B Mesons*, arXiv:1102.4274.

[69] **D0** Collaboration, V. M. Abazov et al., *Measurement of the anomalous like-sign dimuon charge asymmetry with 9 $fb^{-}1$ of $p\bar{p}$ collisions*, Phys.Rev. **D84** (2011) 052007, [arXiv:1106.6308].

[70] **D0** Collaboration, V. Abazov et al., *Measurement of the semileptonic charge asymmetry using $B_s^0 \to D_s \mu X$ decays*, Phys.Rev.Lett. **110** (2013) 011801, [arXiv:1207.1769].

[71] **LHCb** Collaboration, R. Aaij et al., *Measurement of the flavour-specific CP-violating asymmetry $a^s_{\rm sl}$ in B^0_s decays*, arXiv:1308.1048.

[72] N. Carrasco, M. Ciuchini, P. Dimopoulos, R. Frezzotti, V. Gimenez, et al., *B-physics from Nf=2 tmQCD: the Standard Model and beyond*, arXiv:1308.1851.

[73] **Heavy Flavor Averaging Group** Collaboration, Y. Amhis et al., *Averages of B-Hadron, C-Hadron, and tau-lepton properties as of early 2012*, arXiv:1207.1158.

[74] Y. Grossman, *The b/s width difference beyond the standard model*, Phys. Lett. **B380** (1996) 99–105, [hep-ph/9603244].

[75] **CKMfitter** Collaboration. http://ckmfitter.in2p3.fr.

[76] **LHCb** Collaboration, R. Aaij et al., *Measurement of CP violation and the B^0_s meson decay width difference with $B^0_s \to J/\psi K^+K^-$ and $B^0_s \to J/\psi\pi^+\pi^-$ decays*, arXiv:1304.2600.

[77] **LHCb** Collaboration, R. Aaij et al., *Determination of the sign of the decay width difference in the B_s system*, Phys.Rev.Lett. **108** (2012) 241801, [arXiv:1202.4717].

[78] S. Faller, M. Jung, R. Fleischer, and T. Mannel, *The Golden Modes $B^0 \to J/\psi K_{S,L}$ in the Era of Precision Flavour Physics*, Phys.Rev. **D79** (2009) 014030, [arXiv:0809.0842].

[79] I. Dunietz, R. Fleischer, and U. Nierste, *In pursuit of new physics with B_s decays*, Phys.Rev. **D63** (2001) 114015, [hep-ph/0012219].

[80] I. Dunietz and J. L. Rosner, *Time Dependent CP Violation Effects in B0 anti-B0 Systems*, Phys.Rev. **D34** (1986) 1404.

[81] S. Faller, R. Fleischer, and T. Mannel, *Precision Physics with $B^0_s \to J/\psi\phi$ at the LHC: The Quest for New Physics*, Phys.Rev. **D79** (2009) 014005, [arXiv:0810.4248].

[82] R. Fleischer and R. Knegjens, *Effective Lifetimes of B_s Decays and their Constraints on the B^0_s-$\bar{B}^0_s$ Mixing Parameters*, Eur.Phys.J. **C71** (2011) 1789, [arXiv:1109.5115].

[83] K. De Bruyn, R. Fleischer, R. Knegjens, P. Koppenburg, M. Merk, et al., *Branching Ratio Measurements of B_s Decays*, Phys.Rev. **D86** (2012) 014027, [arXiv:1204.1735].

[84] R. Fleischer and R. Knegjens, *In Pursuit of New Physics with $B^0_s \to K^+K^-$*, Eur.Phys.J. **C71** (2011) 1532, [arXiv:1011.1096].

[85] K. Hartkorn and H. Moser, *A new method of measuring Delta(Gamma)/Gamma in the B/s0 anti-B/s0 system*, Eur.Phys.J. **C8** (1999) 381–383.

[86] K. De Bruyn, R. Fleischer, R. Knegjens, M. Merk, M. Schiller, et al., *Exploring $B_s \to D_s^{(*)\pm}K^{\mp}$ Decays in the Presence of a Sizable Width Difference $\Delta\Gamma_s$*, Nucl.Phys. **B868** (2013) 351–367, [arXiv:1208.6463].

[87] **LHCb** Collaboration, R. Aaij et al., *First observation of the decay $B^0_s \to K^{*0}\bar{K}^{*0}$*, Phys.Lett. **B709** (2012) 50–58, [arXiv:1111.4183].

[88] S. Descotes-Genon, J. Matias, and J. Virto, *An analysis of $B_{d,s}$ mixing angles in presence of New Physics and an update of $B_s \to K^{0*}\bar{K}^{0*}$*, Phys.Rev. **D85** (2012) 034010, [arXiv:1111.4882].

[89] J. L. Rosner, *Determination of pseudoscalar charmed meson decay constants from B meson decays*, Phys.Rev. **D42** (1990) 3732–3740.

[90] E. Norrbin and R. Vogt, *Bottom production asymmetries at the LHC*, hep-ph/0003056.

[91] R. Fleischer, *New strategies to extract Beta and gamma from $B_d \to \pi^+\pi^-$ and $B_s \to K^+K^-$*, Phys.Lett. **B459** (1999) 306–320, [hep-ph/9903456].

[92] R. Fleischer, *$B_{s,d} \to \pi\pi, \pi K, KK$: Status and Prospects*, Eur.Phys.J. **C52** (2007) 267–281, [arXiv:0705.1121].

[93] G. Duplancic and B. Melic, *B, B(s) $\to$ K form factors: An Update of light-cone sum rule results*, Phys.Rev. **D78** (2008) 054015, [arXiv:0805.4170].

[94] **LHCb** Collaboration, R. Aaij et al., *Measurement of the effective $B_s^0 \to K^+K^-$ lifetime*, Phys.Lett. **B716** (2012) 393–400, [arXiv:1207.5993].

[95] **LHCb** Collaboration, *Talk given at EPSHEP 2013*, LHCb-PAPER-2013-040 (Feb, 2013).

[96] **LHCb** Collaboration, *Measurement of time-dependent CP violation in charmless two-body B decays*, LHCb-CONF-2012-007 (Feb, 2012).

[97] **BaBar** Collaboration, J. Lees, *Measurement of CP Asymmetries and Branching Fractions in Charmless Two-Body B-Meson Decays to Pions and Kaons*, arXiv:1206.3525.

[98] **Belle** Collaboration, I. Adachi et al., *Measurement of the CP Violation Parameters in $B^0 \to \pi^+\pi^-$ Decays*, arXiv:1302.0551.

[99] R. Fleischer, S. Recksiegel, and F. Schwab, *On Puzzles and Non-Puzzles in $B \to \pi\pi$, πK Decays*, Eur.Phys.J. **C51** (2007) 55–61, [hep-ph/0702275].

[100] K. De Bruyn, R. Fleischer, and P. Koppenburg, *Extracting gamma and Penguin Topologies through CP Violation in $B_s^0 \to; J/\psi K_S$*, Eur.Phys.J. **C70** (2010) 1025–1035, [arXiv:1010.0089].

[101] **UTfit** Collaboration. http://www.utfit.org.

[102] R. Aleksan, I. Dunietz, and B. Kayser, *Determining the CP violating phase gamma*, Z.Phys. **C54** (1992) 653–660.

[103] R. Fleischer, *New strategies to obtain insights into CP violation through B(s) $\to$ D(s)+- K-+, D(s)*+- K-+, ... and B(d) $\to$ D+- pi-+, D*+- pi-+, ... decays*, Nucl.Phys. **B671** (2003) 459–482, [hep-ph/0304027].

[104] **CDF** Collaboration, T. Aaltonen et al., *First observation of $\bar{B}_s^0 \to D_s^{\pm} K^{\mp}$ and measurement of the ratio of branching fractions $B(\bar{B}_s^0 \to \pi^-)$*, Phys.Rev.Lett. **103** (2009) 191802, [arXiv:0809.0080].

[105] **Belle** Collaboration, R. Louvot et al., *Measurement of the Decay $B_s 0 \to D_s - \pi^+$ and Evidence for $B_s 0 \to D_s \pm K^{\pm}$ in $e^+ e_-$ Annihilation at $\sqrt{s}$ 10.87-GeV*, Phys.Rev.Lett. **102** (2009) 021801, [arXiv:0809.2526].

[106] **LHCb** Collaboration, R. Aaij et al., *Measurements of the branching fractions of the decays $B_s^0 \to D_s^{\mp} K^{\pm}$ and $B_s^0 \to D_s^- \pi^+$*, JHEP **1206** (2012) 115, [arXiv:1204.1237].

[107] **LHCb** Collaboration, S. Blusk, *Measurement of the CP observables in $\bar{B}_s^0 \to D_s^+ K^-$ and first observation of $\bar{B}_{(s)}^0 \to D_s^+ K^- \pi^+ \pi^-$ and $\bar{B}_s^0 \to D_{s1}(2536)^+ \pi^-$*, arXiv:1212.4180.

[108] S. Nandi and U. Nierste, *Resolving the sign ambiguity in $\Delta\Gamma_s$ with $B_s \to D_s K$*, Phys.Rev. **D77** (2008) 054010, [arXiv:0801.0143].

[109] A. Buras, J. Gerard, and R. Ruckl, *1/n Expansion for Exclusive and Inclusive Charm Decays*, Nucl.Phys. **B268** (1986) 16.

[110] J. D. Bjorken, *Topics in B Physics*, Nucl.Phys.Proc.Suppl. **11** (1989) 325–341.

[111] M. J. Dugan and B. Grinstein, *QCD basis for factorization in decays of heavy mesons*, Phys.Lett. **B255** (1991) 583–588.

[112] C. W. Bauer, D. Pirjol, and I. W. Stewart, *A Proof of factorization for $B \to D$ pi*, Phys.Rev.Lett. **87** (2001) 201806, [hep-ph/0107002].

[113] R. Fleischer, N. Serra, and N. Tuning, *Tests of Factorization and SU(3) Relations in B Decays into Heavy-Light Final States*, Phys.Rev. **D83** (2011) 014017, [arXiv:1012.2784].

[114] I. Caprini, L. Lellouch, and M. Neubert, *Dispersive bounds on the shape of anti-B $\to$ D(*) lepton anti-neutrino form-factors*, Nucl.Phys. **B530** (1998) 153–181, [hep-ph/9712417].

[115] **BaBar** Collaboration, B. Aubert et al., *Measurement of time-dependent CP-violating asymmetries and constraints on $\sin(2\beta + \gamma)$ with partial reconstruction of $B \to D^{*\mp} \pi^{\pm}$ decays*, Phys.Rev. **D71** (2005) 112003, [hep-ex/0504035].

[116] **BaBar** Collaboration, B. Aubert et al., *Measurement of time-dependent CP asymmetries in $B^0 \to D^{(*)}$ +- $\pi^{\mp}$ and $B^0 \to D^{\pm} \rho^{\mp}$ decays*, Phys.Rev. **D73** (2006) 111101, [hep-ex/0602049].

[117] **BELLE** Collaboration, F. Ronga et al., *Measurements of CP violation in B0 → D*- pi+ and B0 → D- pi+ decays*, Phys.Rev. **D73** (2006) 092003, [hep-ex/0604013].

[118] **Belle** Collaboration, S. Bahinipati et al., *Measurements of time-dependent CP asymmetries in $B \to D^{*\mp}\pi^{\pm}$ decays using a partial reconstruction technique*, Phys.Rev. **D84** (2011) 021101, [arXiv:1102.0888].

[119] I. Dunietz, *Clean CKM information from B(d)(t) → D*-+ pi+-*, Phys.Lett. **B427** (1998) 179–182, [hep-ph/9712401].

[120] G. Duplancic, A. Khodjamirian, T. Mannel, B. Melic, and N. Offen, *Light-cone sum rules for B → pi form factors revisited*, JHEP **0804** (2008) 014, [arXiv:0801.1796].

[121] **Belle** Collaboration, A. Das et al., *Measurements of Branching Fractions for $B^0 \to D_s^+\pi^-$ and $\bar{B}^0 \to D_s^+K^-$*, Phys.Rev. **D82** (2010) 051103, [arXiv:1007.4619].

[122] **BaBar** Collaboration, B. Aubert et al., *Measurement of the Branching Fractions of the Rare Decays $B^0 \to D_s$ (*) + π^-, $B^0 \to D_s$ (*) + ρ^-, and $B^0 \to D_s$ (*) - $K^{(*)}$ +*, Phys.Rev. **D78** (2008) 032005, [arXiv:0803.4296].

[123] A. S. Dighe, I. Dunietz, and R. Fleischer, *Extracting CKM phases and $B_s - \bar{B}_s$ mixing parameters from angular distributions of nonleptonic B decays*, Eur.Phys.J. **C6** (1999) 647–662, [hep-ph/9804253].

[124] S. Stone and L. Zhang, *S-waves and the Measurement of CP Violating Phases in B_s Decays*, Phys.Rev. **D79** (2009) 074024, [arXiv:0812.2832].

[125] R. Fleischer, R. Knegjens, and G. Ricciardi, *Anatomy of $B^0_{s,d} \to J/\psi f_0(980)$*, Eur.Phys.J. **C71** (2011) 1832, [arXiv:1109.1112].

[126] **LHCb** Collaboration, R. Aaij et al., *Analysis of the resonant components in $B_s \to J/\psi\pi^+\pi^-$*, Phys.Rev. **D86** (2012) 052006, [arXiv:1204.5643].

[127] **Belle** Collaboration, J. Li et al., *Observation of $B_s^0 \to J/\psi f_0(980)$ and Evidence for $B_s^0 \to J/\psi f_0(1370)$*, Phys.Rev.Lett. **106** (2011) 121802, [arXiv:1102.2759].

[128] **D0** Collaboration, V. M. Abazov et al., *Measurement of the relative branching ratio of $B_s^0 to J/\psi f_0(980) \to B_s^0 \to J/\psi\phi$*, Phys.Rev. **D85** (2012) 011103, [arXiv:1110.4272].

[129] **CDF** Collaboration, T. Aaltonen et al., *Measurement of branching ratio and B_s^0 lifetime in the decay $B_s^0 \to J/\psi f_0(980)$ at CDF*, Phys.Rev. **D84** (2011) 052012, [arXiv:1106.3682].

[130] N. A. Tornqvist, *Understanding the scalar meson q anti-q nonet*, Z.Phys. **C68** (1995) 647–660, [hep-ph/9504372].

[131] R. L. Jaffe, *Multi-Quark Hadrons. 1. The Phenomenology of (2 Quark 2 anti-Quark) Mesons*, Phys.Rev. **D15** (1977) 267.

[132] G. t. Hooft, G. Isidori, L. Maiani, A. D. Polosa, and V. Riquer, *A Theory of Scalar Mesons*, 0801.2288.

[133] J. D. Weinstein and N. Isgur, *Do Multi-Quark Hadrons Exist?*, Phys.Rev.Lett. **48** (1982) 659.

[134] V. Anisovich, L. Dakhno, and V. Nikonov, *D(s)+ → pi+ pi+ pi- decay: The 1**3 P(0)s anti-s component in scalar isoscalar mesons*, Phys.Atom.Nucl. **67** (2004) 1571–1579, [hep-ph/0302137].

[135] A. Anisovich, V. Anisovich, and V. Nikonov, *Radiative decays of basic scalar, vector and tensor mesons and the determination of the P wave q anti-q multiplet*, Eur.Phys.J. **A12** (2001) 103–115, [hep-ph/0108186].

[136] R. Delbourgo, D.-s. Liu, and M. D. Scadron, *s anti-s dominance of the f(0)(980) meson*, Phys.Lett. **B446** (1999) 332–335, [hep-ph/9811474].

[137] B. El-Bennich, O. Leitner, J.-P. Dedonder, and B. Loiseau, *The Scalar Meson f0(980) in Heavy-Meson Decays*, Phys.Rev. **D79** (2009) 076004, [arXiv:0810.5771].

[138] D. Black, A. H. Fariborz, F. Sannino, and J. Schechter, *Putative light scalar nonet*, Phys.Rev. **D59** (1999) 074026, [hep-ph/9808415].

[139] L. Maiani, F. Piccinini, A. Polosa, and V. Riquer, *A New look at scalar mesons*, Phys.Rev.Lett. **93** (2004) 212002, [hep-ph/0407017].

[140] M. G. Alford and R. Jaffe, *Insight into the scalar mesons from a lattice calculation*, Nucl.Phys. **B578** (2000) 367–382, [hep-lat/0001023].

[141] N. Achasov and V. Ivanchenko, *On a Search for Four Quark States in Radiative Decays of phi Meson*, Nucl.Phys. **B315** (1989) 465.

[142] **OPAL** Collaboration, K. Ackerstaff et al., *Production of f(0)(980), f(2)(1270) and phi(1020) in hadronic Z0 decay*, Eur.Phys.J. **C4** (1998) 19–28, [hep-ex/9802013].

[143] A. Deandrea, R. Gatto, G. Nardulli, A. Polosa, and N. Tornqvist, *The s anti-s and K anti-K nature of f0(980) D(s) decays*, Phys.Lett. **B502** (2001) 79–86, [hep-ph/0012120].

[144] H.-Y. Cheng, C.-K. Chua, and K.-C. Yang, *Charmless hadronic B decays involving scalar mesons: Implications to the nature of light scalar mesons*, Phys.Rev. **D73** (2006) 014017, [hep-ph/0508104].

[145] R. Fleischer, *CP violation in the B system and relations to $K \to$ pi nu anti-nu decays*, Phys.Rept. **370** (2002) 537–680, [hep-ph/0207108].

[146] A. J. Buras, R. Fleischer, S. Recksiegel, and F. Schwab, *Anatomy of prominent B and K decays and signatures of CP violating new physics in the electroweak penguin sector*, Nucl.Phys. **B697** (2004) 133–206, [hep-ph/0402112].

[147] R. Fleischer, *Extracting γ from $B(s/d) \to J/\psi K_S$ and $B(d/s) \to D^+(d/s)D^-(d/s)$*, Eur.Phys.J. **C10** (1999) 299–306, [hep-ph/9903455].

[148] M. Ciuchini, M. Pierini, and L. Silvestrini, *The Effect of penguins in the $B_d \to J/\psi K^0$ CP asymmetry*, Phys.Rev.Lett. **95** (2005) 221804, [hep-ph/0507290].

[149] M. Ciuchini, M. Pierini, and L. Silvestrini, *Theoretical uncertainty in sin 2β: An Update*, arXiv:1102.0392.

[150] A. S. Dighe, M. Gronau, and J. L. Rosner, *Amplitude relations for b decays involving eta and eta-prime*, Phys.Lett. **B367** (1996) 357–361, [hep-ph/9509428].

[151] P. Z. Skands, *Branching ratios for B(d,s) $\to$ J / psi eta and B(d,s) $\to$ eta lepton+ lepton-, extracting gamma from B(d,s) $\to$ J / psi eta, and possibilities for constraining C(10A) in semileptonic B decays*, JHEP **0101** (2001) 008, [hep-ph/0010115].

[152] C.-W. Chiang, M. Gronau, and J. L. Rosner, *Two body charmless B decays involving eta and eta-prime*, Phys.Rev. **D68** (2003) 074012, [hep-ph/0306021].

[153] C. Di Donato, G. Ricciardi, and I. Bigi, *$\eta - \eta'$ Mixing - From electromagnetic transitions to weak decays of charm and beauty hadrons*, Phys.Rev. **D85** (2012) 013016, [arXiv:1105.3557].

[154] P. Colangelo, F. De Fazio, and W. Wang, *$B_s \to f_0(980)$ form factors and B_s decays into $f_0(980)$*, Phys.Rev. **D81** (2010) 074001, [arXiv:1002.2880].

[155] P. Colangelo, F. De Fazio, and W. Wang, *Nonleptonic B_s to charmonium decays: analyses in pursuit of determining the weak phase β_s*, Phys.Rev. **D83** (2011) 094027, [arXiv:1009.4612].

[156] P. Ball and R. Zwicky, *New results on $B \to$ pi, K, eta decay formfactors from light-cone sum rules*, Phys.Rev. **D71** (2005) 014015, [hep-ph/0406232].

[157] **BES** Collaboration, M. Ablikim et al., *Partial wave analysis of chi(c0) → pi+ pi- K+ K-*, Phys.Rev. **D72** (2005) 092002, [hep-ex/0508050].

[158] **BaBar** Collaboration, B. Aubert et al., *Dalitz plot analysis of the decay $B^{\pm} \to K^{\pm}K^{\pm}K^{\mp}$*, Phys.Rev. **D74** (2006) 032003, [hep-ex/0605003].

[159] **LHCb** Collaboration, R. Aaij et al., *Measurement of the B_s effective lifetime in the $J/\psi f_0(980)$ final state*, Phys.Rev.Lett. **109** (2012) 152002, [arXiv:1207.0878].

[160] **LHCb** Collaboration, R. Aaij et al., *Measurement of the CP-violating phase ϕ_s in $\overline{B}^0_s \to J/\psi\pi^+\pi^-$ decays*, Phys.Lett. **B713** (2012) 378–386, [arXiv:1204.5675].

[161] **LHCb** Collaboration, R. Aaij et al., *Analysis of the resonant components in B0J/+-*, Phys.Rev. **D87** (2013), no. 5 052001, [arXiv:1301.5347].

[162] **Belle** Collaboration, Y. Liu et al., *Search for B-0 → J/psi phi decays*, Phys.Rev. **D78** (2008) 011106, [arXiv:0805.3225].

[163] **L3** Collaboration, M. Acciarri et al., *Search for neutral B meson decays to two charged leptons*, Phys.Lett. **B391** (1997) 474–480.

[164] R. Fleischer, *Rescattering and electroweak penguin effects in strategies to constrain and determine the CKM angle gamma from B → pi K decays*, Eur.Phys.J. **C6** (1999) 451–470, [hep-ph/9802433].

[165] R. Fleischer, R. Knegjens, and G. Ricciardi, *Exploring CP Violation and η-η' Mixing with the $B^0_{s,d} \to J/\psi\eta^{(\prime)}$ Systems*, Eur.Phys.J. **C71** (2011) 1798, [arXiv:1110.5490].

[166] F. Ambrosino, A. Antonelli, M. Antonelli, F. Archilli, P. Beltrame, et al., *A Global fit to determine the pseudoscalar mixing angle and the gluonium content of the eta-prime meson*, JHEP **0907** (2009) 105, [arXiv:0906.3819].

[167] **Belle** Collaboration, J. Li et al., *First observation of $B^0_s \to J/\psi\eta$ and $B^0_s \to J/\psi\eta'$*, Phys.Rev.Lett. **108** (2012) 181808, [arXiv:1202.0103].

[168] M. Chang, Y. Duh, J. Lin, I. Adachi, K. Adamczyk, et al., *Measurement of $B^0 \to J/\psi\eta^{(\prime)}$ and Constraint on the $\eta - \eta'$ Mixing Angle*, Phys.Rev. **D85** (2012) 091102, [arXiv:1203.3399].

[169] A. Datta, H. J. Lipkin, and P. J. O'Donnell, *Simple relations for two-body B decays to charmonium and tests for eta eta-prime mixing*, Phys.Lett. **B529** (2002) 93–98, [hep-ph/0111336].

[170] **LHCb** Collaboration, R. Aaij et al., *Evidence for the decay $B^0 \to J/\psi\omega$ and measurement of the relative branching fractions of B^0_s meson decays to $J/\psi\eta$ and $J/\psi\eta'$*, Nucl.Phys. **B867** (2013) 547–566, [arXiv:1210.2631].

[171] C. Thomas, *Composition of the Pseudoscalar Eta and Eta' Mesons*, JHEP **0710** (2007) 026, [arXiv:0705.1500].

[172] **D0** Collaboration, V. M. Abazov et al., *Measurement of the CP-violating phase $\phi_s^{J/\psi\phi}$ using the flavor-tagged decay $B_s^0 \to J/\psi\phi$ in 8 fb^{-1} of $p\bar{p}$ collisions*, Phys.Rev. **D85** (2012) 032006, [arXiv:1109.3166].

[173] **CDF** Collaboration, T. Aaltonen et al., *Measurement of the CP-Violating Phase $\beta_s^{J/\Psi\phi}$ in $B_s^0 \to J/\Psi\phi$ Decays with the CDF II Detector*, Phys.Rev. **D85** (2012) 072002, [arXiv:1112.1726].

[174] **ATLAS** Collaboration, G. Aad et al., *Time-dependent angular analysis of the decay $B_s^0 \to J/\psi\phi$ and extraction of $\Delta\Gamma_s$ and the CP-violating weak phase ϕ_s by ATLAS*, JHEP **1212** (2012) 072, [arXiv:1208.0572].

[175] **ATLAS** Collaboration, *Flavour tagged time dependent angular analysis of the $B_s \to J/\psi\phi$ decay and extraction of $\Delta\Gamma$ and the weak phase ϕ_s in ATLAS*, .

[176] **LHCb** Collaboration, R. Aaij et al., *Measurement of the effective $B_s^0 \to J/\psi K_S^0$ lifetime*, Nuclear Physics **B873** (2013) 275–292, [arXiv:1304.4500].

[177] K. De Bruyn, R. Fleischer, and P. Koppenburg, *Extracting gamma and Penguin Parameters from $B_s^0 \to J/\psi K_S$*, arXiv:1012.0840.

[178] R. Fleischer, *Exploring CP violation and penguin effects through $B_d^0 \to D^+D^-$ and $B_s^0 \to D_s^+D_s^-$*, Eur.Phys.J. **C51** (2007) 849–858, [arXiv:0705.4421].

[179] A. J. Buras and J. Girrbach, *BSM models facing the recent LHCb data: A First look*, Acta Phys.Polon. **B43** (2012) 1427, [arXiv:1204.5064].

[180] C. Bobeth, M. Gorbahn, T. Hermann, M. Misiak, E. Stamou, et al., *$B_{s,d} \to \ell^+\ell^-$ in the Standard Model*, arXiv:1311.0903.

[181] C. Bobeth, M. Gorbahn, and E. Stamou, *Electroweak Corrections to $B_{s,d} \to \ell^+\ell^-$*, arXiv:1311.1348.

[182] T. Hermann, M. Misiak, and M. Steinhauser, *Three-loop QCD corrections to $B_s \to \mu^+\mu^-$*, arXiv:1311.1347.

[183] K. De Bruyn, R. Fleischer, R. Knegjens, P. Koppenburg, M. Merk, et al., *Probing New Physics via the $B_s^0 \to \mu^+\mu^-$ Effective Lifetime*, Phys.Rev.Lett. **109** (2012) 041801, [arXiv:1204.1737].

[184] A. J. Buras, R. Fleischer, J. Girrbach, and R. Knegjens, *Probing New Physics with the $B_s \to \mu^+\mu^-$ Time-Dependent Rate*, arXiv:1303.3820.

[185] J. Albrecht, *Brief review of the searches for the rare decays $B_s^0 \to \mu^+\mu^-$ and $B^0 \to \mu^+\mu^-$*, Mod.Phys.Lett. **A27** (2012) 1230028, [arXiv:1207.4287].

[186] **LHCb** Collaboration, R. Aaij et al., *Measurement of the $B_s^0 \to \mu^+\mu^-$ branching fraction and search for $B^0 \to \mu^+\mu^-$ decays at the LHCb experiment*, arXiv:1307.5024.

[187] **CMS** Collaboration, S. Chatrchyan et al., *Measurement of the $B_s \to \mu\mu$ branching fraction and search for $B_0 \to \mu\mu$ with the CMS Experiment*, arXiv:1307.5025.

[188] **CMS and LHCb** Collaboration, CMS and L. Collaborations, *Combination of results on the rare decays $B^0_{(s)} \to \mu^+\mu^-$ from the CMS and LHCb experiments*, .

[189] A. J. Buras, F. De Fazio, J. Girrbach, R. Knegjens, and M. Nagai, *The Anatomy of Neutral Scalars with FCNCs in the Flavour Precision Era*, arXiv:1303.3723.

[190] W. Altmannshofer, P. Paradisi, and D. M. Straub, *Model-Independent Constraints on New Physics in $b \to s$ Transitions*, JHEP **1204** (2012) 008, [arXiv:1111.1257].

[191] F. Beaujean, C. Bobeth, D. van Dyk, and C. Wacker, *Bayesian Fit of Exclusive $b \to s\bar{\ell}\ell$ Decays: The Standard Model Operator Basis*, JHEP **1208** (2012) 030, [arXiv:1205.1838].

[192] G. Buchalla, A. J. Buras, and M. K. Harlander, *Penguin box expansion: Flavor changing neutral current processes and a heavy top quark*, Nucl. Phys. **B349** (1991) 1–47.

[193] G. Buchalla and A. J. Buras, *The rare decays $k \to \pi\nu\bar{\nu}$, $b \to x\nu\bar{\nu}$ and $b \to \ell^+\ell^-$: An update*, Nucl. Phys. **B548** (1999) 309–327, [hep-ph/9901288].

[194] M. Misiak and J. Urban, *QCD corrections to FCNC decays mediated by Z penguins and W boxes*, Phys.Lett. **B451** (1999) 161–169, [hep-ph/9901278].

[195] M. Voloshin and E. Shabalin, *Contribution of Two Photon Mechanism to Real Part of the K(L) $\to$ mu+ mu- Decay Amplitude and Calculations of Charmed Particle Mass*, JETP Lett. **23** (1976) 107–110.

[196] R. Fleischer, *On Branching Ratios of B_s Decays and the Search for New Physics in $B_s^0 \to \mu^+\mu^-$*, arXiv:1208.2843.

[197] R. Fleischer, N. Serra, and N. Tuning, *A New Strategy for B_s Branching Ratio Measurements and the Search for New Physics in $B_s^0 \to mu^+mu^-$*, Phys.Rev. **D82** (2010) 034038, [arXiv:1004.3982].

[198] D. Becirevic, N. Kosnik, F. Mescia, and E. Schneider, *Complementarity of the constraints on New Physics from $B_s \to \mu^+\mu^-$ and from $B \to K\ell^+\ell^-$ decays*, Phys.Rev. **D86** (2012) 034034, [arXiv:1205.5811].

[199] A. J. Buras, P. Gambino, M. Gorbahn, S. Jager, and L. Silvestrini, *Universal unitarity triangle and physics beyond the standard model*, Phys. Lett. **B500** (2001) 161–167, [hep-ph/0007085].

[200] A. J. Buras, *Minimal flavor violation*, Acta Phys. Polon. **B34** (2003) 5615–5668, [hep-ph/0310208].

[201] M. Blanke, A. J. Buras, B. Duling, S. Recksiegel, and C. Tarantino, *FCNC Processes in the Littlest Higgs Model with T-Parity: a 2009 Look*, Acta Phys.Polon. **B41** (2010) 657–683, [arXiv:0906.5454].

[202] A. J. Buras, F. De Fazio, J. Girrbach, and M. V. Carlucci, *The Anatomy of Quark Flavour Observables in 331 Models in the Flavour Precision Era*, JHEP **1302** (2013) 023, [arXiv:1211.1237].

[203] M. Blanke, A. J. Buras, B. Duling, K. Gemmler, and S. Gori, *Rare K and B Decays in a Warped Extra Dimension with Custodial Protection*, JHEP **03** (2009) 108, [arXiv:0812.3803].

[204] A. J. Buras, F. De Fazio, and J. Girrbach, *The Anatomy of Z' and Z with Flavour Changing Neutral Currents in the Flavour Precision Era*, JHEP **1302** (2013) 116, [arXiv:1211.1896].

[205] H. E. Logan and U. Nierste, *$B_{s,d} \to \ell^+\ell^-$ in a two Higgs doublet model*, Nucl.Phys. **B586** (2000) 39–55, [hep-ph/0004139].

[206] K. Babu and C. F. Kolda, *Higgs mediated $B^0 \to \mu^+\mu^-$ in minimal supersymmetry*, Phys.Rev.Lett. **84** (2000) 228–231, [hep-ph/9909476].

[207] G. Isidori and A. Retico, *Scalar flavor changing neutral currents in the large tan beta limit*, JHEP **0111** (2001) 001, [hep-ph/0110121].

[208] A. J. Buras, P. H. Chankowski, J. Rosiek, and L. Slawianowska, *$\delta m_{d,s}$, $b^0_{d,s} \to \mu^+\mu^-$ and $b \to x_s\gamma$ in supersymmetry at large* $\tan\beta$, Nucl. Phys. **B659** (2003) 3, [hep-ph/0210145].

[209] G. D'Ambrosio, G. F. Giudice, G. Isidori, and A. Strumia, *Minimal flavour violation: An effective field theory approach*, Nucl. Phys. **B645** (2002) 155–187, [hep-ph/0207036].

[210] A. J. Buras, M. V. Carlucci, S. Gori, and G. Isidori, *Higgs-mediated FCNCs: Natural Flavour Conservation vs. Minimal Flavour Violation*, JHEP **1010** (2010) 009, [arXiv:1005.5310].

[211] A. J. Buras, S. Jager, and J. Urban, *Master formulae for $\Delta F = 2$ NLO QCD factors in the standard model and beyond*, Nucl.Phys. **B605** (2001) 600–624, [hep-ph/0102316].

[212] C. Bouchard, E. Freeland, C. Bernard, A. El-Khadra, E. Gamiz, et al., *Neutral B mixing from $2+1$ flavor lattice-QCD: the Standard Model and beyond*, PoS **LATTICE2011** (2011) 274, [arXiv:1112.5642].

[213] A. J. Buras and J. Girrbach, *Complete NLO QCD Corrections for Tree Level Delta F = 2 FCNC Processes*, JHEP **1203** (2012) 052, [arXiv:1201.1302].

[214] **CMS** Collaboration, S. Chatrchyan et al., *Search for narrow resonances in dilepton mass spectra in pp collisions at $\sqrt{s} = 7$ TeV*, Phys.Lett. **B714** (2012) 158–179, [arXiv:1206.1849].

[215] W. Altmannshofer and D. M. Straub, *Cornering New Physics in $b \to s\gamma$ Transitions*, JHEP **1208** (2012) 121, [arXiv:1206.0273].

[216] A. J. Buras, G. Isidori, and P. Paradisi, *EDMs versus CPV in $B_{s,d}$ mixing in two Higgs doublet models with MFV*, Phys.Lett. **B694** (2011) 402–409, [arXiv:1007.5291].

[217] E. Lunghi and A. Soni, *Possible Indications of New Physics in B_d-mixing and in $\sin(2\beta)$ Determinations*, Phys. Lett. **B666** (2008) 162–165, [arXiv:0803.4340].

[218] A. J. Buras and D. Guadagnoli, *Correlations among new CP violating effects in $\Delta F = 2$ observables*, Phys. Rev. **D78** (2008) 033005, [arXiv:0805.3887].

[219] J. F. Gunion and H. E. Haber, *The CP conserving two Higgs doublet model: The Approach to the decoupling limit*, Phys.Rev. **D67** (2003) 075019, [hep-ph/0207010].

[220] **xkcd** Collaboration. http://www.xkcd.com.

[221] **Planck** Collaboration, P. Ade et al., *Planck 2013 results. I. Overview of products and scientific results*, arXiv:1303.5062.

Lay summary

Particle Physics

The laws of physics, at least in principle, underpin all the observations we can make about our world, and thereby also every field of science. To put it very simply, as the cartoon below[3] jokingly does, sociology is just applied psychology, psychology applied biology, biology applied biochemistry, biochemistry applied chemistry and, finally, chemistry just applied physics:

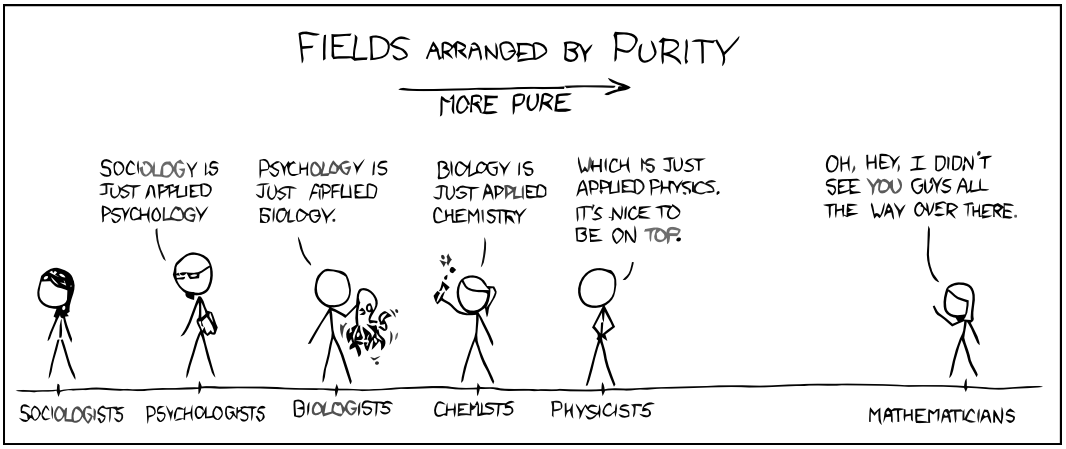

And within the field of physics we may continue this reductionism. We are then eventually led to conclude that all natural phenomena, varying from the weather to the firing of neurons within our brains, can be described in terms of *interactions* between *elementary particles*. In practice this description relies heavily on mathematics, as the cartoon also points out, but in this chapter we will spare the reader from these details.

An elementary particle is a building block of Nature that we currently believe to be indivisible. For example, in our attempt to understand atoms we have discovered that their nuclei are made of protons and neutrons, and that these, in turn, are composed of particles called *quarks*. As quarks do an adequate job of describing subatomic physics (we will say more about this later), they are an example of what we consider to be elementary particles. Electrons, which bind to the atomic nuclei to complete an atom, are another example.

[3]Taken from xkcd comics [220].

Interactions between elementary particles are mediated by fundamental forces. We currently know of four such forces. Namely, the electromagnetic force, the strong force, the weak force and gravity. Interestingly, these forces can themselves be described in terms of elementary particles, specifically so-called *messenger* particles. Messenger particles essentially communicate to other particles whether they should attract or repel each other. With respect to the fundamental forces just listed, the associated messenger particles are the photon (responsible for visible light), the gluon, the W and Z bosons and the graviton.

Of the four fundamental forces, the strong and weak nuclear forces are less familiar from an everyday perspective. The strong force is responsible for binding the neutrons and protons (or quarks to be more precise) of an atomic nucleus together. It is called "strong" because at subatomic distances it is stronger than the competing electromagnetic force that tries to push the (positively charged) protons in the nucleus apart. On the other hand, the weak force is so named because the interactions it mediates are relatively weak and seldom. Nonetheless, it is a very interesting force with important physical consequences. One of its most relevant features for this thesis is that it allows quarks to change a characteristic called their *flavour*, which we will come back to. A possibly familiar example of the weak force in action is radioactive beta decay, which is caused by a neutron decaying to a proton while releasing an energetic electron (the beta particle) and a neutrino particle.

Our current understanding of particle physics is summed up by the aptly named *Standard Model*. The Standard Model predicts how all of the known elementary particles behave with respect to each of the fundamental forces (except for gravity[4]). This model is almost 40 years old and continues to give accurate predictions for particle physics experiments. The state of the art of such experiments is the Large Hadron Collider (LHC) at CERN in Geneva. The LHC is a circular particle accelerator with a 27 km circumference, which can collide protons at close to the speed of light. It began operating in early 2010, and in 2012 it discovered[5] what was considered the last missing piece of the Standard Model: the Higgs boson. Although the Standard Model now appears complete, it is not without shortcomings, some of which we will mention in the next section. The LHC could therefore continue to play an important role by uncovering new physical phenomena, which may help us to extend or replace the ageing Standard Model.

[4]Einstein's theory of general relativity describes gravitational interactions at long distances. It is challenging, however, to incorporate gravity into the quantum mechanical framework of the Standard Model, which is necessary for an understanding at short, subatomic, distances.

[5]Technically a particle with properties very similar to the Higgs boson was discovered. Further tests are needed to confirm that it is certainly the Higgs boson.

Stellar motivations

To point out some of the Standard Model's shortcomings it is sufficient to point at the sky. Given a sufficiently capable telescope, we would observe that the galaxies in our universe are moving away from each other. This observation, that the universe is expanding, is what motivated the popular big bang hypothesis for the beginning of the universe. What is odd, however, is that the rate at which galaxies are currently moving away from each other is not decelerating, as we would expect due to their gravitational attraction, but accelerating! We call the source of this mysterious acceleration *dark energy*, which accounts for 68% of the total energy budget of the universe[6].

Next, if we take a closer look at these galaxies, we observe something else: the outer stars that are in a stable orbit rotate too quickly with respect to the galaxy's visible inner matter (its other stars). For these rotational speeds to make sense, galaxies must contain a significant amount of invisible matter, called *dark matter*. The best explanation for this mysterious dark matter, which also agrees with calculations of how the universe was formed, is that galaxies contain a cloud of tiny, very weakly interacting particles. These dark matter particles are estimated to comprise 27% of the total universe energy budget. However, none of the elementary particles described by the Standard Model qualify.

The contribution of ordinary matter to the total energy budget of the universe, as described by the Standard Model, is thus 5%. That the Standard Model only describes a small fraction of our universe is clearly somewhat of a shortcoming for an otherwise very successful model. Inadequacies such as these, among others, lead us to believe that the model is incomplete. We suspect that if we continue to test it by colliding particles at higher energies or making measurement with increasing precision, we must eventually observe a deviation from its predictions. We refer in general to future physical phenomena that will deviate from Standard Model predictions as *New Physics*. Outlining strategies to hunt for New Physics is one of the main goals of this thesis.

Taking a closer look at the ordinary matter in the universe, with the 5% energy budget, another mystery presents itself: why is it all made of matter and none of it of *antimatter*? This question may seem odd at first because antimatter (not to be confused with the dark matter we defined above) sounds like an exotic substance. However, antimatter is actually perfectly normal stuff. Every matter particle is automatically paired with an antimatter particle that has the same mass but opposite charge. The electron, for example, is paired with the positron, a "positive" electron, which is used in everyday things like medical PET (Positron Emission Tomography) scans. The catch is that when a particle and an anti-particle meet, they annihilate each other and release energy. For this reason it is clear why the Earth has only one kind of each stable particle, and of course these are the ones we initially chose to label as *matter*. However, it could just have easily been made out of stable antimatter particles.

[6]The total energy budget of the universe was recently updated by the new Planck sattelite results [221].

So the Earth is made of matter, but the strange thing is that every galaxy we observe in our universe also appears to be. We would expect that at the beginning of a neutral universe, during the big bang, matter and antimatter were created in equal amounts. So it is a mystery how the antimatter disappeared while matter stuck around. The laws of physics seem to have shown a bias towards matter over antimatter during the evolution of the universe.

In 1967 the Soviet physicist Andrei Sakharov published a paper discussing the conditions that must have been present during the evolution of the universe to explain the current matter–antimatter asymmetry. One requirement is that certain *symmetries* of the laws of physics, which used to be taken for granted, must be broken. As we will soon explain, it turns out that in the Standard Model these symmetries are in indeed broken. However, they are not broken "enough" to explain the huge difference between matter and antimatter we see today. Therefore our quest for New Physics also includes a quest for *symmetry violation*.

Symmetry violation and mesons

According to Sakharov, two symmetries of Nature that must be broken in order to explain the matter–antimatter asymmetry of the universe are *Charge symmetry* (C) and the combination of charge symmetry with *Parity symmetry* (P), known as *CP symmetry*. Charge symmetry intuitively states that if we flip the charges of all particles, for instance make electrons positive and positrons negative, the laws of physics describing their interactions stay the same. Parity symmetry, on the other hand, requires the same laws of physics to hold after flipping every spatial direction. Essentially parity symmetry states that a physical process viewed through a mirror should still behave like a valid physical process.

The charge and parity symmetries seem intuitive, and they are respected by almost all of the fundamental forces. The only exception is the weak force, which violates both symmetries separately and, as it turns out, also their combination: CP symmetry. Thus, as far as we currently know, it is the weak force that is responsible for Nature's bias for matter versus antimatter.

In the Standard Model it is specifically the interaction of quarks via the weak force that violates CP symmetry. As we already mentioned above, quarks are the elementary building blocks of composite particles called *hadrons*, such as neutrons and protons, and they come in different flavours. There are six flavours in total, and these are labeled *up*, *down*, *strange*, *charm*, *beauty*[7] and *top*. Neutrons and protons, for instance, are made from up and down quarks, the two lightest flavours. They are examples of a subgroup of hadrons called *baryons*, each consisting of three quarks. It is also possible for a quark to bind together with an antiquark, due to the strong force, to form a composite particle called a *meson*. Mesons are all unstable and decay quickly, but by studying their decays we can learn a lot about quark interactions.

[7]The beauty quark is also called the *bottom* quark.

The unique feature of the weak force is that it allows a quark of one flavour to change into another. Furthermore, CP symmetry can be violated if, loosely speaking, the chance[8] that a beauty quark transforms into an up quark is not identical to the chance that a beauty antiquark transforms into an up antiquark, for example. Due to the strength of the strong force, however, it is impossible to isolate individual quarks to study them independently. Therefore, as we just mentioned, we can instead study such flavour–changing quark interactions indirectly by observing the transformations and decays of composite meson particles.

Mesons can be studied using particle detector experiments, like the LHC at CERN. By comparing the behaviour of mesons with anti-mesons we can probe how CP symmetry is violated in the underlying quark processes. Furthermore, by measuring such processes very precisely, we can also make a comparison with what the Standard Model predicts to occur. In this way we can probe New Physics. Specifically, the quantum mechanical nature of these processes allows heavy, as of yet undiscovered, new particles to contribute in a subtle way. In order to discover them, however, we need both precise experimental measurements and precise theoretical predictions.

Strange beauty mesons

Certain pairs of neutral mesons can transform into each other before they decay due to a phenomenon called *mixing*. The violation of CP symmetry was in fact first discovered in 1964 due to the mixing of neutral kaons, which are mesons made from combinations of down and strange quarks. The amount of violation observed was, however, very small. It was later discovered that mesons that contain a beauty quark exhibit much more CP symmetry violation, both in their mixing and their decay. In the previous decade neutral mesons comprised of a beauty quark together with a down quark, or an up quark for charged beauty mesons, were extensively studied at particle detectors called *B–factories*. This greatly helped in building a picture of the amount of CP symmetry violation present in the Standard Model. Unfortunately, as we already mentioned earlier, this is not enough to solve the matter–antimatter asymmetry puzzle present in our universe.

When the LHC started up in 2010, and coincidently also this thesis, mesons composed of a beauty quark together with a strange quark, "strange beauty mesons", had not been extensively studied. Since then the particle detectors at the LHC, namely LHCb, ATLAS and CMS, have begun to sharpen this picture. It is therefore conceivable that we will see evidence for New Physics, in the form of new CP symmetry violation or new particles, in the near future. Consequently, the theoretical analysis of these particles is very relevant, because in order to see a deviation from the Standard Model we first require precise theoretical predictions.

[8]We are actually referring here to the coupling strength of these two quarks. The "chance" of this process occurring is the magnitude squared of the coupling strength. CP violation manifests itself as a *complex* coupling strength, so it is only observable if there is interference between multiple couplings present.

The combination of a beauty antiquark with a strange quark is denoted by B_s and a beauty quark with a strange antiquark as $\overline{B}_s$. Because both of these particles are neutral they can mix into each other as we mentioned above. Such mixing transitions are typically depicted by *Feynman diagrams*, which we use extensively throughout this thesis. Here is an example Feynman diagram showing the mixing of a B_s meson into a $\overline{B}_s$ meson:

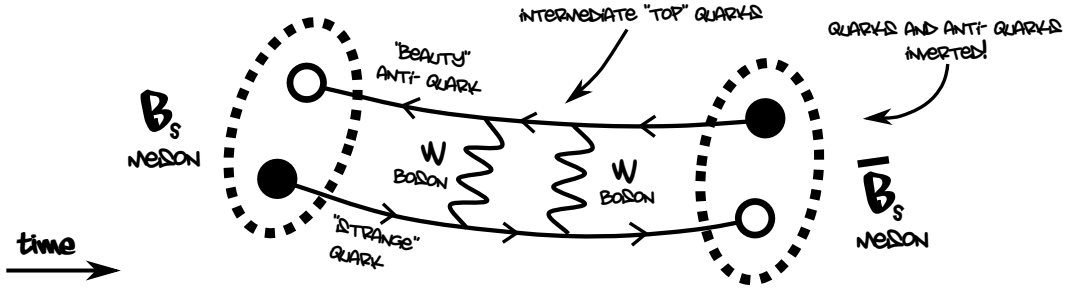

Note in particular that the W bosons, the messenger particles of the weak force, are responsible for mediating such a transition in the Standard Model. In models of New Physics also other particles can contribute to this mixing.

The B_s and $\overline{B}_s$ can be considered each other's anti-particles. One way to study CP symmetry violation is to identify decay processes beginning with one or the other and comparing their results for differences. From an experimental perspective this act of distinguishing between the so-called *flavour states*, B_s and $\overline{B}_s$, is known as *flavour tagging*. Measurements involving this technique can be very sensitive to New Physics. However, the technique is challenging and as a result it only works for a small fraction of events.

A key focus of this thesis is how to search for New Physics using results from experimental measurements that did not rely on flavour tagging. To this end, we can describe the B_s and $\overline{B}_s$ mesons in a different formalism in which they do not mix with each other. In this other formalism the particles are labeled by their relative masses, $B_{s,\mathrm{H}}$ and $B_{s,\mathrm{L}}$ for the heavier and lighter one, respectively, and are referred to as *mass-eigenstates*. Because the particles described in this way do not mix, it is possible to define a lifetime for each particle, which is the duration it lives on average before it decays (about a trillionth of a second). What is special about the strange beauty meson system is that the lifetimes of the two particles differ by a small amount. An experiment can in principle hereby distinguish between the two mass-eigenstates, which can also offer a sensitive probe of New Physics. Typically an experiment measures a single *effective lifetime* for a given strange beauty meson decay, from which interesting physical information has to be decoded.

Strategies to hunt for New Physics

The goal of this thesis is to hunt for New Physics using strange beauty meson decays. We have chosen to focus on these mesons because the underlying quark transitions that

mediate their decays may reveal new CP symmetry violation or give indirect evidence for the existence of new particles. Furthermore, such decays are currently being probed by the LHC experiment at CERN. Currently no large signals of New Physics have been observed, but as the experimental precision improves in the years to come we may very well discover smaller signals. In order to be able to identify such signals as New Physics, it is important to have a precise theoretical understanding of what is being measured. In this thesis we discuss *strategies* for combining experimental measurements in such a way as to minimise the theoretical uncertainty, and thereby maximise our sensitivity to New Physics.

Our ability to theoretically describe the binding of quarks inside a meson due to the nuclear strong force is not perfect. Specifically, although various calculational tools have been developed to this end, their estimates typically have a sizable theoretical uncertainty. To minimise our dependence on this uncertainty, our strategies typically make use of an approximate symmetry of the strong force called *flavour symmetry*. This symmetry essentially states that the three lightest quark flavours – up, down and strange – are approximately indistinguishable from the perspective of the strong force's messenger particles. It thereby allows us to relate different meson decay processes to each other, using experimental measurements from one to fix uncertain parameters in another.

One way to search for New Physics is to test if the violation of CP symmetry predicted by the Standard Model is consistent, particularly the lesser constrained corners[9] of this model. We have proposed strategies to do this using several different strange beauty meson decays. In particular we have chosen decays that can be related by flavour symmetry to other meson decays, such as those already studied by the B–factories as we mentioned earlier. We have found that effective lifetime measurements can be particularly useful in these strategies. Once sufficiently precise experimental data becomes available our strategies should be competitive with existing strategies, and can thereby complement the hunt for new sources of CP symmetry violation.

Another way to search for New Physics is by looking at strange beauty meson decays that the Standard Model predicts to be very rare. A notable example is their decay to two muons, which is predicted to occur only one in 300 million times. On the other hand, in some models of New Physics the chance of this decay occuring is predicted to be far higher. This makes measuring the decay rate a priority for experiments at the LHC. A recent measurement has ruled out a large New Physics signal, however a smaller signal could still be present. In this thesis we have discussed an important correction to the theoretical calculation of this decay rate. We have also highlighted the usefulness of measuring the effective lifetime for this decay, which is sensitive to different New Physics features.

[9]These "corners" are actually the "angles" of triangles in the complex plane that describe the unitarity of quark flavour changing transitions. See Chapter 3 for further details.

Nederlandse samenvatting

Titel vertaling:
Strategieën voor de Jacht op Nieuwe Fysica
met Strange Beauty Mesonen

Deeltjesfysica

De wetten van de natuur onderbouwen, althans in principe, alle observaties die we kunnen maken van onze wereld, en daardoor ook elk gebied van de wetenschap. Simpel gezegd, zoals de bijgaande illustratie[10] dat als grap doet, is sociologie gewoon toegepaste psychologie, psychologie toegepaste biologie, biologie toegepaste biochemie, biochemie toegepaste chemie en, ten slotte, chemie gewoon toegepaste fysica:

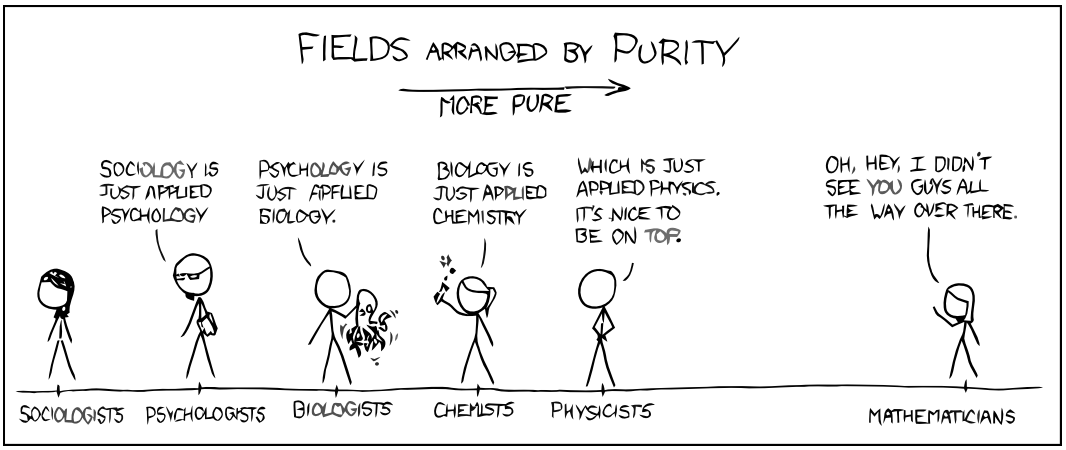

Binnen de fysica kunnen we verder gaan met dit reductionisme. Uiteindelijk kunnen we concluderen dat alle natuurlijke fenomenen, zo gevarieerd als het weer tot het afvuren van neuronen in onze hersenen, omschreven kunnen worden door *interacties* tussen *elementaire deeltjes*. In de praktijk is deze beschrijving gebaseerd op wiskunde, wat ook duidelijk wordt gemaakt in de illustratie, maar in dit hoofdstuk zullen we de lezer deze bijzonderheden besparen.

[10] Genomen van xckd comics [220].

Een elementair deeltje is een bouwsteen van de natuur waarvan we momenteel geloven dat die ondeelbaar is. We hebben bijvoorbeeld ontdekt dat atomen uit protonen en neutronen bestaan, en dat deze deeltjes op hun beurt weer van *quark* deeltjes gemaakt zijn. Omdat quarks tot nu toe een goede omschrijving van subatomaire fysica weergeven (hier komen we later op terug), beschouwen we ze als elementaire deeltjes. Elektronen, die zich aan een atoomkern binden om deze compleet te maken, zijn ook een voorbeeld.

Interacties tussen elementaire deeltjes worden veroorzaakt door fundamentele krachten. We kennen op dit moment vier van dit soort krachten. Namelijk de elektromagnetische kracht, de sterke kernkracht, de zwakke kernkracht en de zwaartekracht. Deze krachten kunnen zelf ook beschreven worden door elementaire deeltjes die *boodschapperdeeltjes* heten. Boodschapperdeeltjes communiceren aan andere deeltjes dat ze elkaar afstoten of aantrekken. Ten opzichte van de net genoemde fundamentele krachten zijn de boodschapperdeeltjes het foton (verantwoordelijk voor zichtbaar licht), het gluon, de W en Z bosonen en het graviton.

Van de vier fundamentele krachten zijn de sterke en zwakke kernkrachten het minst bekend vanuit ons alledaagse perspectief. De sterke kernkracht is verantwoordelijk voor het samenbinden van neutronen en protonen (of quarks om precies te zijn) in een atoomkern. Hij wordt "sterk" genoemd, want op subatomaire afstanden is deze veel sterker dan de concurrerende elektromagnetische kracht die probeert de (positief geladen) protonen in de atoomkern van elkaar weg te duwen. Anderzijds is de zwakke kernkracht zo genoemd omdat de interacties die deze overbrengt relatief zwak en zeldzaam zijn. Toch is de zwakke kracht een interessante kracht met belangrijke consequenties. Eén van de meer relevante functies voor dit proefschrift is dat de zwakke kracht het mogelijk maakt voor quarks om een eigenschap te veranderen die *smaak* heet. Hier komen we later op terug. Een voorbeeld van de zwakke kernkracht in actie is radioactief bètaverval, dat ontstaat door het verval van een neutron naar een proton waarbij een hoog-energetisch elektron (het bètadeeltje) en een neutrino worden uitgestraald.

Ons huidige begrip van de deeltjesfysica is samengevat in het treffend genoemde *Standaard Model*. Het Standaard Model voorspelt hoe alle bekende elementaire deeltjes zich gedragen ten opzichte van elke fundamentele kracht (behalve de zwaartekracht[11]). Het model is bijna 40 jaar oud en het blijft nog altijd nauwkeurige voorspellingen geven voor deeltjesfysica experimenten. De state of the art van zulke experimenten is de Large Hadron Collider (LHC), letterlijk de Grote Hadronen-Botser, te CERN in Genève. Deze deeltjesversneller, in de vorm van een cirkel met een omtrek van 27 km, kan protonen laten botsen met snelheden die dichtbij de lichtsnelheid liggen. De eerste experimentele botsingen zijn begin 2010 van start gegaan, en in 2012 werd het Higgs boson gevonden[12], wat wordt beschouwd als het laatst missend stukje van het Standaard Model. Hoewel het Standaard Model nu compleet lijkt, is het niet zonder tekortkomingen. In de volgende

[11] Einsteins algemene relativiteitstheorie beschrijft gravitationele interacties op lange afstanden. Het blijft een uitdaging om zwaartekracht samen te voegen met de kwantummechanische formulering van het Standaard Model, wat nodig is om de zwaartekracht op korte, subatomaire, afstanden te begrijpen.

[12] Om preciezer te zijn is er een deeltje ontdekt dat heel erg op het Higgs boson lijkt. Verdere testen zijn nodig om vast te stellen dat het echt het Higgs boson is.

sectie zullen we hiervan enkele voorbeelden geven. Bij het zoeken naar nieuwe fysische verschijnselen blijft de LHC een belangrijke rol spelen, en kan het meehelpen om het verouderende Standaard Model uit te breiden of zelfs te vervangen.

Astronomische motivaties

Om sommige van de tekortkomingen van het Standaard Model te bekijken is het voldoende om naar de hemel te kijken. Met een nauwkeurige telescoop zien we dat de sterrenstelsels in ons universum van elkaar weg bewegen. Deze waarneming van een uitdijend heelal heeft de populaire oerknalhypothese gemotiveerd. Wat echter vreemd is, is dat de snelheid waarmee sterrenstelsels uit elkaar bewegen niet kleiner wordt, zoals wij dat zouden verwachten als gevolg van de zwaartekracht, maar juist toeneemt! We noemen de bron van deze mysterieuze versnelling *donkere energie*, die 68% van het totale energiebudget van het universum inneemt[13].

Als we vervolgens nog beter naar de sterrenstelsels zelf kijken, observeren we iets anders: de sterren die in een stabiele baan aan de buitenkant van het sterrenstelsel ronddraaien gaan te snel ten opzichte van de zichtbare interne materie (de andere sterren). Om deze rotatiesnelheden te verklaren is het nodig dat sterrenstelsels een significante hoeveelheid onzichtbare materie bevatten: *donkere materie*. De beste uitleg voor deze mysterieuze donkere materie, die ook de berekeningen van hoe het universum gevormd is kan verklaren, is dat een sterrenstelsel een wolk van kleine deeltjes met zwakke interacties bevat. Geschat is dat deze donkere materie een bijdrage levert van 27% aan het totale energiebudget van het universum. Hier komt geen enkele van de elementaire deeltjes omschreven in het Standaard Model voor in aanmerking.

De uiteindelijke bijdrage van normale materie aan het totale energiebudget van het universum, zoals beschreven door het Standaard Model, is dus 5%. Dat het Standaard Model slechts een kleine fractie van ons universum omschrijft is duidelijk een tekortkoming voor een anders heel succesvol model. Onder andere tekortkomingen zoals deze leidt ons tot de conclusie dat het model incompleet is. We verwachten daarom dat als we doorgaan met testen, door deeltjes te botsen met hogere energieën of door metingen te maken met toenemende precisie, dat we uiteindelijk een afwijking zullen zien van de voorspellingen van dit model. In het algemeen noemen wij toekomstige fysische verschijnselen die zouden afwijken van de voorspellingen van het Standaard Model *Nieuwe Fysica*. Het benoemen van strategieën om op Nieuwe Fysica te jagen is één van de hoofddoelen van dit proefschrift.

Als we de normale materie in het universum, met 5% van het totale energiebudget, nader bekijken, is er nog een mysterie: waarom bestaat het allemaal uit materie en niet uit *antimaterie*? Deze vraag klinkt misschien vreemd, want antimaterie (niet te verwarren met de donkere materie die we net gedefinieerd hebben) klinkt exotisch. Maar eigenlijk is antimaterie volkomen normaal. Elk materiedeeltje is automatisch gepaard

[13]Het totale energiebudget van het universum is recentelijk bijgewerkt door de resultaten van de nieuwe Planck satelliet [221].

met een antimaterie deeltje dat dezelfde massa heeft maar tegenovergestelde lading. Het elektron, bijvoorbeeld, is gepaard met het positron, een "positief" elektron, dat gebruikt wordt in alledaagse dingen zoals medische PET (Positron Emissie Tomografie) scans. Als een deeltje zijn antideeltje tegen komt vernietigen ze elkaar en komt er energie vrij. Daarom is het duidelijk waarom de aarde maar één soort van elk stabiel deeltje heeft, en deze hebben we oorspronkelijk gekozen om *materie* te noemen. Evenwel zou de aarde ook uit stabiele antimaterie deeltjes kunnen bestaan.

De aarde is dus uit materie gemaakt, maar wat vreemd is is dat elk sterrenstelsel wat we kunnen observeren in ons universum dat ook is. We vermoeden dat tijdens het begin van een neutraal universum, net na de oerknal, materie en antimaterie in gelijke hoeveelheden gecreëerd zijn. Daarom is het een mysterie hoe de antimaterie verdwenen is terwijl de materie gebleven is. De fysische wetten lijken een voorkeur te hebben gehad voor materie tegenover antimaterie tijden de evolutie van ons universum.

In 1967 heeft de Sovjet-natuurkundige Andrei Sakharov een artikel gepubliceerd waarin hij de condities omschrijft die nodig waren tijdens de evolutie van het universum om te verklaren hoe de materie–antimaterie asymmetrie ontstaan is. Eén voorwaarde is dat bepaalde *symmetrieën* van de natuur wetten, die eerst vanzelfsprekend leken, gebroken zijn. Zoals we straks zullen uitleggen, blijkt het dat in het Standaard Model deze symmetrieën inderdaad gebroken zijn. Echter, deze symmetrieën zijn niet "genoeg" gebroken om het enorme verschil tussen materie en antimaterie dat we vandaag zien te verklaren. Daarom is onze zoektocht naar Nieuwe Fysica ook een zoektocht naar *symmetrieschending*.

Symmetrie schending en mesonen

Volgens Sakharov zijn er twee symmetrieën van de Natuur die gebroken moeten zijn om de materie–antimaterie asymmetrie van het heelal te verklaren *Charge (Lading) symmetrie* (C) en de combinatie van ladingssymmetrie met pariteitssymmetrie (P), die *CP-symmetrie* is genoemd. Ladingssymmetrie is de intuïtieve gedachte dat als we de lading van alle deeltjes zouden omkeren, bijvoorbeeld elektronen positief maken en positronen negatief, de wetten van de fysica die hun interacties omschrijven hetzelfde zouden blijven. Pariteitssymmetrie, anderzijds, vereist dat de wetten van de fysica nog steeds gelden nadat elke ruimtelijke richting omgekeerd is. In feite stelt pariteitssymmetrie dat een fysisch proces gezien door een spiegel zich nog steeds als een geldig fysisch proces gedraagt.

De ladings- en pariteitssymmetrieën zijn intuïtief, en worden nageleefd door bijna alle fundamentele krachten. De enige uitzondering is de zwakke kernkracht, die ze allebei apart schendt, en ook hun combinatie: CP-symmetrie. Dus, voor zover we nu weten, is het de zwakke kernkracht die verantwoordelijk is voor de partijdigheid van de Natuur voor materie over antimaterie.

In het Standaard Model zijn het specifiek de interacties van quarks via de zwakke kracht die CP-symmetrie schenden. Zoals eerder vermeld zijn quarks de elementaire

bouwstenen van samengestelde deeltjes die *hadronen* heten, zoals neutronen en protonen, en komen quarks in verschillende smaken. Er zijn zes smaken in totaal, die *up*, *down*, *strange*, *charm*, *beauty*[14] en *top* genoemd worden. Neutronen en protonen zijn bijvoorbeeld samengesteld uit up en down quarks, de twee lichtste smaken. Ze behoren tot een subgroep van hadronen die baryonen heten: hadronen die uit drie quarks bestaan. Het is ook mogelijk dat een quark en een antiquark samenbinden door de sterke kracht; deze samengestelde deeltjes worden *mesonen* genoemd. Alle mesonen zijn instabiel en vervallen snel naar andere deeltjes, maar door deze vervallen te bestuderen kunnen we veel leren over quark interacties.

De unieke eigenschap van de zwakke kernkracht is dat het de smaak van een quark kan veranderen. Bovendien kan CP-symmetrie geschonden worden als bijvoorbeeld, losjes geformuleerd, de kans[15] dat een beauty quark transformeert in een up quark niet identiek is aan de kans dat een beauty antiquark transformeert in een up antiquark. Echter, door de sterkte van interactie van de sterke kernkracht is het niet mogelijk om individuele quarks te isoleren zodat we die zouden kunnen bestuderen. In plaat hiervan kunnen we wel zulke smaak–veranderende quark interacties indirect bestuderen door transformaties en vervallen van samengestelde mesondeeltjes waar te nemen.

We kunnen mesonen bestuderen door gebruik te maken van deeltjesdetectoren, zoals de LHC te CERN. Door het gedrag van mesonen te vergelijken met die van antimesonen kunnen we onderzoeken hoe CP-symmetrie is geschonden in de onderliggende quark processen. Bovendien, door zulke processen heel precies te meten, kunnen we ook een vergelijking maken met de voorspellingen van het Standaard Model. Zodoende kunnen we Nieuwe Fysica onderzoeken. Om precies te zijn, de kwantummechanische aard van deze processen laat zware, tot op heden onontdekte, nieuwe deeltjes mee doen op subtiele manieren. Maar om ze te ontdekken hebben we zowel precieze experimentele metingen als precieze theoretische voorspellingen nodig.

Strange beauty mesonen

Bepaalde paren van neutrale mesonen kunnen in elkaar transformeren voordat ze vervallen door middel van een verschijnsel dat *mixing* wordt genoemd. De schending van CP-symmetrie is in feite ontdekt in 1964 door de *mixing* van neutrale kaons (mesonen die samengesteld zijn uit down en strange quarks). De waargenomen hoeveelheid schending was echter erg klein. Later werd ontdekt dat mesonen die een beauty quark bevatten veel meer CP-symmetrie schending vertonen, in hun mixing en in hun verval. In het vorige decennium zijn neutrale mesonen die zijn samengesteld uit een beauty quark met een down quark, of met een up quark in het geval van geladen beauty mesonen,

[14]Het beauty quark wordt ook wel het *bottom* quark genoemd.

[15]We hebben het hier eigenlijk over sterkte van de koppeling tussen deze twee quarks. De "kans" dat dit proces plaats vindt is de grootte in het kwadraat van de koppelingssterkte. CP-schending uit zich als een *complexe* koppelingssterkte, en is dus alleen waarneembaar als er een interferentie is tussen meerdere koppelingen.

uitgebreid bestudeerd bij zogenoemde *B–fabriek* deeltjesdetectoren. Dit heeft ons zeer geholpen in het geven van een beeld van de hoeveelheid CP symmetrie schending in het Standaard Model. Helaas, zoals we al eerder aangegeven hadden, is dit niet voldoende om de puzzel van de materie–antimaterie asymmetrie in ons universum op te lossen.

Toen de LHC begon in 2010, en toevallig ook dit proefschrift, waren mesonen die samengesteld zijn uit een beauty quark met een strange quark, "strange beauty mesonen", nog niet uitgebreid bestudeerd. Sindsdien zijn de deeltjesdetectoren bij de LHC, namelijk LHCb, ATLAS en CMS, begonnen met dit beeld scherper te stellen. Het is daarom aannemelijk dat we bewijzen van Nieuwe Fysica, in de vorm van nieuwe CP-symmetrie schending of nieuwe deeltjes, kunnen zien in de nabije toekomst. Bijgevolg is de theoretische analyse van deze deeltjes erg relevant, want om een afwijking van het Standaard Model te kunnen waarnemen hebben we eerst precieze theoretische voorspellingen nodig.

De combinatie van een beauty antiquark met een strange quark wordt aangeduid met het symbool B_s en een beauty quark met een strange antiquark met $\overline{B}_s$. Omdat beide van deze deeltjes neutraal zijn kunnen ze door mixing in elkaar transformeren, zoals we al eerder hebben opgemerkt. Zulke mixing overgangen worden vaak uitgebeeld door middel van *Feynman diagrammen*, waarvan we uitgebreid gebruik maken in dit proefschrift. Bijgaand een voorbeeld van een Feynman diagram dat de mixing overgang van een B_s meson naar een $\overline{B}_s$ meson voorstelt:

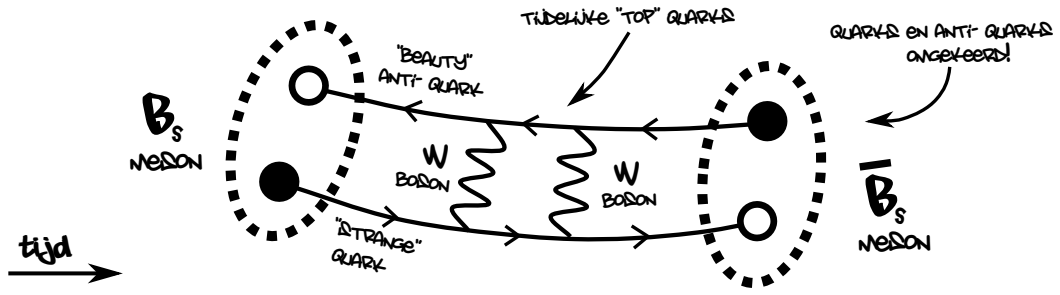

Merk op dat W bosonen, de boodschapper deeltjes van de zwakke kracht, deze overgang bemiddelen in het Standaard Model. In modellen van Nieuwe Fysica kunnen ook andere deeltjes bijdragen aan deze mixing.

De B_s en $\overline{B}_s$ kunnen worden beschouwd als elkaars antideeltjes. Een manier om CP-symmetrie schending te studeren is om vervalprocessen te identificeren die beginnen met de een of met de ander en de resultaten te vergelijken. Vanuit een experimenteel perspectief heet het onderscheiden van deze zogenoemde *smaaktoestanden*, B_s en $\overline{B}_s$, *flavour tagging*. Metingen die gebruik maken van deze techniek kunnen zeer gevoelig zijn voor Nieuwe Fysica. Maar het gebruiken van deze techniek is tegelijkertijd een uitdaging en daarom lukt het maar voor een kleine fractie van gebeurtenissen.

Een belangrijk aandachtspunt van dit proefschrift is hoe wij naar Nieuwe Fysica kunnen zoeken met experimentele metingen die niet afhankelijk van smaak tagging zijn. We kunnen de B_s en $\overline{B}_s$ mesonen omschrijven met een ander formalisme waarin ze niet met elkaar mixen. In dit formalisme worden de deeltjes gelabeld door hun relatieve

massa, $B_{s,\mathrm{H}}$ en $B_{s,\mathrm{L}}$ voor de zwaardere (heavy) en lichtere (light) deeltjes, respectievelijk, en worden ze *massa-eigenstaten* genoemd. Doordat de deeltjes in deze omschrijving niet mixen, is het mogelijk om een levensduur te definiëren voor elk deeltje, dat wil zeggen de gemiddelde tijd dat het deeltje leeft voordat het vervalt (ongeveer een biljoenste van een seconde). Wat het strange beauty meson systeem special maakt is dat er een klein verschil is tussen de levensduur van de twee individuele deeltjes. Een experiment kan in principe hierdoor de twee massa-eigenstaten onderscheiden, een techniek die ook gevoelig kan zijn voor Nieuwe Fysica. Normaal gesproken meet een experiment een enkele *effectieve levensduur* van een strange beauty meson verval, waaruit interessante fysische informatie gedecodeerd kan worden.

Strategieën voor de jacht op Nieuwe Fysica

Het doel van dit proefschrift is om op Nieuwe Fysica te jagen met strange beauty meson vervallen. We hebben gekozen om ons op deze mesonen te richten omdat de onderliggende quark overgangen die de vervallen bemiddelen misschien nieuwe CP-symmetrie schending kunnen blootleggen, of indirect bewijs kunnen leveren voor het bestaan van nieuwe deeltjes. Bovendien worden zulke vervallen momenteel onderzocht door het LHC experiment te CERN. Tot nu toe zijn er geen grote signalen van Nieuwe Fysica waargenomen, maar omdat de experimentele nauwkeurigheid zal verbeteren in de komende jaren zullen we steeds kleinere signalen kunnen ontdekken. Om dit soort signalen te kunnen identificeren als Nieuwe Fysica, is het belangrijk om een nauwkeurig theoretische begrip te hebben van wat gemeten wordt. In dit proefschrift bespreken we *strategieën* voor het zodanig combineren van experimentele metingen dat de theoretische onzekerheid wordt geminimaliseerd, en zodoende de gevoeligheid voor Nieuwe Fysica gemaximaliseerd.

Ons vermogen om het binden van quarks binnen een meson theoretisch te beschrijven is nog niet perfect. Hoewel er diverse wiskundige methodes zijn ontwikkeld die hierbij helpen, hebben schattingen die hieruit volgen typisch een aanzienlijke theoretische onzekerheid. Om onze afhankelijkheid van deze onzekerheden te minimaliseren, maken onze strategieën veelvuldig gebruik van een benaderende symmetrie van de sterke kracht die *smaaksymmetrie* heet. Deze symmetrie zegt in feite dat de drie lichtste quark smaken – up, down en strange – ononderscheidbaar zijn vanuit het perspectief van de boodschapper deeltjes van de sterke kracht. We kunnen daarom verschillende meson vervalprocessen relateren aan elkaar, waarbij we experimentele metingen van de één kunnen gebruiken om onzekere parameters van de ander vast te stellen.

Een manier om naar Nieuwe Fysica te zoeken is te testen of de schending van CP-symmetrie die voorspeld is door het Standaard Model consequent is, vooral met betrekking tot de minder nauwkeurig bepaalde hoeken[16] van dit model. We hebben strategieën voorgesteld om dit te bewerkstelligen met strange beauty meson vervallen. In het bij-

[16]Deze "hoeken" zijn werkelijk hoeken van driehoeken in het complexe vlak die de unitariteit van de quark smaak overgangen omschrijven. Zie Hoofdstuk 3 voor verdere details.

zonder hebben we gekozen voor vervallen die we kunnen relateren aan andere meson vervallen door middel van de smaaksymmetrie, zoals vervallen die al met de B-fabrieken gemeten zijn. We hebben gevonden dat metingen van de effectieve levensduur bijzonder nuttig kunnen zijn voor deze strategieën. Als de nauwkeurigheid van de beschikbare experimentele data eenmaal voldoende is zullen onze strategieën concurrerend zijn met de huidige strategieën, en kunnen deze de jacht naar nieuwe bronnen van CP-symmetrie schending aanvullen.

Een andere manier om naar Nieuwe Fysica te zoeken is om naar vervallen van strange beauty mesonen te kijken die volgens de voorspelling van het Standaard Model zeer zeldzaam zijn. Een opmerkelijk voorbeeld is hun verval naar twee muonen, waar de voorspelling is dat dit maar eens in de 300 miljoen keer voorkomt. Daarentegen is de kans dat dit verval voorkomt veel groter in sommige modellen van Nieuwe Fysica. Daarom is de meting van de vervalsnelheid een prioriteit voor de experimenten van de LHC. Een recente meting heeft een groot Nieuwe Fysica signaal uitgesloten, maar een kleiner signaal kan nog aanwezig zijn. In dit proefschrift hebben we een belangrijke correctie voor de theoretische berekening van de vervalsnelheid gepresenteerd. We hebben ook de bruikbaarheid van de effectieve levensduur voor dit verval gedemonstreerd, welke gevoelig is voor verschillende kenmerken van Nieuwe Fysica.

Acknowledgements

Firstly, thank you dear reader for opening my thesis. As this may be the first chapter you read, let me take this opportunity to also advertise the *Lay summary/Nederlandse samenvatting* chapters, which were written particularly with non-experts in mind.

Now to my acknowledgements. I would like to start by thanking my promotor, supervisor and collaborator Robert Fleischer. I've learnt a great deal from the four years that we've worked together. I was introduced to the subject of B physics from your thorough lecture notes, and it was very useful to dive straight into this topic with our first paper on $B_s \to K^+K^-$. Your enthusiasm for this topic is admirable, and by working efficiently on topical projects we succeeded in publishing many papers together. I'm also very grateful for the many opportunities you helped to organize, including international conferences such as Beauty 2013 and my internship to Munich.

I was fortunate to be able to collaborate with many wonderful people during my PhD, both theorists and experimentalists. Thank you Andrzej Buras for inviting me to visit the IAS in Munich and for your support while I was there. And of course thank you for offering me a job. Thanks also to Jennifer Girrbach, Fulvia De Fazio and Minoru Nagai for the pleasant Munich collaboration. Thank you very much Giulia Ricciardi for a very enjoyable collaboration with Naples. I also really enjoyed your well organized workshop in Capri.

I owe a special thankyou to Kristof De Bruyn, who I worked closely together with on several projects, and who was always happy to discuss. Also thanks for carefully reading over several chapters of this thesis. It was both very educational and enjoyable to work together with experimentalists from LHCb, including Patrick Koppenburg, Marcel Merk, Antonio Pellegrino, Manuel Schiller and Niels Tuning. I'm also grateful for your invitations to join the LHCb workshop every year.

I would like to thank Eric Laenen and Michel Herquet for their collaboration on a paper related to my master thesis (which we published during the start of my PhD). I would further like to thank Eric for his continued support and guidance thereafter, as well as fostering a pleasant working environment in the Nikhef theory group as the head of department. In terms of support I would also like to thank Paul De Jong, my external C3 committee member, as well as Marcel Merk for his frequent words of encouragement.

The reading committee of this thesis deserves a special mention for their time and effort, namely Daniel Boer, Andrzej Buras, Piet Mulders, Gerhard Raven and Giulia

Ricciardi.

During my years at Nikhef I'm fortunate to have met and befriended many great and interesting people, as well as witnessed the theory group transform into a very fun place to work. Sander Mooij you deserve countless credit for beginning the Friday evening Brouwerij het IJ tradition. Damien George I really enjoyed our gym sessions, and how they doubled as brainstorming sessions for Paperscape. Mert Aybat I continue to admire your enthusiasm for burgers and Soundgarden. Giuseppe D'Ambrosi I enjoyed our organization of the day out. Marieke Postma thanks for motivating me to join ultimate frisbee, as well as visit the world table tennis championships. Eric Laenen and Jan Kuipers thanks for the competitive games of squash. In chronological order I would further like to thank Reinier de Adelhart Toorop, Michele Maio, Bert Schellekins, Beatriz Gato Rivera, Jan-Willem van Holten, Jos Vermaseren, Lisa Hartgring, Thomas Reiter, Chris Korthals-Altes, Bart Verouden, Wilco den Dunnen, Jordy de Vries, Thijs van den Broek, Jacob Noordmans, Pietro Falgari, Ivano Lodato, Bernard de Wit, Mike Agathos, Pierre Artoisenet, Robbert Rietkerk, Domenico Bonocore, Valentine Reys, Marteen Buffing, Andrea Signore, Erica Rasch, Marco Volponi, Michael Wiechers, Franz Ciceri, Kalliopi Petraki, Kasper Larsen, Daniel Butter, Otto Rotier, Lodewijk Nauta, and everyone I've forgotten.

Then there are the Nikhefers and non-Nikhefers with which I've had the pleasure to live with at Lamonggracht 17. Jan Weenink, it was a pleasure, especially the basketball, boating and bromance. Also thanks for proofreading the Nederlandse Samenvatting. Mark Beker, Elsabeth van Overbeeke, Joris Heijningen and Lotte Straathof: it still is a pleasure. Thanks for all your support, meals, cleanliness, nights out and the summer swimming in het IJ.

I'm also grateful for all the good times and support I've shared with friends during my PhD, including the past and present Utrecht crowd. Thanks!

Though they were 11 ± 1 hours ahead of me, my family always managed to stay supportive. Thank you Bridget Knegjens, Jan Knegjens, Marry Knegjens, Lucas Knegjens, the twins and Skype. And thanks for proofreading the Nederlandse Samenvatting papa. I'm also very grateful to my extended family in the Netherlands for helping me settle here and offering a home away from home. To my dear grandparents, Piet Bender and the late Mieke Bender, I'm still amazed that you took courses on quantum mechanics and relativity and were able to discuss these so enthusiastically with me!

Paljon kiitoksia Meri Varkilalle kaikesta rakkaudesta ja tuesta viimeisen neljän vuoden aikana.